THE GEOLOGY AND GEOCHEMISTRY OF THE OMAI GOLDFIELD, GUYANA.

ROY GRAHAM ELLIOTT

A thesis submitted in partial fulfilment of the requirements of Oxford Brookes University* for the degree of Doctor of Philosophy.

This research programme was carried out in collaboration with Guyana Geology and Mines Commission (GGMC) and Golden Star Resources (GSR) Ltd., Alberta, Canada.

December 1992

* formerly Oxford Polytechnic.

Now we see but a poor reflection as in a mirror; then we shall see face to face. Now I know in part; then I shall know fully, even as I am fully known.

I Corinthians 13:12.

The geology and geochemistry of the Omai goldfield, Guyana.

by

R. G. Elliott

ABSTRACT

The Omai goldfield consists of mesothermal lode gold mineralisation and associated saprolite-alluvial placer deposits, hosted within Palaeoproterozoic granite-greenstone terrain of the Guiana Shield. Total mining reserves are estimated at 44.8 million tonnes, grading at 1.43 g/t Au. The goldfield lies along an ESE-trending, regional-scale structure referred to as the Issano-Appaparu shear zone. At Omai, the gold deposits are located in two discrete ore zones - the Omai Stock Zone and the Wenot Lake Zone. The bulk of primary mineralisation is centred on a high-Al, quartz diorite-tonalite boss (the Omai Stock), where wall-rock alteration is dominated by a hydrothermal sericite-carbonate assemblage. The primary ore package of Au-W-Te-S mineralisation is contained in a series of narrow (1-5cm), quartz-carbonate (ankerite) veins. Visible gold is commonly associated with galena and microscopic tellurides. Provisional fluid inclusion studies have indicated that the parent hydrothermal fluid was H_2O-CO_2 -bearing ($\approx$5.0 mol% CO_2), of low salinity (0-1.8 wt.% NaCl equiv.) and moderate density (0.96 g/cm^3). The depositional temperature of the fluid was probably in the region of 200-400°C. Preliminary $\delta^{18}O$ values are consistent with a magmatic and/or metamorphic source.

The Majuba Suite greenstones adjacent to the Omai Stock are also partially mineralised. These rocks are dominated by primitive, low-K, high-Fe tholeiitic (HFT) basalts and minor basic intrusives which are characterised by flattish REE patterns of around 10 times chondrite. A subordinate, calc-alkaline series (CAS), of mostly andesitic composition, is intercalated within the volcanic pile. In terms of trace element geochemistry, the Majuba Suite is chemically comparable to volcanic rocks from modern island arc settings.

The REE geochemistry, which proved to be extremely diagnostic throughout, indicates that the Omai Stock is genetically related to the regional Tigri pluton. This and other Trans-Amazonian soda granitoid plutons in the area have chemical affinities akin to calc-alkaline volcanic arc granitoids of Phanerozoic orogenic belts. Several lamprophyric (appinite) pipes are spatially and temporally associated with the Omai Stock. Although the appinites are only weakly mineralised, they may have a genetic significance regarding the source of the gold.

Both the Omai Stock and Majuba Suite are cut by a series of partially mineralised, ultrabasic to intermediate dykes (the Gilt Creek Suite) which intruded along shallow-dipping fracture zones. These rocks are typically Mg-rich, LREE enriched (La_n/Yb_n = 7.84-32.6) and appear to be the product of alkaline arc magmatism. A few post-orogenic mafic dykes (POMDs), of probable Mesozoic age, are also identified in the area. These rocks are strictly non-mineralised and are chemically correlatable with tholeiitic basalts from continental rift-related settings.

In the Wenot Lake Zone, lode mineralisation is hosted within thin bands of high-silica rhyolites (HSRs), also of the Majuba Suite, close to a sheared contact with phyllitic tuffs. The HSRs have a distinct chemistry characterised by elevated SiO_2 (>75.0%), Na, Nb, Zr and REE contents with anomalously low concentrations of Mg, Ti, Ca, K, Rb and Sr. These rocks are further characterised by wing-shaped REE patterns containing deep negative Eu anomalies.

ACKNOWLEDGEMENTS

Anyone who has undertaken a research degree will know that John Donne was right in saying "no man is an island". For sure, this thesis would never have been completed without the help and co-operation of numerous people. Firstly, I would like to thank Chris Barron for introducing me to life and geology in Guyana, way back in 1984, and for his friendship since then. I would also like to thank my former colleagues at the Guyana Geology and Mines Commission (GGMC) where I spent several happy years working as a geologist and where this research was initiated. Dave Fennell, Hilbert Shields and Carlos Bertoni, all of Golden Star Resources (GSR) Ltd, helped to get the project off the ground and provided invaluable logistic support along the way. Funds for the research and production of this thesis were made available by Oxford Brookes University (OBU)*. My thanks are also extended to my main supervisors, Prof. Howard Colley (OBU) and Dr. Bill Perkins (University College of Wales, Aberystwyth) for their guidance and counsel throughout the course. Anton Kearsley provided the expertise with the SEM-EDS facilities at OBU and freely gave countless hours of his time. Jon Wells, Dave Hicks, Simon Deadman and Chris Gilbert, all of OBU, supplied invaluable technical support in the respective fields of thin-sectioning, information technology, photography and geochemistry. Thanks are also due to Dr. Dave Alderton (Royal Holloway) who supervised the fluid inclusion and stable isotope studies and to Ron Hardy (University of Durham) who ran the XRF analyses. I am also very grateful to Drs. Robert De Vletter (Netherlands), Fred Barnard (USA), Asit Choudhuri (Brazil) and Xafi João (Brazil) who kindly supplied inaccessible reference material, as did Catherine Kehoe and Liz Longshaw of the Inter-Library Loan (ILL) office at OBU. Finally, I would like to express my appreciation to my parents, Francis and Margaret, for all their love and support over the years.

* formerly Oxford Polytechnic.

TABLE OF CONTENTS

List of Figures

List of Tables

List of Plates

page

CHAPTER 1

INTRODUCTION

1.1 Opening remarks.

The Omai goldfield is essentially a Precambrian lode gold deposit with published mining reserves of 44.8 million tonnes grading at 1.43 g/t Au (Mining Magazine, Sept., 1991). After a series of abortive exploration programmes spanning several decades, Omai is finally back on stream as a major producing mine following a successful Canadian-based joint-venture operation launched in 1990 by Cambior Inc. and Golden Star Resources Ltd. (GSR).

1.2 Organisation of this research.

This research work was initiated whilst the writer was employed as a geologist with the Guyana Geology and Mines Commission (GGMC) during the period 1984-1988. Permission to visit the Omai property for research purposes was kindly granted in May, 1986 by Golden Star Resources Ltd. This courtesy was extended when Placer Dome Inc. became the senior joint-venture partner the following year.

The field work in the early stages consisted of logging and sampling test pits in the saprolite cover of the Omai Stock Zone. Later, 2125 m of drill-core from the 1986 GSR diamond drilling programme were systematically re-logged and sampled in the field with free access to the original drill-logs and assay results. Regional rocks such as the Tigri and Mariaba plutons were sampled by boat traverse along the Essequibo River at low water. In total, approximately 12 weeks were spent in the field. Seventy-eight geochemical samples, 61 polished sections and 142 thin sections comprise the raw material for this thesis (see Appendix I).

1.3 Aims.

Very little advanced research has been undertaken at Omai, and indeed in Guyana as a whole, for over twenty years. This is due in part to the country's austere investment climate during the period 1966-1985. It is therefore intended that this work will provide a fresh and comprehensive data base for further geological and geochemical research. The aims of this

thesis are five-fold as follows:

1. To critically review the geology and mineralisation of the Omai goldfield in a regional and global context.

2. To determine the geochemical characteristics of the granitoid and meta-volcanic host rocks with a view to regional correlation and to constrain possible petrogenetic and tectonic histories for the Omai area.

3. To accurately identify the main ore-forming phases using SEM-EDS microscopy.

4. To ascertain P-T-X (pressure-temperature-composition) properties and possible sources of the hydrothermal fluids by fluid inclusion studies and stable isotope analyses.

5. To formulate a regional model for gold mineralisation in northern Guyana that may assist in the planning of future exploration programmes.

1.4 Guyana - "the land of many waters".

The Co-operative Republic of Guyana is situated on the northeast seaboard of South America where she nestles between her giant neighbours, Brazil and Venezuela, located to the south and west repectively (see Fig. 1.1). The previously occupied Dutch territory of Surinam forms the eastern frontier along the length of the Corentyne River. In Guyana, less than 850,000 people occupy a land which is roughly the same size as Britain. The majority of the population is concentrated on a narrow fertile coastal plain with some 70,000 inhabitants located in Georgetown, the capital city and Atlantic sea-port. Six ethnic groups are resident and are represented as percentage of the population as follows: East Indian (47%); Afro-Guyanese (35%); Coloureds (12%); Amerindian (5%); Portuguese (0.5%) and Chinese (0.5%).

Traditionally, the former British colony has viewed itself as a Caribbean nation rather than a South American one. English is still the official language and the republic has retained much of its colonial character as reflected by the nature of the commercial, judicial and educational establishments. However, in recent years, emigration and trade links with the U.S.A and Canada have become progressively more dominant as attachments with the U.K. have waned. Despite prolonged internal pressures and foreign influences, the Guyanese people

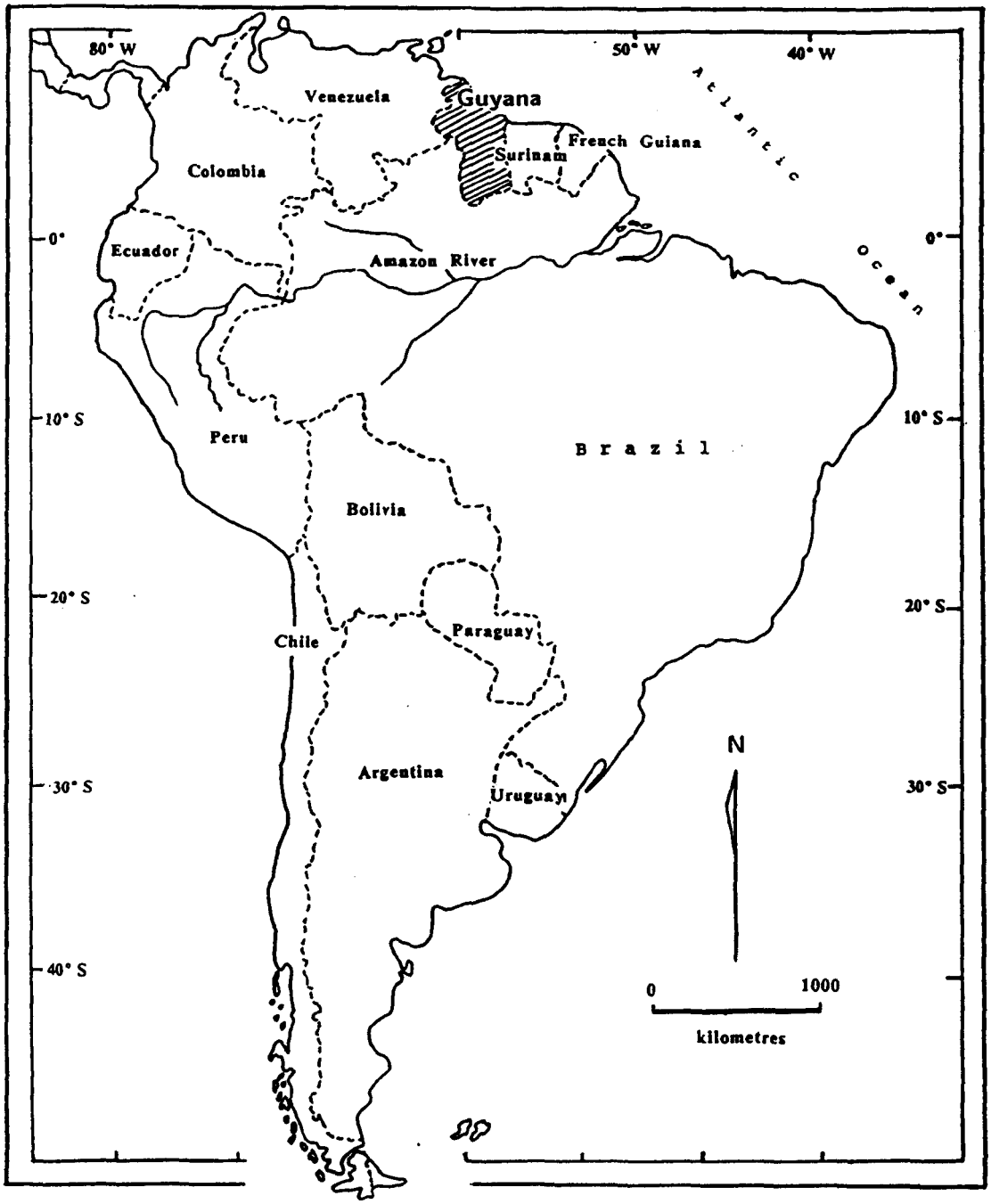

Fig. 1.1: Location Map : Guyana, South America.

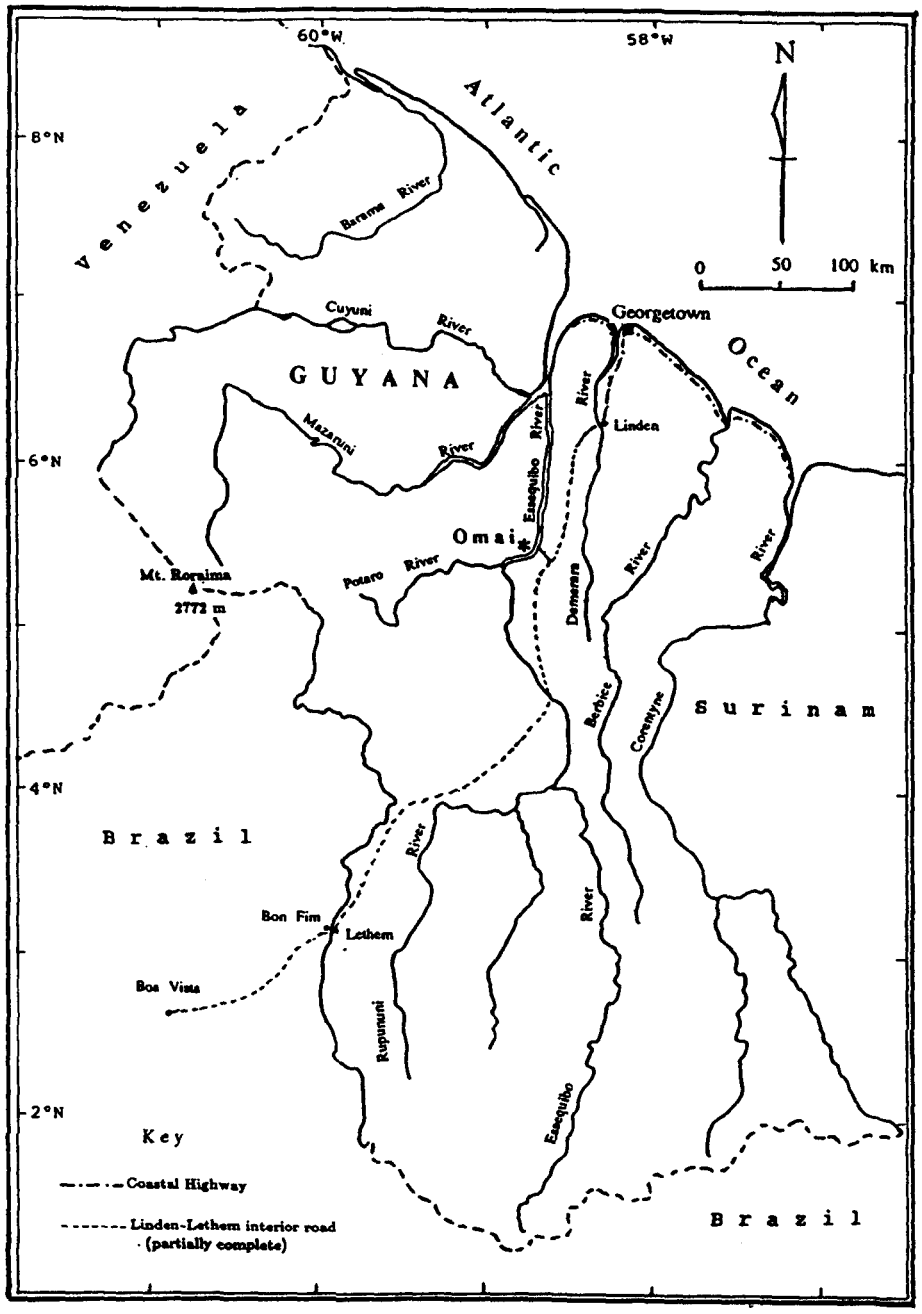

Fig. 1.2: Location Map : The Omai Goldfield, Guyana.

have maintained a rich cosmopolitan cultural heritage, epitomised by their warm-hearted nature and generous hospitality.

After two decades of economic and political experimentation with socialism following independence, Guyana implemented its own brand of perestroika in 1985 under the leadership of President Desmond Hoyte* of the People's National Congress (PNC). Since then, the nation's economic structure has been shaken by a series of devaluations of the Guyana dollar. Bauxite exports and coastal agriculture, such as rice and sugar cane, have traditionally been the backbone of the economy supported by subsidiary forestry and fishing. The gold and diamond industry is currently an important earner of essential foreign exchange though much of the wealth has been dissipated through small-scale operations. In 1988, the per capita GDP was estimated at $US 360. This rather low figure belies the nation's huge natural resource potential.

Undeveloped Amazonian rainforest, interrupted by areas of savanna grassland, blankets about 80% of the country thus confining the road infrastructure (2915 km) mainly to the coast. Generally, access to various interior settlements can only be gained by boat or light aircraft. However, a 200 km-long , all-weather, laterite road is presently under construction aimed at linking Georgetown with the remote Guyana-Brazil border settlement of Lethem and beyond (see Fig. 1.2).

As its name implies, ("Guyana" is the indigenous Amerindian word meaning "land of many waters") the republic is graced with an impressive natural drainage network of considerable magnitude. The main first order water-courses, which virtually dissect the country from north to south, are represented by the Essequibo, Demerara and Berbice rivers. Secondary waterways such as the Mazaruni, Cuyuni and Potaro rivers are also of significant importance and generally drain in an E-W direction.

Guyana lies south of the hurricane and earthquake belts thus avoiding the catastrophes which frequently rock the Caribbean and Central American regions. The average coastal temperature is about 27°C with a diurnal variation of 8°C and a 2°C annual variation. The coast receives an average of 230 cm of rain compared to 265 cm in the rainforested highlands. Rainfall normally occurs in two distinct seasons, namely, May to July and December to January, separated by rather dry spells. Malaria has been totally eradicated from the coast but outbreaks still persist in the interior, especially during the rainy seasons.

* In the general election of October, 1992, Desmond Hoyt was succeeded as president by Dr. Cheddi Jagan of the People's Progressive Party (PPP).

1.5 The Omai goldfield.

1.5.1 Location and access.

The Omai goldfield is situated in dense tropical rainforest in central Guyana, close to the west bank of the mighty Essequibo River (see Plate 1.1 and Fig. 1.2). The property is located 230 km south-southwest of Georgetown at co-ordinates 58°45'W, 05°28'N and covers an area of 24 km^2. The nearest major population centre is the bauxite mining town of Linden, located 120 km to the north. Omai, which can be reached at any time of the year by road from Georgetown in about five to six hours, is the most readily accessible of Guyana's major gold deposits.

1.5.2 Mining and exploration history (1886 - 1992).

The Omai goldfield has a documented mining and exploration history dating back over a century. The main periods of activity are outlined below. For a fuller and more detailed historical account the reader is referred to S.N.C. (1985) and Bertoni et al. (1990).

"Pork-knockers" and the German Syndicate (1886-1911).

In the period 1886-1896 some 1890 kg (60,000 ozs.) of gold were won from the placer deposits of Gilt, Dunclain and L'Esperence creeks by small-scale miners ("pork-knockers") using primitive hand methods. The German Syndicate (later known as the Guiana Syndicate) leased the concession in 1896 and carried out extensive investigation of bedrock quartz lodes by drilling and tunnelling. Hydraulic mining of the saprolite cover produced 1860 kg (59,800 ozs.) between 1900 and 1902. An additional 47 kg (1,500 ozs.) were recovered by stamp-milling of the quartz veins exposed during earlier mining activities.

After limited success in dredging the alluvial flats, the Syndicate surrendered the property to the pork-knockers in 1907. A further 467 kg (15,000 ozs.) were won in the following four years. By 1911 most of the workable ground was exhausted and no accurate production estimates are available subsequent to this period.

Anaconda British Guiana Mines Ltd. (1946-1950).

In order to prove-up reserves, close-formation diamond-drilling was focused on the primary mineralisation contained in the Omai Stock. Seventy-three AX-diameter boreholes were drilled with a total footage of 12,400 m. On the basis of surface drilling assay results, a 120 m shaft was sunk near Red Hill and 900 m of cross-cutting were carried out at the 62 m

Plate 1.1: Aerial view of the Omai Stock Zone showing former open-cut areas.

Plate 1.2: Ground view looking across Wenot Lake.

level. By 1950, Anaconda had targeted a localised primary ore body containing reserves of 54.4 million tonnes grading at 1.19 g/t Au. However, due to a combination of low gold prices and a favourable copper market at the advent of the Korean War, the company decided to relinquish the property.

Regional base metal exploration in the 1960s.

Several linear conductors running ESE across the Omai area were detected by United Nations sponsored airborne magnetic and electromagnetic surveys in the period 1960-1964. The Geological Survey of Guyana (now known as GGMC) carried out a follow-up regional geochemical survey and mapping programme during the last quarter of 1967. In his 1969 report, field geologist F.J.L. Guardia concluded that the majority of the EM anomalies were due to structurally controlled, uneconomic bedrock conductors rather than to base metal mineralisation. Later that year, S.P. Collings, a post-graduate student from the Colorado School of Mines carried out a grid geochemical survey centred on the former mine site. Minor copper and cobalt anomalies were believed to be associated with hydrothermal mineralisation.

Golden Star Resources Ltd. (1985-1987).

In May 1985, Golden Star Resources Ltd., a junior Alberta-based exploration company, signed the Omai Exclusive Exploration Permit (E.E.P.) agreement with the Guyana government. Later, in the same year, the new E.E.P. holders contracted the Canadian engineering consultancy, S.N.C. Inc., to undertake an evaluation-feasibility study of the oxidised zone. The contractors immediately initiated systematic alluvial and saprolite evaluation programmes which consisted of extensive auguring and test-pitting to depths of about 4 m. Indicated alluvial reserves of 750,000 tonnes grading at 3.2 g/t Au and indicated saprolite reserves of 1.2 million tonnes grading at 1.44 g/t Au were subsequently defined. In the following year, on the basis of these encouraging surface results, GSR bored six deep diamond drill-holes, totalling 2125 m, to check out hypogene mineralisation in the Omai Stock Zone.

Placer Dome Inc. - Golden Star Resources Ltd. (1987-1990).

Placer Dome Inc. of Vancouver, British Columbia, became the senior joint-venture partner at Omai in March 1987, though GSR and the Guyana government still retained an interest in the property. Over a three year period Placer carried out a comprehensive, integrated exploration programme which included surface mapping, trenching, soil geochemistry and ground geophysics coupled with approximately 24,000 m of diamond drilling. The localised alluvial deposits in the vicinity of Gilt and Dunclain Creeks were tested using Banka and sonic drilling techniques.

In February 1989, overlapping geochemical and radiometric anomalies drew attention to the Wenot Lake area (see Plate: 1.2), located some 800 m to the south of the Omai Stock. Subsequently, eight exploratory holes were drilled leading to the discovery of a second ore body overlain by a supergene-enriched saprolite blanket. In total, 130 "SAP" and "DDH" holes totalling 10,550 m were drilled in order to accurately define the Wenot Lake ore zone.

Early in 1990, Placer were in a position to estimate the combined primary, saprolite and alluvial reserves of the Omai gold deposits. Using a 0.7 g/t and 0.5 g/t cut-off value for hard rock and saprolite respectively, geological (indicated) reserves were calculated at 52.8 million tonnes grading at 1.35 g/t Au (see Table 1.1). However, on 30 April, the same year, Placer withdrew from the original agreement for "economic reasons" and complete control of the Omai E.E.P. reverted back to GSR.

Cambior Inc. - Golden Star Resources Ltd. (1990 - to date).

On 24 May, 1990, GSR entered into a joint-venture agreement with Cambior Inc. of Val d'Or, Quebec. Thereafter, 8,500 m of definition drilling were carried out to confirm grade continuity and geological boundaries in the respective mineralised zones. Following the completion of a successful feasibility study at the end of 1990, Cambior Inc and GSR signed a deal with the government of Guyana which effectively launched Omai into the production stage under the auspices of the newly-formed subsidiary, Omai Gold Mines Ltd. Construction of the mine plant is presently well under way with a target start-up date set for early 1993. The published mining reserves of 44.8 million tonnes, grading at 1.43 g/t Au, will permit an average annual production in excess of 8.2 tonnes (255,000 ozs.) over the first three years (Mining Magazine, Sept., 1991). Additional Cambior-GSR mining data are given in Table 1.2.

1.5.3 Previous research (1899 - 1992).

In 1899, E. E. Lungwitz, the former manager of the German Syndicate operations at the Omai mine, submitted a doctoral thesis to Rostock University, Leipzig. Lungwitz apparently recorded the ore minerals as gold, gold-tellurides and scheelite. He also noted that the ore included pyrite but the pyrite itself did not contain gold.

In his publication entitled "The geology of the goldfields of British Guiana", Dulau & Co, 1908, Sir J. B. Harrison, who pioneered much of the geological mapping and exploration in early colonial times, proposed that the gold contents of the "aplite" stock were derived from the overlying diabase (gabbro). In addition, Harrison submitted petrographic and chemical analyses of Omai drill-core specimens which had been surrendered to the colony by the German Syndicate in 1901. The occurrence of numerous small eluvial diamonds at Omai are

also recorded in Harrison's 1908 publication.

R. Johnston made a detailed petrographic study of 110 drill-core samples and various outcrop specimens collected by the Anaconda's former geologist at Omai - Mr. Glenn C. Waterman. The results of this study were tabled in the form of a dissertation to the University of St. Andrews, Scotland in 1960. Johnston proposed the Omai Stock was of trondhjemitic affinity and that the albitisation was caused by inherent, late-stage, residual fluids which antedated gold mineralisation. The same author postulated that the hydrothermal fluids occupied post-emplacement fractures in the stock and that they originated from an underlying, deep-seated magmatic source.

During the late 1960s, S.P. Collings conducted a 10-week geochemical survey spanning 25 km^2 of the Omai area. Over 1000 soil, saprolite, stream-sediment, heavy mineral concentrate and oxidised whole-rock samples were collected and examined for a wide range of elements by atomic absorption spectrophotometry (AAS) and semi-quantitative spectrographic analysis. Collings identified a weakly anomalous Cu-Co-Ni signature on the south flank of Quartz Hill. A further Cu-Co-Ni-(Au) target was pin-pointed in a N-S trending shear zone immediately east of Omai River. The results of this work were presented as an M.Sc. thesis to the Colorado School of Mines in 1969.

As an integral part of the undergraduate geology programme at the University of Alberta, R. P. Shaw (1986) carried out a mineralogical investigation on two gold-bearing, soil-saprolite samples collected near the abandoned mine shaft at Red Hill. SEM-EDS analysis revealed that native gold grains in the saprolite sample displayed high degrees of fineness and showed no evidence of transportation.

Table 1.1

Placer-GSR Evaluation of Geological Reserves at Omai

Omai Stock Zone

Material	Ore ($x10^3$ tonnes)	Grade (g/t Au)
Fresh rock	41,806	1.340
Saprolite	3,338	1.194
Alluvium	1,820	1.610
Subtotal	46,964	1.338

Wenot Lake Zone

Material	Ore ($x10^3$ tonnes)	Grade (g/t Au)
Fresh Rock	1,352	1.228
Saprolite	4,455	1.538
Subtotal	5,807	1.446
Grand total	**52,771**	**1.353**

Data source: Bertoni et al., (1990).

Table 1.2

Cambior-GSR Mining Data

Joint-Venture Interest:	Cambior (60%); GSR (35%); Guyana Government (5%).
Capital Cost of Project:	$US 152 million.
Total Resource:	64.1 tonnes (2.06 million ozs.) gold.
Mining Reserves:	44.8 million tonnes at 1.43 g/t gold.*
Main Ore Zones:	Omai Stock Zone; Wenot Lake Zone.
Projected Production:	8.2 tonnes (255,000 ozs.)/year over first 3 years.
Mining Methods:	Open pit; grinding-ballmilling - carbon-in-leach process.
Estimated Recovery:	93.5%
Initial Operating Cost:	$US 185/oz. gold.
***Proposed* Start-up Date:**	*early* 1993

* Approximately 25% of mining reserves consist of saprolite and alluvial deposits.

Data source: Mining Magazine (Sept., 1991).

CHAPTER 2

TECTONIC SETTING AND GEOLOGICAL FRAMEWORK

2.1 Aims of chapter.

This chapter sets out to demonstrate how the mineralised Precambrian granite-greenstone terrain of northern Guyana relates to the regional tectonic setting of northern South America. Having established this, the intent is to focus on the geological and structural framework of the Omai area, and in particular, the Omai goldfield. The main lithological units of the goldfield, especially the mineralised host rocks, are discussed in detail and wherever applicable, reference is made to stratigraphic counterparts in the region.

2.2 Tectonic setting.

The Amazon Craton forms the cornerstone of the South American continent and is divided into two main tectonic units, the Guiana Shield and the Brazilian Shield, by the Phanerozoic sediments infilling the Amazon basin (see Fig. 2.1). Adverse terrain, geo-political barriers and diversity of languages - Spanish, Portuguese, English, Dutch and French - have previously precluded any serious regional interpretation of the available data. However, recent multi-disciplinary studies, co-ordinated under the auspices of IGCP Project 204 (1983-1987), have given fresh insight into the tectonic evolution of one of the world's lesser known Precambrian cratons.

In a review of the geochronological data, Teixeira et al., (1989) recognised that the Amazonian Craton is comprised of an Archaean nucleus (the Central Amazonian Province) fringed by a series of sub-parallel Palaeoproterozoic to Mesoproterozoic mobile belts which decrease in age away from the nucleus. The structurally coherent Maroni-Itacaiunas mobile belt dominates much of the geology of the Guiana Shield. It sweeps northwestwards in an arcuate fashion for over 3000 km from the eastern Brazilian Shield through French Guiana, Surinam, Guyana and Venezuela. This belt was consolidated during the Trans-Amazonian tectono-thermal orogeny (ca. 2.25 - 1.95 Ga.) and contains expansive areas of low grade, meta-volcanic and meta-sedimentary supracrustal rocks which have been interpreted by Gibbs (1980) as analogues of the more celebrated Archaean greenstone belts of the Canadian, Australian and South African Precambrian shields.

Fundamental geological and structural similarities between the Precambrian of the Guiana Shield and the Man Shield of the West African Craton were recorded by McConnell (1969). The Type 1 Birimian greenstone belts of the Ivory Coast and Burkina Faso, as described by Black (1980), were correlated with similar Palaeoproterozoic stratigraphic units in the Guiana Shield by Gibbs and Barron (1983). Moreover it was apparent that the Eburnean event (2.1 - 1.9 Ga.) which affected the western Man Shield was of comparable age to the Trans-Amazonian orogenic cycle of northeast South America. Matheis (1987) stressed the former alignment of Proterozoic gold-iron-manganese-diamond metallogenetic belts across the Atlantic in support of this model whilst Caen-Vachette (1988) emphasised the concordance of geochronological and palaeomagnetic data from mylonites occupying major tectonic lineaments.

2.3 Geological outline of Guyana.

The geology of Guyana, as outlined by McConnell (1958) and Barron (1986), is traditionally discussed in terms of northern and southern geological provinces, respectively located either side of the Takutu Break. Alternatively, the geology may be reviewed according to the six tectono-stratigraphic domains which comprise the national geological framework (see Fig. 2.2). As far as mineralisation is concerned, the Guyanese lode gold deposits, Omai included, show a compelling spatial association with the Palaeoproterozoic granite-greenstone terrain of the northern geological province (see Fig. 7.1 and Walrond, 1987a; 1987b). The precise timing of regional mineralisation has yet to be ascertained, though the stratigraphic evidence places it in within the time frame of the Trans-Amazonian orogeny and certainly prior to the onset of post-orogenic mafic magmatism which commmenced around 1.7 Ga.

2.3.1 The Palaeoproterozoic granite-greenstone terrain of northern Guyana.

The geological foundation of northern Guyana consists of a basement of closely folded belts of Palaeoproterozoic supracrustal rocks separated by extensive areas of granitoid-gneiss intrusions (Fig. 2.2, unit 2). This tectono-stratigraphic domain which covers an area of some 65,000 km^2 between the Pakaraima Mountains and the Atlantic coast is comfortably constrained within the confines of the Maroni-Itacaiunas mobile belt (see Fig. 2.1).

The meta-volcanic and meta-sedimentary rocks which constitute the NW-SE trending, Guyanese greenstone belts have been re-defined as the Barama-Mazaruni Supergroup (BMS) by Gibbs (1980). Three main belts can be identified from north to south and are respectively known as the Barama, Cuyuni and Mazaruni belts (see Fig. 2.2). According to Gibbs, a typical stratigraphic succession consists of meta-basalts at the base, passing up through metamorphosed andesites, dacites and rhyolites into meta-greywackes, phyllites and

tuffaceous sediments at the top. The successions which reach thicknesses of 8 km to 10 km are often synclinally folded and metamorphosed to amphibolite grade at the margin and greenschist facies in the interior. In neighbouring countries, the Barama-Mazaruni Supergroup is readily correlatable with stratigraphically similar supracrustal units such as the Pastora Supergroup (Venezuela), Marowijne Group (Surinam), Paramacca Supergroup (French Guiana) and the Vila Nova of northeastern Brazil.

In northern Guyana, the greenstone belts are separated by extensive, syn- to late tectonic, calc-alkaline, granitoid complexes which intruded during the Trans-Amazonian orogeny. Collectively, these complexes are known as (P1-type) Trans-Amazonian granitoids (see also section 4.5) and include the voluminous granite-gneiss terrain of the Bartica Assemblage. According to Barron (1986), the relatively small cogenetic intrusions which make up the huge batholiths range in composition from diorite to granite and are usually soda-rich. Structurally, they may either cross-cut or run parallel to the metamorphic foliation of the adjacent supracrustal rocks, occasionally occupying fold hinges. The individual intrusions have been classified by Gibbs and Barron (1992) into three main petrographic associations as follows; 1) quartz-augite syenites and quartz-augite diorites; 2) granodiorite-tonalite and 3) granite-adamellite. These authors propose that the granodiorite-tonalite association is the most volumetrically and spatially abundant one, moreover it is often linked with hydrothermal alteration and gold-quartz lodes occupying fractures and shear zones at the contact with supracrustal rocks. A series of ultramafic to gabbroic rocks, previously known as the "Older Basic Intrusive Suite", is also incorporated in the basement. These rock types, which display varying degrees of metamorphism, have been correlated with the Badidku Suite of the southern geological province.

In northern Guyana, both basement and cover rocks have been intruded by three anorogenic mafic dyking episodes, though only two of these have any regional significance. The first main phase is represented by the large-scale, erratically-shaped, differentiated gabbro-norite sills and dykes of the Avanavero Suite which were emplaced during the Mesoproterozoic between 1.7 and 1.5 Ga (see Gibbs and Barron, 1983). The second main phase generated the swarms of regularly-orientated Permo-Triassic basic dykes which have been assigned to the Apatoe Suite. A more detailed regional overview of post-orogenic mafic magmatism is given in Chapter 5.

2.4 Regional geology and structure of the Omai area. (see Table 2.1 and Fig.2.3)

2.4.1 Geology.

Surface mapping of the Omai area, centred on the 20 km E-W stretch of the Essequibo River,

was pioneered by Cannon (1963), Guardia (1969) and Collings (1969). The region is heavily forested with fresh bedrock geology obscured by a thick (30-60 m) weathered mantle and local surficial deposits. The paucity of mappable exposure has limited the scope for detailed geological and structural interpretations, with fresh outcrops usually confined to river and creek sections. Moreover, the dense forest seriously hinders mobility and rules out feature mapping from the ground. As one geologist poetically put it "you feel like a flea in a deep-pile carpet". On the plus side, the topography is gently undulating and rarely exceeds 75 m, though some laterised ridges may rise to 200 m.

In a broader regional context, the Omai area is located on the eastern extremity of the Mazaruni greenstone belt and despite the adverse terrain, the area affords an excellent opportunity for studying mineralised granite-greenstone basement. The base of the stratigraphic sequence at Omai is marked by the Palaeoproterozoic Mazaruni Group which consists of basic to acid volcanic cycles with intercalated sediments and minor basic intrusives. The volcano-sedimentary sequence has been metamorphosed from sub- to lower greenschist facies, though Cannon (1963) has recorded amphibolite facies rocks in the contact aureoles bordering granitoid batholiths. Also in the Omai area, a major series of intermediate sills (e.g. the Captain Mann Sill) is observed within the greenstone belt following a consistent ESE to SE trend. Guardia (1969) has mapped these units as an integral part of the Mazaruni Group though the petrographic and geochemical evidence presented later in this thesis seems to suggest that the sills were emplaced after greenstone volcanism and metamorphism.

On a regional scale, the geology of the greenstone sequence at Omai is comparable to the upper portions of the volcano-sedimentary succession at Issineru, located on the Mazaruni belt some 250 km northwest of Omai. This correlation is significant as Gibbs (1980) considers Issineru as the type-locality of the Barama-Mazaruni Supergroup. The age of regional proto-greenstone volcanism in northern Guyana has been constrained by Gibbs and Olszewski (1982) at 2.25 Ga using U-Pb systematics on zircons extracted from weathered meta-greywackes.

In the central Essequibo region, several structurally controlled, syn- to late-tectonic, granitoid batholiths intruded into the Mazaruni Group during the Trans-Amazonian orogeny. The Tigri and Mariaba plutons are of particular importance to this study because of their relatively close spatial relationship with the Omai Stock as illustrated in Fig. 2.3. Cannon (1963) described the Tigri (Kumaka) pluton as a granodiorite with a an adamellite core and observed a weak foliation concordant with the regional metamorphic structure whilst Johnston (1960) recognised certain petrographic affinities between the Omai Stock and the Tigri pluton. Snelling and McConnell (1966) have dated the Tigri pluton at 1945 ± 45 Ma by the K:Ar

Table 2.1

General Stratigraphic Table for the Omai Area, Guyana

(modified after Guardia, 1969)

Tertiary

Fluviatile sands (Berbice Formation)

Residual laterite

Permo-Triassic

Doleritic dykes (Apatoe Suite)

Mesoproterozoic

Gabbro-norite sills and dykes (Avanavero Suite)

Trans-Amazonian Tectono-Thermal Event (ca. 2.25-1.95 Ga)

Intermediate sills and dykes (e.g. Captain Mann Sill)

Omai Stock; Tigri pluton; Mariaba pluton (Younger Granite Group)

Lamprophyres (Appinites) (Badidku Suite ?)

Palaeoproterozoic Supracrustals - Mazaruni Group (ca. 2.25 Ga)

Conglomerates and greywackes

Tuffaceous sediments

Acid volcanic rocks

Basic to intermediate volcanic flows and minor basic intrusions (e.g. Majuba Suite)

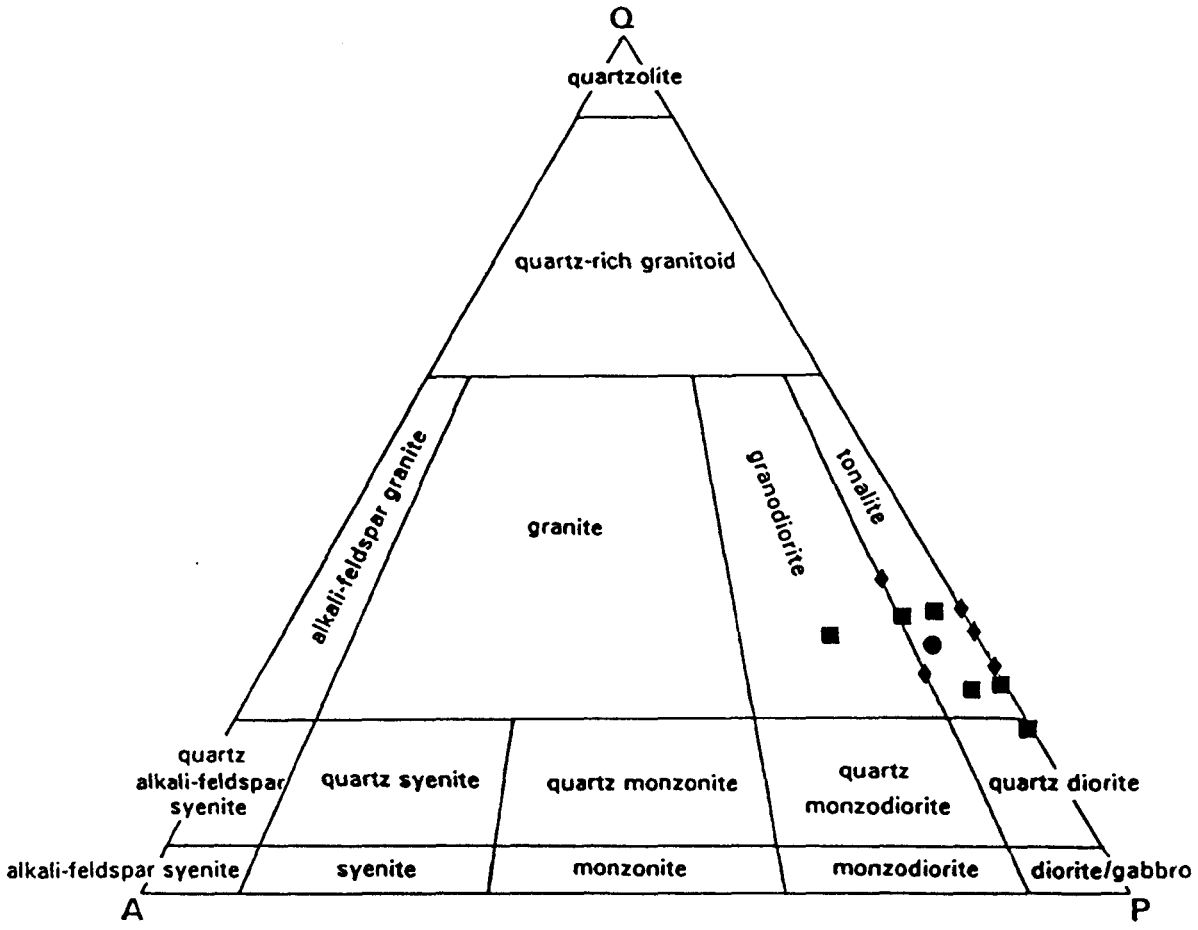

Fig. 2.4: QAP (quartz - alkali feldspar - plagioclase feldspar) plot of regional granitoid rocks in the Omai area. Petrographic data from this study (see Appendix II). Field boundaries after Streckeisen (1976).

Symbols: squares - Tigri pluton; diamonds - Mariaba pluton; circle - Mowasi pluton (located 40 km southwest of Omai).

radiometric method on hornblende. In the same work, the Mariaba pluton, or "biotite trondhjemite" of Cannon (1963) was dated at 1710 ± 50 Ma. A fresh petrographic classification (this study), as shown in the QAP plot of Fig. 2.4, indicates that these regional granitoid rocks are largely of tonalitic affinity. Also, the plutons appear to have suffered the effects of low-grade regional metamorphism as expressed by mild propylitic alteration.

At least one main pulse of post-orogenic mafic magmatism can be identified in the Omai region. This phase is represented by the two regional-scale, unmetamorphosed, gabbroic to doleritic dykes which intersect 3.2 km southeast of the Omai Stock Zone. The linear, regular morphology of these intrusions, hereafter referred to as Point and Ya-ya dykes respectively, is more characteristic of the Apatoe Suite, as opposed to Avanavero-type magmatism.

Throughout most of the Phanerozoic, in the Omai region at least, there followed a prolonged period of weathering which led to the formation of deep lateritic soils and regoliths eroded to a common base-level. The unconsolidated continental-deltaic white and brown sands of the Berbice Formation were subsequently deposited on top of this uneven surface during Plio-Pleistocene times.

2.4.2 Structure.

For reasons already mentioned, i.e. paucity of outcrop, deep weathering etc., the regional structural framework of the Omai area is still poorly understood. Data obtained from the various drilling programmes have been helpful but too localised to be of any great assistance. However, there is a general consensus of opinion that ESE- to SE-trending regional structures have greatly influenced the geological make-up of the area.

On the basis of sparse structural data and apparent repetition of stratigraphic units, Guardia (1969) proposed that the Omai goldfield is located on the southern limb of an asymmetrical, antiformal anticline with an axis running ESE. Although primary structures in the volcano-sedimentary rocks are rare, Cannon (1963) stressed the widespread occurrence of steeply-dipping, ESE- and SE-trending, cataclastic foliation. Further afield, this foliation is well expressed in phyllonitic belts located at Potaro Mouth and Yesi Island on the Essequibo River. Similar observations were made by Collings (1969) in the mafic meta-volcanic country rocks surrounding the Omai Stock whilst Guardia (1969) recorded two, narrow, steeply dipping, ESE-trending shear zones in the region. Additional evidence of shearing was observed by company geologists in Placer-GSR drill-core sections across the contact between felsic meta-volcanic rocks and phyllitic tuffs in the Wenot Lake Zone (Bertoni et al., 1990).

About 1.1 km due west of the Omai Stock, Collings (1969) located a 100m-wide, N-S trending shear zone running along the Omai River. His definitive criteria for such reasoning included apparent displacement in the "meta-andesite" unit coupled with localised brecciation and shearing, though such observations are difficult to confirm in the field due to the extensive alluvial cover. Moreover the N-S trend would appear to cut across the grain of the regional structure. However, it is of interest to note that localised, discordant, N-S faults have been mapped in the Wenot Lake Zone by Placer and Cambior-GSR geologists.

The prevalent fault trends in the area appear to strike in a conjugate NE-SW/NW-SE direction. Johnston (1960) noted two sets of fractures in the Omai Stock, a major NE-SW set and a subordinate NW-SE one. Strong field evidence suggests that this conjugate fracture pattern also controlled regional post-orogenic mafic dyke emplacement. For example the X-shaped configuration of Point and Ya-ya dykes conforms well to this fracture trend. In addition, Gibson (1987) proposes that the ENE trend of creeks draining the Omai Stock is also fault-controlled.

To summarise, an ESE to SE structural trend, expressed mainly by cataclastic foliation and minor shear zones, is dominant in the Omai area. Superimposed on this trend is a conjugate NE-SW/NW-SE fracture system which has controlled joint directions in the Omai Stock and regional-scale, post-orogenic mafic dyke emplacement.

2.5 The geology of the Omai goldfield.

Primary gold mineralisation at Omai is concentrated in two discrete ore zones, namely the Omai Stock Zone and the Wenot Lake Zone (see Fig. 2.3). A third component of the goldfield consists of saprolitic and alluvial placer deposits mantling the primary ore bodies and is known as the oxidised zone. Detailed study of the geology of the area was facilitated by the 1986 GSR diamond-drilling programme which focused on the Omai Stock Zone. In all, eight vertical boreholes (GSR 86:1 to 86:8) were drilled up to a maximum depth of 305 m, giving a total footage of 2125 m. The location of these boreholes with respect to the Omai Stock are shown in Fig. 2.5. The Wenot Lake Zone was developed subsequent to the writer's departure from Guyana and therefore only a few samples are available for analysis. In addition to the drill-core collection, several surface samples of regional lithologies were collected, mainly from river and creek exposures (see Appendix I).

2.5.1 The Omai Stock Zone.

The Omai Stock Zone is located 2.5 km inland from Omai Point on the Essequibo River (see Fig. 2.3). The geology of the Zone is dominated by a small, altered granitoid stock, known

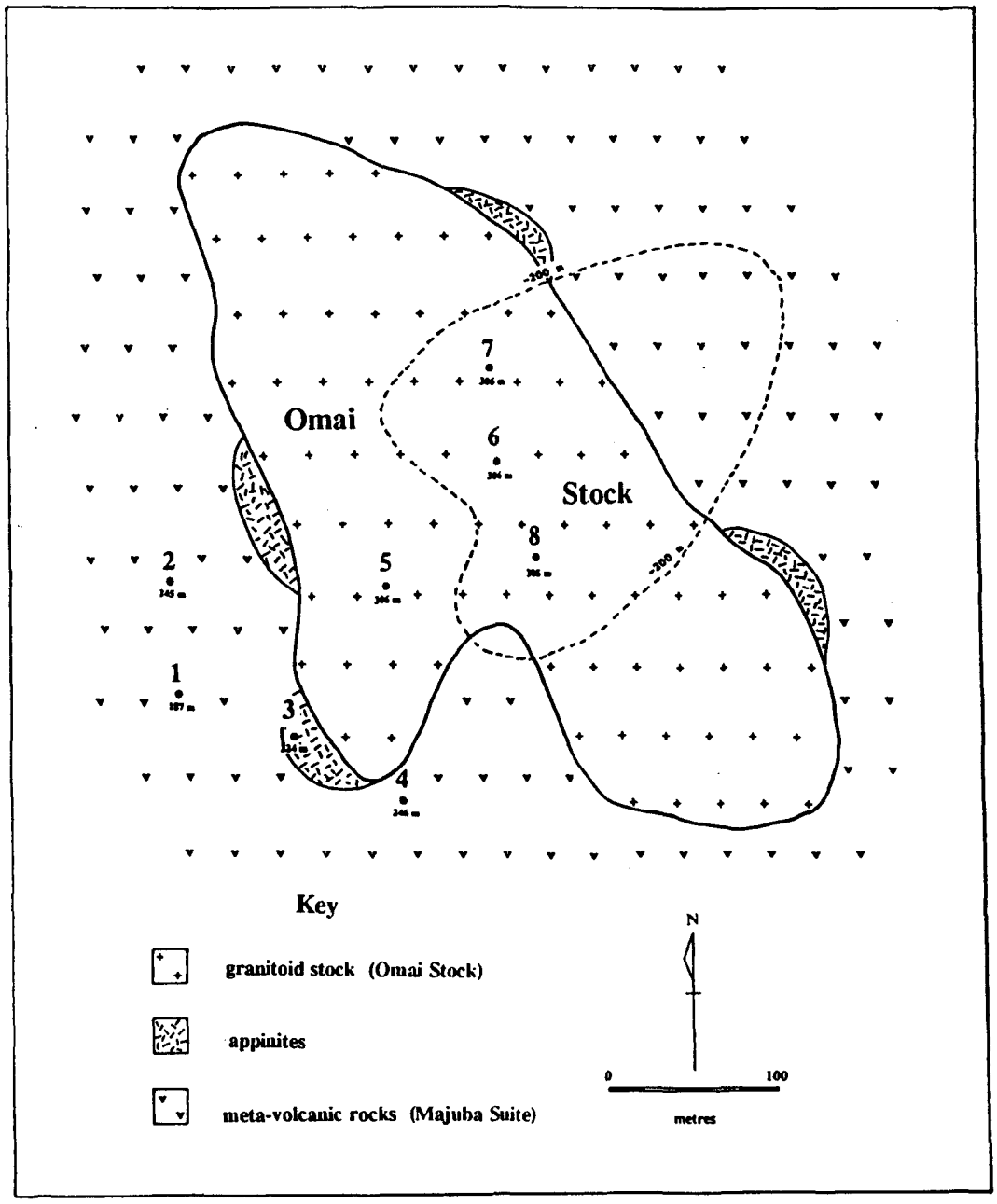

Fig. 2.5: Schematic plan of the Omai Stock Zone showing the location and depth of GSR boreholes 86:1 to 86:8 with respect to the outline of the Omai Stock at mean sea-level and at -200 m. (Modified after Placer-GSR analysis of Anaconda drilling data; approximate location of appinite pipes from Bertoni et al., 1990).

Note: A modified version of this diagram indicates the the appinites form an intermittent ring around the Stock (see Bertoni et al., 1991).

as the Omai Stock, which hosts the bulk of mineralisation. Various minor intrusive phases are associated with the Stock and collectively the igneous body is referred to as the Omai Intrusive Complex. The ore zone also extends a short distance into a suite of meta-volcanic country rocks belonging to the Mazaruni Group. This suite is here defined as the "Majuba Suite", after the former name of the Red Hill area. Plate 2.1 illustrates a schematic cross-section through the Omai Stock Zone, highlighting the main lithologies and the chief areas of mineralisation.

The Majuba Suite.

The lateral extent of the Majuba Suite is poorly constrained and estimates vary from author to author. However, there is general agreement that the rocks are steeply-dipping and strike in an ESE direction. Previous petrographic classifications are also variable and testify of the heterogeneous nature of the rocks. Johnston (1960) and Collings (1969) loosely described the rocks as "meta-andesites" whilst Guardia (1969) described them under the umbrella term of "intermediate flows and tuffs". These descriptions are supported, to a certain extent, by the petrographic and geochemical data presented in this thesis. In essence, the Suite consists of basalt dominated, basic to intermediate volcanic cycles with associated minor basic intrusives and intermediate tuffaceous components.

Owing to the effects of episodic hypogene alteration, great difficulty arises in distinguishing intraformational boundaries with any degree of certainty. Even petrographic determinations are tentative, considering the widespread textural degradation of the pristine mineral phases. The breakdown of primary mineral phases is here attributed to the substantial influx of metamorphic and/or hydrothermal fluids rather than to the intensity of deformation. This observation is borne out by elevated loss-on-ignition (LOI) values of up to 11.35%. Therefore, ultimate compositional classification of these rocks may rely on the application of immobile trace elements such as Ti, Zr, Nb and Y as demonstrated in Chapter 3.

Basalts

The basaltic components of the Majuba Suite are best examined in borehole GSR 86:3 where they form continuous intersections spanning several tens of metres. In hand specimen, the rocks are massive, melano- to mesocratic, medium to dark greenish-grey and aphanitic to medium-grained. Chlorite and epidote are common throughout and are the main indicator minerals of low-grade regional metamorphism. Quartz-albite-epidote stringers are numerous and may be related to ductile deformation. In the more brittle specimens, chlorite occurs in slickenslides associated with epidote and colourless, amorphous carbonates smeared along the fracture planes. Pyrite occurs pervasively in diverse forms, such as euhedral cubes,

coarse blebs and narrow veinlets, indicating several phases of paragenesis. Networks of cross-cutting carbonate and silica veinlets are also ubiquitous. Evidence of tectonic brecciation, silica flooding and annealed fracturing is widespread.

Hydrothermal activity is recorded by a series of narrow, irregular quartz-carbonate veins. In the vicinity of these veins the meta-volcanic wall-rocks are commonly bleached for several centimetres and the resultant halo often carries concentrations of pyrite. The relationship between regional metamorphism and hydrothermal alteration is clearly demonstrated by hand specimen 2-0915. In this sample (see Plate: 2.2) narrow hydrothermal quartz veins with associated alteration haloes are seen to overprint dark-green, sub-parallel, chlorite bands of metamorphic origin.

In thin section, the rock-forming mineralogy of the basaltic rocks is dominated by a chlorite-actinolite-epidote-albite-quartz-sericite assemblage which is typical of greenschist facies metamorphism. In addition, most samples appear to have been affected by at least two phases of carbonatisation. The first phase pervasively altered phenocryst and groundmass constituents alike and was probably contemporaneous with regional metamorphism. A later, fresher phase, characterised by rhombic cleavage, is restricted to cross-cutting veinlets and would appear to be synchronous with hydrothermal alteration. Thorough carbonatisation and sericitisation greatly hinder petrographic observations as they preclude reliable anorthite determinations on primary plagioclase crystals. Generally, the more basic members of the Majuba Suite are rich in opaque oxides which may account for up to 10% of the mode. The oxides occur in veinlets, as drop-like disseminations uniformily distributed throughout the sections or as large skeletal grains pseudomorphing mafic minerals.

Some specimens show moderately well-preserved igneous textures. For example, thin sections 3-1681 and 3-0905 exhibit well-defined, relict sub-ophitic to ophitic textures which are characterised by sericitised plagioclase laths up to 2 mm in length. Relict amygdaloidal and porphyritic textures are observed in thin section 4-2022 (see Plate: 2.3). In this slide, several oval to rounded amygdales, up to 4 mm across, can be positively identified. In cross-polarised light, these features are characterised by a core of polycrystalline quartz mantled by broad rims of sericite-carbonate aggregate. Despite the widespread retrogression, numerous six- and eight-sided equant mafic phenocrysts are also recorded whereas in similar samples the pre-tectonic phenocryst phases have been altered to such an extent that they are virtually indistinguishable from the groundmass.

Specimens 4-2409 and 5-1750 display relatively coarse ophitic to nematoblastic textures and are typified by chloritised acicular needles set in a fine-grained sub-ophitic groundmass. The coarse grain-size suggests that their igneous precursors were hypabyssal basic rocks rather

than volcanic extrusive ones. These samples also contain small corroded quartz-filled vesicles which host radiating needles of a pale green mineral, tentatively identified here as pumpellyite or zeolites. The occurrence of pumpellyite, if confirmed, is evidence for sub-greenschist facies metamorphism whilst the presence of abundant zeolites may partially account for the hydrous nature of the greenstone rocks.

Minor basic intrusives

These rocks, which occur as narrow sills and dykes, were emplaced prior to peak regional metamorphism and appear to be contemporaneous with the basaltic rocks described above. In the past, the intrusives have been variously described as "masked hornblende porphyry" (Anaconda, 1946-1950); "epidiorite" (Johnston, 1960) and "amphibolite" (Payne, 1989a).

Two texturally distinct minor basic intrusives were identified in the GSR drill-core. The first type, which was encountered in borehole GSR 86:4 between 118 m and 177 m and in GSR 86:3 between 106 m and 116 m, is typically dark green, homogeneous and medium- to coarse-grained (see Plate: 2.4) In thin sections 4-1272 and 4-1650 this rock is characterised by simply twinned, sheaf-like amphibole needles, up to 1 cm in length, which form radial and branching patterns and account for about 50% of the mode. The groundmass consists of heavily altered plagioclase which may show relict granophyric textures. Locally, this unit bears a strong megascopic resemblance to the appinites of the Omai Intrusive Complex.

The second type of basic intrusive displays a compact, hypidiomorphic, isogranular texture. Three individual bodies of this type, varying in apparent thickness from 3 m to 8 m, were encountered in the drill-core. The representative thin sections, 1-0523, 2-1110 and 2-1598, all show well-preserved igneous features. Relict, subhedral, 3 mm to 4 mm crystals of amphibole-chlorite, after clinopyroxene, ophitically and sub-ophitically enclose murky, euhedral plagioclase laths of about 0.5 mm in length (see Plate: 2.5).

Andesites

True andesites are relatively rare in the Majuba Suite, at least, in the sample collection. In hand specimen they resemble the basalts described above and using such criteria as colour index to discriminate between the two volcanic types may lead to erroneous conclusions.

The andesitic rocks are best represented by thin section 1-1555. This specimen displays a relict porphyritic-seriate texture characterised by lozenge-shaped amphiboles and equant mafic phenocrysts, some in excess of 1 cm, which account for about 40% of the mode. Another andesitic specimen (3-1372) may be comparable to Anaconda's "Caviar bed" and

Plate 2.2: Mafic meta-volcanic rock (Majuba Suite) showing hydrothermal quartz veins, with alteration haloes, cutting across metamorphic fabric. Drill-core specimen, 2-0915.

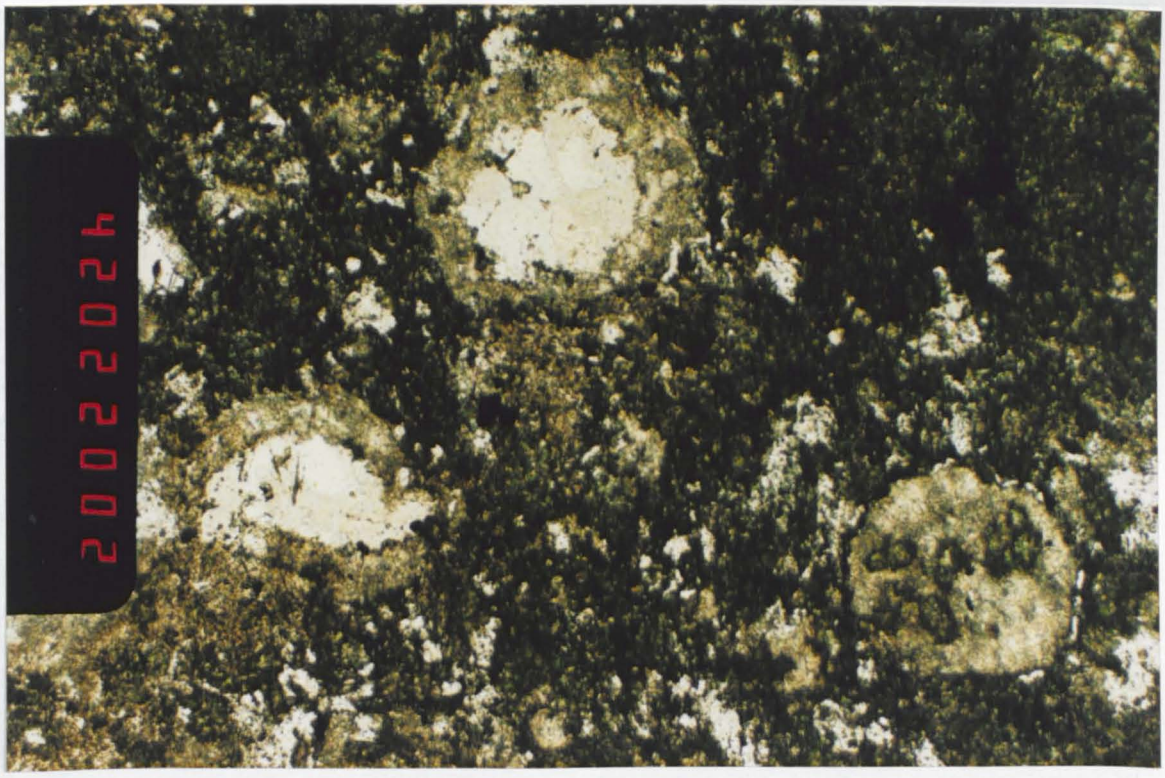

Plate 2.3: PPL micrograph of a mafic meta-volcanic rock (Majuba Suite) showing relict amygdaloidal and porphyritic textures. Thin section, 4-0220; Mag. x 40.

Plate 2.4: Minor basic intrusive (Majuba Suite) with blebs of pyrite. Drill-core specimen, 4-1270.

Plate 2.5: PPL micrograph of a minor basic intrusive (Majuba Suite) showing a relict ophitic texture. Thin section, 1-0523; Mag. x 40.

to Johnston's "porphyritic andesite" which is reported to be exposed in Gilt Creek. The main characteristic of this lithology is its spotted or ophimottled texture which consists of rounded, light-coloured patches, up to 8 mm across, set in a fine-grained, greenish-grey, chloritic groundmass. The spots, which may represent former amygdales or feldspar phenocrysts, are best viewed in hand specimen.

Tuffaceous intermediate rocks

The tuffaceous horizons of the Majuba Suite are very conspicuous due to their banded textures and striking sea-green colour when wet. These tuffs were intersected in borehole GSR 86:4 between 12 m and 105 m where they are interstratified with other components of the suite. Thin section 4-0657 is a good representative of the tuffs and consists of ghostly, sub-rounded, light-coloured rock fragments up to 1 cm across, which are best viewed under a microfiche reader. Excellent examples of centimetre-scale banding are illustrated by specimens 1-0579 and 4-1050. The former specimen consists of bands of dirty brown, micro-laminated, silty ash material interbedded with relatively more felsic and crystalline layers which exhibit a "tapioca" texture. Thin section 4-0775 very much resembles a lapilli tuff and is characterised by bands of aligned, flattened, elliptical, totally carbonated grains up to 1.2 cm across the long axis, which are set in fine grained chlorite-sericite-albite-quartz groundmass.

The Omai Intrusive Complex.

The Omai Intrusive Complex consists of four distinct intrusive phases. In chronological order, these are, 1) lamprophyric (appinite) pipes; 2) the Omai Stock; 3) ultramafic to dioritic sills and dykes and 4) a gabbroic sheet. The former three phases appear to have been successively intruded during the Trans-Amazonian orogeny but emplaced prior to mineralisation. In stark contrast, the gabbro clearly shows a post-orogenic affinity and is non-mineralised.

Lamprophyres (appinites)

Field Relations

Volumetrically, the appinites are a minor but significant component of the Intrusive Complex. Surface exposure is restricted to a few large boulders cropping out at the head of Dunclain Creek on the north east margin of the Stock. The Anaconda boreholes intersected another body on the southwest lobe of the stock and heaps of excavated appinite debris can be seen in the tailing dumps adjacent to Red Hill shaft. A vertical section through the shaft, based

on the Anaconda data, is shown on page 15 of Johnston's (1960) thesis. Here the appinite takes the form of a 30 m-diameter, subvertical pipe which thickens out and bifurcates at a depth of 80 m. This same body was also intersected during 1986 GSR drilling programme and intersections of appinite can be observed in boreholes GSR 86:3, 86:4 and 86:5. Further drilling by Placer-GSR (1987-1990) revealed that a cluster of four appinite bodies occur along the periphery of the Stock (see Fig. 2.5).

Cross-cutting relationships in the GSR drill-core strongly suggests that the appinites intrude the meta-volcanic country rocks of the Majuba Suite. The low to moderate degrees of alteration observed macroscopically, and in thin section, demonstrate that the timing of the intrusion post-dated the peak regional metamorphism. However, the relationship between the appinite and the Omai Stock is not so clear in spite of the number of observed intrusive contacts reported. Johnston (1960) advocates that the appinite "has the appearance of an earlier intrusion, followed probably at no great interval by the trondhjemite (Omai Stock)". In contrast, Bertoni et al., (1990) record the presence of chill textures in the appinite at the contacts with the Stock and therefore propose that the appinites are the later intrusive phase. The most plausible explantion for the ambiguous field relations is the the two rock types are broadly coeval with appinite intrusion overlapping that of the Omai Stock.

Petrography

This texturally distinct rock type been variously described by numerous petrographers over the last 40 years as "hornblende porphyry", (Anaconda, 1946-1950); "appinite", (Johnston, 1960); "hornblende diorite porphyry", (Collings, 1969) and "pegmatitic mafic diorite", (Payne, 1989a). The term "lamprophyre", which translates as "glistening porphyry" is indeed an apt description of the Omai rocks (see Plate: 2.6). However, the lamprophyre lithological class is highly heterogeneous and a more specific term is therefore necessary. Strictly speaking, the Omai lamprophres are categorised as "spessartites" under the recent IUGS petrographic classification presented by Le Bas and Streckeisen (1991), though according to Rock's (1991) classification the term "appinite" (plutonic spessartite) is equally valid. In light of the similarities between the Omai lamprophyres and the type-locality appinites at Appin, Scotland, the term "appinite" is preferred in this study.

In hand specimen, this rather beautiful rock is characterised by dark green, fresh, elongate, bladed, branching amphibole phenocrysts, 1 cm to 6 cm in length, which are hosted in creamy-white, interstitial groundmass of plagioclase with sub-ordinate quartz and calcite (see Plate 2.6). The rock type which has a colour index of 35 to 60 is variably cut by narrow hydrothermal veins of quartz-carbonate which bleach the wall-rocks on a centimetre scale.

Locally, epidote-rich veins are common and may signify thermal metamorphic effects exerted by the Stock. Close to lithological contacts the grain size progressively diminishes so that the appinite may be mistaken for a minor basic intrusive of the Majuba Suite. Generally there is no evidence to suggest that the appinites have suffered regional metamorphism.

Microscopically, the appinite thin sections are dominated by coarse amphibole phenocrysts up to a modal amount of 55%. Generally, this phase consists of hornblende which varies in habit from columnar prismatic crystals to stumpy equant basal sections. Disintegration and retrogression to actinolite-chlorite along cleavage planes is a common feature of the hornblende phenocrysts. Simple twinning, lamellar twinning, overgrowth and poikilitic textures are also much in evidence. In some sections, biotite occurs as an accessory mafic phase in the form of small wispy plates with buckled cleavage traces.

Plagioclase, for the most part, occurs interstitially as broad, subhedral grains which are often heavily altered by sericite and epidote. Some of the more prismatic grains show sericitised cores and relict albite twinning. Well-defined micrographic and granophyric textures, especially in thin section 5-1142, are common petrographic features of this lithology (see Plate: 2.7). The average anorthite composition of the plagioclase is provisionally constrained in the sodic end of the spectrum with values less than An35. However, only a limited number of determinations were possible due to alteration.

Apatite is an important accessory phase occurring ubiquitously in the groundmass and phenocryst phases alike. Sphene is another common accessory mineral which is represented by fresh subhedral, diamond-shaped wedges with overgrowths. Quartz occurs as rare, clean, fresh interstitial grains displaying moderate degrees of undulose extinction. Calcite grains are also observed and may either be primary and/or secondary in origin. Three types of opaque minerals are identified in thin section. Coarse, subhedral skeletal grains are most likely relict leucoxene pseudomorphing ilmenite. Relict cube-shaped opaques partially replaced by quartz are probably pyrite remnants. Small rounded opaque forms often contained in amphibole are probably magnetite.

Regional correlation

In the context of northern Guyana, the Omai appinite cluster would appear to be unique. However, Barron (pers. comm., 1992) reports the presence of a "hornblendite" adjacent to the Temple Bar granite. This appinite-granitoid spatial relationship is sited at the Temple Bar Falls on the Konawaruk River, some 30 km southwest of Omai. Other so-called appinites in the northern geological province may be the product of one of two processes. Firstly, in-situ differentiation of thick Avanavero-type gabbroic sills such as the Itaki complex may produce

Plate 2.6: Appinite (Omai Intrusive Complex) showing bladed hornblende phenocrysts with epidotisation of interstitial plagioclase feldspar. Drill-core specimen, 5-1145.

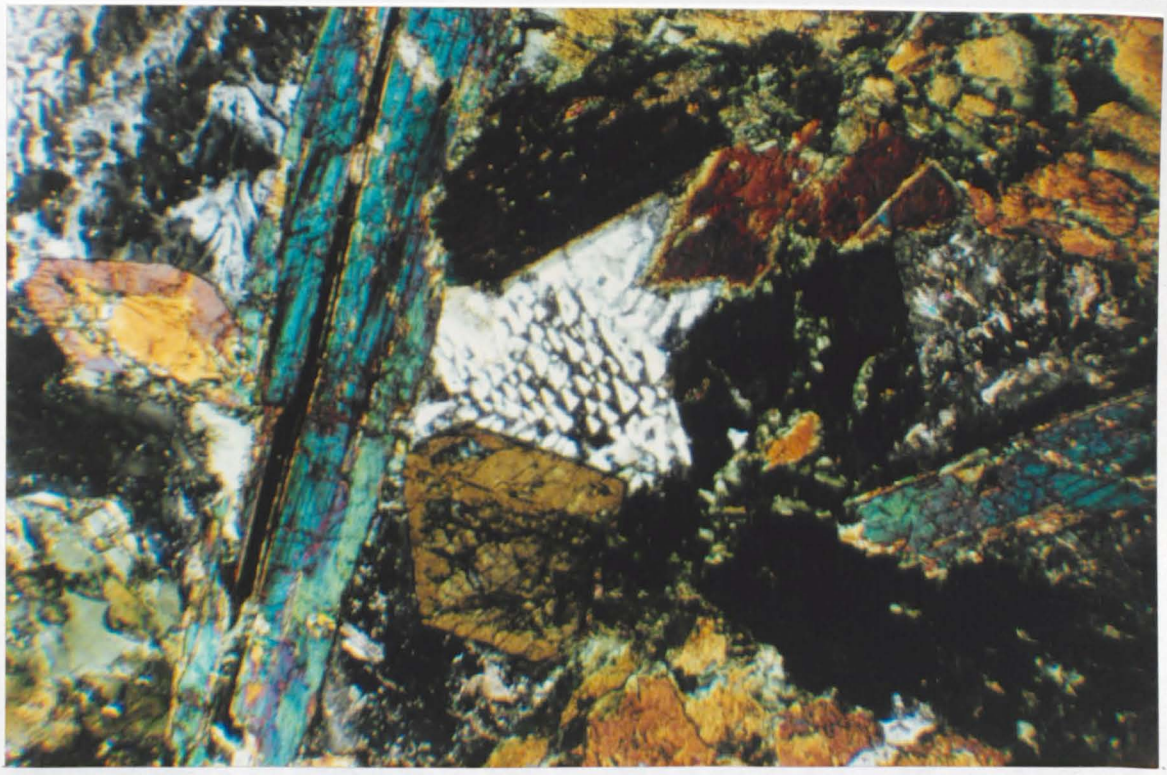

Plate 2.7: XPL micrograph of appinite (Omai Intrusive Complex) showing interstitial micrographic texture in plagioclase feldspar and lamellar twinning and compositional zoning in hornblende phenocrysts. Thin section, 5-1142; Mag. x 55.

cumulate layers rich in amphibole phenocrysts. At Omai, the small-scale nature of the intrusions definitely disqualifies differentiation as a viable mechanism. Secondly, variably metamorphosed, minor basic intrusives of the Mazaruni Group may display hornblendic textures similar to magmatic appinites. Examples of these metamorphic derivatives are well illustrated by the Omai minor basic intrusives as discussed above.

Owing to the rare nature of Omai appinites and uncertainty regarding the exact timing of emplacement, regional stratigraphic correlation is somewhat tentative. However, the field relations, backed by geochemical evidence, constrain their emplacement within the time frame of the Trans-Amazonian orogeny. One possibility is that the appinites were generated by the same pulse of magmatism that gave rise to the ultrabasic to gabbroic rocks of the Badidku Suite (see section 2.3.1). On the other hand, if the appinites are indeed cogenetic with the Omai Stock then classification into the Younger Granite Group would be more appropriate.

In a global context, lamprophyric bodies show compelling spatial and temporal distributions with Archaean and post-Archaean lode gold deposits. This matter has been comprehensively addressed by Rock and Groves (1988) among others. The significance of the Omai appinites with respect to mineralisation will be discussed in more detail in Chapter 7.

The Omai Stock.

Field relations

The Omai Stock forms the bulk and core of the Omai Intrusive Complex and is the main host of mineralistion. In plan, it is roughly elongate in a NW-SE direction and has an irregular lobate expression with approximate surface dimensions of 450 m by 250 m. Surface mapping by Placer Dome Inc. indicted that the present plan of the Stock may have been influenced by two major ENE-trending, left-lateral faults which dissected the body into three main blocks (Gibson, 1987). Drilling projections of the Anaconda data, compiled by Placer Dome Inc. have demonstrated a mushroom-shaped, three-dimensional geometry for the Stock with a moderate degree of plunge to the northeast (see Fig 2.5).

Cross-cutting relations in the field and drill-core sections clearly show that the Stock post-dates the meta-volcanic rocks of the Majuba Suite, whereas relations with the appinites, as mentioned above, are ambiguous. In turn, the Stock is cut by a stockwork of narrow (1-5 cm) mineralised quartz-carbonate veins which make up 1% to 2% volume of the intrusive body.

Petrography

The Omai Stock has remained a petrographic enigma for over 80 years. This is largely due to the combined effects of soda-metasomatism and hydrothermal alteration which have seriously obscured the primary mineral components. The alteration is also refelected by LOI values of up to 6.9%. Therefore, in an attempt to resolve the petrography, 17 representative thin-section samples were systematically examined under the microscope using the point-counting method. The results, which were plotted on a standard QAP plot (Fig. 2.6), show that the composition of the Stock varies from diorite to granodiorite, though the vast majority of data define a tight cluster straddling the quartz diorite and tonalite fields. However, it must be stressed that this classification is somewhat tentative, especially in the highly altered samples where accurate modal amounts of plagioclase are very difficult to establish.

"Aplite" versus "Granite"

Traditionally, two apparent granitoid rock-types have been recognised in the Omai Stock (see Table 2.2). The first of these is a strongly altered, leucocratic variety which was originally given the field name of "aplite" by Harrison (1908). The second type, which is relatively less altered, corresponds to Harrison's "granite". Examination of the GSR drill-core sections, especially boreholes 86:6 and 86:8, suggests that the former dominates the upper 100 m of the Stock.

In hand specimen, the "aplite" is a pale greenish-grey leuco-type with a colour index of about 10. (see Plate 2.8). It is homogeneously massive, holocrystalline and is characterised by a fine- to medium-grained saccharoidal texture, more typical of a microgranite. Microscopic analysis carried out during this study shows that the modal mineralogy of this rock-type is dominated by altered subhedral to euhedral plagioclase crystals which account for 50% to 65% of the mode. Evidence of Na-metasomatism is reflected by albitised crystals showing broad, wavy, poorly-defined multiple twinning. The majority of plagioclase grains, however, display relatively fresh polysynthetic twinning and yield anorthite compositions in the range An5 to An35. Compositional zoning of the plagioclase crystals is conspicuously absent which may reflect a degree of recrystallisation during metasomatism. Following albitisation, these grains were pervasively altered, in some cases up to the point of complete textural destruction, by radiating plates of sericite-muscovite aggregates associated with the main hydrothermal veining episode (see Plate 2.9). The sericitic (phyllic) alteration, which may account for up to 20% of the mode, is also responsible for the complete obliteration of the mafic mineral phases. The alteration paragenesis is further complicated by significant amounts of carbonate which have been introduced to the wall-rocks during hydrothermal alteration. The remaining modal mineralogy of the "aplite" is dominated by interstitial

anhedral quartz grains (10-15%) with accessory amounts of perthitic alkali feldspar. Other accessory phases include opaque oxides, apatite and zircon. Locally, concentrations of euhedral pyrite cubes occur in the wall-rocks adjacent to quartz-carbonate veins.

Table 2.2

Field and Petrographic Nomenclature of the Omai Stock

Strongly Altered Facies	Less Altered Facies	Author
Aplite	Granite	Harrison (1908)
-	Trondhjemite	Johnston (1960)
-	Granodiorite	Collings (1969)
Quartz albitite	Quartz leucodiorite	Morton (1987)
-	Quartz diorite	Payne (1989a)
Propylitised tonalite	Sericitised-albitised tonalite	Morton (1990)
Quartz diorite / tonalite	Quartz diorite / tonalite	This study (1992)

The "granite", on the other hand, is a mesocratic grey to pinkish grey with a colour index of around 30 (see Plate 2.10). In most specimens, dark green relict mafic grains, ranging from 2 mm to 8 mm in length, are megascopically discernible. Thin section studies show that propylitisation is the prevalent alteration type and is expressed by chloritised-epidotised relicts of amphibole and possibly biotite (see Plate 2.11), though phases of albitisation and relatively mild sericitisation are also observed. The presence of fresh accessory sphene also characterises this propylitised rock-type.

Generally, the modal felsic mineralogy and QAP classification of "aplite" and "granite" are broadly comparable. This observation is supported by the petrographic work of Morton (1990) who proposes that the two rock-types are simply contrasting alteration facies of the original "tonalitic" stock. Morton (1990) further implies that the alteration is zonal and draws analogy with other mineralised felsic porphyry systems where the intensity of the alteration diminishes with distance from the core of the body. However, the drill-core data do not uphold this hypothesis. The key to the problem may be found in thin section analysis of the lesser altered "granite" facies where the alteration paragenesis can be resolved as: albitisation

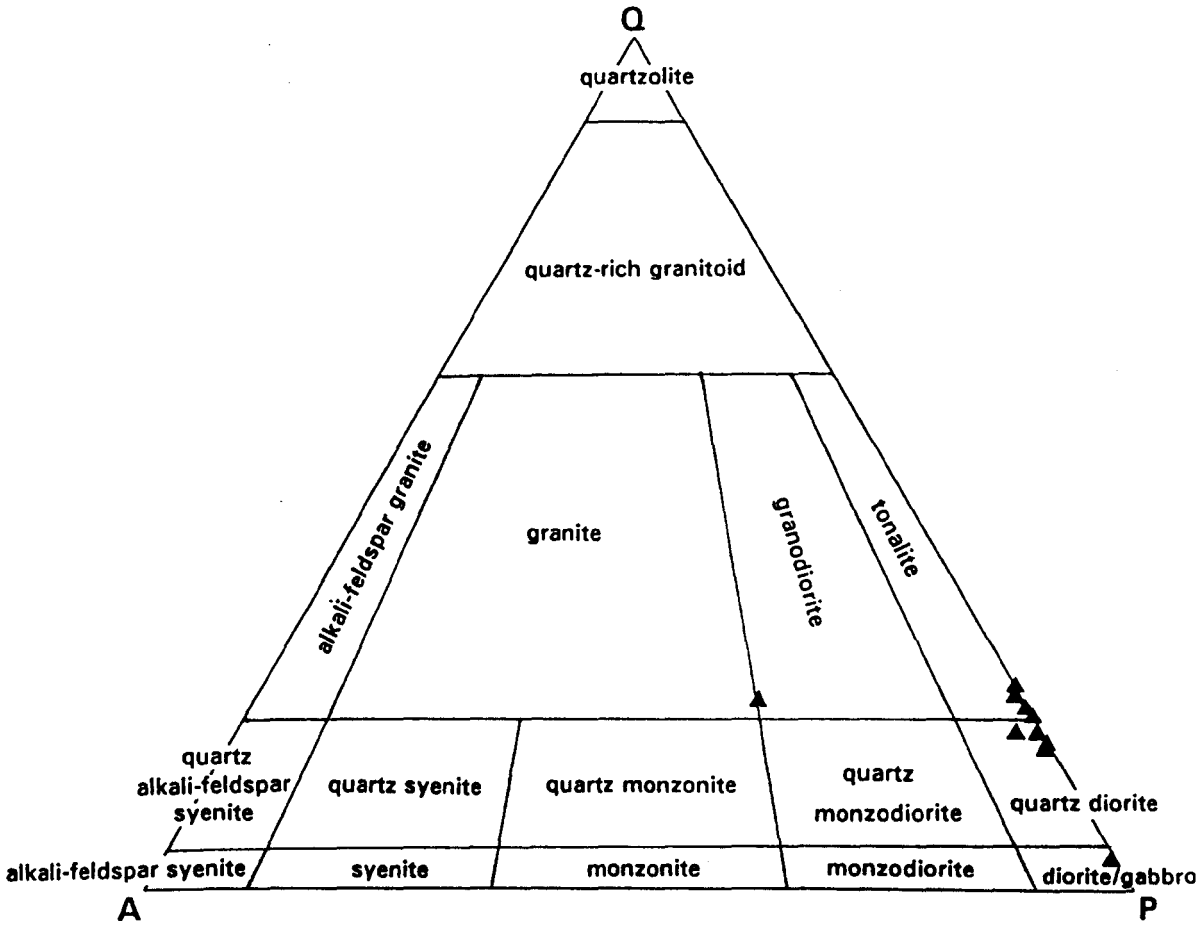

Fig. 2.6: QAP (quartz - alkali feldspar -plagioclase feldspar) plot of samples from the Omai Stock. Petrographic data from this study (see Appendix II). Field boundaries after Streckeisen (1976).

Note: To avoid congestion, not all data are shown.

Plate 2.8: Strongly altered quartz diorite / tonalite ("aplite"), Omai Stock. Note also the two narrow hydrothermal quartz veins. Drill-core specimen, 6-0420.

Plate 2.9: XPL micrograph of strongly altered quartz diorite / tonalite ("aplite"), Omai Stock. Note the incipient to intense sericitisation of the plagioclase feldspar crystals. Thin section, 6-0786; Mag. x 40.

Plate 2.10: Lesser altered quartz diorite / tonalite ("granite"), Omai Stock. Note relict acicular mafic minerals in light-coloured areas. Drill-core specimen, 6-0626.

Plate 2.11: PPL micrograph of lesser-altered facies ("granite"), Omai Stock, showing propylitised amphibole and/or biotite crystals and accessory sphene in the felsic groundmass. Note: this sample plots as a granodiorite in Fig. 2.6. Thin section, 7-1300; Mag. x 40.

- propylitisation - sericitisation. By drawing on the petrographic observations made in the Tigri and Mariaba granitoid rocks it is here proposed that the propylitisation identified in the Omai Stock is a low-grade regional metamorphic effect and not a local hydrothermal one. This reasoning would indicate that the strongly altered, "aplite" portions of the Stock are simply areas of intense hydrothermal alteration where sericitisation has overprinted and obliterated any trace of propylitic alteration. The matter of contrasting alteration facies in the Omai Stock is re-addressed in Chapter 4 using the chemical data. A summary of the alteration paragenesis is also given in Chapter 6.

Regional correlation

The array of data in Figs. 2.4 and 2.6 show that the Omai Stock has close petrographic affinities to the Tigri pluton as opposed to the Mariaba pluton, though at this stage, it is not possible to establish if any genetic relationship exists. However, the field relations suggest that all granitoid bodies in the Omai area are members of the Trans-Amazonian Younger Granite Group. On a regional scale, several small granitoid stocks, all with variable degrees of gold mineralisation, are hosted within the greenstones of the Barama-Mazaruni Supergroup. These include, Eagle Mountain, Mahdia distict; Million Mount, Puruni SE; Aurora (Mad Kiss), Cuyuni River and Ianna-Yakishuri, Barama River. The significance of minor felsic intrusions as hosts of lode-gold deposits is well documented in other Precambrian granite-greenstone terrains (see Cherry, 1983).

Ultramafic to dioritic sills and dykes (Gilt Creek Suite).

Ostensibly, these lithological units form a heterogeneous series, however, their trace element contents suggest that they define a compositional spectrum related by crystal fractionation (see Chapter 5). These rocks, which are here defined as the Gilt Creek Suite, typically occur as 1 m-thick, intrusive sheets which were preferentially emplaced in the Stock along shallow-dipping fracture or shear zones. Along their margins, the sills and dykes show widespread evidence of quartz-carbonate veining which indicates that they were emplaced prior to the main hydrothermal episode. Two of the largest intrusive sheets are worth a mention in detail.

A subhorizontal, 10 m-thick, ultramafic body was encountered in four boreholes (GSR 86:4, 86:6, 86:7 and 86:8) within a depth range of 180 m to 200 m. The body appears to be laterally continous over 200 m and extends into the meta-volcanic country rocks of the Majuba Suite. In hand specimen, the rock-type is melanocratic, granular, medium to coarse-grained and extremely dense. Another diagnostic feature is the pervasive carbonatisation which gives rise to LOI values of up to 22.7%. Several samples are further characterised by a sheared fabric as shown in Plate 2.12. In the meta-volcanic drill-core intersections, such

as borehole GSR 84:4, this shearing may be easily mistaken for a metamorphic fabric. Likewise, in the Stock, drill-core intersections of narrow (<1.5 m), chilled basic dykes have been erroneously described as "mafic meta-volcanic xenoliths".

In borehole GSR 86:7, a major dioritic body was observed cutting the central portion of the Stock between 76 m and 111 m, heavily fracturing the wall-rocks in the process. In the Placer-GSR borehole DDH 24, an intersection of the same unit was examined between 29 m and 45 m. From the limited field data available it is here suggested that this unit forms a 15 m- to 25 m-thick intrusive sheet dipping 20° to 25° E or ESE. Several company geologists appear to have interpreted this unit as raft of greenstone country rock, caught up in the Stock. The sharp intrusive contacts, however, clearly disqualify such an hypothesis.

Macroscopically, the diorite is massive, mesocratic (colour index 40 to 45), medium grained and mildly porphyritic. Petrographic evidence from thin sections 7-0819 and 7-0979 clearly demonstrates that the lithology is strongly propylitised and consists of rare euhedral amphibole and plagioclase phenocrysts set in a medium-grained granular matrix (see Plate 2.13). Quartz is a noticeable constituent of the groundmass, though some of it may be secondary in origin.

On the whole, several members of the Gilt Creek Suite share a number of common petrographic features. These include, sheared and buckled plagioclase grains, high modal carbonate contents (10-35%) and high modal values (10-15%) of opaque oxides. However, the porphyritic diorite, as described above, may be the exception to the rule. In general, all the intermediate components of the suite are characterised by ubiquitous and abundant accessory apatite, monazite and zircon.

Within the Omai region, this suite of rocks does not appear to have an obvious stratigraphic equivalent. Macroscopically, the porphyritic diorite resembles the "amygdaloidal andesites" of Guardia (1969) as typified by the Captain Mann Sill (see section 2.4.1 and Fig. 2.3). The field relations bracket the timing of intrusion for the suite between the emplacement of the Omai Stock and the main mineralising event, i.e. probably towards the end of the Trans-Amazonian orogeny.

Gabbro (GSR dyke)

The pervasive effects of hydrothermal alteration which are the hallmarks of the other components of the Intrusive Complex are noticeably absent in this gabbroic unit. In short, the gabbro is unmetamorphosed, non-deformed and non-mineralised. For the sake of easy

Plate 2.12: Sheared ultramafic rock (Gilt Creek Suite), Omai Stock Zone. Wispy white streaks denote areas of carbonatisation. Drill-core specimen, 4-1618.

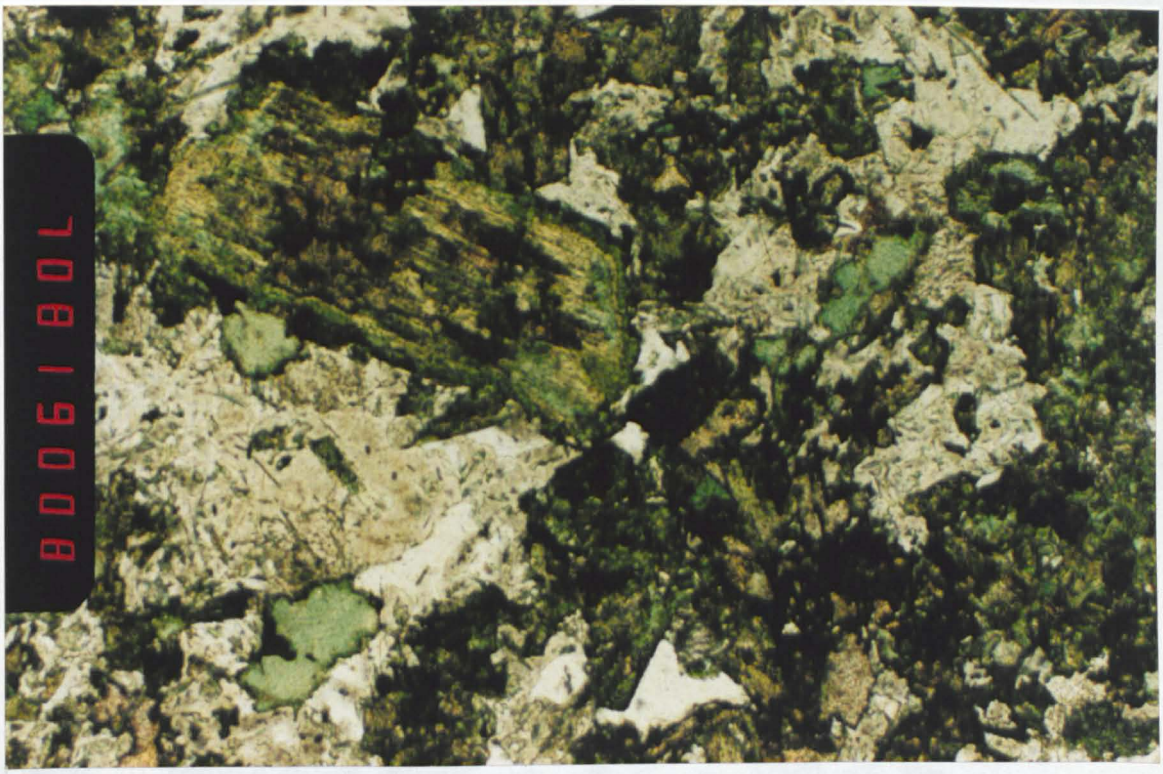

Plate 2.13: PPL micrograph of porphyritic diorite (Gilt Creek Suite), Omai Intrusive Complex, showing propylitised amphibole phenocryst. Note also the needles of apatite in the felsic groundmass. Thin section, 7-0819; Mag. x 40.

Plate 2.14: Speckled gabbro (GSR dyke), Omai Intrusive Complex. Drill-core specimen, 6-3028.

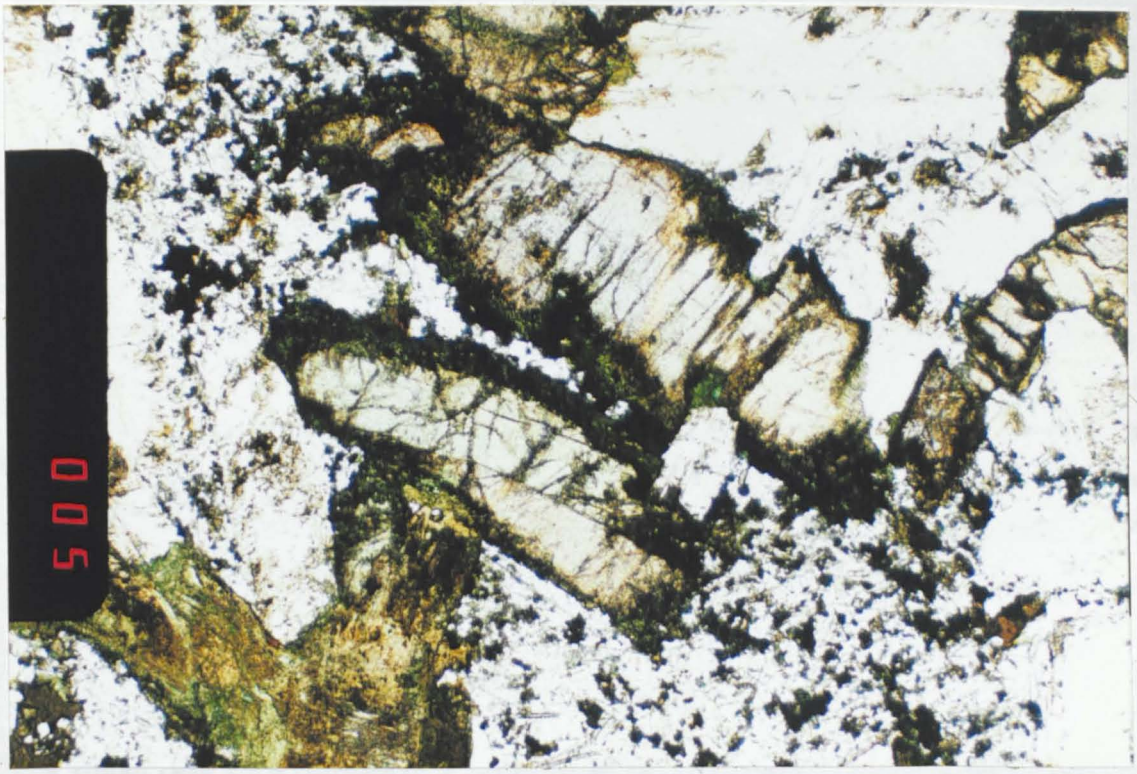

Plate 2.15: PPL micrograph of speckled gabbro (GSR dyke), Omai Intrusive Complex, showing uralitisation and simple twinning in clinopyroxene (augite) crystals. Thin section 7-3021; Mag x 40.

reference this gabbroic body is hereafter referred to as the GSR dyke.

The GSR dyke was encountered at the bottom of boreholes GSR 86:6, 86:7 and 86:8 where it intruded along the contact between the Omai Stock and the country rocks. In Plate 2.1 the gabbro is portrayed as a thick subhorizontal intrusive body, underpinning the Stock around the 300 m level. In borehole GSR 86:6, over a 20 m vertical intersection, the gabbro megascopically grades from a melanocratic, chilled microgabbro at the contact with the Stock to a coarsely crystalline, melano- to mesocratic, speckled facies at depth. A hand specimen of the latter is shown in Plate 2.14.

Generally, the gabbro is homogeneous and holocrystalline with a mineralogy dominated by sub-ophitic arrangements of plagioclase and clinopyroxene (augite). On average, these two phases comprise about 60% and 35% of the mode respectively. All thin sections show variable degrees of uralitisation in which the rims of the pyroxenes are altered to a rather frayed, fibrous, deep-green amphibole and in extreme cases small plates of biotite are also evident. Uralitisation is most advanced in thin sections 6-3028 and 7-3021 which represent the speckled facies (see Plate: 2.15).

Microscopically, the speckled facies is characterised by well-defined inter-granular, poikilitic and granophyric textures. Anhedral to subhedral clots of clinopyroxene occur interstitially between the idiomorphic wedges of plagioclase. Phenocrysts of plagioclase up to 6 mm across, poikilitically enclose blebs of clinopyroxene less than 1 mm across. Other plagioclase phenocrysts show excellent sieve textures. Splendid granophyric textures are typically common adjacent to granular masses of quartz and alkali feldspar which combine to form about 5% of the mode. Large skeletal opaque oxides show strong spatial relationships with the clinopyroxenes whereas smaller opaque forms tend to occur along side subordinate biotite grains. Concentrations of accessory apatite are preferentially located in the felsic phases.

Field relations, combined with petrographic observations made in this study, indicate that the GSR dyke readily correlates with the two large diabase intrusions, i.e. Point dyke and Ya-ya dyke, which intersect 3.2 km to the southeast. As noted in section 2.4.1 these dykes appear to correlate with the Permo-Triassic dyke swarms of the Apatoe Suite.

2.5.2. The Wenot Lake Zone.

The Wenot Lake Zone consists of a 1.6 km long, ESE-trending belt of intercalated, mafic to acid meta-volcanic rocks of the Mazaruni Group. The Zone maintains a uniform thickness of 200 m and is apparently contiguous on its northern boundary with the rocks of the Majuba Suite. The southern margin of the Zone, according to Bertoni et al., (1990), is shear-bounded

by a steeply-dipping, sub-parallel belt of phyllitic tuffs, (also known as carbonaceous meta-siltstones and meta-sandstones) whilst the east and west extents of the Zone remain undetermined. Broadly speaking, the Wenot Lake Zone is bimodal and can be discussed in terms of two distinct lithological units: 1) mafic to intermediate meta-volcanic rocks and tuffs or 2) felsic meta-volcanic rocks.

Mafic to intermediate meta-volcanic rocks and tuffs.

This suite is volumetrically superior and occupies approximately 70% to 75% of the Zone. However, the rocks generally tend to be non-mineralised. It is apparent from the petrographic descriptions afforded by Morton (1990) that this suite of rocks is readily correlatable with the Majuba Suite as described in section 2.5.1.

Felsic meta-volcanic rocks (soda-dacite and soda-dacite porphyry).

These massive, highly siliceous and extremely competent rocks are the chief hosts for gold-quartz mineralisation in the Wenot Lake Zone. Recent borehole data show that the units occur as strung-out bands and lenses, from 2 m to 25 m thick, surrounded by mafic to intermediate meta-volcanic rocks and tuffs (see Bertoni et al., 1990, Fig. 4.3.1). The thicker units are laterally continuous for over 100 m and are frequently offset by N-S trending faults. Petrographic work by Payne (1989b) and Morton (1990) confirm that two texturally distinct felsic lithologies are present. These are known respectively as "soda-dacite" and "soda-dacite porphyry".

Soda-dacites

The soda-dacites are buff-coloured, fine-grained, cherty rocks (see Plate 2.16) and occur in discrete bands, largely in the northern part of the Zone. They were initially given the field name of "quartzites" by Placer Dome Inc. but were later deemed to be soda-dacites after a detailed petrographic assessment by Payne (1989b).

Thin section 67-1474 demonstrates that this lithology is comprised of a fine-grained microcrystalline quartzo-feldspathic groundmass with albite as the dominant feldspar phase. The slide also contains a delicate network of sericite and carbonate which infill microfractures and wrap around former grain boundaries. These minerals are secondary and are indicative of hydrothermal alteration. Corroded opaque minerals, probably pyrites, occur as a minor phase.

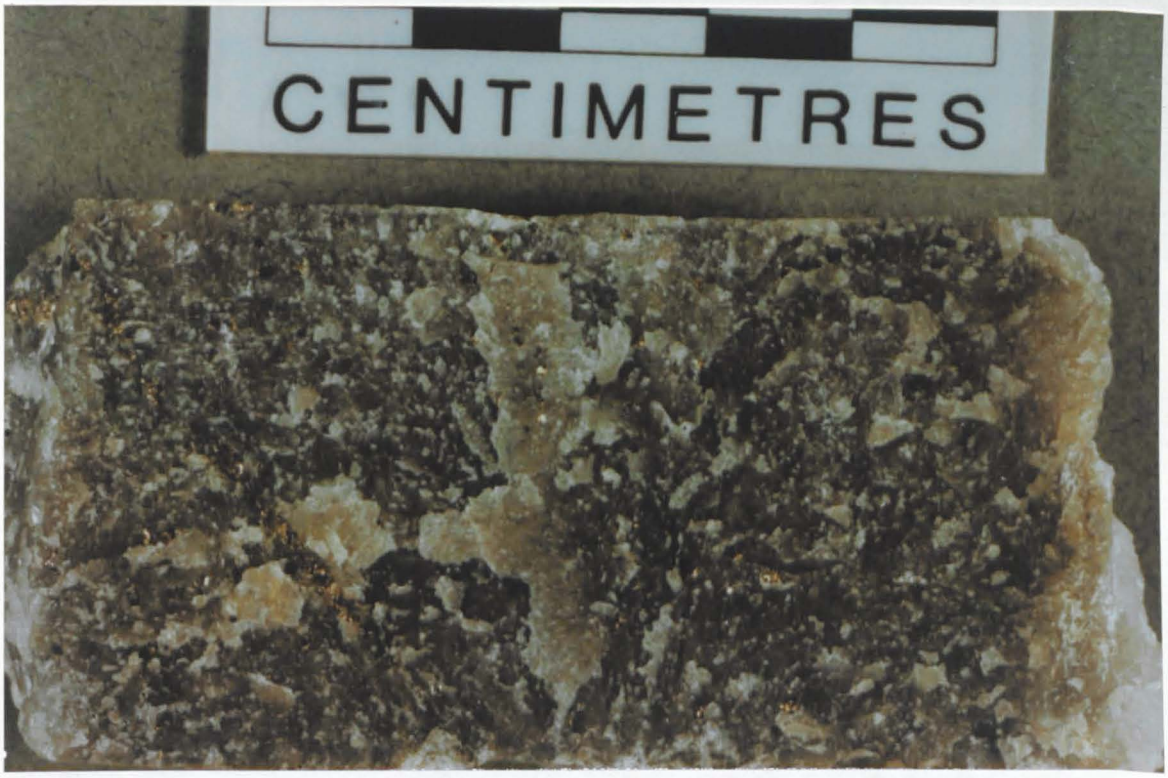

Plate 2.16: Soda-dacite, Wenot Lake Zone. Note diagonal pyrite veinlet on the left. Drill-core specimen, 67-1474.

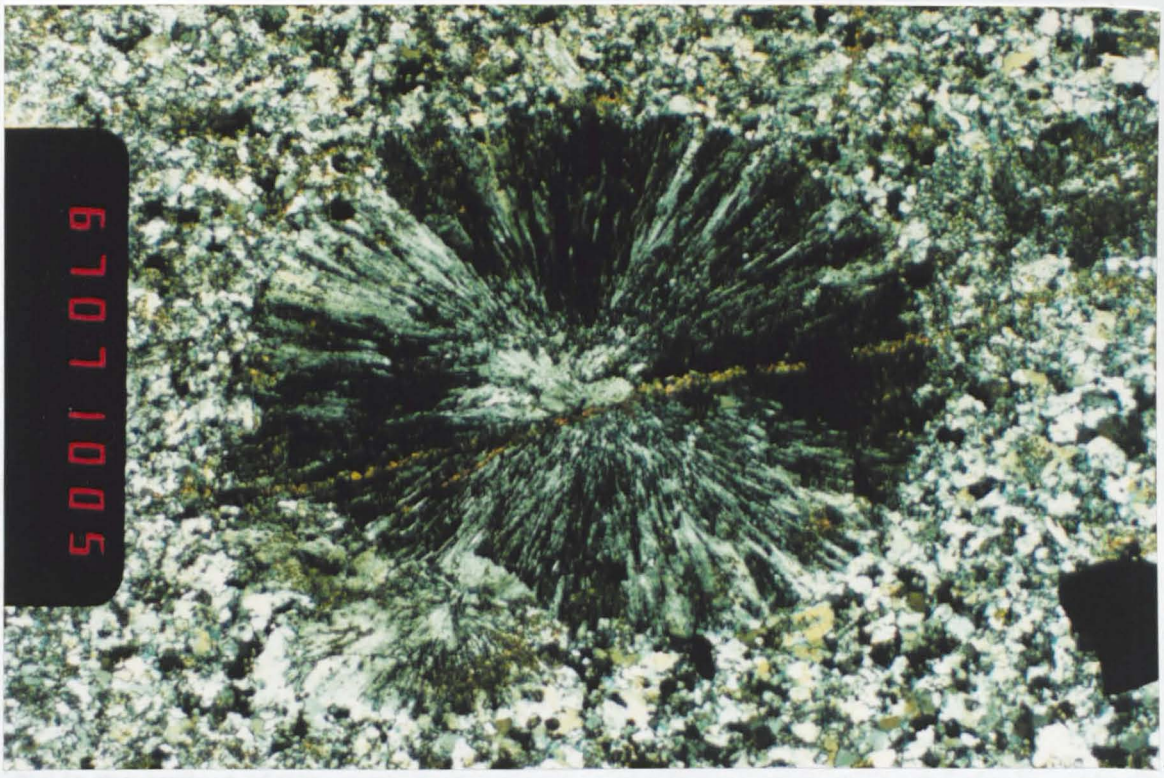

Plate 2.17: XPL micrograph of soda-dacite porphyry, Wenot Lake Zone, showing a quartzo-feldspathic spherulite dissected by a sericite veinlet. Thin section, 67-0716; Mag. x 40.

Soda-dacite porphyry

The bands of soda-dacite porphyry are preferentially located near the southern margin of the Zone and show sheared contacts with the phyllitic tuffs. In hand specimen the porphyry is leucocratic, off-white and is characterised by 40% modal, light-coloured, sub-rounded to sub-prismatic porphyroblasts, 2 mm to 8 mm in diameter. Slide 67-0716 illustrates that the porphyroblastic phase consists of beautifully preserved spherulites, or aggregates of spherulites, containing radially disposed quartzo-feldspathic needles (Plate:2.17). The groundmass mineralogy and texture are very similar to the bulk composition of the soda-dacite as described above.

Morton (1990) interprets the porphyry as a coarser-grained equivalent of the soda-dacite. This hypothesis is substantiated in part by the geochemical analyses presented in this thesis (see Table 3.4) which show that the two felsic lithologies are chemically identical. Moreover, these analyses suggest that the rocks show strong affinities to high-silica rhyolites which are widely documented in similar geological terrains. However, the Wenot Lake felsic meta-volcanic rocks appear to be a very localised phenomenon in contrast to the relatively thick acid volcanic flows which have also been mapped in the Omai area as part of the Mazaruni Group (see Fig. 2.3). The genesis and correlation of the former is briefly debated in Chapter 3.

2.5.3 The oxidised zone (see also section 6.6).

The oxidised zone at Omai, which attains a maximum thickness of 50 m, is an unique gold depositional environment operating under very different constraints to those of the underlying primary mineralisation. The oxidised zone, or weathered zone as it is sometimes called, consists of the laterite profile (saprolite zone) mantling the primary ore bodies of the Omai Stock and Wenot Lake Zones and includes the overlying alluvial deposits.

Laterisation processes

Humid tropical conditions, tectonic stability, prolonged sub-aerial weathering and the absence of Pleistocene glaciation are the main factors which have contributed to the formation and development of deep, lateritic weathering profiles which mantle the crystalline rocks of the Guiana Shield. Unfortunately, the word "laterite" has been loosely applied in the literature, but in the context of this study it will be used as a blanket term for any weathered, residual material overlying fresh bedrock. Synonymous terms for laterite include "saprolite" and "regolith". However, strictly speaking, an intensely weathered rock may only be referred to as saprolite when relict primary textures or structures can be discerned.

Topp et al. (1985) stipulate that the essential requirements for laterisation are a high annual rainfall, intense leaching and a strongly oxidising environment. The leaching of solutions tend to flush out the more mobile constituents, such as the alkalis and alkaline earths, leaving a residue of aluminum, titanium and ferric oxides/hydroxides. Generally, individual laterite profiles have been subdivided into three or four major stratigraphic components, each with distinct physical and mineralogical characteristics (see Davy and El Ansary, 1986; Butt, 1988 and Schellman, 1989). However, on a universal scale, variations in the climatic history, geomorphology and bedrock geology have given rise to complex and varied laterite profiles which make general classification and correlations rather difficult.

Owing to fieldwork constraints at Omai, only the laterite profile overlying the Omai Stock Zone was investigated. However, from the field observations presented by Bertoni et al., (1990) it is evident that the weathered profile of the Wenot Lake meta-volcanic rocks closely parallels the oxidised sections of the Majuba Suite which are discussed below. Nevertheless, a point worth noting is that the duricrust horizon is well developed in the Wenot Lake area but is missing from the laterite sequence in the Omai Stock Zone. A generalised classification for the vertically zoned laterite profile for the Omai area, irrespective of bedrock geology, is illustrated in Table 2.3 below.

Table 2.3

Generalised Laterite Profile for the Omai Area

Material	Description	Av. Thickness (m)
Colluvium	transported surficial material (soil and slope wash).	1
Duricrust	residual indurated latosol.	5
Mottled zone	intensely leached and weathered in-situ material.	4
Saprolite	extremely weathered residual rock with relict textures or structures.	20
	Total	30 m

Plate 2.18 shows the top of this profile exposed north of Wenot Lake. In places, the colluvium has been stripped off by erosion, thus exposing the duricrust horizon at the surface.

The laterite profile of the Omai Stock Zone.

The weathered profile mantling the Majuba Suite and the main Intrusive Complex was examined to a depth 10 m in open-cut areas and to 6 m in test-pit sections. Diamond drilling has indicated that weathering penetrates to depths of nearly 50 m. However, hydraulic mining, particularly over the mineralised Stock has reduced the thickness of cover to 2 m locally.

A typical weathered section overlying the meta-volcanic country rocks closely resembles the idealised profile proposed by Butt and Zeegers (1989). Here, a thin layer of humus mantles 1 m to 2 m of colluvium, which is the product of mass movement or slope wash. The colluvium consists of an orange-brown clay matrix supporting abundant grey-brown, pea-sized, lateritic pisoliths and angular quartz fragments. The pisoliths, according to Collings (1969), are composed primarily of goethite and hematite with minor quantities of kaolinite and quartz. Spectrographic analyses (Collings, 1969) demonstrated that the pisoliths are enriched in iron, vanadium and chromium with respect to bedrock values. Vermicular and vesicular, indurated cobbles are also contained in this section of the profile with occasional evidence of grading. These cobbles are the erosional remnants of duricrust, though the duricrust itself is not evident in the Omai Stock Zone. The base of the colluvium is frequently marked by an accumulation of lithic debris, introduced by slope wash and gravity settling. This phenomenon is here referred to as the stone line, though Bertoni et al., (1990) imply that a stone line is a pisolith-rich zone transitional between the duricrust and mottled horizons.

Beneath the colluvial layer a very distinct mottled horizon can usually be identified within a depth range of 1 m to 5 m. Purple-red hematitic spots and ochreous kaolinite blotches are hosted within a rusty massive clay matrix. Intense leaching and bioturbation have all but destroyed any primary structures, however some relict quartz veining may be evident. This horizon shows strong similarities to the Mottled Clay Layer (H 111), described by Ambrosi and Nahon (1986), in the weathered profile of Birimian meta-basic rocks in Burkina Faso, West Africa.

The mottled zone gives way to a variegated, orange-red saprolite clay at a depth of 5 m to 6 m. Generally, the degree of redness is a function of the basicity of the parent rock. The saprolite, which locally displays relict foliation or banding persists until slightly weathered rock ("saprock") or fresh bedrock is encountered at at an average depth of 30 m.

Plate 2.18 Top of the laterite profile exposed 400 m north of Wenot Lake.

Plate 2.19: Excavation through the oxidised mantle overlying the Omai Stock Zone. Note the contact between the reddish-brown saprolite of the Majuba Suite and the pale to buff saprolite of the Omai Stock.

The laterite profile overlying the Omai Stock is much simpler in form than the meta-volcanic one of the Majuba Suite. In essence, the intermediate mottled zone would appear to be absent in the former. This may be explained by the hydraulic mining activity previously mentioned. However, S.N.C (1986) suggest that the shallower weathering profile over the Stock is an erosional factor due to higher bedrock elevation. The granitic saprolite consists of leucocratic, pale to buff clay unit characterised by a distinct, relict granular texture. Envelopes of intensely altered wallrock are observed along the margins of moderately fresh quartz-carbonate veins. The heavy mineral concentrates derived from the granitic saprolite are rich in black to iridescent cubes of pyrite with subordinate fresh octahedral magnetite crystals, minute bipyramidal zircons and rare gold grains.

The colour contrast between the meta-volcanic saprolite of the Majuba Suite and the granitic saprolite of the Omai Stock is well illustrated in the oxidised contact zone as shown in Plate: 2.19.

Alluvial placer deposits.

Volumetrically, the alluvial deposits are a minor components and account for approximately 3.5% of the total geological reserves. They are contained in Dunclain, Gilt and L'Esperence Creeks which drain in a southwest direction away from the primary ore zones. The original drainage courses have been very much altered by past dredging operations. The alluvial material itself is somewhat unconventional and consists chiefly of reworked tailing dumps from the former hydraulic workings. These secondary alluvial deposits, which are only a few metres thick, give rise to a hummocky topography and consist of very poorly sorted laterite pisoliths, angular quartz-vein fragments and cobbles of weathered country rock. In contrast, the underlying primary alluvial deposits are characterised by a stiff, blue-grey, silty clay which rests on top of clean, quartz pebble "pay" gravels.

CHAPTER 3

GEOCHEMISTRY OF THE MAJUBA SUITE AND THE CAPTAIN MANN SILL

3.1 Aims of chapter.

Prior to this study, virtually no geochemical data existed for any of the greenstone rocks at Omai. Therefore, the primary aim of this chapter is to elucidate the geochemical characteristics of the Majuba Suite and to attempt a chemical correlation with regional and global equivalents wherever possible. The geochemical data also permit an ancillary study of element mobility in ancient terrains which have been transformed by low-grade regional metamorphism and hydrothermal alteration. Two andesitic samples from the Captain Mann Sill were also analysed.

3.2 Description of the geochemical sample subset (26 samples).

The sample subset is mainly comprised of GSR drill-core specimens of the Majuba Suite taken from a small target area on the southwest margin of the Omai Stock Zone (see Fig. 2.5 and Table 3.1). Representative samples of basic to intermediate composition were selected from drill-core intersections within a vertical depth range of 15 m to 250 m. A surface sample of the Suite (CM-02), taken from a fresh outcrop in Captain Mann Creek, outside the ore zone, is also included. The sample subset also includes two felsic meta-volcanic drill-core specimens (67-0716 and 67-1460) from the Wenot Lake Zone, courtesy of the Placer-GSR drilling programme of 1989. In addition, two samples (CM-03 and CM-04) of the Captain Mann Sill were collected from non-oxidised exposures in Captain Mann Creek (see Fig. 2.3 for sample locations). Each sample in the subset was selected on the basis that it was devoid of metamorphic and/or hydrothermal veining and visible mineralisation. All, but one geochemical sample (3-1098), has a corresponding thin section specimen (see Appendix I).

3.3 Elemental analyses.

Major element analysis was carried out on rock powder pellets at the University of Durham using a Philips PW-1400 XRF system. Previously determined Loss-on-Ignition (LOI) values were programmed into the mass absorption correction data. Concentrations of the trace elements Rb, Ba, Sr, Li, Zr, Nb, Hf, Th, U and Pb were determined from sample solutions

using a VG Elemental Plasmaquad at the University College of Wales, Aberystwyth. Selected samples were analysed for rare earth elements (REE) and Y, also by this method. At Oxford Brookes University*, all samples solutions were analysed for Co, Cr, Ni, V, Sc, Y, Cu and Zn by ARL 3510 ICP spectrometer facilities. Selected samples were also tested for As using the Perkin-Elmer 500 AAS- MHS-20 hydride generator system, also at Oxford Brookes. The complete range of geochemical data for the Majuba Suite and Captain Mann samples is presented in Table 3.4, located at the end of this chapter. Unless otherwise stated, all data presented in tables and diagrams in this chapter are taken from Table. 3.4. Additional information regarding sample preparation and analytical techniques is given in Appendix III.

Table 3.1

Breakdown of Geochemical Subset (Majuba Suite and Captain Mann Sill)

Sample Location	No. of Samples
Majuba Suite, Omai Stock Zone	21
Majuba Suite, Captain Mann Creek	1*
Majuba Suite, Wenot Lake Zone	2
Captain Mann Sill, Captain Mann Ck.	2*
Total	26

Note: * denotes surface samples, all others are drill-core specimens

3.4 Constraints.

At the outset of this geochemical approach it is necessary to acknowledge the limitations of the sample subset. Firstly, the rather small sample population may not be adequate to accurately define petrogenetic trends. Secondly, few of the samples have an aphyric texture and more often, porphyritic and amygdaloidal textures are present. However, on the positive

* formerly Oxford Polytechnic

side, none of the samples could be described as cumulates or adcumulates. Thirdly, the subset includes several pyroclastic samples which are not useful in defining magmatic trends. Fourthly, excessive LOI values of up to 11.35 wt. % reflect elevated fluid:rock ratios in which some degree of element mobility and/or net elemental enrichment/depletion is anticipated.

Nonetheless, in view of the paucity of geochemical data at Omai, and Guyana as a whole, a decision was made to proceed with caution, emphasising petrogenetic trends and immobile element ratios rather than absolute chemical abundances of isolated samples. In retrospect, this strategy has proved successful and demonstrates that valuable petrogenetic data can be determined from variably altered samples when fresh rocks are not available.

3.5 Alteration.

The majority of specimens were selected from "fresh" rock beneath the oxidised zone and therefore the effects of tropical weathering in the subset are minimal. Nevertheless, petrographic observations demonstrate that many samples were subjected to phases of hydrous hypogene alteration involving low-grade regional metamorphism (chloritisation, epidotisation, carbonatisation and sericitisation) and hydrothermal alteration (sericitisation, carbonatisation). In addition, minor amounts of albitisation may have been introduced into the rocks by sea-floor metasomatism, regional metamorphism or by Na-metasomatism from the Omai Stock. Intense epidote veining in the Majuba Suite is most likely the result of contact metamorphism, though, obviously altered samples such as these were excluded from the subset.

The degree of chemical alteration sustained by basaltic (46-53 % SiO_2) rocks can be gauged graphically using a NaO_2-CaO co-variation diagram. This technique is applied to the basaltic rocks of the Majuba Suite (16 samples) as shown in Fig. 3.1. It is evident from the diagram that about 70.0% of the samples plot as altered basalts, with a tendency towards Na depletion, whilst the remainder are classified as unmodified normal basalts. One sample (4-0145), has a CaO/NaO_2 ratio equivalent to those found in soda-rich spilites.

Floyd et al. (1991) have implemented a scheme whereby the LOI values of basic volcanic rocks can be used as an index of hydrous alteration intensity. This coding system, which can be used to screen samples for geochemical analysis, has been applied to the Majuba Suite and Captain Mann Sill samples (see Table 3.2). In ideal situations, only samples with an alteration code of 1 or 2 (LOI < 8.0 wt %) may be analysed. However, strict adherence to this Floyd "rule" is virtually impossible if the host-rock compositions to hydrothermal mineralisation at Omai are to be studied.

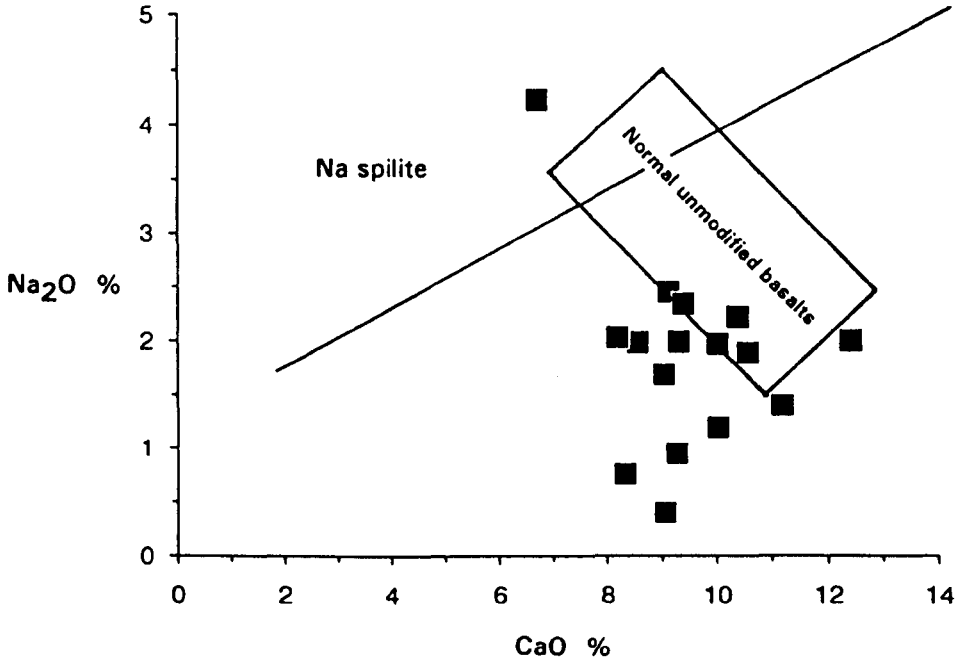

Fig. 3.1: Na_2O - CaO diagram for basaltic rocks (46-53 % SiO_2) of the Majuba Suite, Omai Stock Zone. The diagonal lines divides the spilitic field from other basalts (see Graham, 1976) and the rectangle outlines the field of normal unmodified basalts (see Stillman and Williams, 1979).

Within the sample subset, several factors are operative in controlling the degree of alteration in a particular sample. The first factor pertains to location. Samples located in the Omai Stock Zone tend to have the highest alteration codes. In contrast, the three samples collected from Captain Mann Creek, some 900 m north of the mineralised area all have alteration codes of 1 with LOI values less than 1.2 wt %. However, a time factor may also be involved in this case as the two samples from the Captain Mann Sill are probably post-metamorphic. Secondly, the acidity of a rock appears to govern the degree of alteration sustained. For example, the more basic rocks generally have higher alteration codes than those rocks with SiO_2 contents above 58%. However it must be stressed that intense silicification, which often results in chronic element dilution, may generate low LOI values thus reflecting a false impression of pristine composition. This phenomenon may apply to the highly felsic meta-volcanic host rocks of the Wenot Lake Zone, e.g. samples 67-1460 and 67-0716. A third factor to be considered is texture. It is interesting to note that the three basic intrusive rocks which exibit coarse-grained sub-ophitic to ophitic textures all yield LOI values less than 3.2 wt % (alteration code 1).

Table 3.2

Alteration Coding of the Majuba Suite and Captain Mann Sill.

Alteration Code	LOI (wt. %)	Alteration Intensity	No. of Samples
1	< 4.0	Mild	12
2	4.0 - 8.0	Strong	2
3	> 8.0	Severe	12
		Total	26

Definitive criteria after Floyd et al., (1991)

Note: The range of LOI values for the Majuba Suite and Captain Mann Sill samples is 0.71 wt.% to 11.35 wt. %. See also Table 3.4

3.6 Element mobility in the Majuba Suite (Omai Stock Zone).

The absolute concentrations of mobile elements in altered igneous rocks rarely reflect primary magmatic values. Therefore, before any geochemical characteristics can be constrained, it is first of all necessary to ascertain what elements (if any) were mobile during secondary processes and to what extent. Moreover, the processes which have influenced mobility also require identification. The twenty-two, basic to intermediate meta-volcanic samples (including sample CM-02) which represent the Majuba Suite rocks of the Omai Stock Zone provide suitable material for a preliminary investigation of element mobility of hydrothermally altered greenstone rocks.

3.6.1 Major elements.

With reference to the Harker-type diagrams of Fig. 3.2 (a to i), it is evident that the vast majority of major oxides follow chemically coherent linear trends, implying that the major elements were relatively immobile, with respect to SiO_2, during episodic alteration. Moreover, the trends are consistent with low-pressure crystal fractionation in an evolving magmatic suite. However, the validity of these trends is dependent on the fact that silica also behaved in an immobile manner. This hypothesis can be tested by plotting SiO_2 against the relatively inert trace element, Zr. The linearity of the line defined by the SiO_2-Zr data in Fig 3.3 endorses the fact that there was no significant silica migration in the Majuba Suite samples. However, each sample must be judged on its own merits. For example, the petrographic features of quartz-filled amygdales and quartz veinlets shown by thin section 4-2022 indicate that silica may have been mobilised and enriched in the corresponding geochemical sample.

At his juncture, the following point needs to be stressed. Although an element may demonstrate apparent immobile behaviour, the overall primary values of that element may have experienced net enrichment or dilution due to the addition or subtraction of other elements to or from the system. In other words, if all the samples have suffered the same degree of alteration, elements may retain primary trends but not primary values.

The shot-gun scatter displayed by K_2O-SiO_2 diagram (Fig. 3.2 f) indicates that K was readily prone to mobilisation during post-magmatic processes. Excesses of K_2O in certain geochemical samples can be directly correlated with pervasive sericitisation in the thin section specimens, though it is not possible to determine if the alteration is metamorphic or hydrothermal in origin. The moderate degree of scatter shown by the NaO_2-SiO_2 data (Fig. 3.2 e) signifies small-scale mobility of Na. Deviations from the linear trend in the P_2O_6-SiO_2 (Fig. 3.2 i) are most likely due to subtle differences in modal apatite abundances between samples, rather than element mobility. Samples yielding anomalously high MnO values also

tend to have relatively high As values and are usually tuffaceous in nature. These trends are consistent with localised circulation of hydrothermal fluids in a submarine environment.

3.6.2 Trace Elements.

Three key groups of trace elements are considered in the dicussion below. These are: large-ion-lithophile (LIL) elements, high field strength (HFS) elements and the rare earth elements (REE).

LIL elements (Rb, Ba, Sr).

In broadly analogous meta-igneous terrains across the globe the LIL elements have been readily moblised by various low-grade alteration processes including sea-floor metasomatism (Hart et al., 1974); regional metamorphism (Brewer and Aitken, 1989) and hydrothermal alteration (Humphris and Thompson, 1978). As demonstrated above, selective sericitisation gave rise to scatter of potassium (another LIL element) values in the Majuba Suite. A strong constant ratio for K-Rb data (Fig 3.4 a) and to a lesser extent for K-Ba and Rb-Ba data (Figs. 3.4 b and c respectively) show that the distribution of Rb and Ba were also controlled by the same process. Such consistent co-enrichments may be explained by the substitution of Rb and Ba for K in sericite-muscovite grains as the host rocks equilibriated with the invading fluids carrying these elements.

The negative linear relationship between Ca and Sr (Fig 3.5 a) is converse to primary magmatic trends, which therefore suggests that the present Sr values have been modified by secondary processes. However, Sr does not display any linear correlation with the other LIL elements, e.g. Rb (Fig 3.5 b), indicating that Sr distribution is not directly related to sericitisation in the Majuba Suite. The inverse relationship between Ca and Sr data also rules out modification by Ca-rich agencies such as epidotisation and carbonatisation. However, Sr does displays a vague positive correlation with Na (Fig. 3.5 c). One may therefore speculate that some Sr (and Na) were introduced to the rocks from a sea-water source.

In general, LIL element behaviour appears to be related to plagioclase feldspar stability. The trends outlined above can be generated by the leaching of Ca, Na and Sr from the feldspar during sericitisation, replacing it with K, Rb and Ba.

HFS elements (Ti, Zr, Nb, Y, Hf, Ta).

The high ionic potential of the HFS elements invokes strong resistance to transportation by aqueous fluids during secondary processes (Pearce and Cann, 1973). For this reason, the

elements Ti, Zr, Nb and Y have been used extensively in the petrogenetic studies of modern and ancient volcanic rocks to define lava types (Winchester and Floyd, 1977); fractionation trends (Pearce and Norry, 1979) and palaeotectonic settings (Pearce 1982). However, it must be noted that HFS elements are susceptible to chemical migration under certain conditions. For example, Hynes (1980) proposed that Ti, Zr and Y behaved highly erratically due to elevated CO_2 levels associated with greenschist facies metamorphism. In exceptional hydrothermal conditions the occurrence of zircon in ore veins has demonstrated the potential for Zr mobility (Claoué-Long et al., 1990). Moreover, the evidence of hydrothermal rutile and sphene recorded in Au lode deposits of the Superior Province, Canada, (Jemielita et al. 1990), indicates that Ti may also be extremely mobile in certain hydrothermal conditions.

The problem of elemental contamination during sample preparation and/or analysis also needs to be addressed at this point. Wood et al., (1979) estimate that carbon tungstide temas may contaminate samples with up to 0.5 ppm Ta and similar or slightly higher concentrations of Nb. Tantalum concentrations obtained in this study (1992), by ICP-MS analysis, were erratically enriched by values up to 1.00 ppm. Consequently all Ta values were deemed unreliable and omitted from the data set. Although a carbon tungstide tema was used in sample preparation, it is more likely that such high levels of Ta were introduced from "build-ups" on the sampling cone in the VG Plasmaquad. Surprisingly, Nb concentrations in the Omai samples appear to be unaffected by external sources.

The mobility of the HFS elements in the Majuba Suite can be tested using the graphical methods outlined by Whitford et al., (1989). The underpinning principle of this technique is based on constant ratio relationships of incompatible elements. For example, in a suite of rocks, any two elements which are immobile, with respect to each other, will define a linear array of data pointing towards the origin on binary variation diagrams. These trends are interpreted to reflect the immobility of the elements tested, with any movement up and down the linear arrays being controlled by the net addition or subtraction of other elements to or from the system.

The broadly linear distribution defined by the Nb-Zr, Hf-Zr and Ti-Y data sets (Fig. 3.6, a,b, and c respectively) strongly suggest that Nb/Zr, Hf/Zr and Ti/Y ratios in the Majuba Suite represent primary values. Minor deviations from linear trends are attributed to localised mobility, analytical uncertainties or sub-sampling error (see Whitford et al., 1989). The most widely used inter-element ratios in petrogenetic studies are Ti/Zr, Zr/Y and Nb/Y. Therefore these element ratios, in particular, need to be tested for their reliability.

The arrays of data for these elements, as shown in Fig. 3.7 a, b, and c, consist of bimodal linear trends pointing towards the origin, giving the impression of relative elemental

immobility. The bimodal nature of the distribution patterns is thought to be generated by compositional variations within the Majuba Suite, though the ultimate controls behind the patterns are not fully understood. For example, in the Zr-Y diagram (Fig. 3.7b) the uppermost array is comprised of rocks chemically identified as andesites whereas the trend close to the Y axis consists of rocks with the chemical composition of basalts. In the Nb-Y diagram (Fig. 3.7c) the position is ambiguous. The dominant array consists of chemically classified basalts and andesites whereas the subordinate trend close to the Y axis is mostly made up of chemically identified basaltic rocks. The picture may be further complicated by element ratios involving Ti, as this element appears to behave compatibly (see Fig. 3.2g). This trend may be explained by continuous magnetite-ilmenite fractionation.

REE (La to Lu).

Owing to their congruent chemical behaviour as immobile incompatible elements, REE have been widely used in geological research to detect and identify petrogenetic trends. However, some REE mobility has been recorded in low-grade volcanic terrains comparable to Omai (see Hellman et al., 1979; Brewer and Aitkin, 1989). The REE group of elements may be discussed in terms of two distinct sub-groups. These are respectively known as the light rare earth elements (LREE, i.e La to Eu) and the heavy rare earth elements (HREE, i.e. Gd to Lu).

Selective transport of individual REE elements in particular rock samples may be recognised by pronounced departures from smooth chondrite-normalised trends, though positive and negative Eu anomalies usually mirror primary magmatic trends. In the Majuba Suite, several samples show sharply positive Ce anomalies (see Figs. 3.10a, 3.11a and 3.12a). Globally, this phenomenon is extremely rare, though positive Ce anomalies have been documented in Recent sediments in the Indian Ocean. According to Desprairies and Bonnot-Courtois (1980) and Tlig and Steinberg (1982) these anomalies are produced by the submarine alteration of volcanic glass to smectite which in turn fractionates Ce from sea-water.

At Omai, the positive Ce anomalies probably reflect the mobility of Ce in the tetravalent state during alteration, rather than a primary magmatic feature. The anomalies do not correspond with any obvious petrographic characteristic, though the fact that they are restricted to the greenstone rocks of the Majuba Suite suggests that they may have been generated during greenschist facies metamorphism or by submarine weathering processes. Moreover, the Ce anomalies mainly occur in samples showing LREE enrichment relative to HREE, which may indicate that the LREE have been collectively mobilised in these samples, albeit, to a much lesser degree than Ce. However, it is worth noting that there is a serious analytical uncertainity for Ce in basalts (see Table C, Appendix III) and it is very possible that this has contributed to the positive Ce anomalies recorded in the basaltic rocks of the Majuba Suite.

Two of the Majuba Suite samples (i.e. 2-2360, Fig. 3.12a and 67-1460, Fig. 3.13a) show very minor negative Ce anomalies on the chondrite-normalised patterns. Elsewhere, this feature has been attributed to sea-water alteration (Ludden and Thompson, 1979; Colley and Walsh, 1987) and to the incorporation of subducted sediment during magmatic arc genesis (Hole et al., 1984). Mildly erratic Ho, Tm and Yb values for a few of the Majuba Suite sample probably represent analytical error at low elemental detection limits.

3.6.3 Element mobility: summary.

It is evident from the discussion above that LIL element mobility was primarily governed by plagioclase feldspar stability. K, Rb, and Ba, were extensively mobilised and co-enriched by sericitic alteration. On the other hand, Na and Sr values were modified by early albitisation but were subsequently mobilised and depleted by the later sericitisation. Whitford-type bi-element plots demonstrate that the primary HFS element ratios of Nb/Zr, Hf/Zr and Ti/Y were moderately well-preserved whilst the position concerning Ti/Zr, Zr/Y and Nb/Y is less clear, though comparable immobility is anticipated. Tantalum contamination during sample preparation and/or ICP-MS analysis was widespread, and consequently, all Ta data have been omitted from the data set. Sharply positive Ce anomalies, as expressed on LREE-enriched chondrite-normalised REE profiles, showed that Ce, and possibly the other LREE, may have been selectively mobilised and enriched with respect to HREE, probably during greenschist facies metamorphism.

Fig. 3.2 a to i (overleaf): Harker diagrams for basic to intermediate rocks of the Majuba Suite in the Omai Stock Zone (22 samples).

a) Al_2O3 - SiO_2

b) $Fe_2O_3^T$ - SiO_2

c) MgO - SiO_2

d) CaO - SiO_2

e) Na_2O - SiO_2

f) K_2O - SiO_2

g) TiO_2 - SiO_2

h) MnO - SiO_2

i) P_2O_5 - SiO_2

Note: All major oxide values given in weight percent (wt. %). In Fig. 3.1 h, the highly anomalous MnO value of 1.74 % for sample 4-1050 is off-scale and is not plotted.

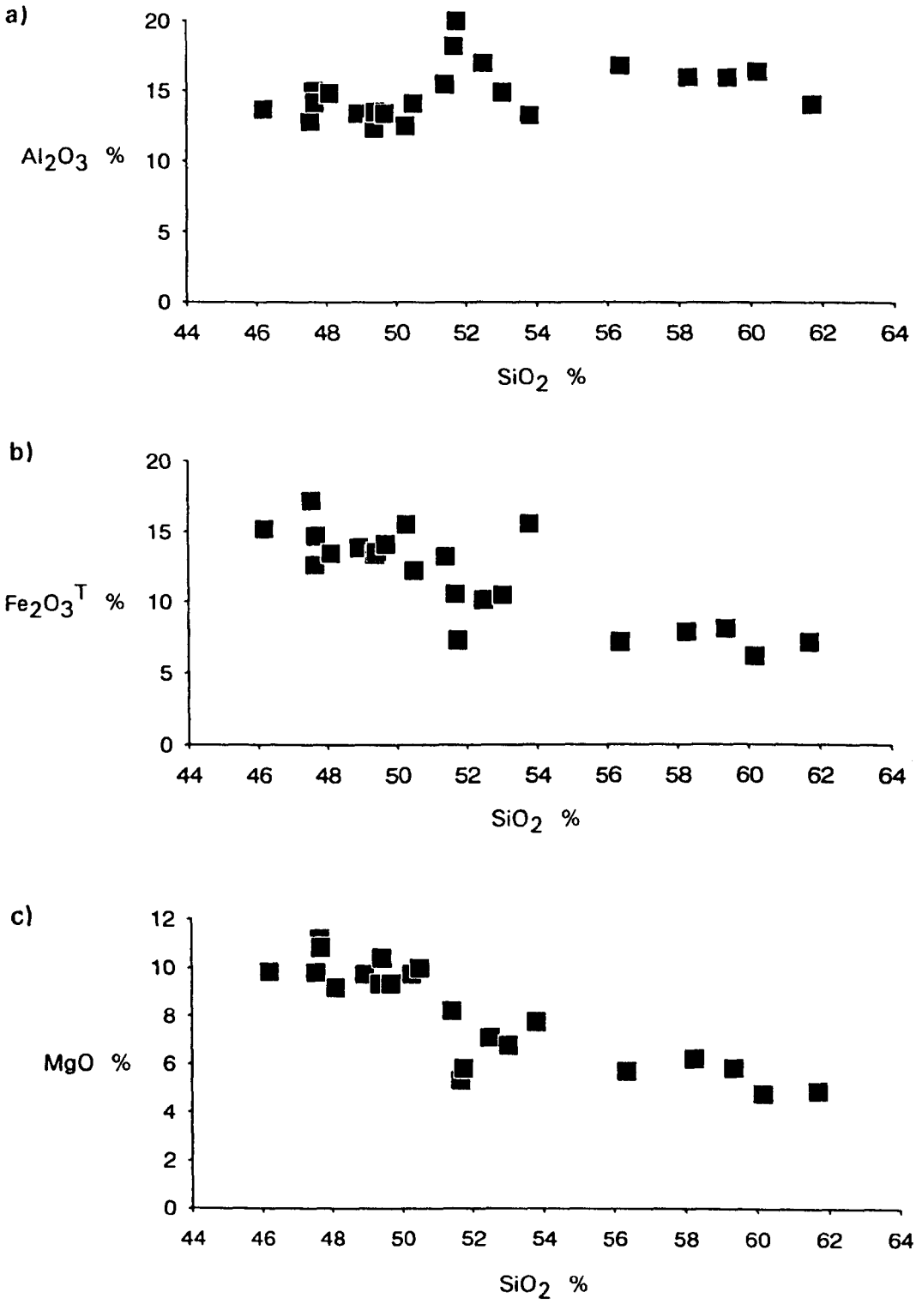

Fig. 3.2: a) Al_2O_3 - SiO_2; b) $Fe_2O_3^T$ - SiO_2 and c) MgO - SiO_2.

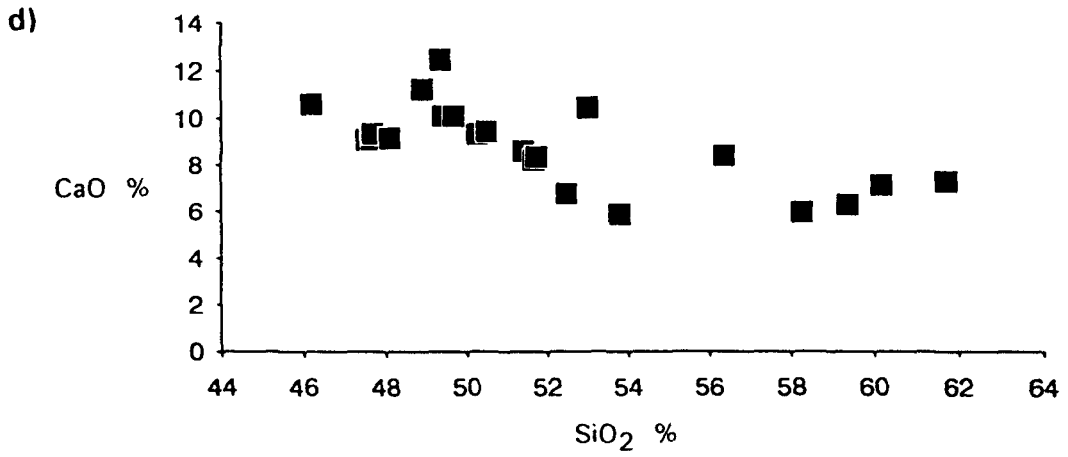

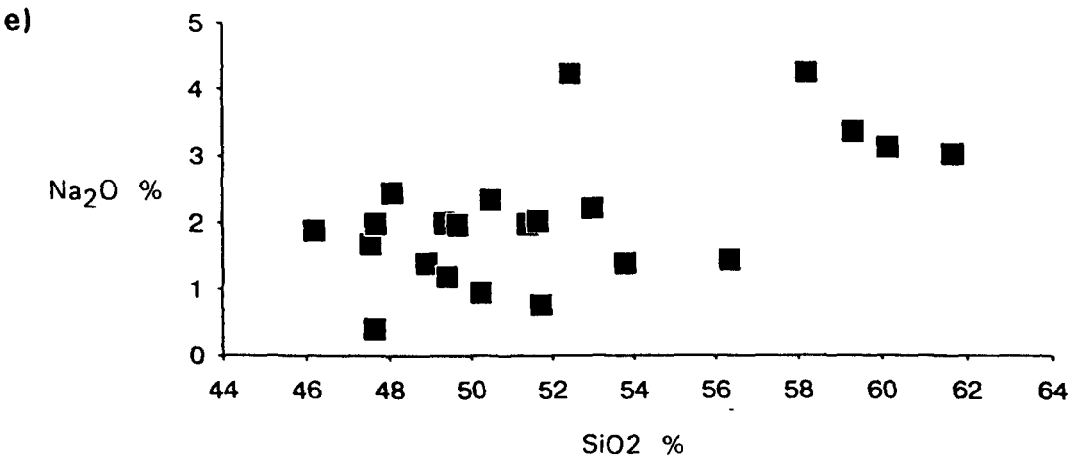

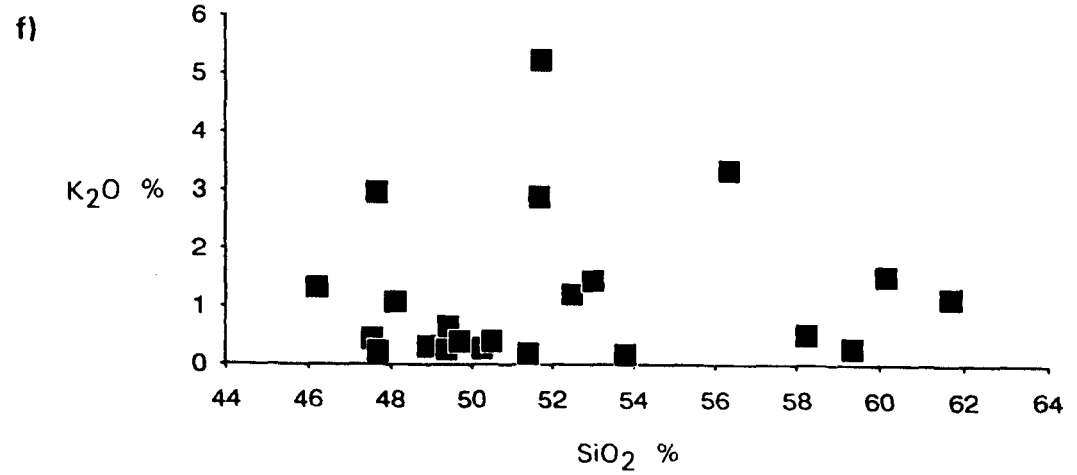

Fig. 3.2 (cont'd): d) $CaO - SiO_2$; e) $Na_2O - SiO_2$ and f) $K_2O - SiO_2$.

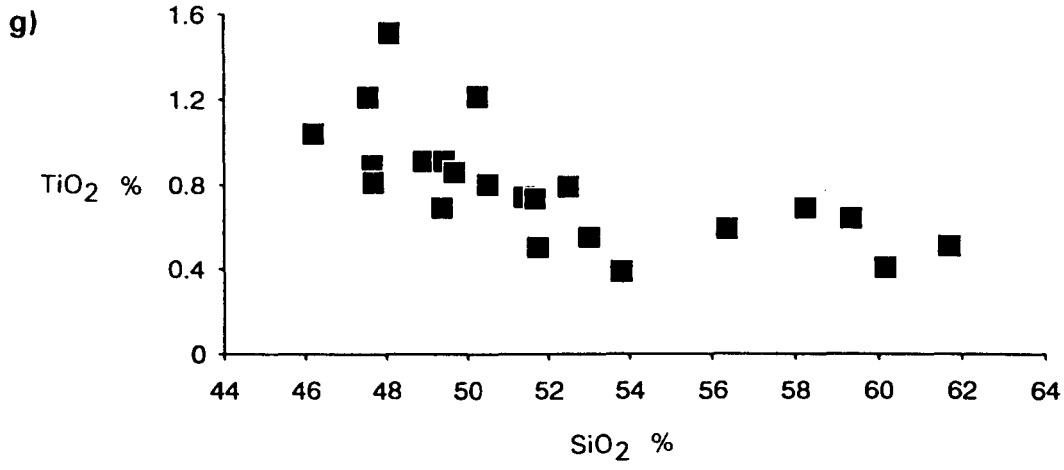

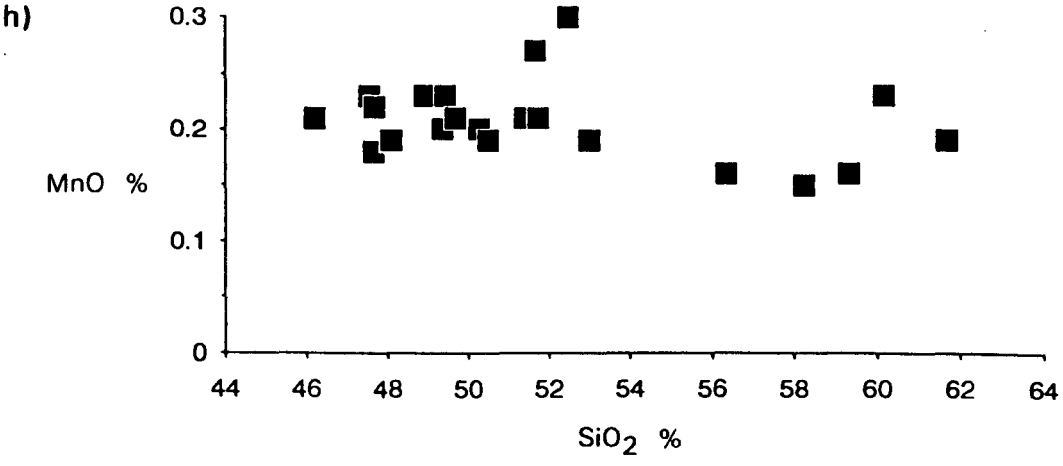

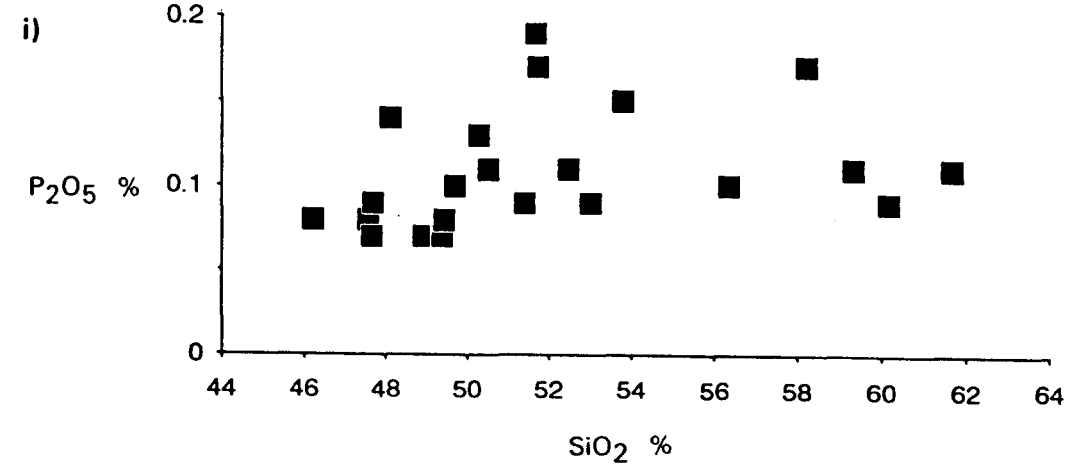

Fig. 3.2 (cont'd): g) TiO_2 - SiO_2; h) MnO - SiO_2 and i) P_2O_5 - SiO_2.

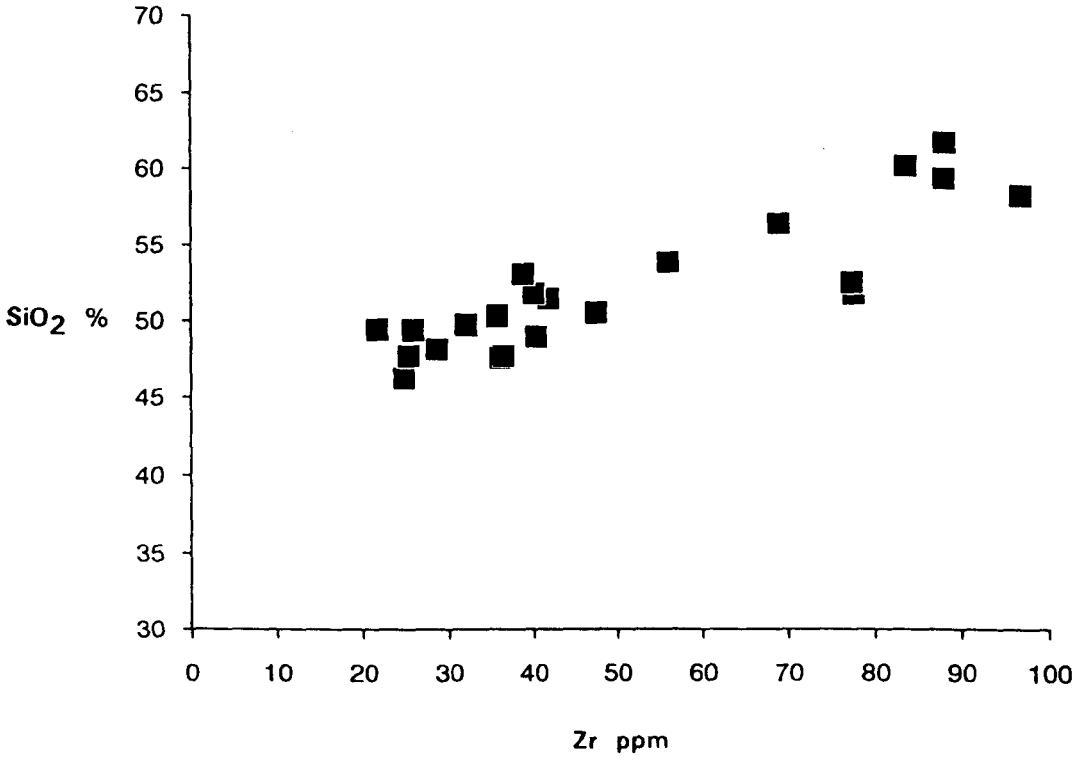

Fig. 3.3: SiO_2 - Zr diagram for rocks of the Majuba Suite, Omai Stock Zone. The linear distribution of the data indicates that silica was relatively immobile with respect to the inert trace element Zr during alteration. Moreover, the positive linear correlation between the elements is typical of island arc volcanic suites (see Wilson, 1989, Fig. 6.13).

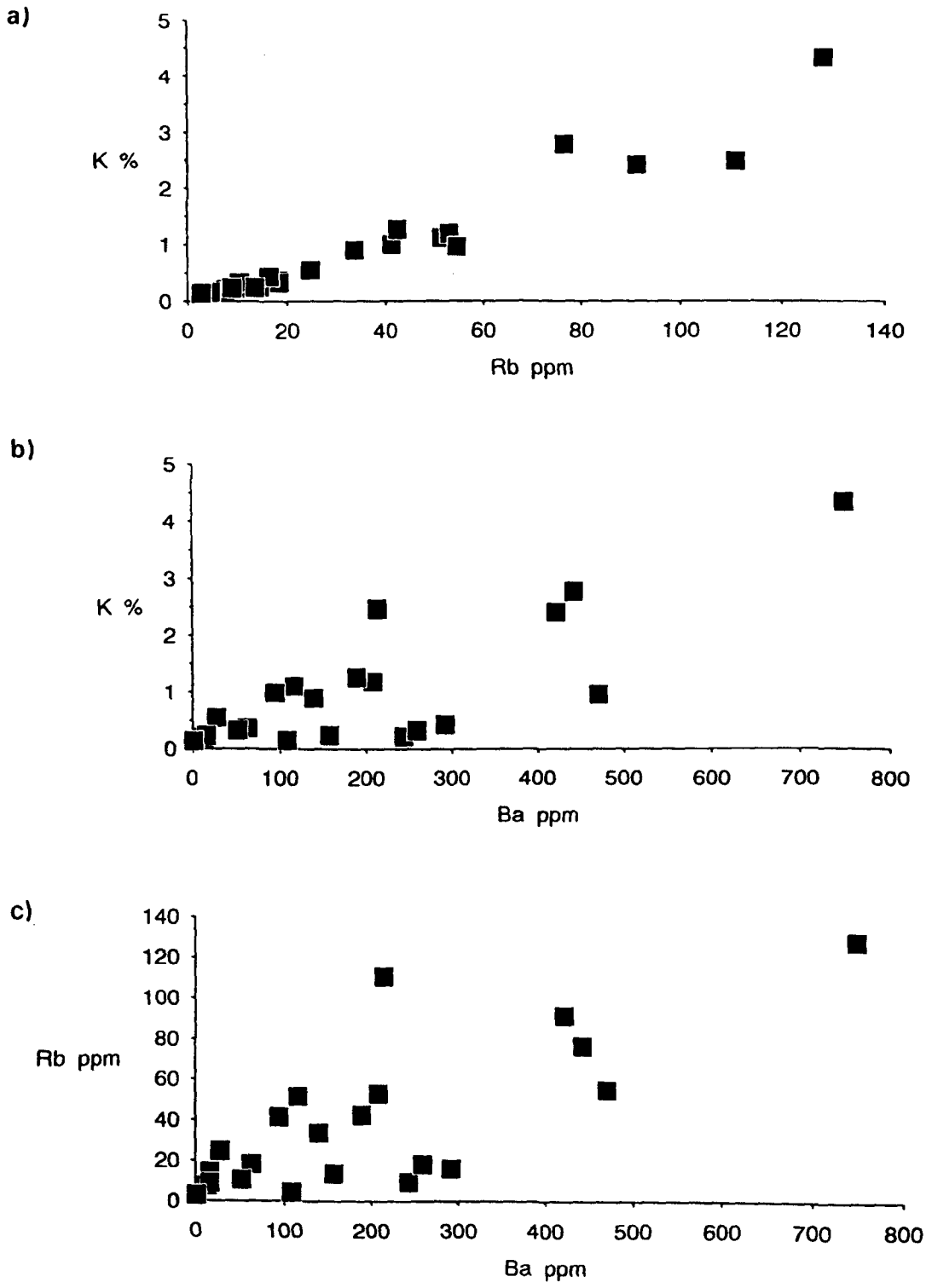

Fig. 3.4: Co-variation diagrams showing the constant ratio relationships of the LIL elements K, Rb, and Ba in the Majuba Suite, Omai Stock Zone: a) K - Rb; b) K - Ba and c) Rb - Ba (see text for details)

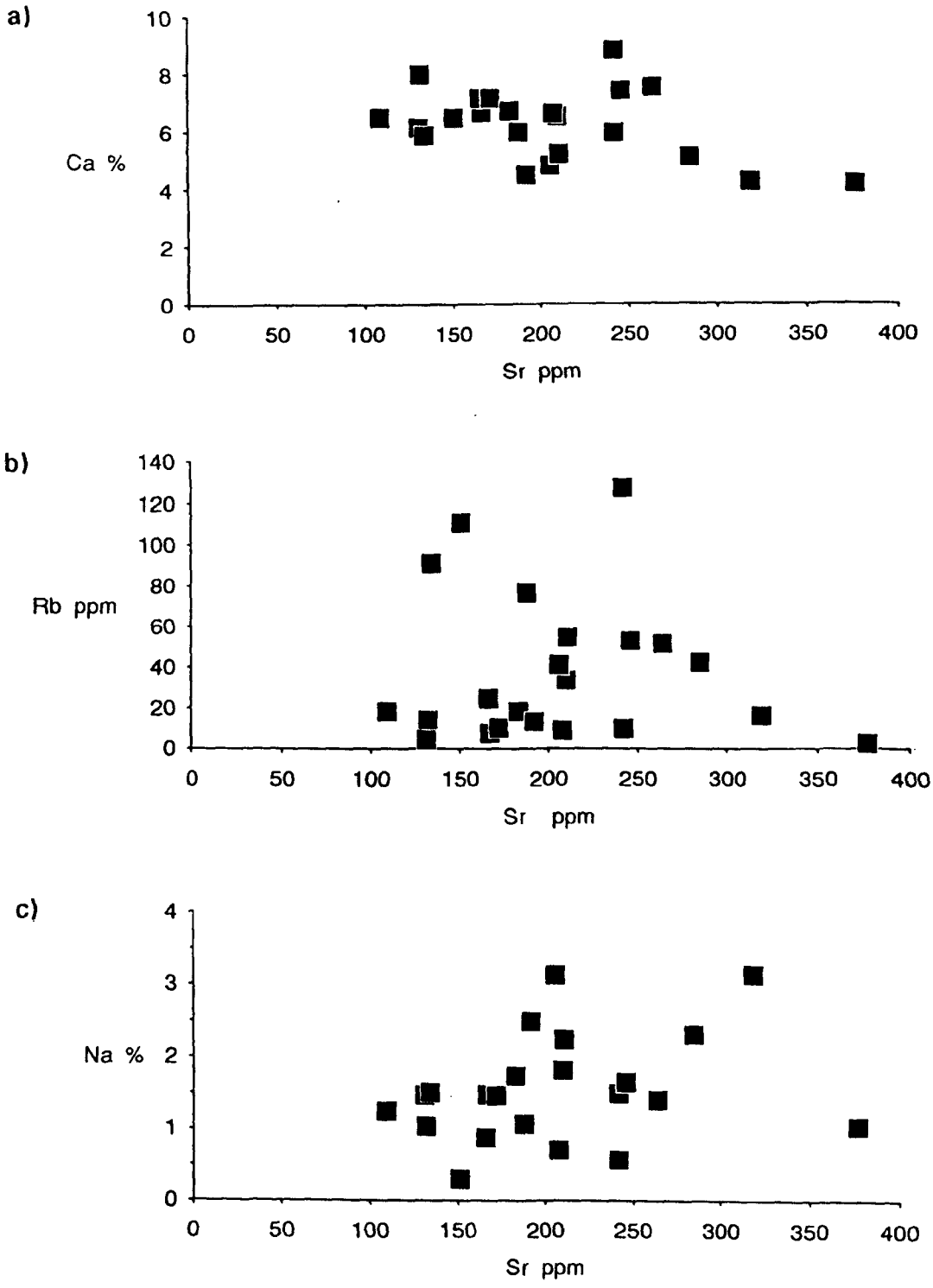

Fig. 3.5: Co-variation diagrams showing the relationship of Sr with a) Ca, b) Rb and c) Na in the Majuba Suite, Omai Stock Zone (see text for details).

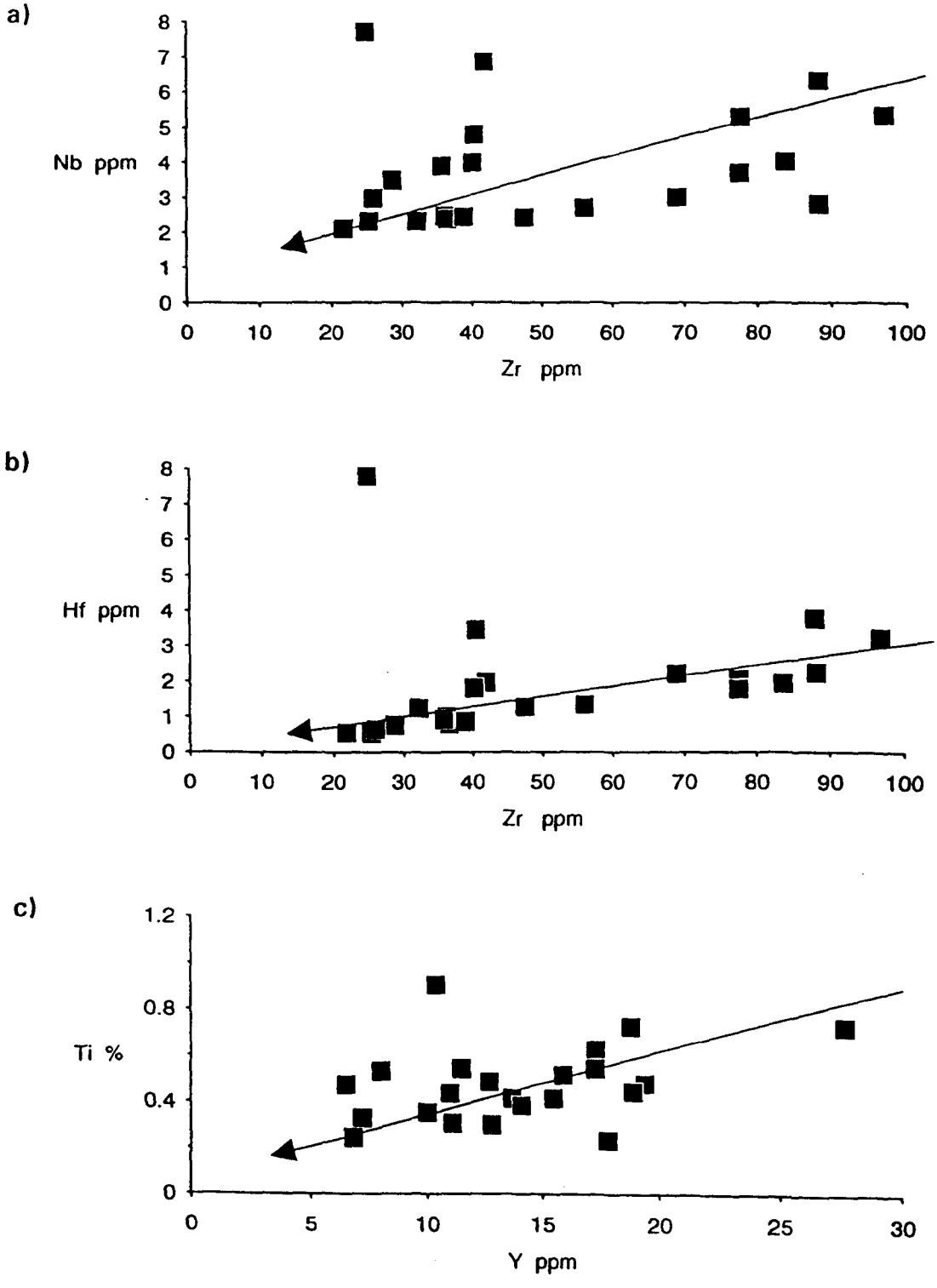

Fig. 3.6: Co-variation diagram showing the relative immobile behaviour of various HFS elements in the Majuba Suite, Omai Stock Zone: a) Nb - Zr; b) Hf - Zr; and c) Ti - Y. The arrows pointing towards the origin represent idealised trends of immobile behaviour between the elements (see text for further details).

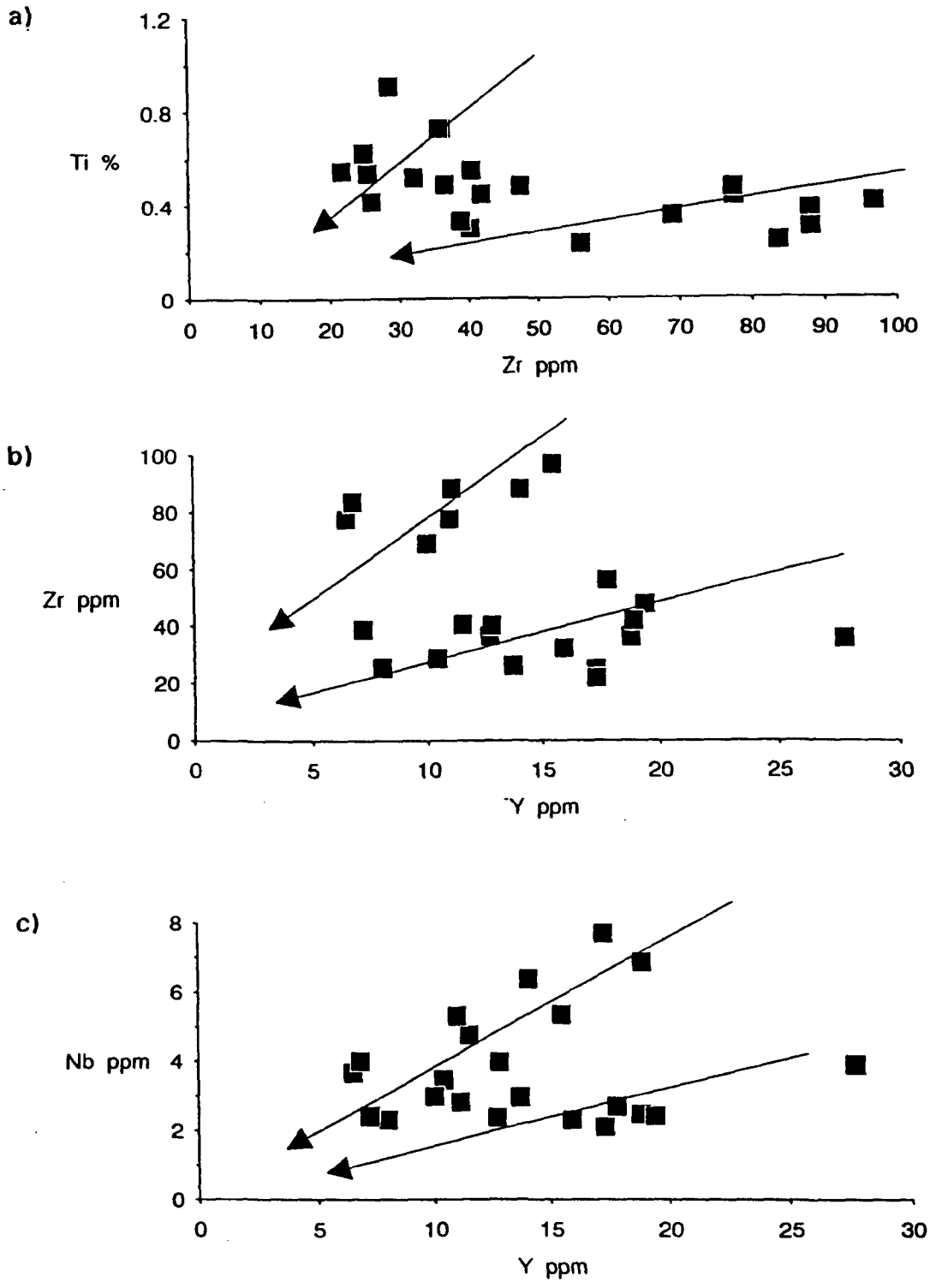

Fig. 3.7: Co-variation diagrams showing the relative immobile behaviour of various HFS elements in the Majuba Suite, Omai Stock Zone: a) Ti - Zr; b) Zr - Y and c) Nb - Y. The arrows pointing towards the origin represent idealised trends of immobile behaviour between the elements. The bi-modal nature of the distribution patterns probably reflects compositional variation within the Majuba Suite (see text for further details).

3.7 Geochemistry of the Majuba Suite.

3.7.1 Compositional classification.

As outlined in Chapter 2, satisfactory petrographic classification, especially of the Majuba Suite rocks has been precluded by widespread mineralogical and textural degradation inflicted during post-magmatic processes. Moreover, compositional classification using conventional Total Alkali Silica (TAS) diagrams is limited due to the mobility of K and Na. Table 3.3 attempts an arbritary chemical classification of the Majuba Suite samples using SiO_2 wt. % as the sole discriminant. However, this method is limited in its application, firstly by localised silica migration in the subset and secondly by the fact that it fails to provide any information regarding the magmatic affinity of the rocks. Recourse is therefore made to the discrimination diagram constructed by Floyd and Winchester (1978) which uses the immobile element ratios Zr/TiO_2 and Nb/Y to constrain lava groups (see Fig. 3.8). The advantage of this diagram is that it differentiates between sub-alkaline rocks and those with an alkaline affinity. However, the fact that sub-alkaline basalts and basaltic andesites are categorised in the same field is an obvious limitation.

Table 3.3

Classification of the Majuba Suite using SiO_2 contents

Lithology	SiO_2 Limits (wt. %)	Number of Samples
Basalt	45 - 52	14
Basaltic andesite	52 - 57	4
Andesite	57 - 63	4
Dacite	63 - 68	-
Rhyolite	> 68	2*
	Total	24

Note: SiO_2 limits from adapted from Le Bas and Streckeisen (1991); * denotes samples from the Wenot Lake Zone

With reference to Fig. 3.8 it is apparent that the Majuba Suite samples are dominated by rocks in the compositional range basalt to andesite. The two highly acidic samples from the Wenot lake Zone plot just inside the field of comendites and pantellerites. However, the Zr and Nb values in this case were obtained by semi-quantitative analysis (see Table 3.4, note 10) and therefore this classification must remain tentative until more conclusive data are produced. In the meantime, these rocks may be classified, according to their SiO_2 contents, as "high-silica rhyolites" (HSRs).

By and large, the presentations of data in Table 3.3 and Fig. 3.8 are mutually supportive and provide fairly accurate compositional classifications in the absence of reliable petrographic data. For simplicity, the SiO_2 classification scheme (Table 3.3) is here adopted, though caution must be exercised regarding localised silica mobility. Moreover, it must be stressed that chemical assessments are not to be used independently of petrographic observations. For example, three of the Majuba Suite "basalts" are actually basic intrusives (see Table 3.4). Initial petrographic screening was also necessary in order to remove several of the fine-grained, mafic dyke samples of the Gilt Creek Suite. Without screening, these samples would have comfortably plotted as Majuba Suite greenstones according to the chemical criteria of Table 3.3 and Fig 3.8.

3.7.2 Magmatic affinity

In Fig. 3.8, all the Majuba Suite samples from the Omai Stock Zone show sub-alkaline tendencies with Nb/Y ratios less than 0.6. Unfortunately, owing to K and Na mobility in the sample subset these tendencies cannot be confirmed by the K_2O-SiO_2 and Na_2O-SiO_2 diagrams proposed by Middlemost (1975). For the same reason, i.e. alkali mobility, the Jensen cation plot (Fig. 3.9) is preferred over conventional AFM ternary plots to discriminate between tholeiitic and calc-alkaline trends within the sub-alkaline series. The distribution of data in Fig. 3.9 intimates that the Majuba Suite samples of the Omai Stock Zone follow a common fractionation path in which early high-Fe tholeiites have differentiated into a relatively more evolved, but numerically sub-ordinate, calc-alkaline series. The petrogenesis of these rocks is discussed in detail in section 3.7.4.

The two high-silica rhyolite samples from the Wenot Lake Zone show mildly alkaline tendencies on the Zr/TiO_2 - Nb/Y plot of Fig.3.8. However, these rocks have a clear tholeiitic character on the basis of their P_2O_5 and Zr contents (see Winchester and Floyd, 1976). According to the Jensen cation diagram (Fig. 3.9) the two rhyolitic samples show a marginal tholeiitic affinity. However, trace abundances of Fe, Mg and Ti in the two samples preclude a satisfactory assessment by this method. Nevertheless, the petrogenetic evidence (see section 3.7.4) intimates that these rocks are low Fe-Mg tholeiites.

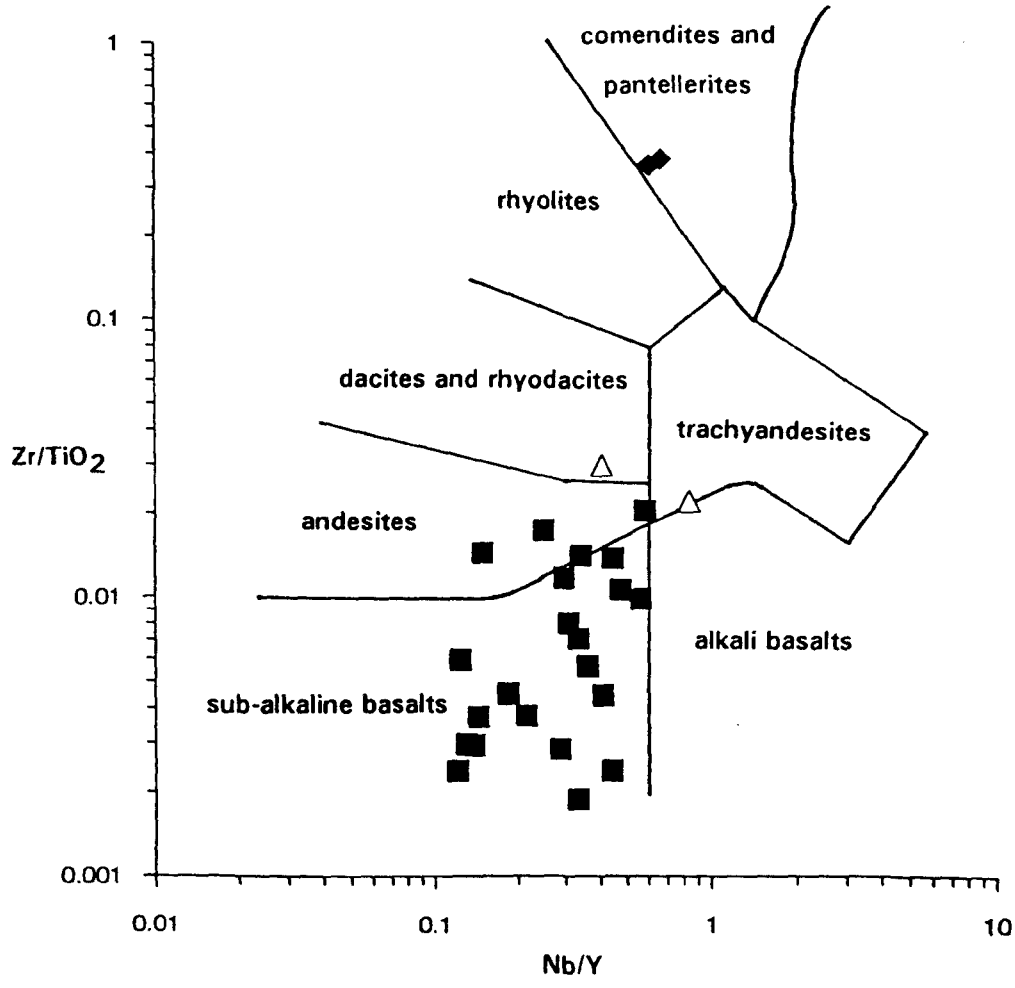

Fig. 3.8: Zr/TiO_2 - Nb/Y diagram for rocks of the Majuba Suite and Captain Mann Sill. Field boundaries after Floyd and Winchester (1978).

Symbols: solid squares - Majuba Suite, Omai Stock Zone; solid diamonds - Majuba Suite, Wenot Lake Zone; open triangles - Captain Mann Sill.

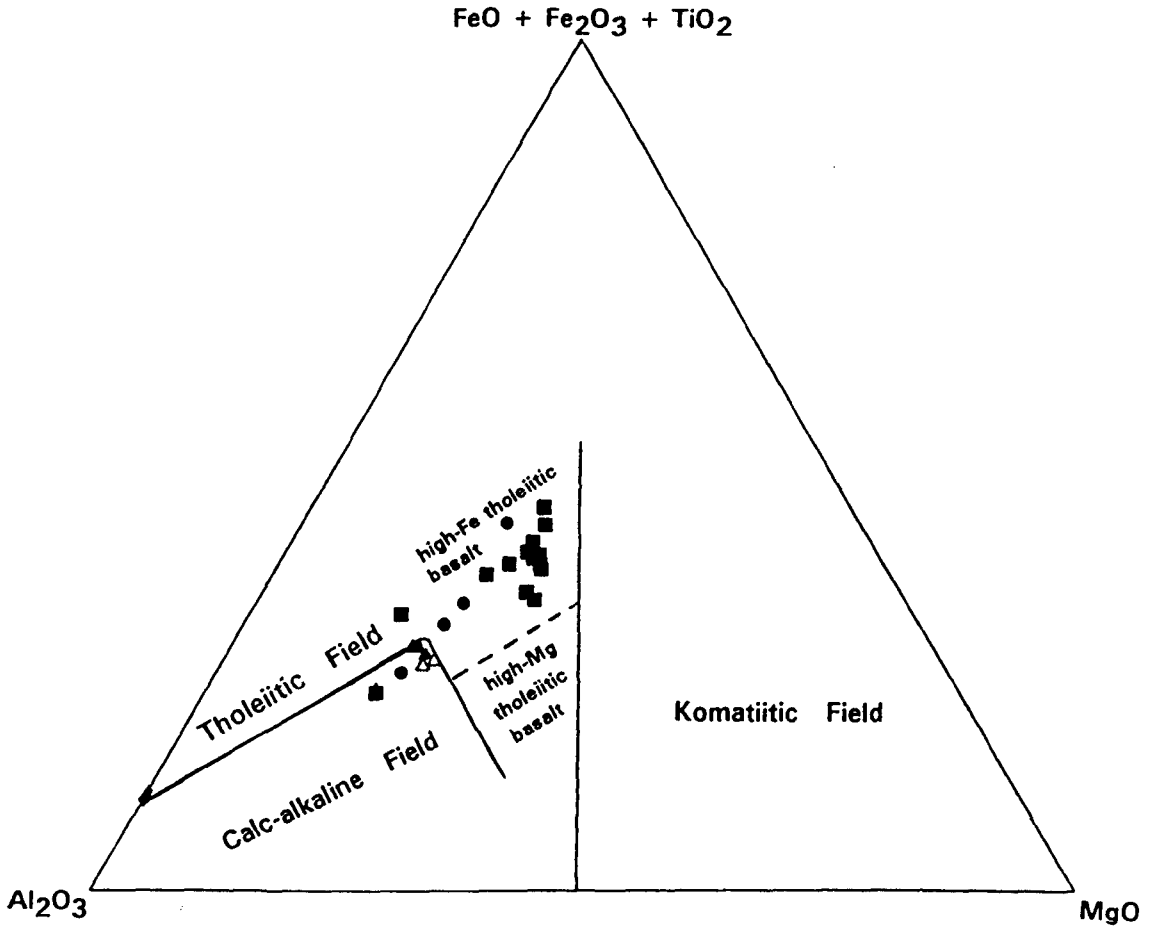

Fig. 3.9: Jensen cation diagram for the rocks of the Majuba Suite and Captain Mann Sill. Field boundaries after Jensen (1976). Total Fe in the Omai rocks is represented by $Fe_2O_3^T$.

Symbols: solid squares - basalts; solid circles - basaltic andesites; solid triangles - andesites; all Majuba Suite, Omai Stock Zone. Solid diamonds high-silica rhyolites, Majuba Suite, Wenot Lake Zone; open triangles - Captain Mann Sill.

3.7.3 Geochemical characteristics.

The geochemical characteristics of the Majuba Suite are best described according to the three litho-magmatic groups outlined in section 3.7.2. To recapitulate, these are: high-Fe tholeiites (HFTs); calc-alkaline series (CAS) and low Fe-Mg tholeiites / high-silica rhyolites (HSRs). In all cases, chondrite-normalised REE patterns prove to be extremely diagnostic.

High-Fe tholeiites (HFTs) (16 samples)

The HFT group is dominated by basalts but also contains a small number of minor basic intrusives and basaltic andesites (see Table 3.4). On a chemical basis, the basalts and minor basic intrusives are virtually indistinguishable. The field relations with the other members of the Majuba Suite are not clear, though the drill-core data suggest that the HFTs and the CAS rocks are intercalated within the volcanic pile. Chemically, the HFTs are characterised by relatively primitive REE contents and low LIL and HFS element concentrations. Mg-numbers (100xMgO/(MgO + FeO), atomic ratio) are moderate and fall within the range 51 to 65. The HFTs also share several of the hallmarks which typify standard Fe-rich tholeiitic basalts as defined by the B.V.S.P (1981). These include: high total Fe contents (e.g. 12- 17% $Fe_2O_3^T$), flat to slightly fractionated chondrite-normalised REE patterns and an abundance of opaque oxides.

Primary LIL element values can be inferred from the least evolved and least altered of the HFT rocks e.g. K_2O, 0.18-0.45%; Rb, 4-18 ppm; Ba, 50-260 ppm and Sr, 100-185 ppm. Alternatively, the true magnitude of LIL elements in altered volcanic rocks can be interpolated from the level of the relatively immobile LIL element, Th, on MORB-normalised diagrams (Saunders and Tarney, 1985). The HFT basalts and minor basic intrusives are typically low-Ti and low-Zr rocks with average values of 0.95% TiO_2 and 36 ppm Zr. Copper and Zn concentrations tend to reflect backround values and do not appear to be modified by mineralisation. In the Majuba Suite, as a whole, these elements show a negative correlation with differentiation, which suggests that Cu and Zn were orginally hosted within mafic mineral phases. Lead values are also low and normally fall within the range of 2 to 20 ppm, though Pb values up to 94 ppm are recorded.

As already intimated, the most diagnostic chemical features of the HFTs are the chondrite-normalised REE patterns. Two types of REE pattern can be identified. The first type consists of flat to slightly fractionated, sub-horizontal profiles with La_n/Yb_n* ratios in the order of 1.24 to 1.40 and overall REE abundances of 8 to 12 times chondrite (see Fig. 3.10a). This type of primitive pattern, which is displayed by HFT samples with 46-49% SiO_2, is considered to be characteristic of island arc tholeiites (see Jakes and White, 1972).

* Note: n subscript denotes chondrite-normalised values. Normalising values from Nakamura (1974).

The few minor disturbances to otherwise smooth profiles shown in Fig. 3.10a merit a brief mention. The small positive Ce anomaly (Ce/Ce* = 1.22)* displayed by sample 3-0905 is attributed either to Ce mobility during regional metamorphism or to analytical uncertainity (see section 3.6.2). Plagioclase accumulation may account for the minor positive Eu anomaly (Eu/Eu* = 1.15) shown by sample 4-0294, and indeed, the relatively high CaO and Sr values obtained from this sample would appear to support this hypothesis. However, petrographic observations in the corresponding thin section specimen indicate that thorough carbonatisation has generated the anomalous Eu, Ca and Sr values. The reason for the small positive Ho anomaly (Ho/Ho* = 1.20) shown by the REE profile of sample 5-1750 is not known, though alteration effects or analytical error are the most likely causes.

The second type of REE pattern is noted for its slight to moderate LREE/HREE fractionation, as exemplified by the three samples in Fig. 3.11a. The La_n/Yb_n ratios for these samples, which have SiO_2 values of 50-53%, range from 2.11 to 3.65. In addition, all the samples display sharply positive Ce anomalies (Ce/Ce* = 1.61 to 2.62). As already mentioned, this phenomenon may suggest that the LREE were collectively mobilised and enriched during regional metamorphism, though analytical irregularity may also be a contributing factor. Moreover, it is unlikely that the fractionated LREE/HREE profiles are purely the result of differentiation as the difference in SiO_2 contents between these samples and the ones showing flat REE patterns is only a matter of a few percent.

The Calc-alkaline Series (CAS) (6 samples).

The CAS group of rocks define a SiO_2 range of 51.7% to 61.7% with a strong bias in the sample set towards the more intermediate compositions. Like their HFT counterparts, the CAS rocks are characterised by low HFS element abundances though the latter appear to be more LIL-enriched. Inspite of being more evolved, compositionally, the CAS andesites have comparable Mg-numbers with several of the HFT basalts.

The most striking chemical attribute of the CAS group is the sub-parallel arrays of moderately fractionated REE patterns (see Fig 3.12a). At first glance, these appear to resemble the LREE-enriched HFTs as described above. However, a closer inspection of the data reveals that the CAS rocks, which in the case of Fig. 3.12a are all andesites, have noteably higher La_n/Yb_n ratios, i.e in the order of 4.60 to 6.50. The well-developed positive Ce anomalies shown by samples 1-1555 and 5-2492 once again alerts us to the fact that the fractionated LREE portions of the profiles may not be a pure magmatic effect. However, the fractionated REE trends shown by the the Omai CAS rocks are of the same magnitude as those found in modern calc-alkaline volcanic rocks of island arc settings (see Jakes and White, 1972).

* Ce/Ce* indicates analysed Ce value / Ce value interpolated from REE patterns. Same for Eu/Eu* and Ho/Ho*.

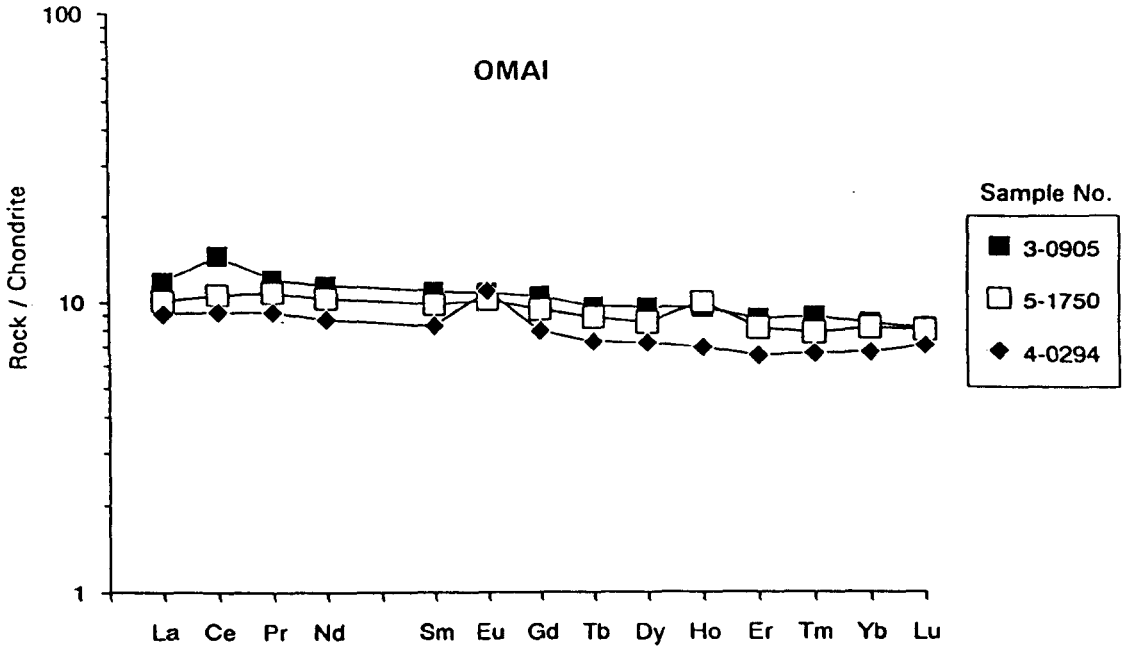

Fig. 3.10a: Chondrite-normalised REE patterns of HFT basaltic rocks from the Majuba Suite, Omai (see text for details). Normalising values from Nakamura (1974).

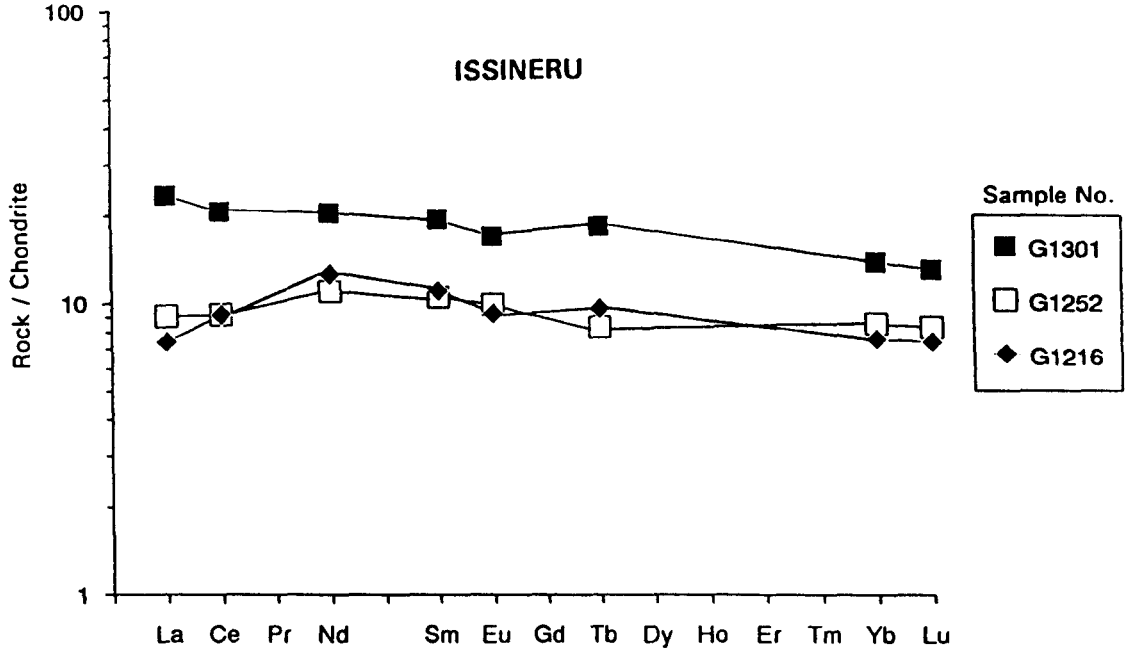

Fig. 3.10b: Chondrite-normalised REE patterns of Fe-rich tholeiitic basalts from the Issineru Formation, Issineru (see text for details). Data from Renner and Gibbs (1987). Normalising values from Nakamura (1974).

For discussion see p. 94.

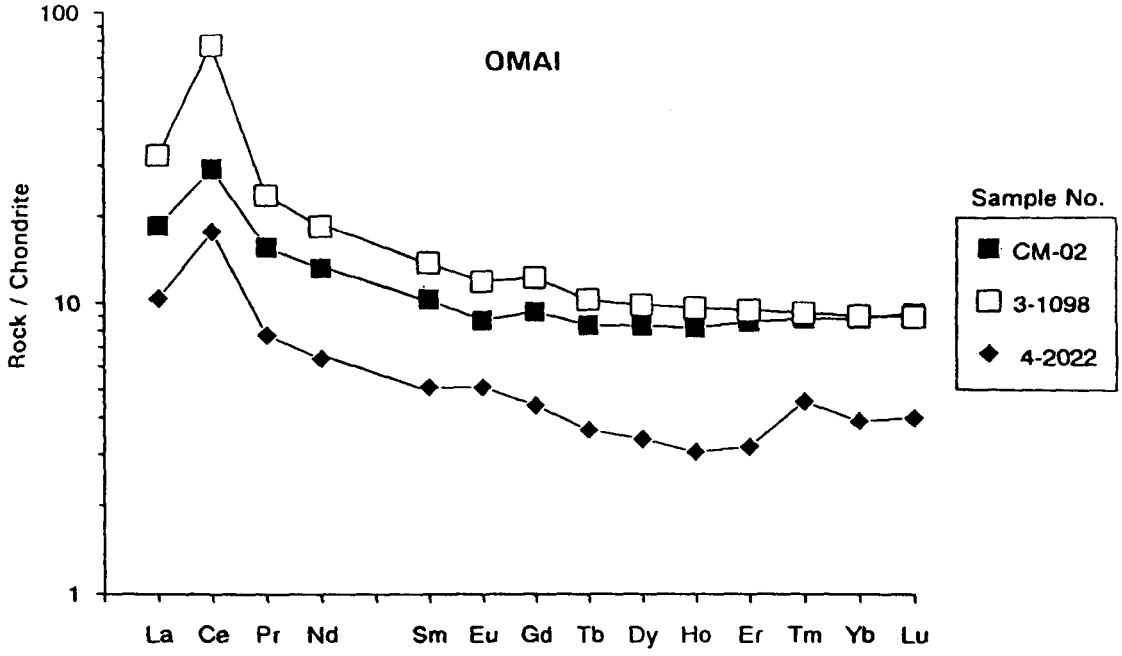

Fig. 3.11a: Chondrite-normalised REE patterns of HFT basaltic rocks from the Majuba Suite, Omai, showing LREE-enriched trends and sharply positive Ce anomalies (see text for details). Normalising values from Nakamura (1974).

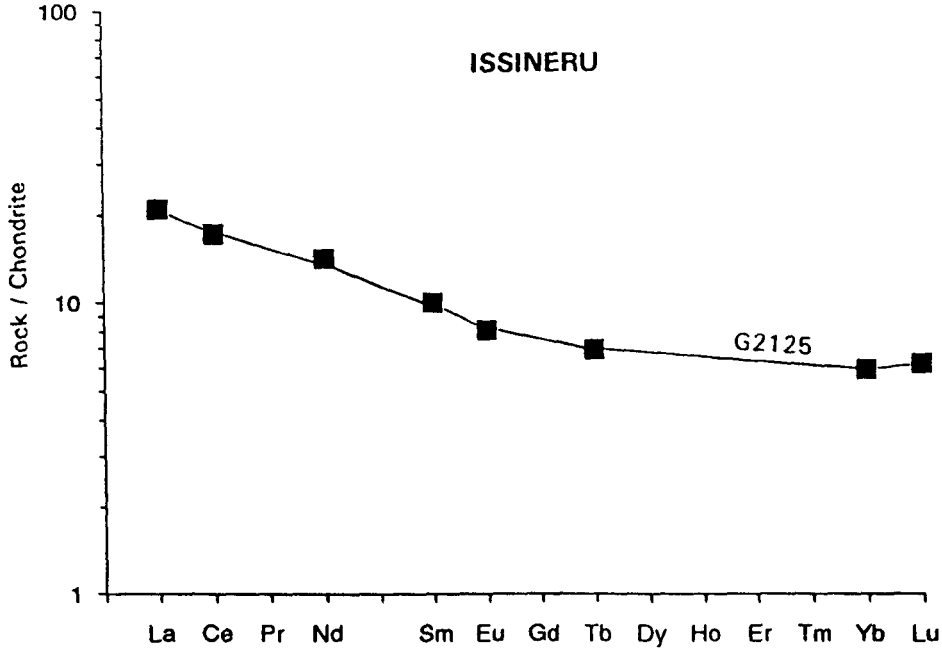

Fig. 3.11b: Chondrite-normalised REE pattern of a porphyritic (tholeiitic ?) basalt from the Issineru Formation, Issineru (see text for details). Data from Renner and Gibbs (1987). Normalising values from Nakamura (1974).
For discussion see p. 94.

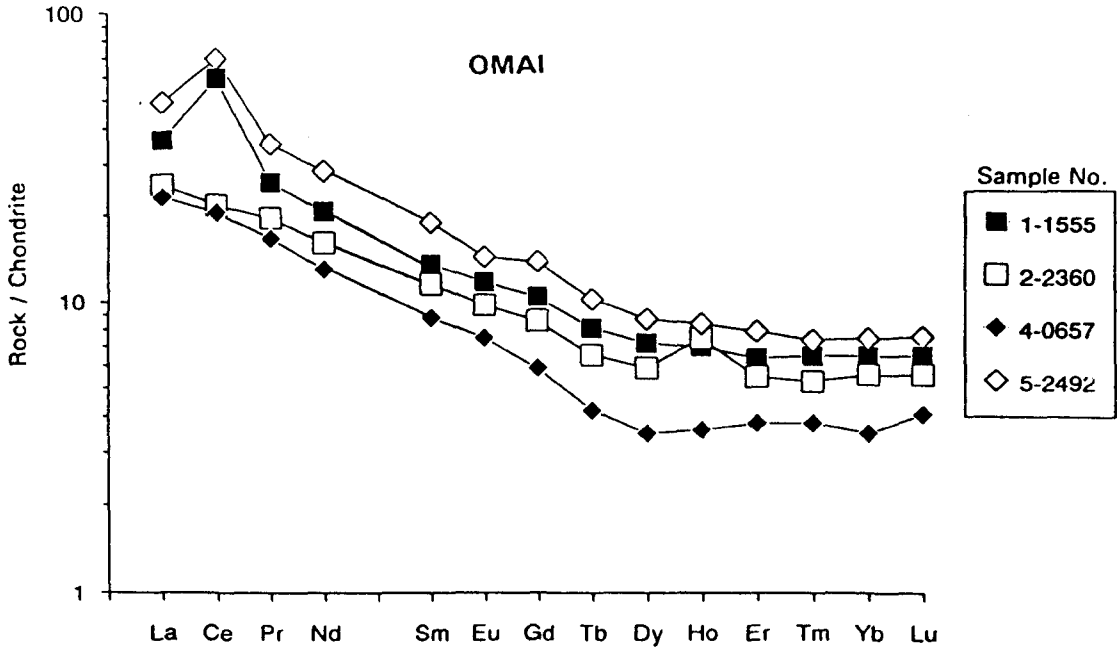

Fig. 3.12a: Chondrite-normalised REE patterns of CAS andesites from the Majuba Suite, Omai, showing fractionated LREE trends and positive Ce anomalies (see text for details). Normalising values from Nakamura (1974).

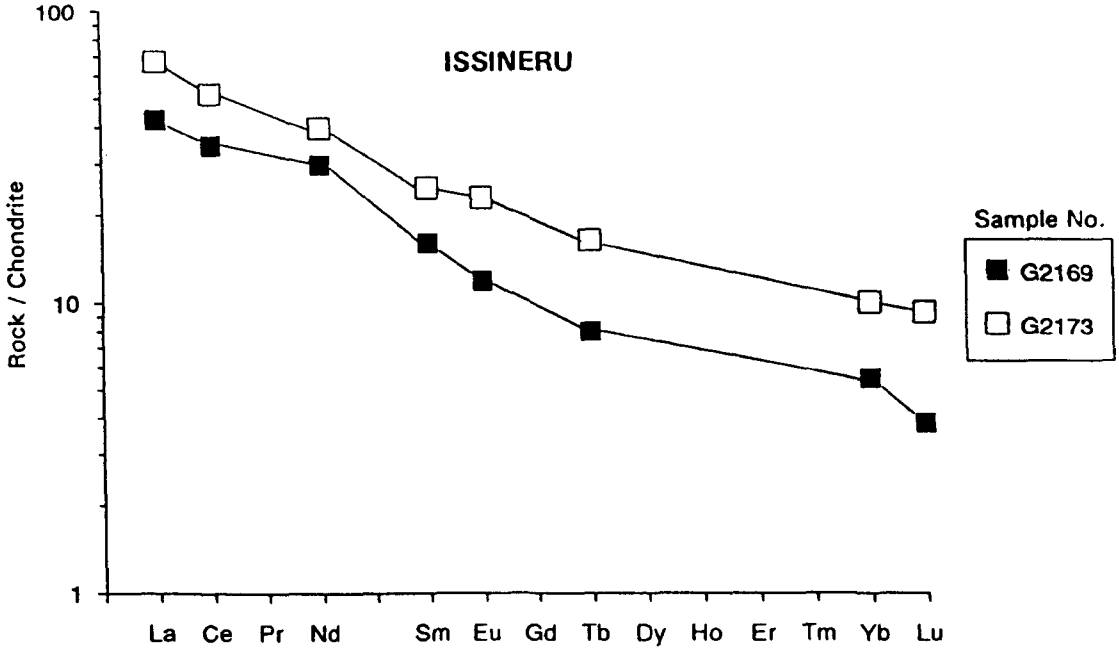

Fig. 3.12b: Chondrite-normalised REE patterns of calc-alkaline hornblende basaltic andesites from the Issineru Formation, Issineru (see text for details). Data from Renner and Gibbs (1987). Normalising values from Nakamura (1974).
For discussion see p. 96.

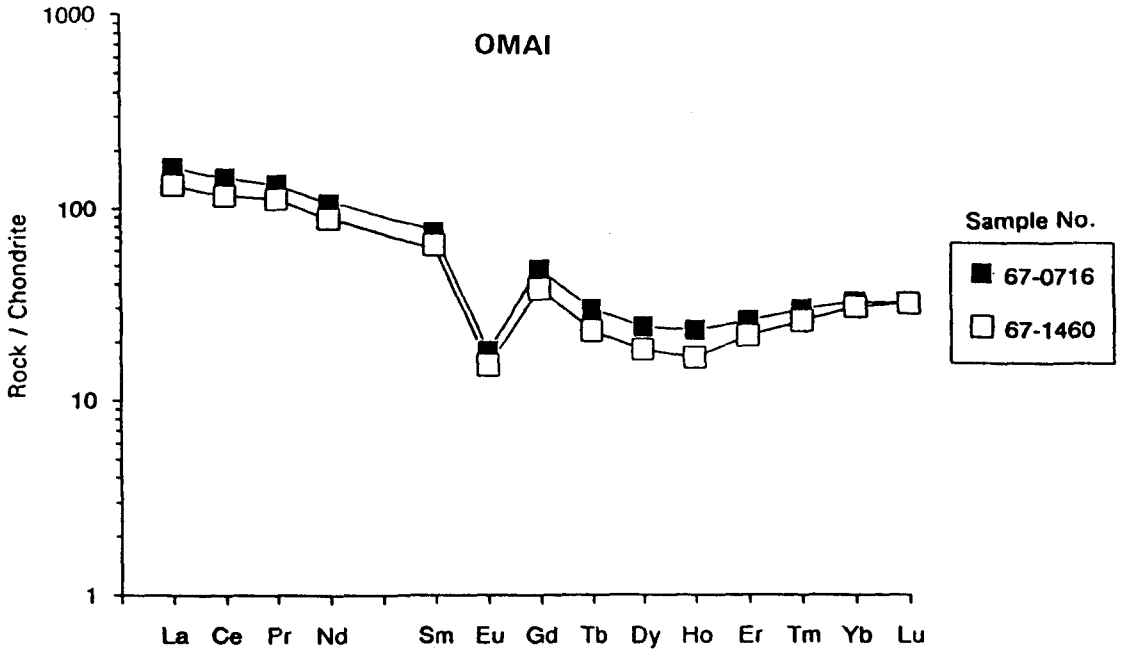

Fig. 3.13a: Chondrite-normalised REE patterns of high-silica rhyolites (HSRs) from the Majuba Suite (Wenot Lake Zone), Omai. Normalising values from Nakamura (1974).

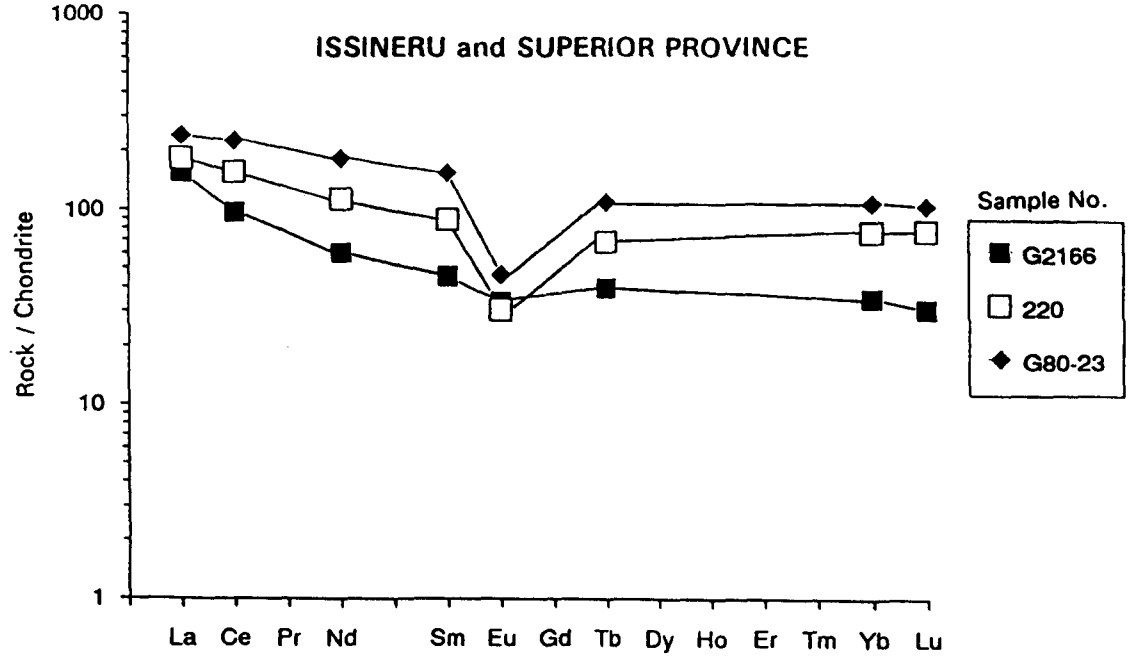

Fig. 3.13b: Chondrite-normalised REE patterns of high-silica rhyolite samples from Issineru and the Superior Province, Canada (see text for details). G2166, Issineru Formation (Renner and Gibbs, 1987); 220, Kamiskotia area, Abitibi belt; G80-23, Confederation Lake area, Uchi belt. Data for Superior Province samples (220 and G80-23) cited in Lesher et al., (1986). Normalising values from Nakamura (1974). For discussion see p. 98.

Low Fe-Mg Tholeiites / High-silica Rhyolites (HSRs) (2 samples).

In this study, analyses of the "soda-dacite" and "soda-dacite porphyry" samples from the Wenot Lake Zone have shown the two rocks to be chemically identical, thus upholding the petrographic observations made by Morton (1990). These chemically distinctive rocks, as their name implies, are first and foremost characterised by their high SiO_2 contents of over 75%. Other conspicously high element contents include, Na_2O (5.3-7.5%), Zr (370-415 ppm), Nb (31-38 ppm), Hf (12-14 ppm) and total REE (257-315 ppm). Zinc values of 180-300 ppm are also relatively high compared to other volcanic rocks of the Majuba Suite. At the other extreme, MgO, TiO_2, CaO, K_2O and P_2O_6 occur in trace amounts along with anomalously low concentrations of Rb, Sr and Ba. The elevated Na_2O/K_2O ratios of 4.4 to 11.8 suggests that these felsic rocks were affected by severe Na metasomatism.

The moderately fractionated wing-shaped REE patterns, with pronounced negative Eu anomalies (Eu/Eu* = 0.25) and deeply concave HREE "tails", further characterise these high-silica rhyolites (see Fig. 3.13a). Total REE abundances are in ther order of 30 to 37 times chondrite with La_n/Yb_n ratios of 4.41 to 5.51.

3.7.4 Petrogenesis.

Petrogenetic origin.

In the absence of isotopic data, the petrogenetic origin of the Majuba Suite cannot be accurately constrained. However, the chemical aspects of the most primitive members of the Suite, i.e the HFT basaltic rocks, provide a few pointers. For example, a strong tholeiitic character coupled with flat to slightly fractionated REE patterns of around 10 times chondritic abundance imply that the HFTs are mantle derivitives. However, their moderate Mg-numbers intimate that the parental magma was clearly not a primary, high-pressure mantle melt, but rather, that low-pressure crystal fractionation processes played a significant role in during genesis.

The coherent linear trends shown by the Harker-type diagrams (Figs. 3.2 and 3.3) imply that the HFTs and the CAS rocks form a co-genetic suite related by simple crystal fractionation mechanisms. However, the dichotomous patterns defined by the data distribution in the Mg-number-SiO_2 and Ce_n/Yb_n-SiO_2 diagrams (Figs. 3.14 a and b respectively) demonstrate that the petrogenentic evolution of the Majuba Suite is not as simple as first thought. For example, Fig 3.14a clearly shows that the HFT and the CAS rocks evolved from a hypothetical parental magma along different fractionation paths. Discrete tholeiitic and calc-alkaline trends can also be identified in Fig. 3.14b, though, here, more data are required to

confirm these trends.

Further insight into petrogenesis of the Majuba Suite may be gained from the study of analogous Palaeoproterozoic greenstone successions. At Cartwright Lake, northwest Manitoba, quantitative modelling by Peck and Smith (1989) indicated that sub-ordinate calc-alkaline andesites were derived from primitive (Mg) tholeiitic basalts by a fractional crystallisation/crustal contamination mechanism followed by low-pressure fractionation. The authors also concluded that their model accounted for the close spatial relationship between the dominant tholeiitic basalts and minor calc-alkaline andesites. It is interesting to note the same field relationships exist in the Majuba Suite at Omai.

In other Precambrian shield areas, high-silica rhyolitic rocks are common constituents of bimodal mafic-silicic volanic sequences, similar to those found in the Wenot Lake Zone (see Lesher et. al., 1986). Moreover, these felsic rocks are reported to have crystallised from the most fractionated and lowest temperature magma erupted (Sisson, 1991). At Omai, according to the Ce_n/Yb_n-SiO_2 diagram of Fig. 3.14b, the HSRs appear to be direct genetic derivitives of the HFTs, generated by extreme fractionation of tholeiitic melts. This hypothesis is supported by the mineral vector diagrams of Figs. 3.15 a and b, though it cannot be substantiated due to insufficient data and the large compositional gap betweeen the HFTs and HSRs. For global HSRs, another petrogenetic model worth consideration includes partial sialic fusion and magma mixing instigated by the ponding of mafic magma at the the base of the lower crust (see Hildreth, 1981; Thurston and Fryer, 1983). The latter authors further propose that the deep negative Eu anomalies, which characterise the HSRs, cannot be accounted for by plagioclase fractionation alone, but are more consistent with volatile fluxing in compositionally zoned magma chambers.

Petrogenetic trends in mineral vector diagrams and chondrite-normalised REE patterns.

Mineral vector diagrams have been successfully used to ascertain the main fractionating mineral phases behind HFS elemental variation in volcanic suites and to provide information regarding eruptive environment (Pearce and Norry, 1979). Using Zr as a differentiation index, this technique is applied to the Majuba Suite in an attempt to elucidate the controlling factors behind the distribution of two key trace elements, Ti and Nb.

The dominant trend (Trend 1) in the TiO_2-Zr diagram of Fig 3.15a demonstrates that Ti variation within the Majuba Suite was strongly influenced by the systematic removal of magnetite from the melt. The chemical data is endorsed by petrographic observations which show an abundance of opaque oxides, especially in the HFT basaltic rocks. According to Pearce and Norry (1979) Ti, Nb and Y distributions are largely governed by clinopyroxene-

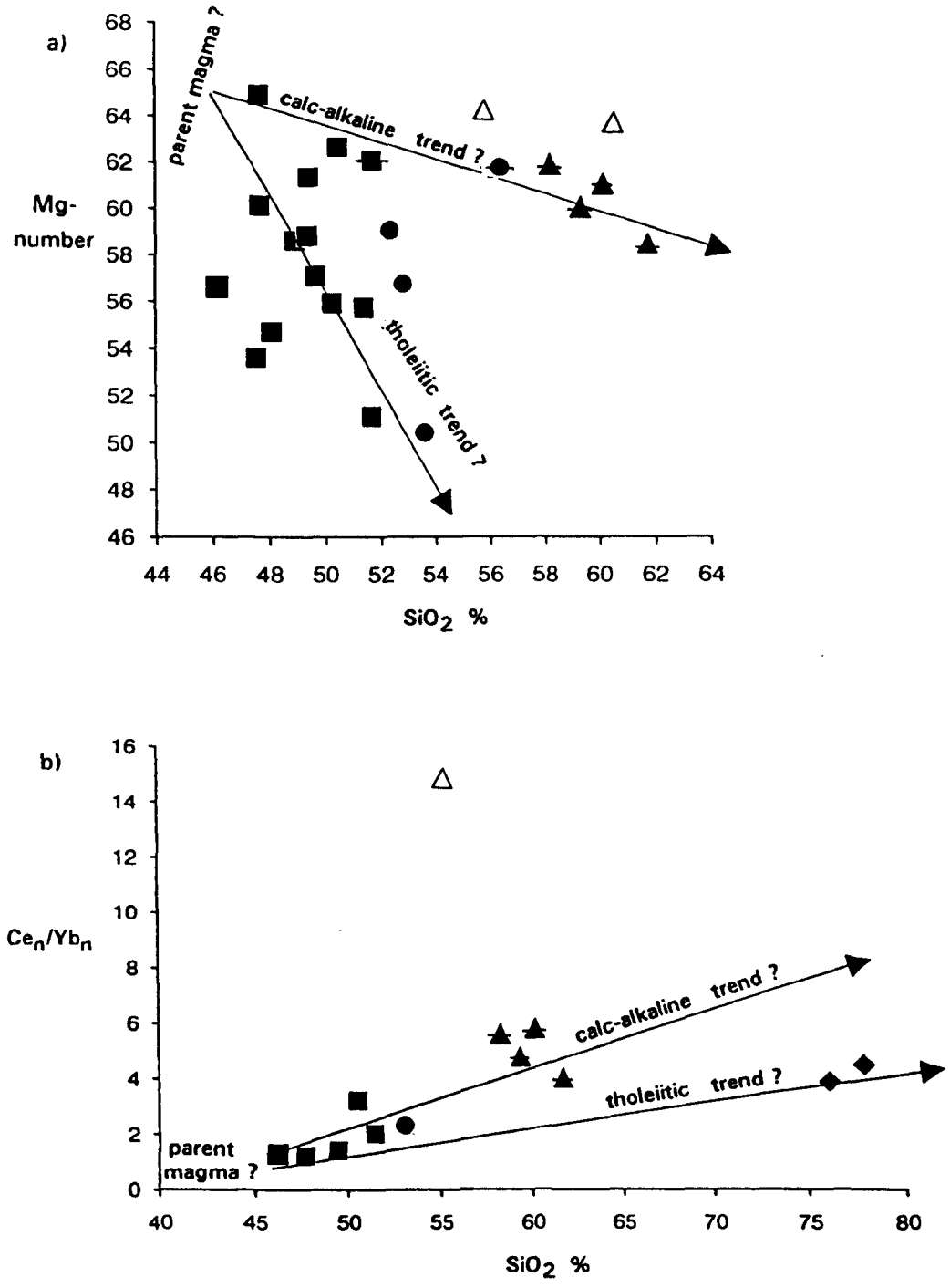

Fig. 3.14: Co-variation diagrams showing possible petrogenetic trends within the Majuba Suite. a) Mg-number -SiO_2; b) Ce_n/Yb_n - SiO_2. HFTs and HSRs tend to lie along a tholeiitic trend whilst the CAS rocks follow a separate, calc-alkaline one (see text for details). Mg-number = 100xMgO/(MgO + FeO) atomic ratio, where FeO is calculated as a function of $Fe_2O_3^T/1.15$. In Fig. 3.14a the HSRs plot off scale and are not shown.

Symbols: solid squares - basalts (with minor basic intrusives); solid circles - basaltic andesites; solid triangles - andesites. Barred symbols represent CAS rocks whilst all others are HFTs, except, solid diamonds - HSRs (Wenot Lake Zone) and open triangles - Captain Mann Sill samples (included for comparison).

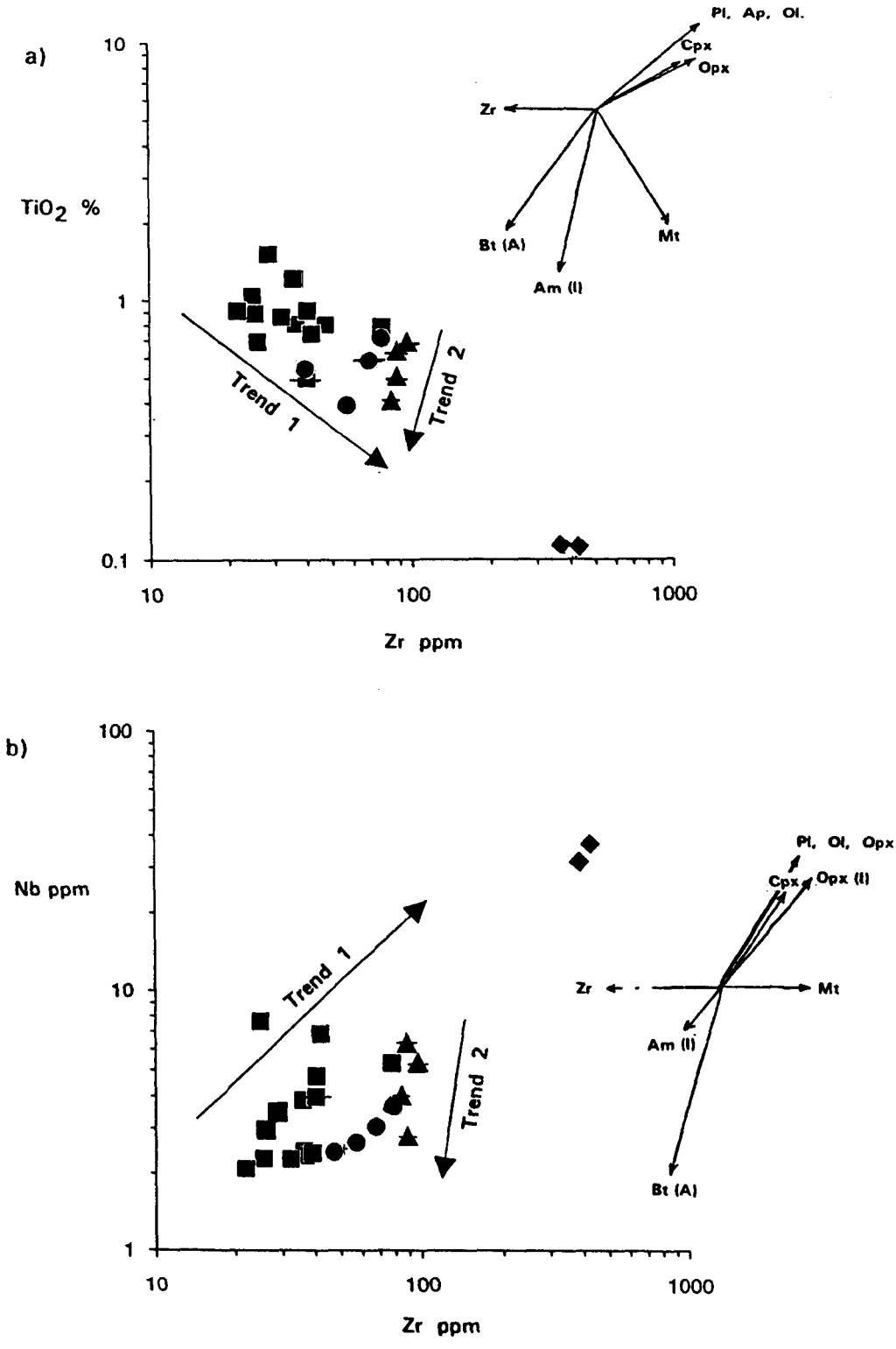

Fig. 3.15: Mineral vector diagrams showing petrogenetic trends within the Majuba Suite (see text for details). a) TiO_2 - Zr; b) Nb - Zr. Mineral vectors from Pearce and Norry (1979); symbols as for Fig. 3.14.

dominated fractionation in island arc settings and amphibole ± biotite fractionation in Andean arcs. In Fig 3.15a, a secondary trend (Trend 2) is defined by the CAS andesites, indicating that amphibole and/or biotite were the main fractionating influences on Ti distribution in these rocks. Supporting petrographic evidence for this trend is somewhat limited, though the evolution of the REE patterns displayed by the CAS andesites in Fig 3.12a is typical of classic amphibole fractionation. This evolution, which is progressive with increasing silica contents, includes a systematic decrease in total REE abundances, a transition from a minor negative Eu anomaly to a small positive one and the development of a concave HREE "tail". The REE patterns of the LREE-enriched HFT basalts also appear to follow these trends (Fig 3.11a), though as already mentioned, the validity of these trends is questionable. Moreover, extensive amphibole fractionation is more commonly associated with intermediate melts as opposed to basic ones.

In the Nb-Zr mineral vector diagram (Fig 3.15b), the dominant trend (Trend 1) reflects the combined influence of plagioclase-olivine-orthopyroxene-clinopyroxene removal from the melt during differentiation of the Majuba Suite, whilst an amphibole/biotite secondary trend (Trend 2) appears to have been the main controlling factor behind the genesis of the CAS andesites. In the HFTs, relicts of olivine, pyroxene and plagioclase have been identified with variable degrees of confidence in thin section whilst the small negative Eu anomalies in the REE patterns testify that plagioclase began to fractionate from the HFT melt at around 50-51% SiO_2.

3.7.5 Tectonic association.

So far, several lines of evidence have suggested that the Majuba Suite has field and petrological affinities akin to volcanic rocks of modern arc settings. First of all, the regional geological setting of basic to acid volcanic cycles overlain by immature clastic sediments (see Table 2.1) point to eruption/deposition in an arc-related environment. More specifically, the Majuba Suite rocks have demonstrated low-pressure crystal fractionation trends (Figs. 3.2 and 3.3) and chondrite-normalised REE patterns (Figs. 3.10a and 3.12a) both of which are consistent with contemporary island arc settings. At this juncture, however, it is necessary to stress that the Precambrian plate tectonic processes are still poorly understood and therefore rocks from ancient terrains do not necessarily have modern analogues in terms of tectonic setting. Nevertheless, as long as this point is borne in mind, comparative studies serve a useful purpose.

In the section below, evidence from discrimination diagrams and MORB-normalised multi-element plots is presented in an attempt to confirm the palaeotectonic affinities of the Majuba Suite, with wider implications for the tectonic association of the Omai region as a whole.

Implications from discrimination diagrams.

The data distribution in the discrimination diagrams of Figs. 3.16 and 3.17 intimate that both HFT and CAS basaltic rocks of the Majuba Suite show a strong tectonic affinity to contemporary primitive island arcs in terms of Ti-Zr, Ti-V and Zr-Y data. Strictly speaking, the Ti-V plot (Fig. 3.16b) may only be applied to volcanic suites not affected by magnetite fractionation. In volcanic arc suites, such fractionation, which is usually confined to calc-alkaline rocks, produces exaggerated Ti/V ratios, and thus, erroneous tectonic affinities (see Shervais, 1982). Although the HFTs have been influenced by magnetite fractionation (Fig 3.15a), this does not seem to radically interfer with the assessment of tectonic setting using Ti-V data. Further evidence for an arc-related eruptive environment is provided by the CAS andesites. In terms of La/Yb and Th/Yb ratios these rocks show excellent correlation with modern orogenic andesites from island arc settings (see Fig 3.18).

The Th-Hf-Ta ternary diagram (Fig 3.19) is useful for discriminatory purposes on three counts. Firstly, it has the capacity to resolve the tectonic association for the complete range (basic to silicic) volcanic rocks as opposed to basalts or andesites only. Secondly, it can be used to discriminate between tholeiitic and calc-alkaline series and thirdly it is a sensitive indicator of crustal contamination (Wood, 1980). The distribution of Majuba Suite data shown in Fig. 3.19 clearly indicates that the majority of samples reflect a destructive plate margin setting. Several samples, however, appear to be anomalous, showing an apparent E-type MORB / within-plate affinity. With respect to the five HFT samples in this group, the anomaly may have been generated by small degrees of crustal contamination introduced to arc tholeiites, though a more likely explanation is that the abundances of Fe-Ti oxides, which characterise the HFTs, have preferentially accomodated Ta(Nb/17) over Hf and Th (see Schock, 1979; Wood, 1980). This hypothesis is substantiated on two scores. Firstly, the petrographic observations show the two most anomalous samples (3-0739 and 4-2409) on the Th-Hf-Ta diagram are rich in opaque oxides. Secondly, the same samples also contain anomalously high TiO_2 values of 1.51% and and 1.21% respectively. The two HSR samples from the Wenot Lake Zone also plot in the E-type MORB / within plate field in Fig. 3.19. This trend can be used to support the model which proposes that universal HSRs are formed in response to partial fusion of juvenile continental crust and subsequent magma mixing with sub-crustal tholeiitic melts.

Unfortunately, the Th-Hf-Ta diagram fails to discriminate between tholeiitic and calc-alkaline rock-types in the Majuba Suite. The fact that many of the HFTs plot in the calc-alkaline field is unusual in that tholeiitic rocks rarely have Hf/Th ratios of less than 3 (Wood, 1980). However, some E-type MORB samples have been documented from 36°N and FAMOUS areas of the Mid-Atlantic ridge with Hf/Th ratios of between 2.3 and 2.5 (Wood, 1980).

Implications from MORB-normalised multi-element plots[**]

HFTs

In total, three distinct MORB-normalised spidergram signatures are identified amongst the HFT basaltic rocks. The first type, which is the most typical of the series, shows a striking similarity to the average Island Arc Tholeiite of Pearce (1982), in which most of the elements, with the exception of the LIL elements, are depleted with respect to MORB (see Fig. 3.20a). Distortion in the LIL elements of the HFT sample can be accounted for by the enrichment of these elements during secondary processes.

The second type of signature is demonstrated by the minor basic intrusive sample 3-1098 in Fig 3.20b. This pattern shows a strong Subduction Zone Component (SZC), i.e. enhanced LIL and LREE elements and depleted HFS contents with respect to MORB. The occurrence of SZCs, especially those with a pronounced Ta-Nb trough, are usually diagnostic of calc-alkaline rocks in evolved arcs. The formation of SZCs have been attributed to various processes including the input of slab-derived fluids and/or subducted sediment in the mantle wedge (see Saunders and Tarney, 1979; Pearce, 1982 and Hole et al., 1984).

The third type of MORB-normalised signature displayed by basaltic rocks of the Majuba Suite is ambiguous and cannot be used to constrain tectonic association. This type of signature which is ostensibly transitional between arc and within-plate settings has also been recorded in Palaeoproterozoic metavolcanic rocks of the Baltic Shield (see Fig. 3.21 a and b). Such signatures may have been produced by a number of processes including 1) extreme LIL enrichment of arc tholeiites (e.g samples 4-2022 and K86, Fig. 3.21a); 2) small degrees of crustal contamination in arc-generated magma or, 3) enhanced Ta, Nb, Hf and Ti values due magnetite-ilmenite accumulation. In Fig 3.21a, the ambiguous MORB-normalised trend of sample 5-1750 can be resolved by a combination of processes 1 and 3.

CAS andesites

The spiky MORB-normalised profile defined by the average CAS andesite (sample AMS, Fig. 3.23b) also testifies to an orogenic origin for the rocks of the Majuba Suite. With respect to the arc tholeiite patterns shown by the HFTs in Fig 3.20a, the average CAS MORB-normalised profile is more fractionated in terms of LIL/HFS element ratios such as Th/Ta, Ce/Nb and Sm/Ti. Such elevated ratios reflect a greater SZC in the CAS rocks.

** The following notes apply to all MORB-normalised multi-element spidergram plots shown in this thesis.
1. K, P and Ti actually denote major oxide values of these elememts.
2. If not reported, tantalum values (Ta*) are calculated as a function of Nb/17 (see Jochum et al., (1986).
3. Interpolated Ce values are used for all samples showing strong positive Ce anomalies (see Table 3.4, note 9).

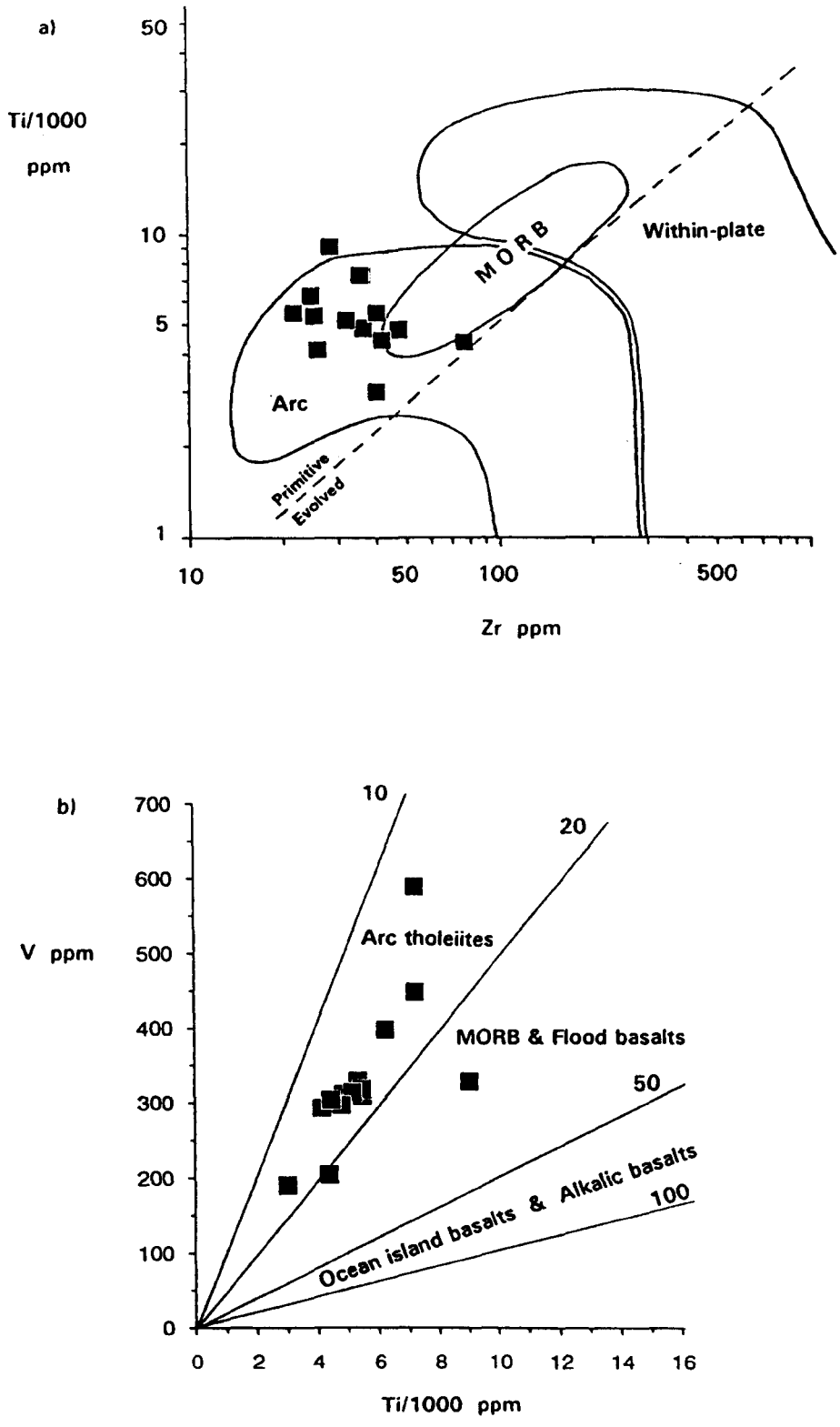

Fig. 3.16: Discrimination diagrams showing palaeotectonic affinites of Majuba Suite basalts (and minor basic intrusives) with respect to contemporary tectonic settings. a) Ti - Zr diagram (field boundaries from Pearce, 1982). b) V - Ti diagram (field boundaries from Shervais, 1982). Numbers in Fig. 3.16b refer to Ti/V ratios.

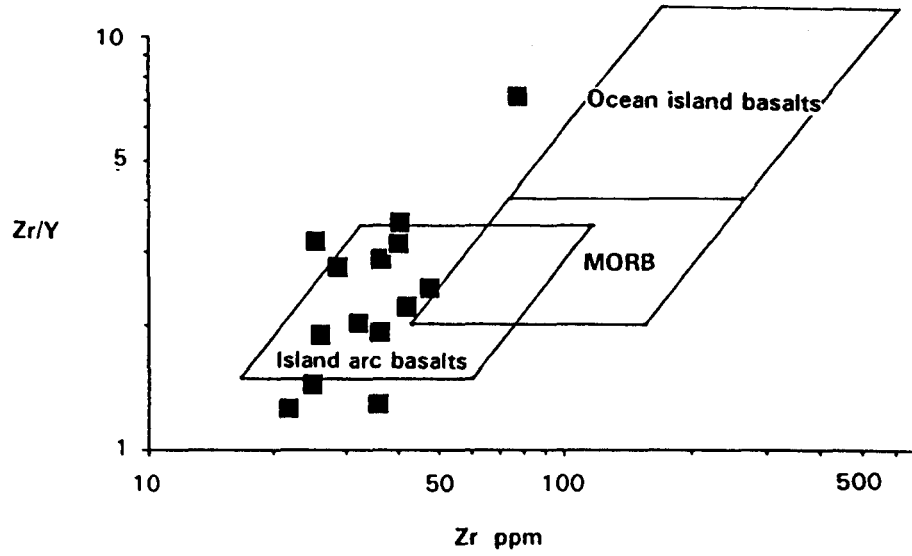

Fig. 3.17a: Zr/Y - Y discrimination diagram showing palaeotectonic affinities of Majuba Suite basalts (and minor basic intrusives) with respect to contemporary tectonic settings. Field boundaries from Pearce and Norry (1979).

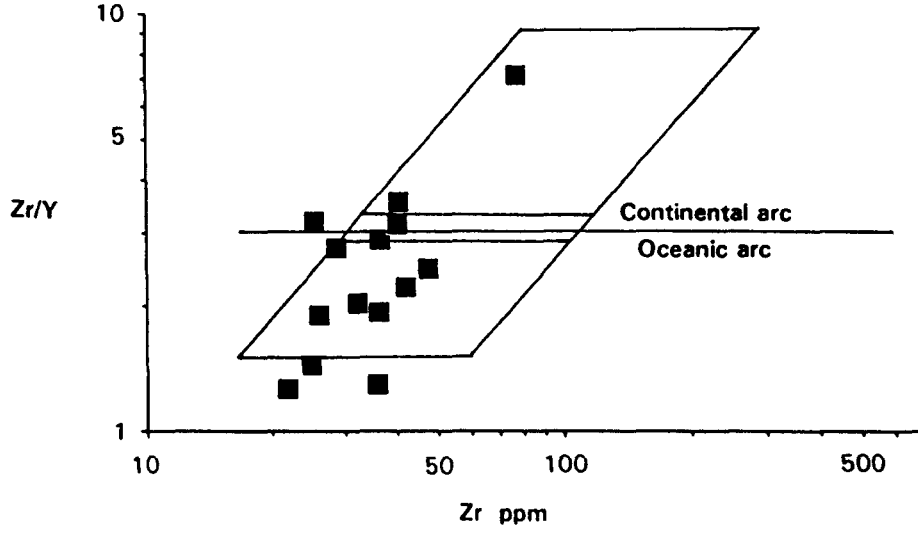

Fig. 3.17b: Zr/Y - Y discrimination diagram indicating that the Majuba Suite basalts (and minor basic intrusives) have modern oceanic arc affinities as opposed to continental arc. Field boundaries from Pearce (1983). This diagram may only be applied to volcanic suites that demonstrate an island arc affinity in the Zr/Y - Zr diagram of Fig. 3.17a.

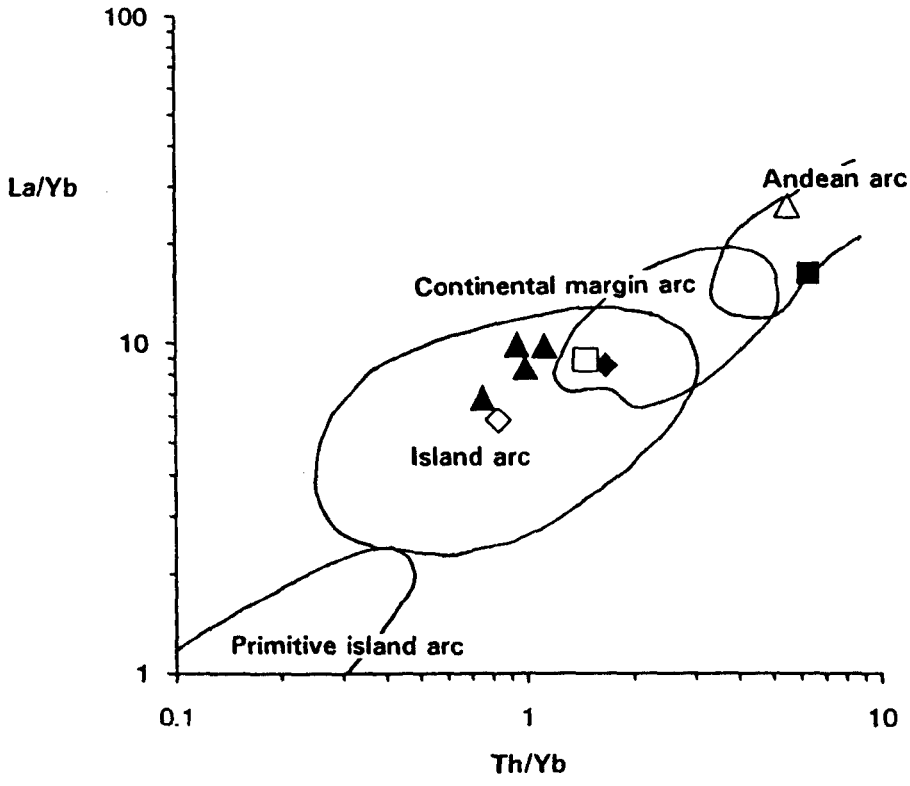

Fig. 3.18: La/Yb - Th/Yb discrimination diagram showing the palaeotectonic affinities of various Precambrian greenstone andesites with respect to the tectonic settings of modern orogenic andesites. Field boundaries from Condie (1989).

Symbols:

Solid diamond - average Archaean (3500-2500 Ma) andesite (Condie, 1989).

Open diamond - average Proterozoic (2500-1500 Ma) andesite (Condie, 1989).

Solid triangles - CAS andesites, Majuba Suite, Omai.

Open triangle - basaltic andesite, Captain Mann Sill (sample CM-03), Omai.

Solid square - average two-pyroxene andesite, Issineru Formation, Issineru (Renner and Gibbs, 1987).

Open square - average calc-alkaline hornblende andesite, Issineru Formation, Issineru (Renner and Gibbs, 1987).

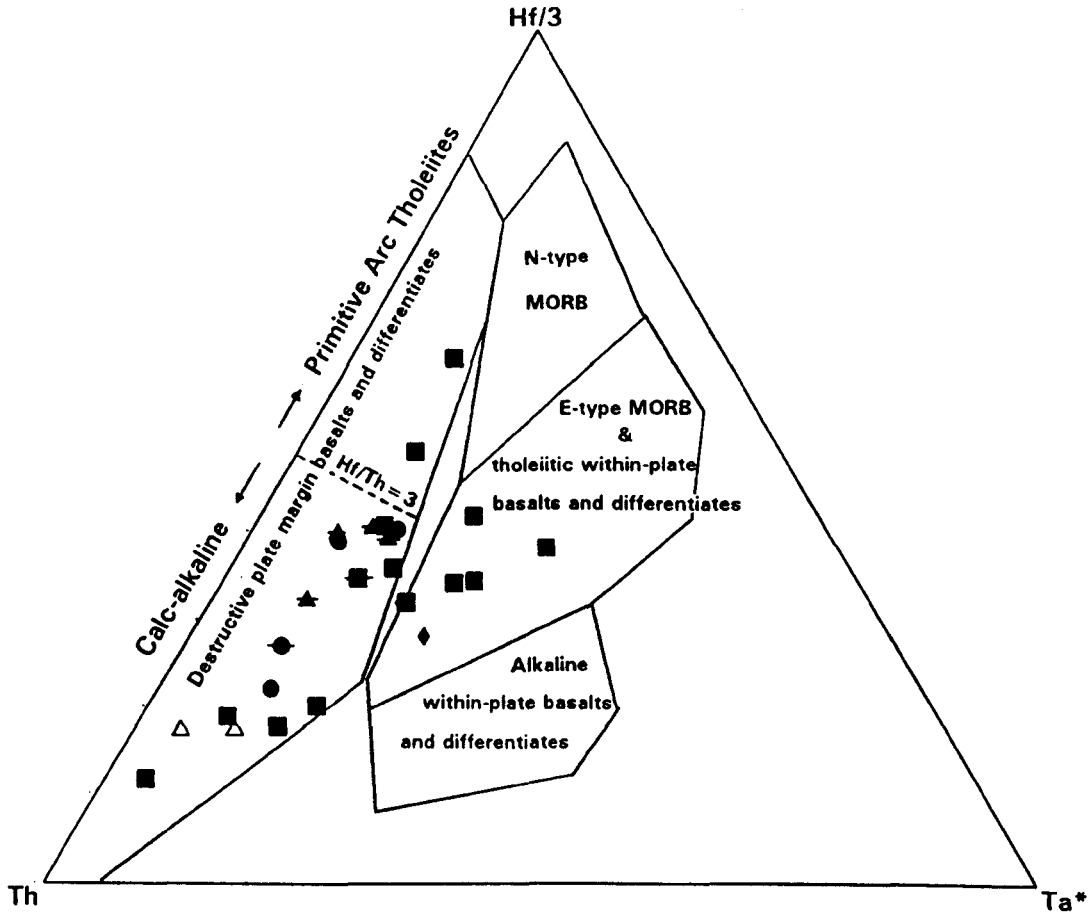

Fig. 3.19: Th-Hf-Ta discrimination diagram showing the palaeotectonic affinities of the Majuba Suite and Captain Mann Sill rocks with respect to contemporary tectonic settings (see text for details). Field boundaries from Wood (1980).

Symbols: solid aquares - basalts (with minor basic intrusives); solid circles - basaltic andesites; solid triangles - andesites. Barred symbols represent CAS rocks whilst all other are HFTs, except, solid diamonds - high -silica rhyolites (HSRs), Wenot Lake Zone and open triangles - Captain Mann Sill samples.

Note: Ta* denotes that all tantalum values are calculated as a function of Nb/17 (see Jochum et al., 1986).

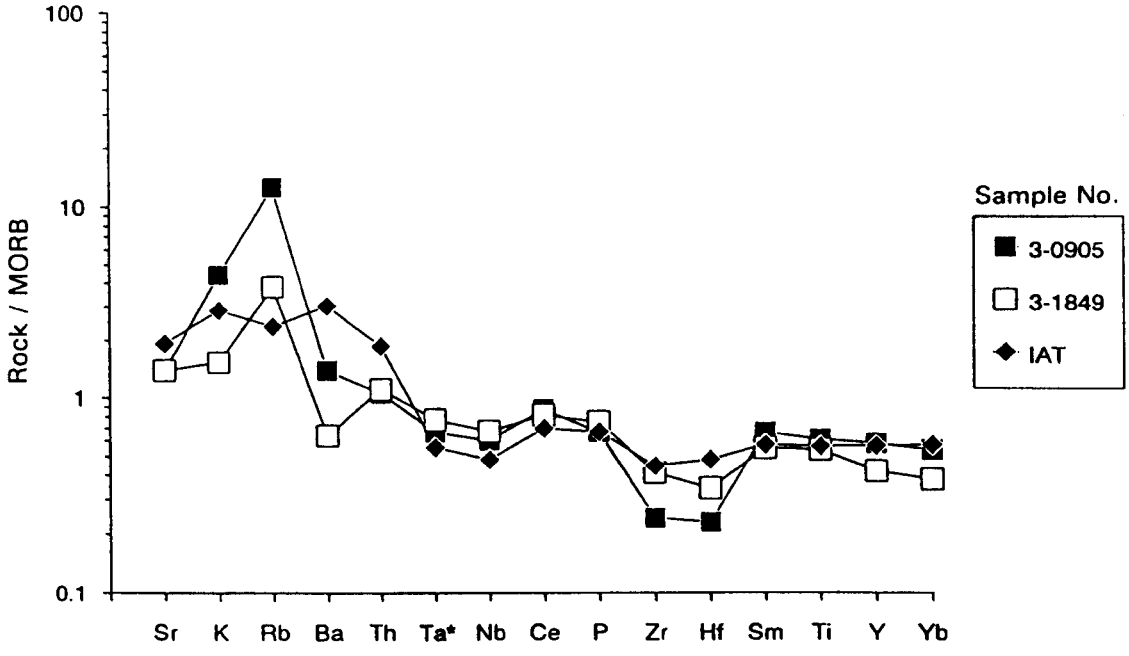

Fig. 3.20a: MORB-normalised multi-element diagram showing the similar trace element compositions between HFT basalts of the Majuba Suite (samples 3-0905 and 3-1849) and the average Island Arc Tholeiite (IAT) of Pearce (1982). Normalising values from Pearce (1982).

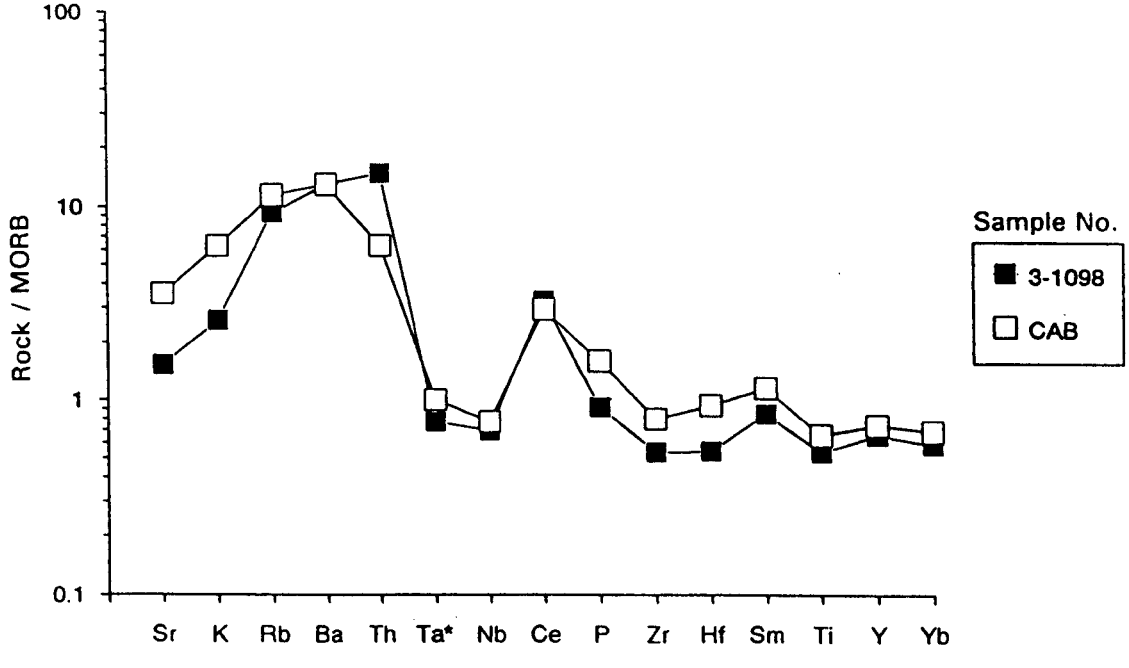

Fig. 3.20b: MORB-normalised multi-element diagram showing the similarity in trace element compositions between a LREE-enriched HFT minor basic intrusive of the Majuba Suite (sample 3-1098) and the average Calc-alkaline Arc Basalt (CAB) of Pearce (1982). Normalising values from Pearce (1982).

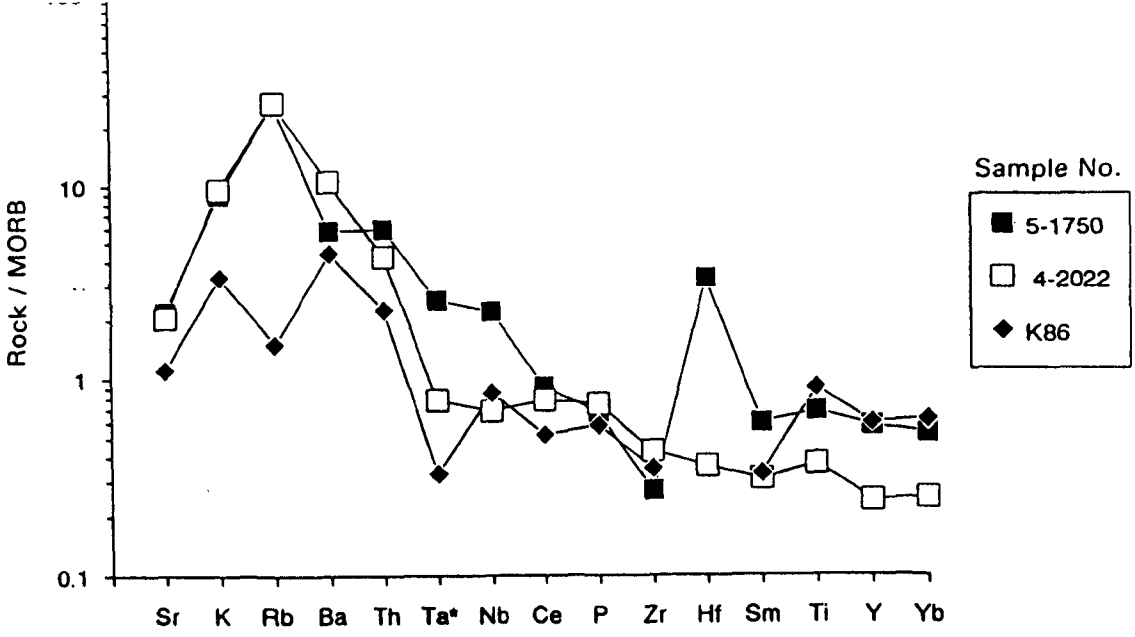

Fig. 3.21a: MORB-normalised multi-element diagram showing the broadly comparable trace element patterns between HFT basalts of the Majuba Suite (samples 5-1750 and 4-2022) and a contemporaneous basalt (K86) from the Vittangi Greenstone Group, Baltic Shield. These patterns are ambiguous and cannot be used to ascertain tectonic affinities (see text for details). K86 sample data from Pharaoh and Pearce (1984); normalising values from Pearce (1982).

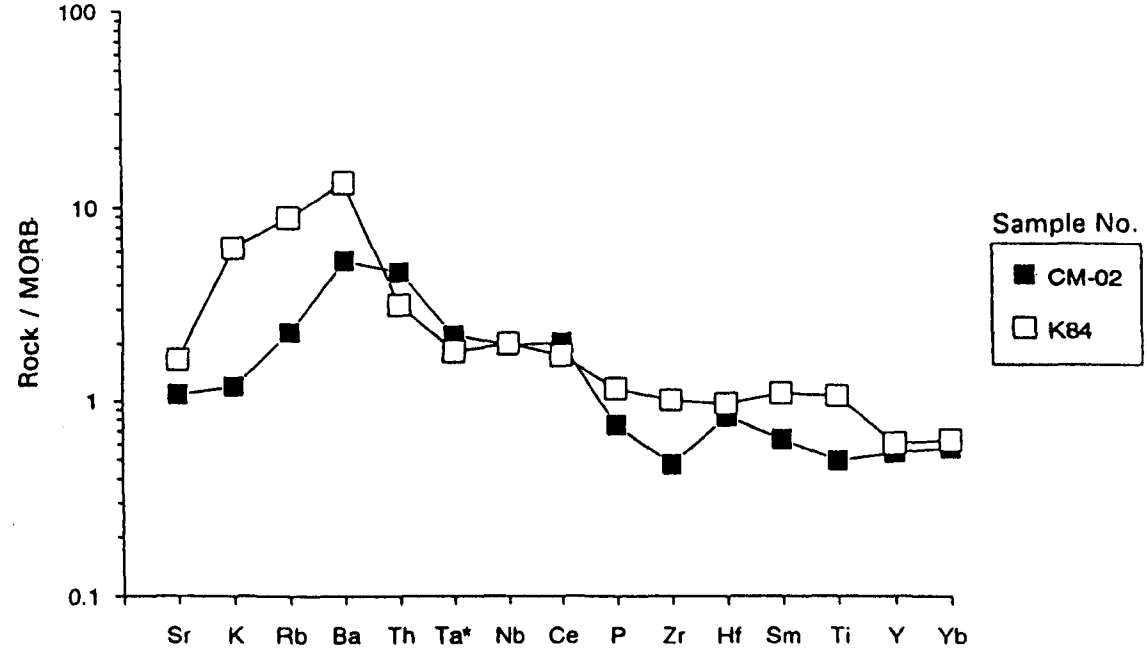

Fig. 3.21b: MORB-normalised multi-element diagram showing the broadly comparable trace element patterns between a HFT basalt (sample CM-02) of the Majuba Suite and a contemporaneous basalt (sample K-84) from the Vittangi Greenstone Group, Baltic Shield. These patterns are ambiguous and cannot be used to ascertain tectonic affinities (see text for details). K84 sample data from Pharaoh and Pearce (1984); normalising values from Pearce (1982).

3.7.6 Regional correlation.

As previously mentioned, very little detailed geological research has been conducted within Guyana over the past two decades owing to former political policy, adverse terrain and poor communications. This statement also rings true for several other Guiana Shield countries. Nonetheless, the regional review of the Barama-Mazaruni Supergroup by Allan Gibbs (PhD thesis, 1980) remains Guyana's most comprehensive geological study to date and provides an excellent platform for further research. In more recent years, two complimentary MSc theses (O'Day, 1984; Renner, 1985) were carried out under Gibbs supervision in the Issineru area of the Mazaruni greenstone belt. (see location map, Fig. 3.22). The Issineru area which is located 250 km northwest of Omai was selected because it afforded the most representative, least deformed and best exposed stratigraphic section (i.e. the Issineru Formation) of the Mazaruni belt and probably the Barama-Mazarui Supergroup as a whole.

Renner's (1985) work is particularly pertinent to this study because it focuses on the geochemistry of the meta-volcanic portions of greenstone stratigraphy whereas O'Day's study emphasises the geology and petrography of the overlying meta-sedimentary rocks. Review papers by Gibbs (1987a) and Renner and Gibbs (1987) have also proved to be useful and readily accessible sources of data. In the following sections an attempt is made first and foremost to correlate the Majuba Suite rocks with the documented lithologies of the Mazaruni Group at Issineru. Secondly, a brief reference is made to the greenstone successions of the Guiana Shield at large, though here too, trace element data are rather sparse. Finally, the Majuba Suite rocks are examined in terms of their geochemical properties relative to global Precambrian greenstone sequences and modern analogues.

The lithostratigraphy of the Omai area correlates reasonably well with the upper 2 km of the Issineru Formation where tholeiitic basalts and contemporaneous gabbroic intrusions are interbedded with calc-alkaline intermediate and felsic rocks. The large volumes of sediment in the greater Omai area (see Fig. 2.3) also indicate that the Omai supracrustals rocks are close to the top of the greenstone succession.

<u>HFT basalts</u>

On the grounds of field, petrographic and geochemical properties the Omai HFTs can be readily correlated with the sub-ophitic, low-K, Fe-rich tholeiitic basalts recorded at Issineru by Renner (1985). Like the Omai HFT basalts, their counterparts at Issineru are mainly characterised by near-horizontal chondrite-normalised REE patterns of around 10 times chondrite (see Figs. 3.10 a and b). Depleted LREE patterns have also been identified at Issineru but not at Omai as yet. The LREE-enriched patterns of some Omai HFTs may have

an equivalent at Issineru (see Figs. 3.11 a and b). Renner and Gibbs (1987) suggest that their porphyritic basalt sample (G2125) which displays this the LREE-enriched pattern may actually be calc-alkaline. However as outlined in section 3.6.2, LREE enrichment in the Omai HFTs may have been induced by secondary processes. No data is avaliable for the gabbroic components at Issineru, though by analogy with Omai, it is assumed that they are chemically identical to the tholeiitic basalts with which they are associated. Slightly further afield, primitive low-K tholeiitic basalts, known as the Brokolonko metabasalts, dominate the Marowijne Group greenstones at Stonbroekoe in neighbouring Surinam (see Fig. 3.22 and Veenstra, 1978). Stratigraphically, these supracrustal rocks are contiguous with the Barama-Mazaruni Supergroup of Guyana.

In contrast to the Omai HFTs, which demonstrate strong affinities to contempory island arc tholeiites, Renner (1985) concluded that the Issineru tholeiites showed tectonic affinities similar to modern ocean floor basalts (OFBs), though the general picture proved to be unclear. Gibbs (1987a) demonstrated that basalts from across the Guiana Shield plotted in all three fields (arc, MORB and within-plate) on the Ti-Zr discrimation diagram of Pearce (1982). In this respect, the Guiana Shield basalts are similar to global basalts from Precambrian greenstone terrains (see Condie, 1989). However, it is interesting to note that individual greenstone terrains may express a specific tectonic association. For example, Leube et al., (1990) propose that the Palaeoproterozoic tholeiitic basalts of the Birimian Supergroup, Ghana, show a consistent MORB-type chemistry.

The MORB-normalised profiles shown in Fig. 3.23a attempt to compare the Omai HFT basalts with global basalts from Precambrian greenstone terrains. Here, the similarity in the MORB-normalised patterns between the various average basalts in style and incompatible element abundances is remarkable. Generally, the patterns are LIL-enriched with respect to MORB and show a characteristic Ta-Nb trough. Making allowances for LIL enrichment due to secondary processes at Omai, the average HFT basalt appears to be more compatible with the average Archaean (3500-2500 Ma) basalt than the average Proterozoic (2500-1500 Ma) basalt. Overall, the Omai HFTs are stongly depleted in Zr with respect to other Precambrian basalts.

CAS andesites

By way of REE patterns (Fig. 3.12a) and La/Yb-Th/Yb ratios (Fig 3.18) the CAS andesites have already demonstrated strong chemical similarities to modern orogenic andesites from island arc settings. Within the Mazaruni greenstone belt, the CAS andesites appear to show a good stratigraphic and chemical correlation with the rather rare calc-alkaline hornblende andesites documented at Issineru by Renner (1985) and Renner and Gibbs (1987). This

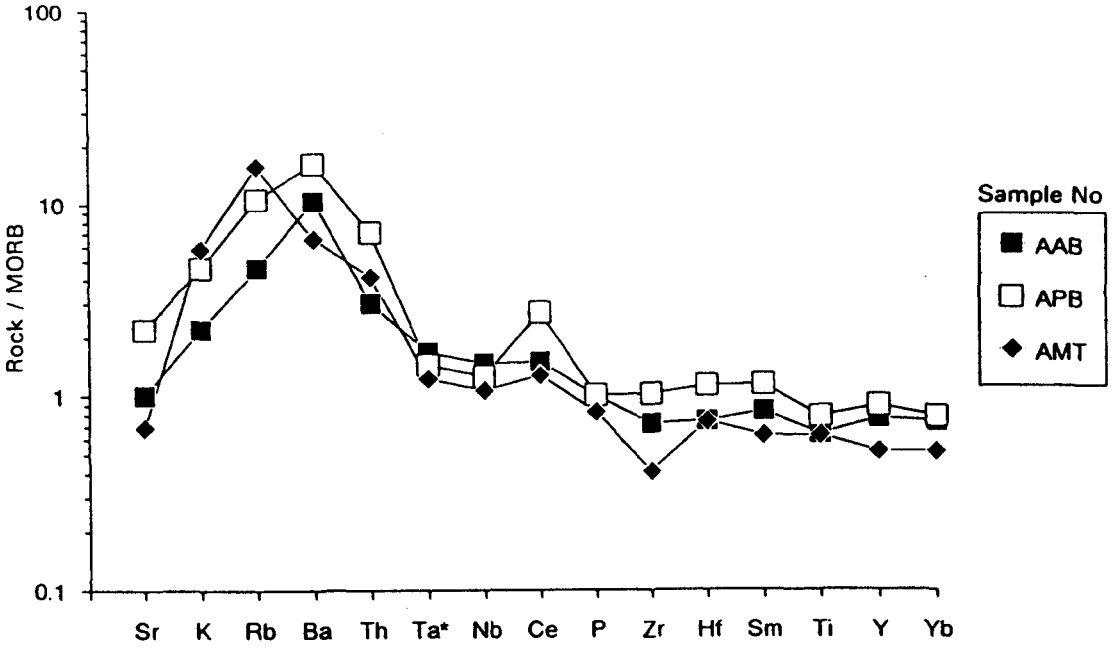

Fig. 3.23a: MORB-normalised multi-element diagram comparing the trace element composition of the average Majuba Suite HFT basalt and minor basic intrusive (AMT) with average global Precambrian greenstone basalts. AAB - average Archaean (3500-2500 Ma) basalt; APB - average Proterozoic (2500-1500 Ma) basalt. Global data from Condie (1989); normalising values from Pearce (1982).

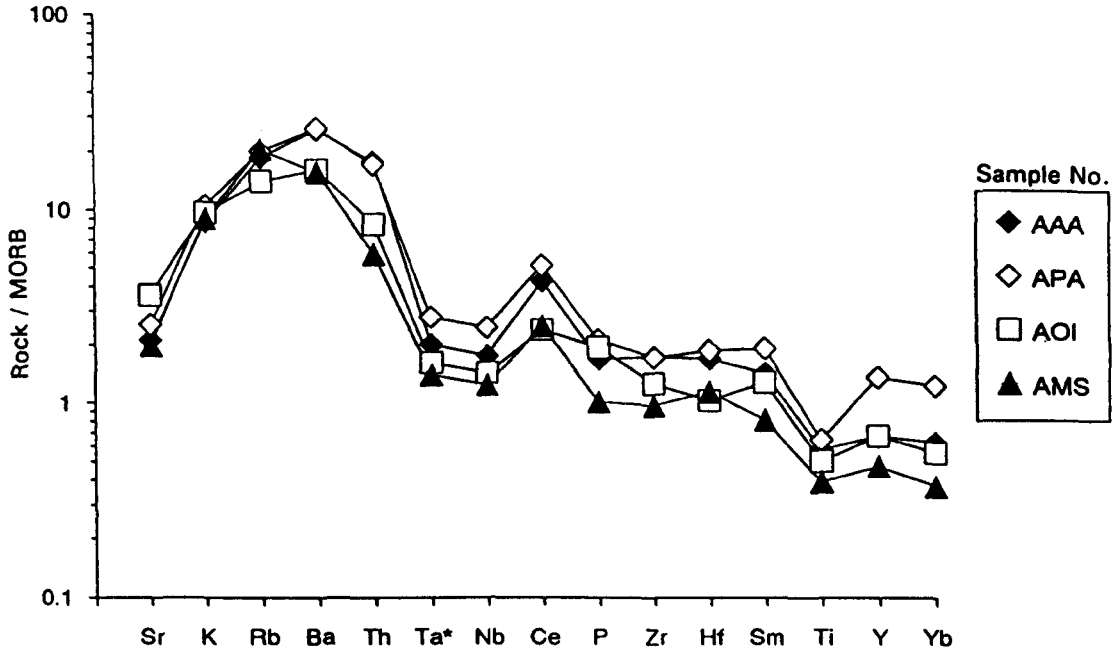

Fig. 3.23b: MORB-normalised multi-element diagram comparing the trace element compositions of the average Majuba Suite CAS andesite (AMS) with average Precambrian to Recent orogenic andesites. AAA - average Archaean (3500-2500) greenstone andesite; APA - average Proterozoic (2500-1500 Ma) greenstone andesite (both from Condie, 1989). AOI - average "other" oceanic island arc andesite (Bailey, 1981). Normalising values from Pearce (1982).

correlation is epitomised by the similar fractionated REE patterns as illustrated in Fig. 3.12 a and b.

The MORB-normalised multi-element plot of Fig. 3.23b compares the incompatible trace element patterns of the average CAS andesite with average andesites from global Precambrian greenstone belts and Tertiary to Recent oceanic island arc settings. The diagram demonstrates that all the signatures show a striking similarity in style and elemental abundances, though the Omai CAS andesites appear to show a marginally better correlation with modern, as opposed to Precambrian, andesites. In all cases, the signatures are characteristed by fractionated profiles and enhanced SZCs which are universally diagnostic of orogenic volcanic rocks.

HSRs

Low-volume spherulitic felsic volcanic rocks of tholeiitic and calc-alkaline affinities have also been recorded at Issineru (Renner, 1985). These rocks are apparently common throughout the Barama-Mazaruni Supergroup of northern Guyana. The Omai HSRs can be readily correlated with tholeiitic rhyolitic rocks at Issineru which are also characterised by distinct wing-shaped REE patterns with conspicuous negative Eu anomalies and elevated total REE contents (see Fig. 3.13b). On the other hand, the Issineru calc-alkaline rhyolites are noted for their fractionated REE patterns (Renner and Gibbs, 1987) which closely resemble those displayed by the CAS andesites at Omai.

On a world scale, the Omai HSRs show good field and chemical correlation with similar rocks in the Superior Province of Canada (see Fig. 3.13b). In particular, the Omai HSRs are comparable to the FIIIb felsic volcanic horizons defined by Lesher et al. (1986). In the Superior Province, these horizons are of vital economic importance as they host substantial volcanogenic massive sulphide (VMS) deposits. Similar VMS deposits have yet to be discovered within the Guyanese greenstone belts.

3.8 Geochemistry of the Captain Mann Sill

Despite the apparent conformable field relationships with the Mazaruni Group greenstones, the petrographic and chemical data suggest that the Captain Mann Sill is a late-tectonic intrusive feature, post-dating greenstone volcanism and metamorphism. In thin section, the two Captain Mann samples (CM-03 and CM-04) are relatively fresh compared to their greenstone counterparts and are characterised by a seriate-porphyritic texture in which plagioclase, amphibole and pyroxene phenocrysts are readily identifiable. The sections also show a strong mineral alignment which was probably induced during emplacement as

opposed to regional metamorphism.

On the basis of silica contents, the two Captain Mann samples are classified as basaltic andesite (CM-03) and andesite (CM-04), though the magmatic affinity of these samples is ambiguous. For example, according to the Zr/TiO_2-Nb/Y diagram of Fig. 3.8, sample CM-04 has a mild alkaline character, plotting in the trachyandesite field, whereas sample CM-03 is sub-alkaline. Both samples plot in the calc-alkline field in the Jensen cation diagram (Fig. 3.9), though the elevated La_n/Yb_n ratio displayed by sample CM-03 is more typical of alkalic or shoshonitic volcanic rocks.

The Captain Mann andesites are distinguished from the CAS andesites by their anomalous trace element characteristics which include enhanced LIL (Rb, Ba, Sr, Th), Zr, Nb, Hf, U, P, LREE, Ni and Cr concentrations. In this respect, the Captain Mann andesites closely correlate with the dioritic dykes of the Gilt Creek Suite which cut the Omai Stock. Both rock types are characterised by highly fractionated REE patterns as shown in Fig. 3.24a. From a petrogenetic point of view, this anomalous trace element geochemistry, implies that the Captain Mann Sill is not cogenetic with the CAS andesites, nor is it geneticaly related to the HFTs or HSRs. This hypothesis is borne out by the aberrant datum plot of CM-03 on the Ce_n/Yb_n-SiO_2 diagram of Fig. 3.14b. The petrogenesis of the Captain Mann Sill is discussed along with the Gilt Creek Suite Suite in Chapter 5, section 5.7.2.

Regarding tectonic association, the Captain Mann sample, CM-03, shows a well-defined arc signature on the MORB-normalised multi-element plot of Fig. 3.25. This pattern may reflect a substantial crustal component, as in modern continental-margin andesites. This supposition is apparently supported by the fact that sample CM-03 plots within the Andean arc field on the La/Yb-Th/Yb diagram of Fig. 3.18.

At Issineru, Renner and Gibbs (1987) identified relatively pristine, porphyritic sills of andesitic-trachyandesitic composition. These intrusive bodies occupy a similar stratigraphic position to the Captain Mann Sill at Omai. Moreover, the Omai and Issineru post-greenstone sills share a similar trace element geochemistry as epitomised by comparable REE patterns (see Figs. 3.24 a and b), MORB-normalised signatures (Fig. 3.25) and Andean arc tectonic affinities (Fig. 3.18). On a wider regional scale, Gibbs (1987a) proposed that the Issineru two-pyroxene andesites may be related to the voluminous continental felsic volcanic rocks of the Uatuma Supergroup (ca 1.92 to 1.69 Ga.) which is widely distributed throughout the Guiana Shield. In central Guyana, this mainly alkaline anorogenic suite is represented by the Iwokrama which outcrops about 80 km south of Omai. Gibbs hypothesis, however, appears to be repudiated by the fact that both the Omai and Issineru post-greenstone sills show strong orogenic tendencies as opposed to anorogenic ones.

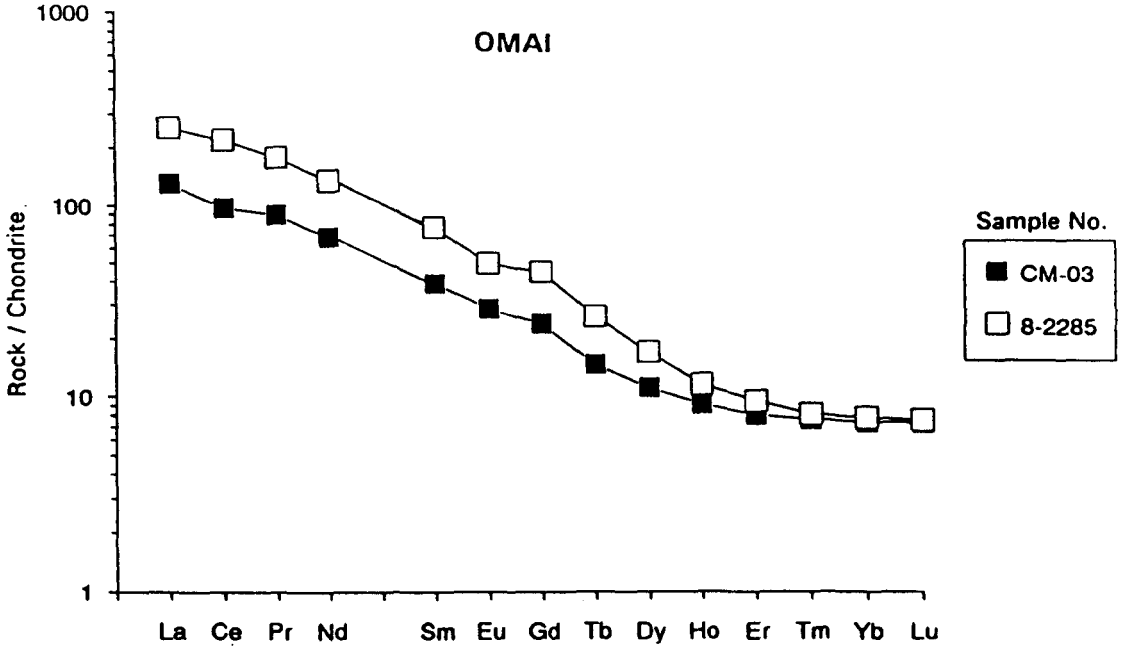

Fig. 3.24a: Chondrite-normalised REE patterns showing the comparable trends between a basaltic andesite (CM-03) from the Captain Mann Sill and a dioritic dyke sample (8-2285) from the Gilt Creek Suite, Omai Stock Zone. Normalising values from Nakamura (1974).

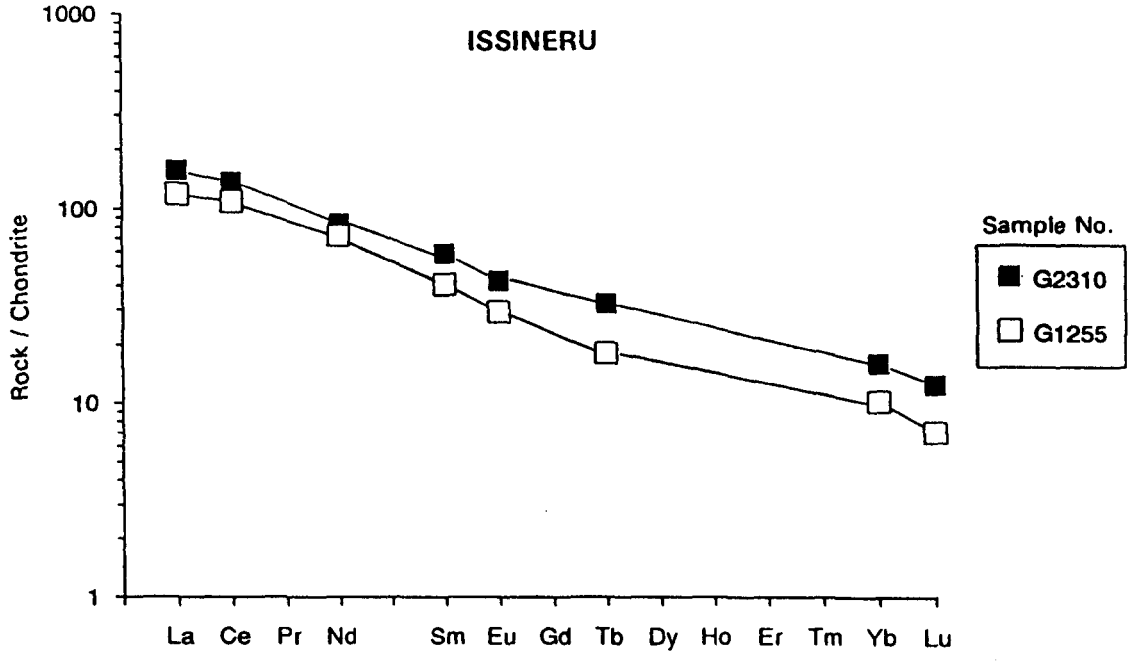

Fig. 3.24b: Chondrite-normalised REE patterns for two-pyroxene andesites of the Issineru Formation, Issineru. Data from Renner and Gibbs (1987). Normalising values from Nakamura (1974)

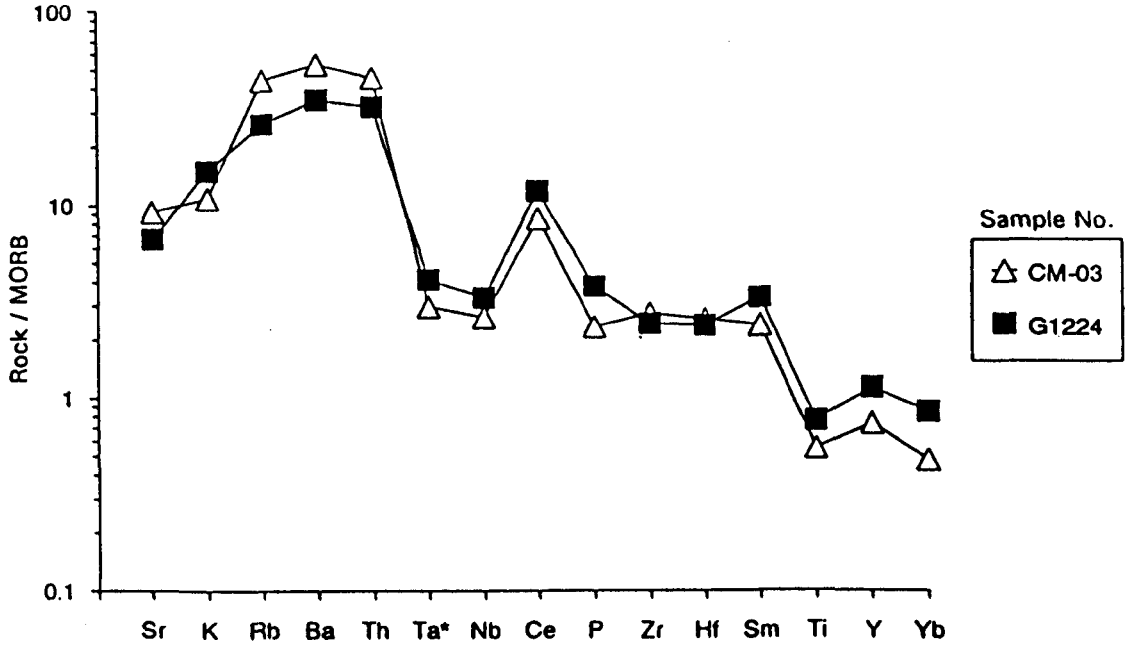

Fig. 3.25: MORB-normalised multi-element diagram showing the comparable trace element compositions between the Captain Mann Sill (CM-03), Omai and a two-pyroxene andesitic sill (G1224) from the Issineru Formation. Issineru data from Renner and Gibbs (1987); normalising values from Pearce (1982).

Table 3.4 (overleaf)

Geochemical analyses of the Majuba Suite and Captain Mann Sill

Notes:

1. Samples are listed according to increasing silica contents.
2. Majuba Suite: HFT - high-Fe tholeiite; CAS - calc-alkaline series; HSR - high-silica rhyolite (Wenot Lake Zone).
3. ! denotes minor basic intrusive, ^ indicates pyroclastic sample.
4. Major oxides are re-calculated on a 100 % anhydrous basis.
5. Major oxide values in weight percent (wt. %), trace element concentrations in ppm.
6. Total Fe analysed as Fe_2O_3 and represented by $Fe_2O_3^T$
7. LOI denotes loss-on-ignition values (wt. %).
8. Mg-number = 100 x MgO/(MgO + FeO) atomic ratio, where FeO = $Fe_2O_3^T/1.15$.
9. + indicates positively anomalous Ce values. Interpolated Ce values (Ce*) are estima are as follows in ppm: sample 3-0905 - 10.3; 3-1098 - 25.1; CM-02 - 15.6; 4-2022 - 7.8; 5-2492 -35.9; 1-1555 - 26.8.
10. * indicates semi-quantitative data by ICP-MS analysis.

Table 3.4: Geochemical analyses of the Majuba Suite and Captain Mann Sill

	Majuba Suite							
	5-1750 HFT	4-12721 HFT	3-1681 HFT	3-1849 HFT	3-0739 HFT	1-0401 HFT	4-0294 HFT	3-0905 HFT
SiO2	46.20	47.55	47.65	47.68	48.10	48.92	49.37	49.44
Al2O3	13.65	12.75	14.89	14.12	14.77	13.34	12.28	13.45
$Fe_2O_3^T$	15.19	17.20	12.66	14.69	13.45	13.90	13.39	13.58
MgO	9.83	9.81	11.22	10.85	9.18	9.74	9.33	10.43
CaO	10.58	9.05	9.07	9.32	9.13	11.19	12.41	10.03
Na2O	1.89	1.68	0.40	1.99	2.45	1.40	2.00	1.19
K2O	1.33	0.44	2.97	0.23	1.08	0.30	0.26	0.66
TiO2	1.04	1.21	0.89	0.81	1.51	0.91	0.69	0.91
MnO	0.21	0.23	0.18	0.22	0.19	0.23	0.20	0.23
P2O5	0.08	0.08	0.07	0.09	0.14	0.07	0.07	0.08
Total	100.00	100.00	100.00	100.00	100.00	100.00	100.00	100.00
LOI	9.35	3.52	8.70	9.81	11.15	11.35	10.95	9.91
Mg-number	56.6	53.6	64.9	60.1	54.7	58.6	58.8	61.3
$Fe_2O_3^T$/MgO	1.55	1.75	1.13	1.35	1.47	1.43	1.44	1.30
Rb	51.7	18.3	111	7.60	33.8	14.4	9.70	24.7
Sr	264	109	151	167	210	132	242	166
Ba	116	62.9	214	12.8	139	15.8	243	27.6
Li	51.2	12.8	31.6	23.1	23.2	43.6	24.8	35.1
Y	17.3	18.8	8.00	12.7	10.4	11.5	13.7	17.3
Zr	24.9	36.2	25.4	36.6	28.7	40.5	26.0	21.8
Nb	7.67	2.45	2.30	2.36	3.46	4.74	2.96	2.09
Hf	7.78	1.00	0.53	0.81	0.76	3.46	0.64	0.54
Th	1.17	1.23	0.65	0.22	0.19	0.85	0.64	0.21
U	0.79	0.15	0.08	0.10	0.07	0.31	0.08	0.06
Co	91	102	85.3	75.1	82.0	70.0	71.4	77.5
Cr	151	127	246	94.6	230	155	130	159
Ni	114	125	168	121	174	137	154	150
V	397	588	329	310	328	309	293	317
Sc	48.4	61.3	49.6	48.5	33.6	43.0	40.2	46.7
Cu	146	262	197	146	170	188	192	169
Pb	5.43	36.4	5.91	2.68	2.14	8.31	93.5	2.08
Zn	104	150	127	122	107	109	95.7	110
As	8.8	36.1	9.6	1.5	2.5	53.8	7.5	3.0
La	3.31			3.09			2.99	3.86
Ce	9.14			8.10			7.97	12.60 +
Pr	1.31			1.24			1.12	1.46
Nd	6.44			6.21			5.43	7.14
Sm	1.97			1.80			1.67	2.19
Eu	0.78			0.65			0.83	0.82
Gd	2.57			2.14			2.18	2.87
Tb	0.46			0.35			0.37	0.50
Dy	2.89			2.11			2.45	3.26
Ho	0.75			0.55			0.53	0.72
Er	1.81			1.35			1.46	1.95
Tm	0.27			0.20			0.22	0.30
Yb	1.79			1.68			1.47	1.85
Lu	0.27			0.20			0.24	0.28
La_n/Yb_n	1.24			1.23			1.04	1.40

Note: Where REE data are given, Y concentrations are determined by ICP-MS, in all other cases Y values are determined by ICP. This applies to all geochemical analyses presented in this thesis.

Table 3.4 (cont'd): Geochemical analyses of the Majuba Suite and Captain Mann Sill

	Majuba Suite						
	2-1598! HFT	4-2409 HFT	3-1098! HFT	CM-02 HFT	4-0775 HFT	5-1515 CAS	4-0145* HFT
SiO2	49.68	50.27	50.50	51.41	51.66	51.74	52.49
Al2O3	13.31	12.46	14.03	15.38	18.11	19.89	16.87
$Fe_2O_3^T$	14.12	15.48	12.23	13.22	10.59	7.33	10.17
MgO	9.33	9.75	10.00	8.22	5.34	5.84	7.13
CaO	10.03	9.28	9.41	8.57	8.19	8.33	6.72
Na2O	1.97	0.95	2.34	1.98	2.03	0.76	4.22
K2O	0.39	0.27	0.39	0.18	2.89	5.23	1.20
TiO2	0.86	1.21	0.80	0.74	0.73	0.50	0.79
MnO	0.21	0.20	0.19	0.21	0.27	0.21	0.30
P2O5	0.10	0.13	0.11	0.09	0.19	0.17	0.11
Total	100.00	100.00	100.00	100.00	100.00	100.00	100.00
LOI	2.21	4.20	3.17	1.19	8.66	8.29	9.47
Mg-number	57.1	55.9	62.6	55.7	51.1	62.0	59.0
$Fe_2O_3^T$/MgO	1.51	1.59	1.22	1.61	1.98	1.26	1.43
Rb	10.4	8.90	18.5	4.60	91.3	128	41.4
Sr	172	208	183	131	134	242	206
Ba	51.9	15.9	259	108	422	750	94.2
Li	19.6	18.1	16.8	16.3	13.4	16.8	25.4
Y	15.9	27.7	19.4	18.9	11.0	12.8	6.50
Zr	32.2	35.8	47.6	41.9	77.6	40.2	77.5
Nb	2.29	3.86	2.41	6.84	5.29	3.96	3.68
Hf	1.26	0.93	1.29	1.97	2.05	1.82	1.79
Th	0.45	0.34	2.96	0.94	0.86	0.86	0.63
U	0.13	0.11	0.18	0.30	0.41	0.41	0.25
Co	106	107	77.5	76.8	73.5	45.7	67.6
Cr	156	100	203	151	100	37.3	62.2
Ni	215	90.9	160	75.1	125	71.4	61.4
V	313	447	296	303	204	190	232
Sc	45.0	69.5	44.7	43.5	28.3	22.3	36.1
Cu	175	251	218	121	84.5	56.5	135
Pb	1.70	3.53	3.60	20.4	5.60	5.10	3.50
Zn	111	123	106	127	72.9	65.5	102
As	10.4	3.4	9.7	0.9	54.9	9.5	29.8
La			10.7	6.10			
Ce			65.8+	25.2+			
Pr			2.78	1.90			
Nd			11.4	8.34			
Sm			2.77	2.08			
Eu			0.88	0.66			
Gd			3.40	2.56			
Tb			0.53	0.43			
Dy			3.34	2.84			
Ho			0.72	0.62			
Er			2.10	1.92			
Tm			0.32	0.30			
Yb			1.96	1.94			
Lu			0.31	0.31			
La_n/Yb_n			3.65	2.10			

Table 3.4 (cont'd): Geochemical analyses of the Majuba Suite and Captain Mann Sill

	Majuba Suite						
	4-2022 HFT	4-1050* HFT	1-1657 CAS	5-2492 CAS	1-1555 CAS	4-0657* CAS	2-2360 CAS
SiO2	53.01	53.80	56.36	58.25	59.35	60.17	61.70
Al2O3	14.84	13.21	16.77	15.98	15.91	16.40	14.04
Fe_2O_3T	10.49	15.53	7.19	7.85	8.09	6.17	7.12
MgO	6.79	7.75	5.70	6.21	5.83	4.76	4.89
CaO	10.39	5.87	8.36	5.96	6.28	7.14	7.28
Na2O	2.22	1.40	1.44	4.23	3.35	3.11	3.01
K2O	1.43	0.16	3.33	0.51	0.28	1.52	1.15
TiO2	0.55	0.39	0.59	0.69	0.64	0.41	0.51
MnO	0.19	1.74	0.16	0.15	0.16	0.23	0.19
P2O5	0.09	0.15	0.10	0.17	0.11	0.09	0.11
Total	100.00	100.00	100.00	100.00	100.00	100.00	100.00
LOI	8.83	3.85	5.64	0.95	2.32	9.26	0.83
Mg-number	56.9	50.4	61.7	61.8	60.0	61.0	58.3
$Fe_2O_3^T$/MgO	1.54	2.00	1.26	1.26	1.39	1.30	1.46
Rb	53.2	2.80	76.7	16.4	13.5	42.6	54.8
Sr	246	377	188	319	192	285	211
Ba	208	1.30	443	292	157	189	471
Li	24.7	10.9	12.0	18.6	21.2	21.7	27.2
Y	7.20	17.8	10.0	15.5	14.1	6.8	11.1
Zr	38.9	56.1	69.0	96.9	88.1	83.7	88.2
Nb	2.42	2.68	2.99	5.33	6.36	4.01	2.81
Hf	0.87	1.35	2.21	3.21	3.77	1.95	2.25
Th	0.84	1.01	0.93	1.85	1.40	0.73	0.92
U	0.23	0.41	0.33	0.77	0.55	0.33	0.39
Co	58.4	53.0	42.4	48.7	39.5	61.7	83.7
Cr	83.2	86.2	90.4	230	143	103	99.1
Ni	69.8	137	64.5	82.7	59.3	104	92.0
V	217	202	145	191	167	104	140
Sc	31.7	20.1	18.9	23.4	20.7	16.3	18.3
Cu	105	159	92.2	93.8	56.0	78.4	224
Pb	46.6	21.4	56.9	6.1	28.1	11.6	5.40
Zn	81.2	129	87.1	78.9	93.9	102	72.6
As	5.9	7.4	14.6	1.2	2	6.7	1.5
La	3.41			16.2	12.0	7.64	8.43
Ce	15.3+			60.2+	51.4+	17.7	18.8
Pr	0.94			4.32	3.18	2.02	2.39
Nd	4.02			17.9	13.0	8.19	10.1
Sm	1.03			3.81	2.73	1.79	2.33
Eu	0.39			1.10	0.90	0.58	0.75
Gd	1.22			3.8	2.88	1.62	2.37
Tb	0.19			0.53	0.42	0.22	0.34
Dy	1.16			2.97	2.46	1.21	2.04
Ho	0.23			0.64	0.53	0.27	0.57
Er	0.72			1.77	1.45	0.86	1.24
Tm	0.16			0.25	0.22	0.13	0.18
Yb	0.86			1.65	1.42	0.77	1.23
Lu	0.14			0.26	0.22	0.14	0.19
La_n/Yb_n	2.66			6.56	5.66	6.63	4.58

Table 3.4 (cont'd): Geochemical analyses of the Majuba Suite and Captain Mann Sill

	Majuba Suite (Wenot Lake Zone)		Captain Mann Sill	
	67-0716 HSR	67-1460 HSR	CM-03	CM-04
SiO2	77.80	76.01	55.43	60.15
Al2O3	13.53	13.40	16.61	15.16
$Fe_2O_3^T$	1.69	1.50	7.92	6.85
MgO	0.04	0.03	6.94	5.90
CaO	0.27	0.84	6.65	5.32
Na2O	5.30	7.44	3.61	3.75
K2O	1.21	0.63	1.62	1.76
TiO2	0.11	0.11	0.82	0.75
MnO	0.02	0.02	0.12	0.10
P2O5	0.03	0.02	0.28	0.26
Total	100.00	100.00	100.00	100.00
LOI	1.64	1.38	1.15	0.71
Mg-number	4.7	4.0	64.1	63.6
$Fe_2O_3^T$/MgO	42.3	50.0	1.14	1.16
Rb	27.1*	12.7*	88.2	67.2
Sr	28.5*	56.4*	1112	657
Ba	283*	222*	1047	568
Li			26.2	13.6
Y	61.6	46.9	22.2	16.6
Zr	394*	415*	245	166
Nb	37.7*	31.1*	9.12	14.0
Hf	12.2*	13.9*	6.15	4.45
Th	6.6*	6.7*	8.93	5.98
U	2.9*	3.1*	4.00	2.14
Co	3.3	1.8	69.2	56.8
Cr	3	2.2	289	223
Ni	8.3	4.7	198	164
V	27.2	27.2	203	148
Sc	0.7	0.8	17.5	15.0
Cu	19.8	13.8	147	115
Pb			47.2	16.5
Zn	305	187	103	82.3
As			1.5	1.5
La	53.7	43.5	42.7	
Ce	124	100	83.6	
Pr	16.1	13.4	10.8	
Nd	65.6	54.5	42.7	
Sm	14.9	12.7	7.82	
Eu	1.37	1.16	2.17	
Gd	13.0	10.3	6.50	
Tb	1.52	1.17	0.76	
Dy	8.12	6.18	3.80	
Ho	1.72	1.24	0.69	
Er	5.72	4.80	1.80	
Tm	0.99	0.86	0.26	
Yb	7.02	6.59	1.62	
Lu	1.07	1.07	0.25	
La_n/Yb_n	5.11	4.41	17.6	

Note: The concentrations of Co, Cr, and Sc in samples 67-0716 and 67-1460 are close to, or below, the limits of detection (LOD) for the ICP analytical technique (see Table G, Appendix III).

CHAPTER 4

GEOCHEMISTRY OF THE OMAI GRANITOID ROCKS

4.1 Aims of chapter.

The primary aim of this chapter is to elucidate the geochemical characteristics of the Trans-Amazonian granitoid rocks which outcrop in the Omai area - in particular the Omai Stock, the main host of gold mineralisation at Omai. Attempts are also made to determine the petrogenetic and tectonic histories of the Omai granitoids with a view to regional and global correlation. Some attention is given the effects of hydrothermal alteration on element mobility in the Omai Stock.

To date, no comprehensive chemical data are available for the Trans-Amazonian granitoid complexes of Guyana, though some historical major oxide values are presented in Gibbs and Barron (1992). This fact emphasises the importance of the results tabled in this thesis. Essential trace element data, particularly the rare earth elements, are not only crucial in establishing the geochemistry of the Omai granitoid rocks, but also in laying the foundation for future regional geochemical research.

4.2 Description of the geochemical subset (30 samples).

The subset mostly consists of drill-core specimens taken from the Omai Stock. A number of surface samples, however, were collected from the regional Tigri and Mariaba plutons. One other sample, collected from the Mowasi pluton, some 40 km southwest of Omai, is also included to give the subset a broader regional perspective. Strictly speaking, this sample falls outside the Omai area but for the purposes of this study it is referred to as an "Omai granitoid rock". All geochemical samples, with the exception of 7-0258, have corresponding thin section specimens (see Appendix I). The latitude-longitude co-ordinates of the regional granitoids are also recorded in Appendix I.

The Omai Stock (18 samples).

Eighteen representative samples were selected from the 1986 Golden Star Resources drill-core collection. These samples include both "aplite" and "granite" types as defined

petrographically in Chapter 2. The specimens were taken from four separate boreholes (GSR 86-5, -6, -7 and -8) between depths of 13.9 m and 243.3 m. The location of these boreholes with respect to the Stock is shown in Fig 2.5. All selected samples are devoid of subaerial weathering, mineralisation (except pyrite) and excessive hydrothermal alteration.

The Tigri pluton (6 samples).

Six fresh samples were collected by boat traverse from island exposures in the Essequibo River at low water. Sampling was centred along a 3.2 km traverse between the mouth of Kumaka River and Tigri rapids (see Fig. 2.3 for sample locations).

The Mariaba pluton (5 samples).

Five surface samples were taken from fresh low-water outcrops in the southern portion of the pluton along a 4.5 km NNE-SSW boat traverse of the Essequibo River between the mouths of Akenna Creek and Clear Water Creek.

The Mowasi pluton (1 sample).

This solitary sample was collected from a pristine surface outcrop in the middle reaches of the Mowasi River during a previous (cassiterite-gold) geochemical sampling expedition (Elliott, 1985). The Mowasi pluton is undoubtedly part of the Temple Bar granitoid complex which is exposed in the neighbouring Konawaruk River (see Cannon, 1963).

4.3 Elemental analyses.

All granitoid samples have been analysed for a comprehensive range of major and trace elements, including the rare earth elements (see Table 4.2). Unless otherwise stated, all data presented in tables and diagrams in this chapter have been taken from Table 4.2). Analytical techniques and sample preparation are the same as for the Majuba Suite and Captain Mann samples (see section 3.3 and Appendix III).

4.4 Constraints.

The granitoid subset is subject to less limitations than the meta-volcanic sample collection discussed in Chapter 3. For example, the granitoid samples are relatively fresher, especially the regional ones, in terms of LOI values and petrographic features. Secondly, the larger granitoid sample population for a limited number of homogeneous lithologies provides greater

confidence in determining petrogenetic trends. Thirdly, granitoid field relations are more clearly defined than those rocks with greenstone associations.

4.5 Trans-Amazonian granitoid complexes - a regional overview.

Two peak periods of acid plutonism are recognised within the Trans-Amazonian orogeny which prevailed throughout the Guiana Shield from 2.25 to 1.95 Ga. In general terms, these correspond to: 1) early, syn- to late-tectonic, calc-alkaline, soda granitoid complexes, referred to as P1-type; and 2) late, pink, potassic, anorogenic (?) granitoid complexes, known as P2-type (see Gibbs and Barron (1992). These authors also suggest that a pulse of mafic magmatism, which gave rise to the Badidku Suite, separates P1 and P2 plutonism. The huge granitoid batholiths of northern Guyana's granite-greenstone basement are generally of the P1-type and are comprised of small cogenetic intrusions which range in composition from granite to diorite. These intrusions correspond to the Younger Granite Group of Allen (1963). According to Gibbs and Barron (1992) the granodiorite-tonalite association is the dominant granitoid type and is commonly associated with hydrothermal alteration and gold-quartz lodes occupying fractures and shear zones at the contact with the greenstone country rocks.

In southern Guyana, south of the Takutu Break, the Trans-Amazonian granitoid complexes, which are of the P2-type, are even more voluminous than their northern counterparts, forming an extensive 90 km-wide, E-W trending belt across the country (see Walrond, 1987a). These southern complexes are fairly homogeneous, mostly granodioritic to granite in composition, and enclose enclaves of amphibolite-grade meta-sedimentary rocks of the Kwitaro Group which have been interpreted as the stratigraphic equivalents of the Barama-Mazaruni greenstones (Barron 1986). The southern granitoid rocks which have been grouped under the banner of the Southern Guyana Granite Complex show strong petrological associations with the Agua Branca Granite of northern Brazil whereas the Trans-Amazonian granitoids of northern Guyana are contiguous with granitoid terrains in eastern Venezuela (Gibbs and Barron, 1992).

In northern Guyana, the most reliable Trans-Amazonian age to date (2.23 Ga) has been determined by U-Pb methods on zircons extracted from a biotite gneiss of the Bartica Assemblage (Gibbs and Olszewski, 1982). This age is significant with respect to this present study as the Mariaba pluton intrudes the Bartica Assemblage and therefore a maximum age of emplacement can be invoked for the former.

Reconnaissance K:Ar dating was carried out in the Omai area by Snelling and McConnell (1966). Hornblende from the Tigri pluton and biotite from the Mariaba pluton yielded respective ages of 1945 ± 100 Ma and 1710 ± 50 Ma. Given the potential for argon loss

these ages are somewhat tentative but they still provide useful "ball-park" data which generally conform to the time frame of the Trans-Amazonian orogeny. On first impressions, the estimated Mariaba age appears to be anomalously low, however it is worth noting that Trans-Amazonian granitoid rocks from the Amazonas territory of Venezuela yield Rb:Sr and U:Pb radiometric ages of between 1.86 and 1.76 Ga (Gaudette and Olszewski, 1985).

In this present study, abortive attempts were made to elucidate the timing of granitoid intrusion in the immediate Omai area. Four 20-kg bulk saprolite samples collected from open-cuts in the Omai stock were panned-down and passed through a heavy liquid separation procedure to produce heavy-mineral concentrate fractions. In addition, 11 heavy mineral separates derived from crushed hand specimens of the Tigri and Mariaba plutons were also processed. After the removal of the magnetic fractions all samples were sent to Professor R. Doig of McGill University, Quebec for zircon extraction and subsequent U-Pb dating. Unfortunately the relatively small samples contained insufficient quality zircons to permit reliable radiometric dating.

4.6 Alteration and element mobility.

The Omai Stock

As demonstrated in Chapter 2, some portions of the Stock have suffered pervasive sericitisation and minor carbonatisation associated with hydrothermal alteration whilst other portions of the body have been affected by the relatively milder propylitic (chlorite-epidote) alteration, also related to hydrothermal activity. LOI values for the Stock which range from 1.62% to 6.87% show a negative correlation with SiO_2 (Fig. 4.1a) indicating that the more acid samples are less susceptible to hydrous alteration than their intermediate counterparts. Petrographic observations indicate that the LOI values vary proportionally with the degree of sericitic alteration. In turn, the geochemical data presented below confirm that the intensity of sericitisation is directly related to modal amounts of plagioclase feldspar present in the samples. These trends are substantiated by the strong positive correlations shown by the K_2O-LOI and Al_2O_3-LOI data in Figs. 4.1b and 4.1c respectively.

This selective sericitisation has given rise to a corresponding potassic enrichment which is reflected by K_2O values up to 4.42%. The relationship between potassic alteration and modal plagioclase contents is further demonstrated by the positive slope defined by the Al_2O_3-K_2O data in Fig.4.2a. This trend is converse to normal primary magmatic trends. Rubidium shows positive correlations with K (Fig. 4.2b) and Ba (Fig. 4.2c) which suggests that Rb and Ba concentrations were also controlled by sericitic alteration. This hypothesis is supported by

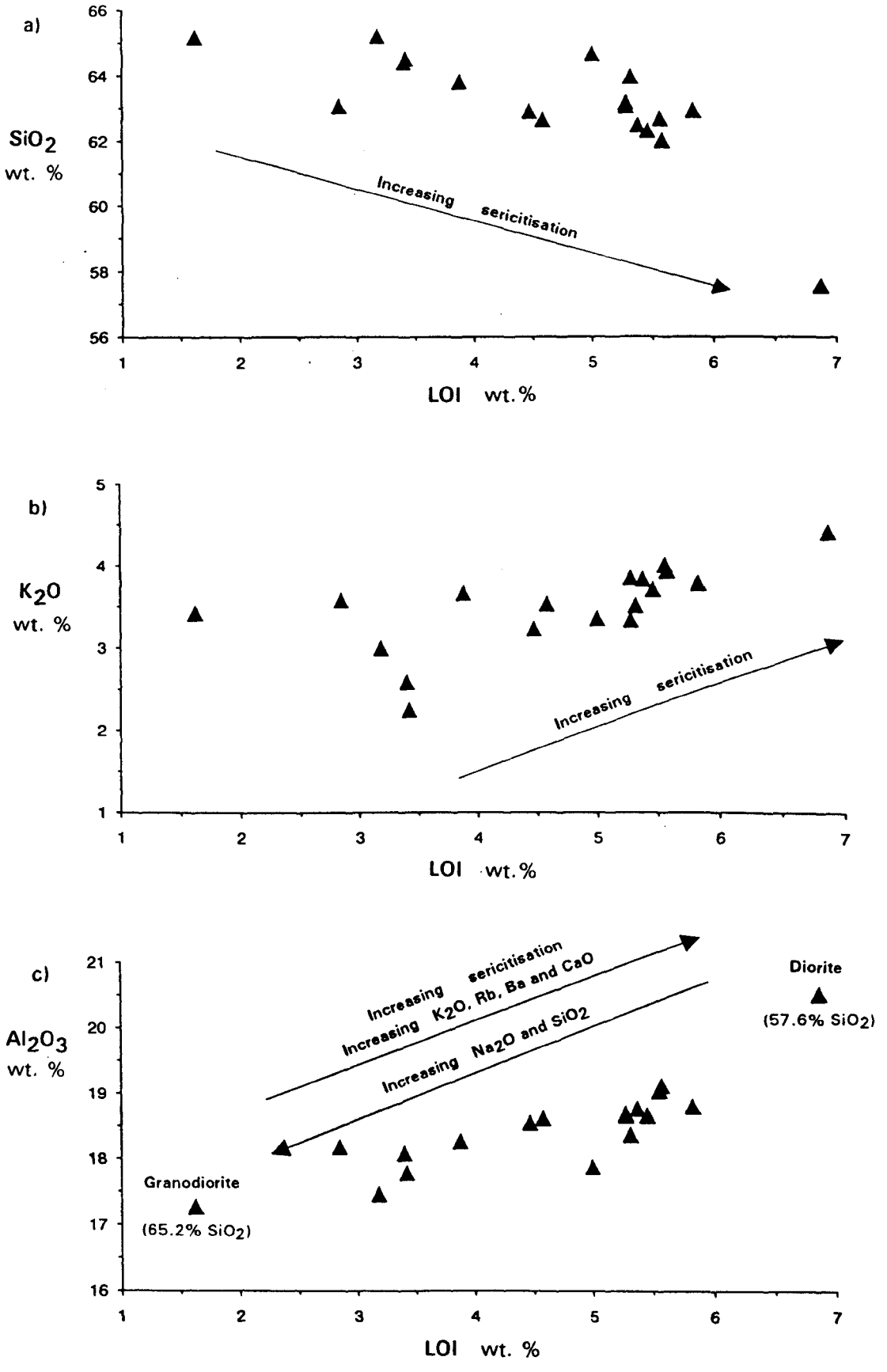

Fig. 4.1: SiO_2, K_2O and Al_2O_3 variation with loss-on-ignition (LOI) for the Omai Stock showing the effects of hydrothermal alteration (sericitisation). a) SiO_2 - LOI; b) K_2O - LOI and c) Al_2O_3 - LOI (see text for details).

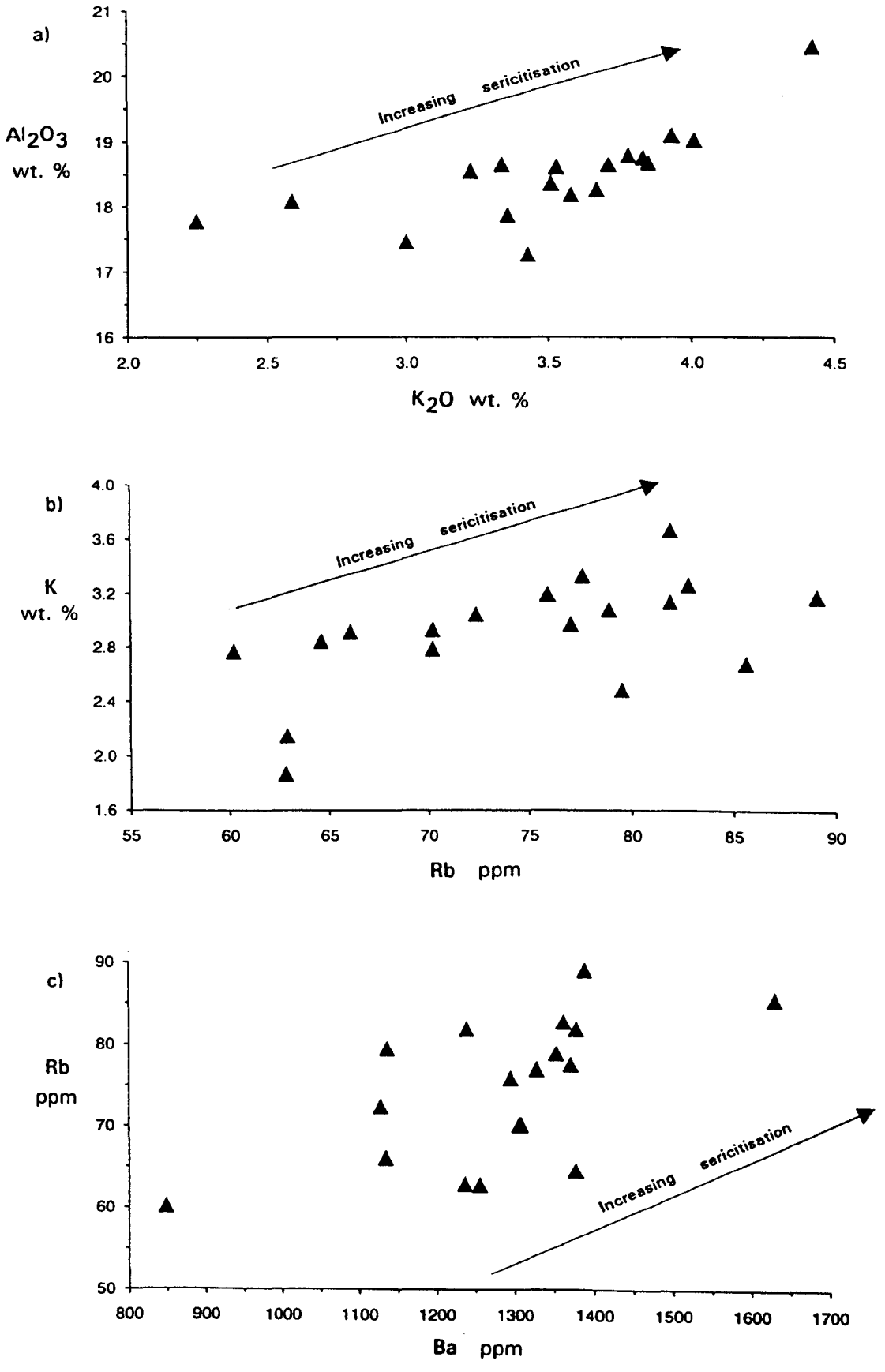

Fig. 4.2: Co-variation diagrams for the Omai Stock showing the effects of hydrothermal alteration (sericitisation). a) Al_2O_3 - K_2O; b) K - Rb and c) Rb - Ba (see text for details).

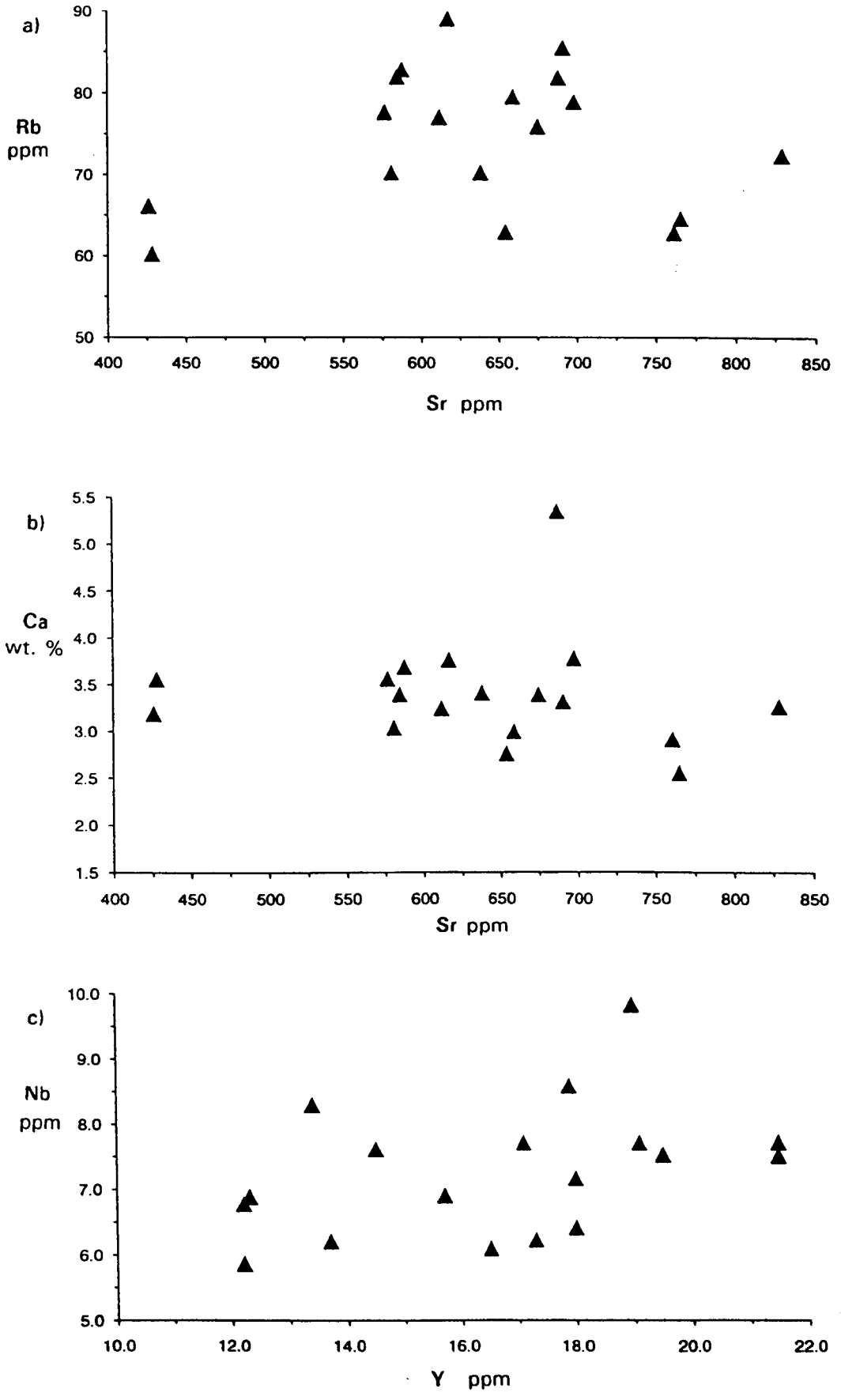

Fig. 4.3: Co-variation diagrams for the Omai Stock. a) Rb - Sr; b) Ca - Sr and c) Nb - Y (see text for details).

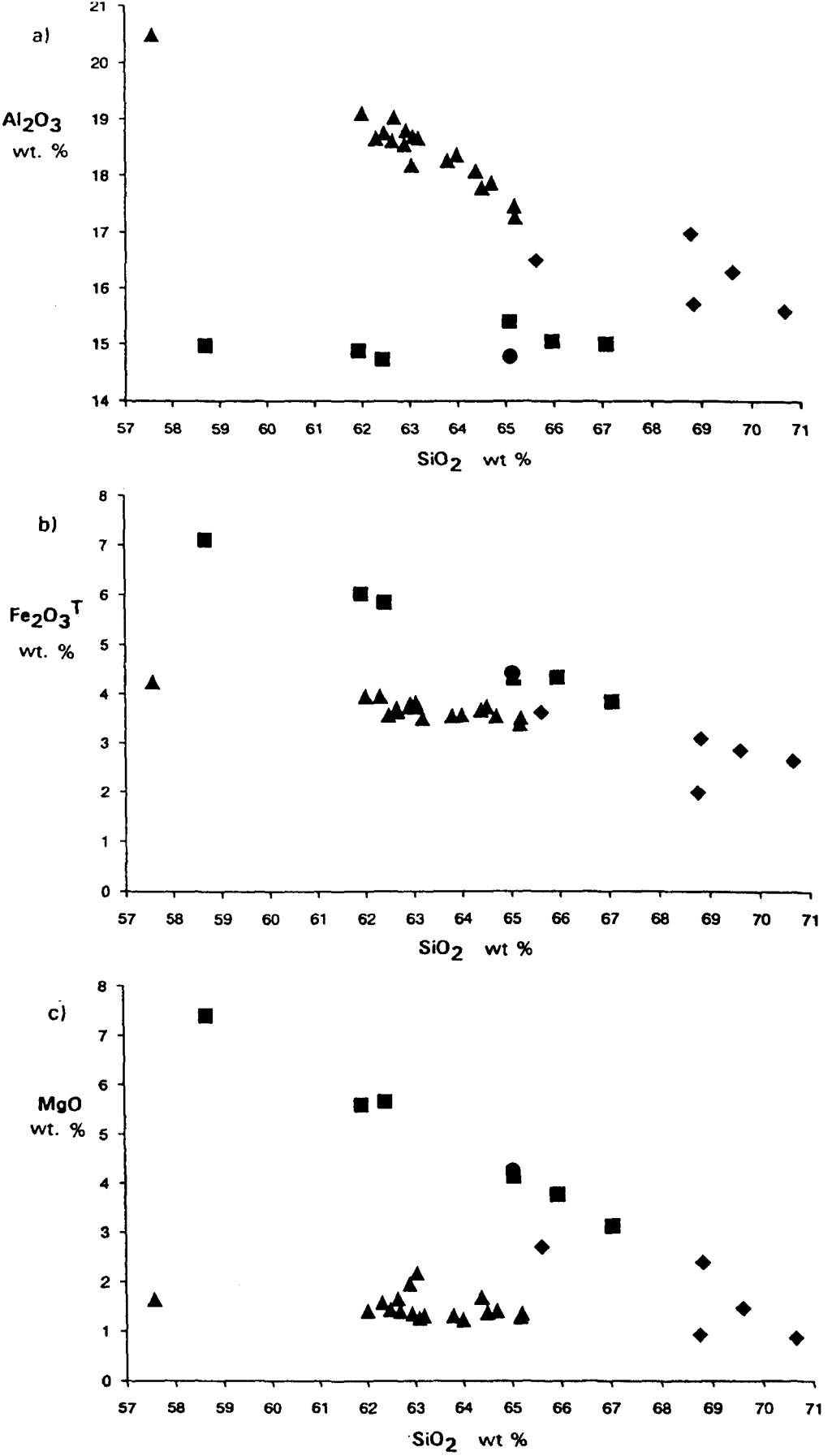

Fig. 4.4: Co-variation diagrams showing major oxide variation with SiO_2 for the Omai granitoid rocks. a) Al_2O_3 - SiO_2; b) $Fe_2O_3^T$ - SiO_2 and c) MgO - SiO_2.

Symbols: triangles - Omai Stock; squares - Tigri pluton; diamonds - Mariaba pluton; circle - Mowasi pluton.

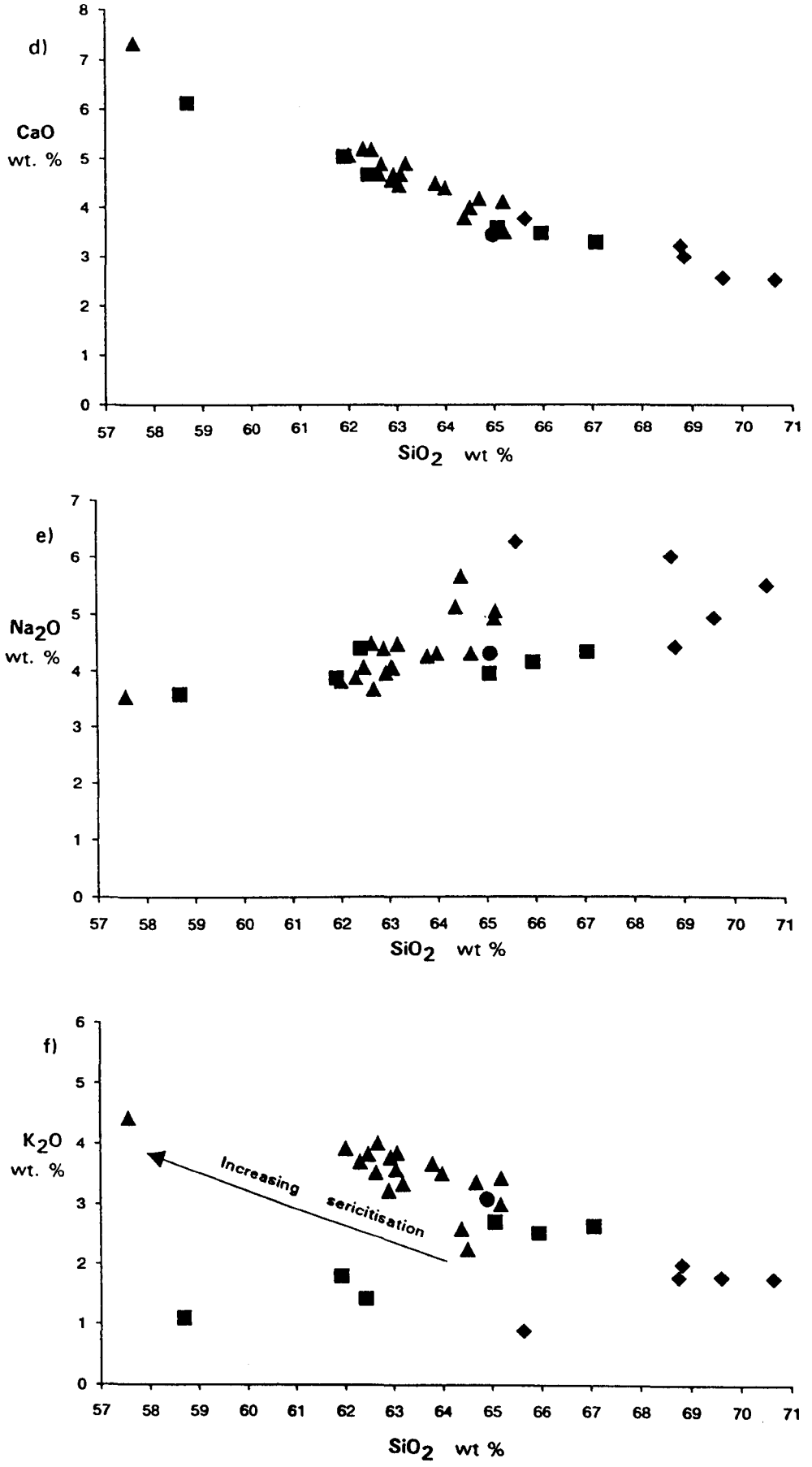

Fig. 4.4: (cont'd): d) $CaO - SiO_2$; e) $Na_2O - SiO_2$; f) $K_2O - SiO_2$

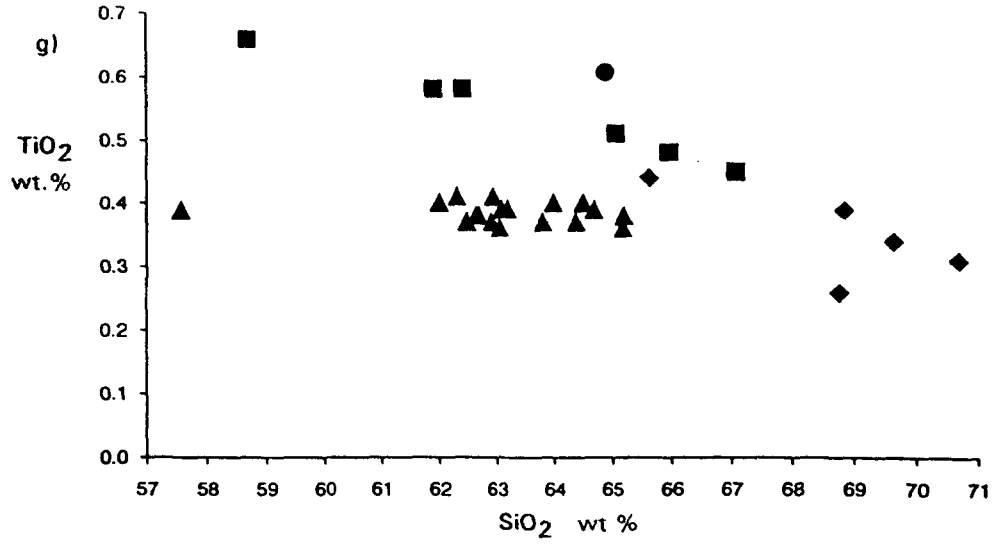

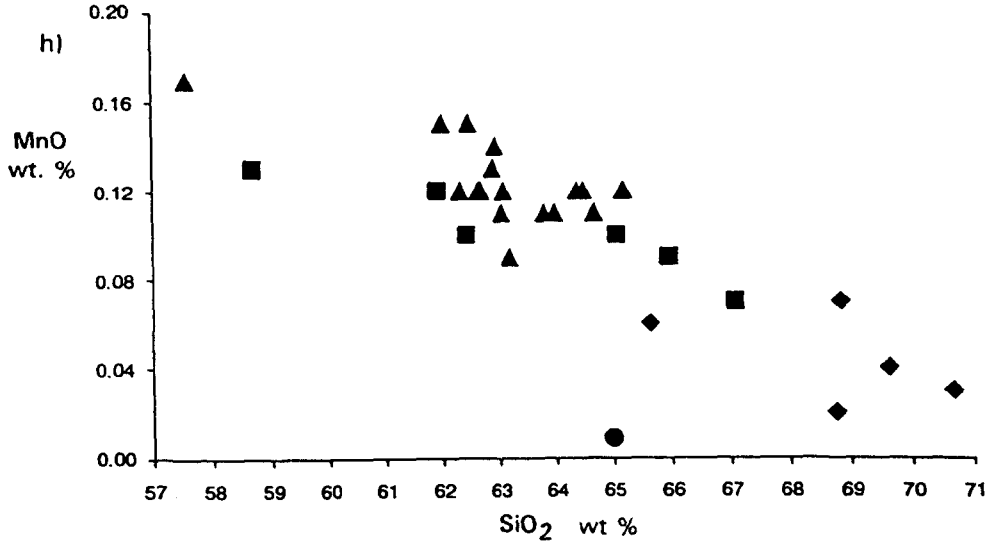

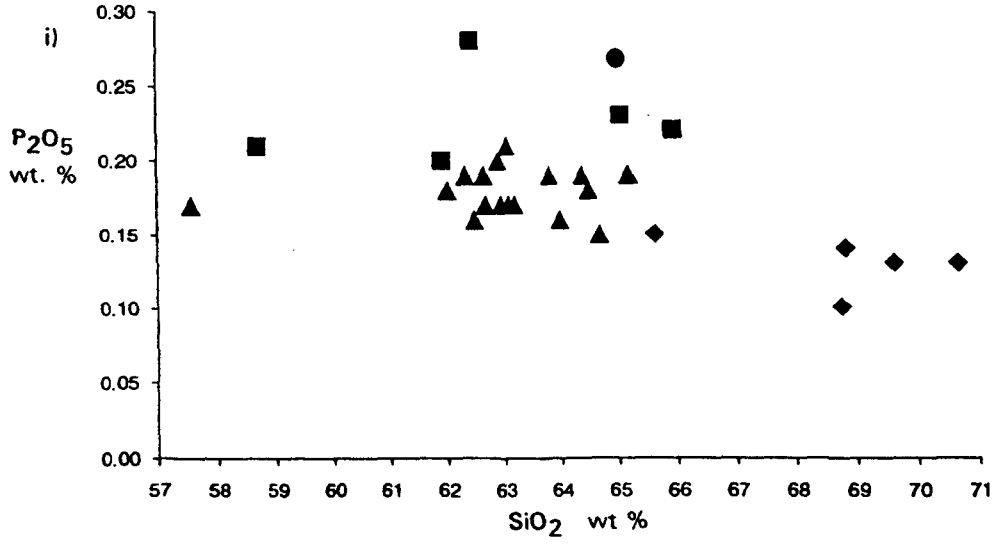

Fig. 4.4 (cont'd): g) TiO_2 - SiO_2; h) MnO - SiO_2 and i) P_2O_5 - SiO_2.

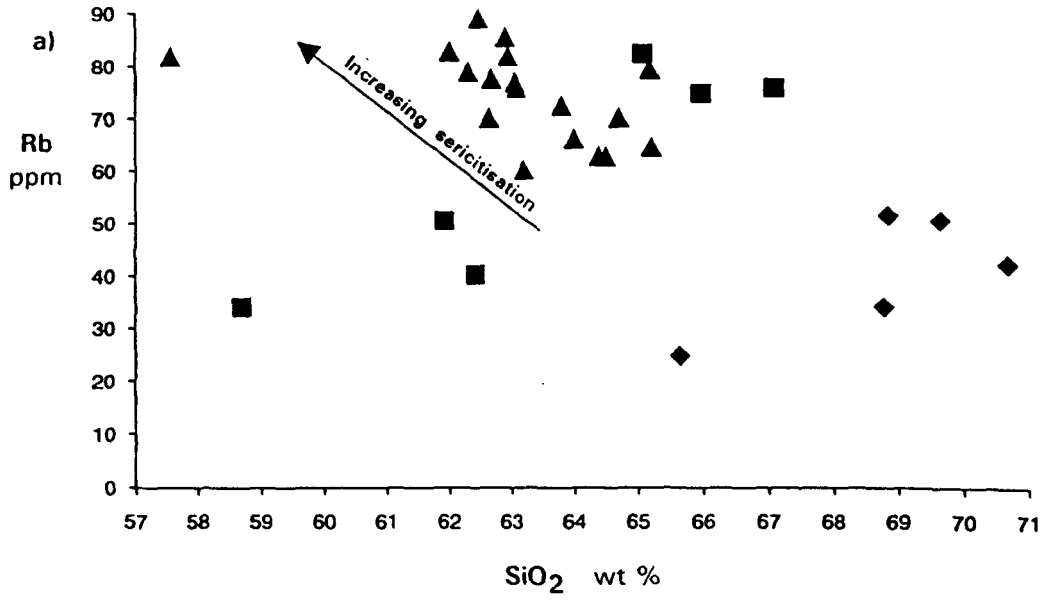

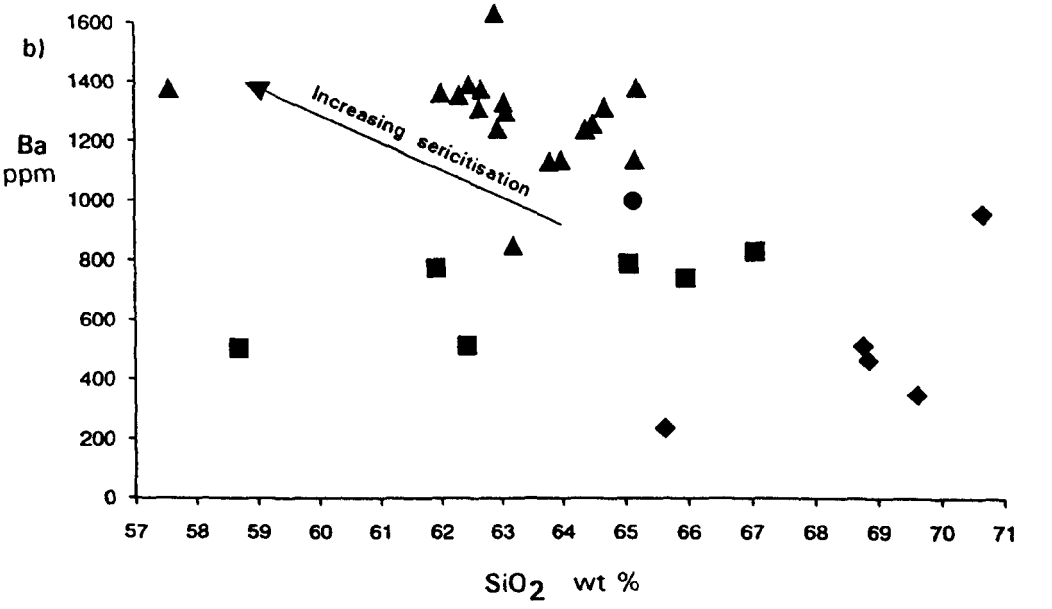

Fig. 4.5: Co-variation diagrams of selected trace elements versus SiO_2 for the Omai granitoid rocks. The sericitisation vector for the Omai Stock is also shown (see text for details). Symbols as for Fig. 4.4. a) Rb - SiO_2; b) Ba - SiO_2

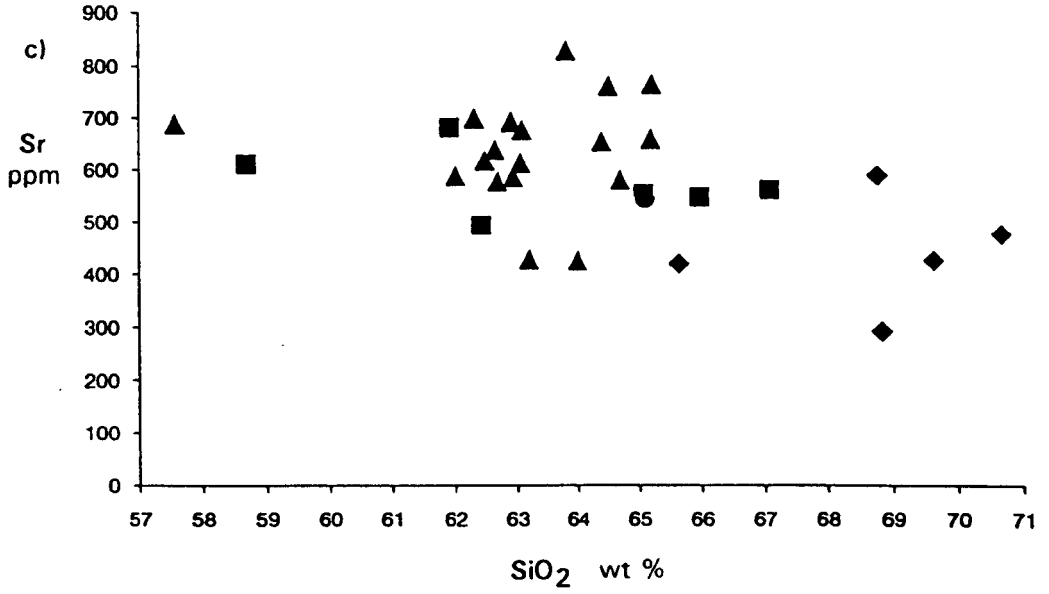

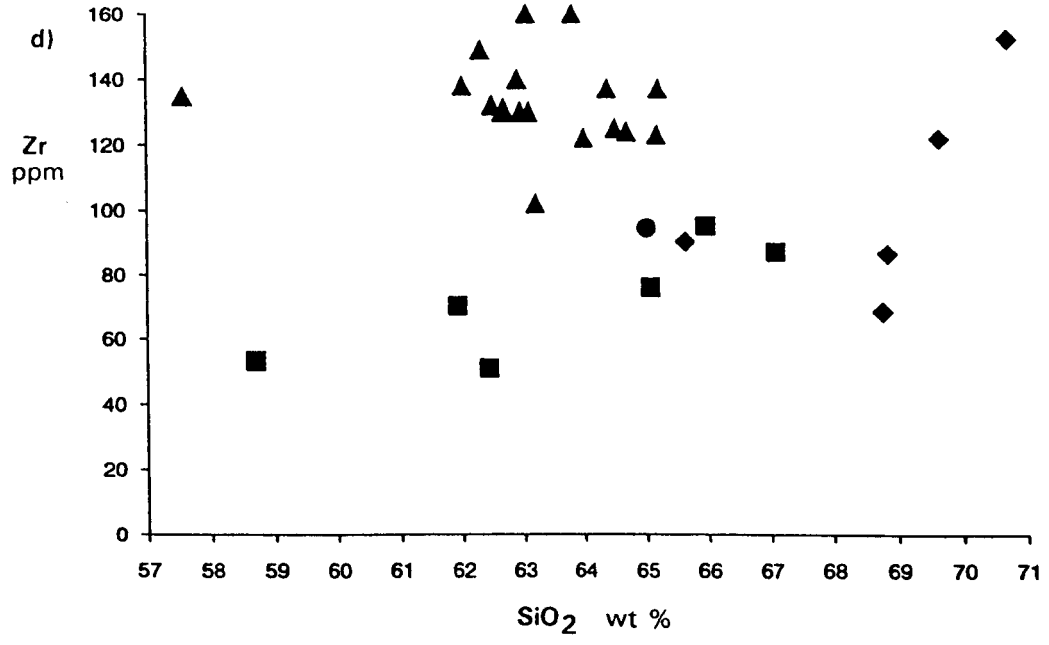

Fig. 4.5 (cont'd): c) Sr - SiO_2; d) Zr - SiO_2.

the fact that Rb displays a negative linear relationship with SiO_2 (Fig. 4.5a) - a trend which is converse to normal differentiation processes.

The scatter of Rb-Sr data shown in Fig. 4.3a intimates that Sr concentrations are not directly indexed to sericitic alteration. The inverse relationship between Ca and Sr (Fig. 4.3b) may be explained by one of two processes. Firstly, the most plausible explanation is that Sr did not substitute for Ca^{2+} in plagioclase feldspar to any great extent, but behaved in an incompatible manner during differentiation. A second consideration is that Sr was preferentially leached from plagioclase feldspar during sericitisation, though for this to be true, one would expect a negative linear trend for the Rb-Sr data, which is clearly not the case (see Fig. 4.3a).

As shown schematically in Fig. 4.1c, Na_2O has definitive inverse relationships with Al_2O_3, CaO, K_2O, Rb, Ba and LOI and a positive correlation with SiO_2. The petrographic data affirms that the elevated Na_2O values correspond to samples containing K-feldspar and/or relatively high modal amounts of primary albite. The geochemical and petrographic trends therefore imply that albitisation was generated by Na-autometasomatic processes which preferentially affected late-stage (tonalitic-granodioritic) components of the Omai Stock. Moreover, these components were not readily susceptible to later sericitic alteration, but instead, responded to the hydrothermal activity by forming a propylitic mineral assemblage. In contrast, the more calcic (dioritic-tonalitic) components of the Stock readily accommodated the potassic-rich hydrothermal fluids by the breakdown of plagioclase feldspar to sericite.

Petrographic observations confirm that silica was relatively immobile in those Stock samples selected for analyses, whilst the well-defined, tight, linear, magmatic trends displayed in Fig. 4.4 indicate that the relative concentrations of major elements, with the exception of K_2O, were little affected by hypogene alteration. However, comparatively depleted values of $Fe_2O_3^T$, MgO, TiO_2, Co, Cr, V, and Sc may reflect chronic element dilution in response to the breakdown of mafic minerals and Fe-Ti oxides during alteration. On the other hand, the coherent data distribution (e.g. Figs. 4.4 b, c and g) suggests that primary magmatic trends of these elements have been preserved, if not primary elemental abundances. The broad linear array of data projecting towards the origin (Fig. 4.3c), implies that the critical trace elements Nb and Y did not suffer serious chemical migration during alteration. Sub-sampling error and/or analytical uncertainties may account for the moderate degree of scatter shown by the data.

Smooth and closely compatible chondrite-normalised REE patterns were obtained for all analysed samples of the Omai Stock. This indicates that the relative REE concentrations were little affected by secondary processes. This observation is supported by the work of

Corey and Chatterjee (1990) who propose that the redistribution of REE during the alteration of a granitic rock is primarily controlled by the stability of the accommodating secondary mineral phases rather than the composition of the invading fluid. On this principle, an altered granitic rock may therefore yield a similar REE profile to a fresh equivalent. Moreover, in evolved granitoid rocks, the bulk of the REE are normally held in accessory minerals such as apatite, zircon, monazite and allanite which are generally resistant to alteration. Microscopic examination of the Omai Stock samples has confirmed the presence and stability of such phases as apatite and zircon.

The Tigri, Mariaba and Mowasi plutons.

Pristine petrographic features and LOI values generally less than 2.0% testify to the relatively fresh nature of these regional plutons. Apart from low to moderate degrees of epidotisation in some of the Tigri and Mariaba samples, evidence of post-magmatic alteration is absent and consequently no significant element mobility is anticipated or observed.

4.7 Magmatic affinity and peraluminosity (Shand Index).

As illustrated by the AFM diagram (Fig. 4.6a), the Tigri, Mariaba and the Mowasi samples all display clear-cut calc-alkaline trends. Determination of the Omai Stock's magmatic affinity by this method is not feasible owing to the K_2O enrichment brought about by sericitisation. However, on the $Fe_2O_3^T$-$Fe_2O_3^T$/MgO diagram (Fig. 4.6b), all the Omai granitoids, including the Omai Stock, show a strong calc-alkaline affinity which appears to be harmonious with the greater regional trend.

In the Shand Index diagram (Fig 4.7a), the Na-metasomatism and sericitisation vectors cancel each other out giving a net metaluminous trend for the Omai Stock. In Fig. 4.7b, the Tigri and Mowasi samples also show a marked metaluminous tendency whereas the Mariaba samples range from metaluminous to weakly peraluminous with A/CNK (molar) ratios in the order of 0.82 to 1.11.

4.8 Geochemical characteristics.

4.8.1 The Omai Stock.

Elevated Al_2O_3 values ranging from 17.27% to 20.50% distinguish the Omai Stock from the regional granitoid plutons. These high Al_2O_3 values can be directly correlated with high modal

contents of plagioclase feldspar. The enhanced mean Ba concentration of just under 1300 ppm is a further diagnostic feature of the Stock, though this in part is attributed to the effects of sericitic alteration. This hydrous alteration precludes a satisfactory compositional classification of the Stock by chemical means. However, the least hydrothermally-altered samples, i.e. the sodic ones, which yield relatively low LOI values of 1.62% to 3.24% plot in the "granodiorite" field of the Na_2O-CaO-K_2O ternary diagram as shown in Fig. 4.8. This trend is partially supported by the thin section studies in which significant amounts of K-feldspar are only observed in Na-rich samples such as 7-1300. By and large, the Stock's main chemical trends, as summarised in Fig. 4.1c, confirm the petrographic trends displayed in Fig. 2.6, which show that the Stock evolved from an early diorite into a late-stage soda-granodiorite.

On the whole, the Stock has SiO_2, CaO and Na_2O contents concordant with those of the Tigri pluton, but the low $Fe_2O_3^T$, MgO and compatible trace element abundances are more comparable with the Mariaba pluton. Rb/Sr ratios in the Stock roughly coincide with those in the Tigri pluton (see Fig. 4.9), which is surprising, as one would expect exaggerated Rb values in the former due to sericitisation. However, Rb values for the Stock are moderate and fall within the narrow range of 60-90 ppm. Mean Zr and Hf concentrations in the Stock tend to be slightly higher than those of the regional granitoids and are probably a consequence of higher modal zircon abundances.

As illustrated in Fig. 4.10a, samples from the Omai Stock display a narrow, regular range of fractionated chondrite-normalised REE signatures which are typified by La_n/Yb_n ratios in the order of 10.8 to 15.8 with an average value of 12.9. The HREE components of the profiles form a distinctive flat to slightly concave "tail" with relative enrichment from Er through to Lu. Negligible to minor negative Eu anomalies further characterise the Stock's REE patterns. Absolute REE contents are consistently moderate with a mean total REE value of around 160 ppm.

In spite of the high levels of Au-W-Te-S mineralisation in the Omai Stock, the base metal (Cu,Pb,Zn) concentrations contained therein are much the same as the non-mineralised regional plutons. Arsenic values in the Stock's wall-rocks reach a few parts per million at best.

4.8.2 The Tigri pluton.

The SiO_2 contents recorded for the Tigri pluton fall within the limits of 58.69% and 67.07% with a mean value of 63.52% SiO_2. The pluton is distinguished from its granitoid neighbours by relatively high $Fe_2O_3^T$ and MgO values of 5.45% and 5.25% respectively at the 63.0%

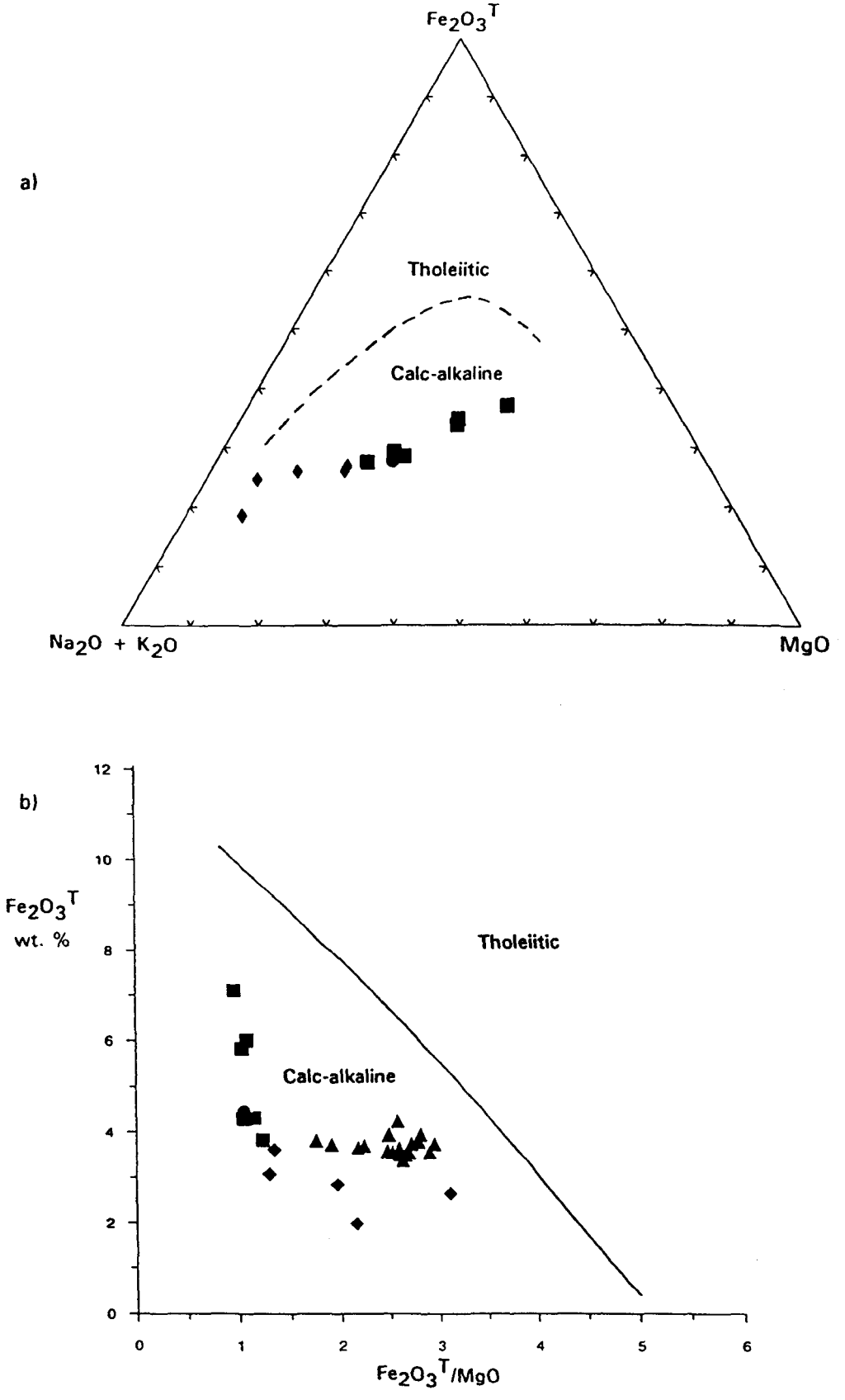

Fig. 4.6: Diagrams showing the magmatic affinity of the Omai granitoid rocks. a) Na_2O+K_2O - $Fe_2O_3^T$ - MgO (AFM) ternary diagram (Omai Stock samples excluded); field boundary from Irvine and Baragar (1971). b) $Fe_2O_3^T$ - $Fe_2O_3^T$/MgO diagram; field boundary from Miyashiro (1974). Symbols as for Fig. 4.4.

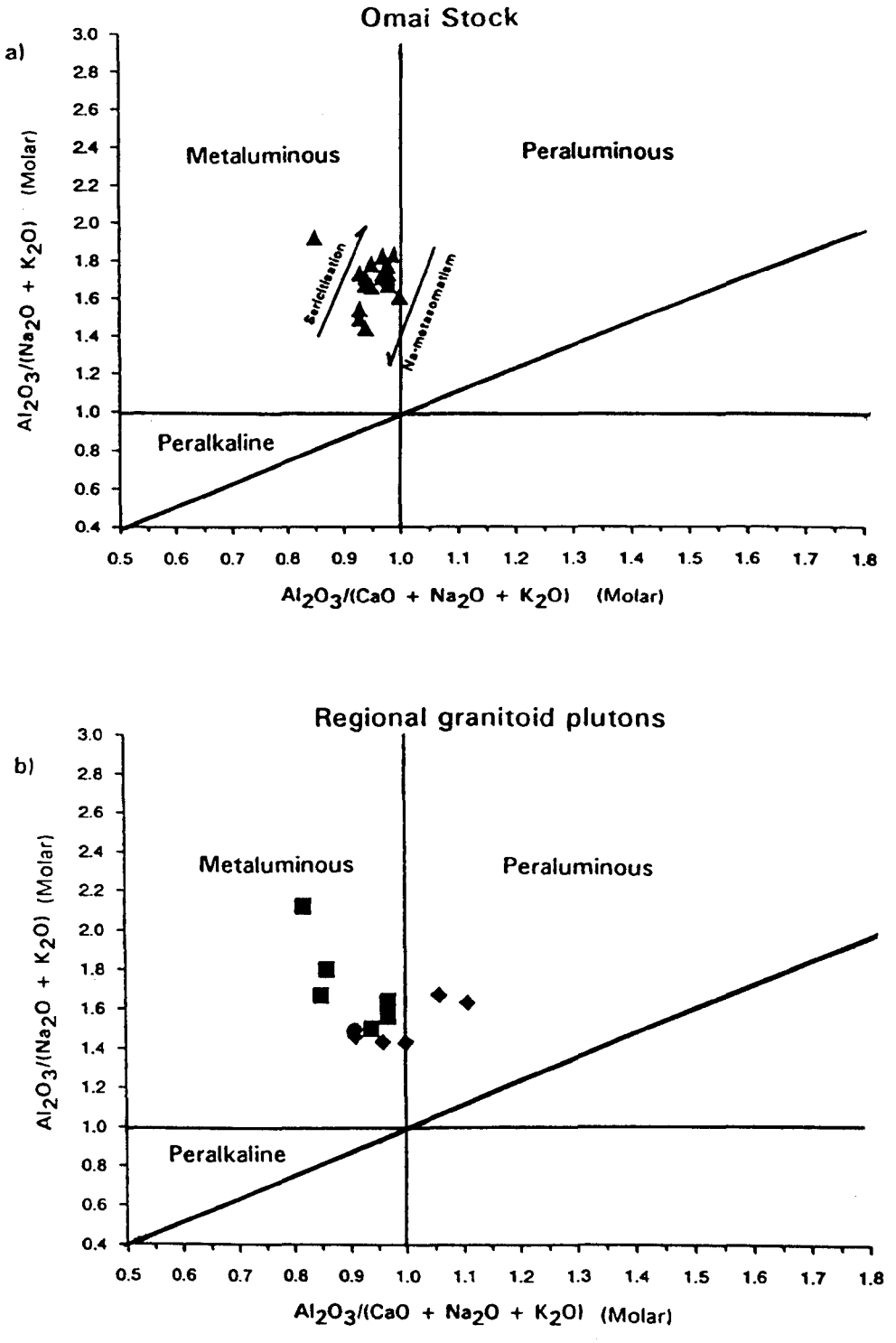

Fig. 4.7: Shand Index diagrams for the Omai granitoid rocks. a) the Omai Stock (with alteration vectors); b) regional (Tigri, Mariaba and Mowasi) granitoid plutons. Symbols as for Fig. 4.4.

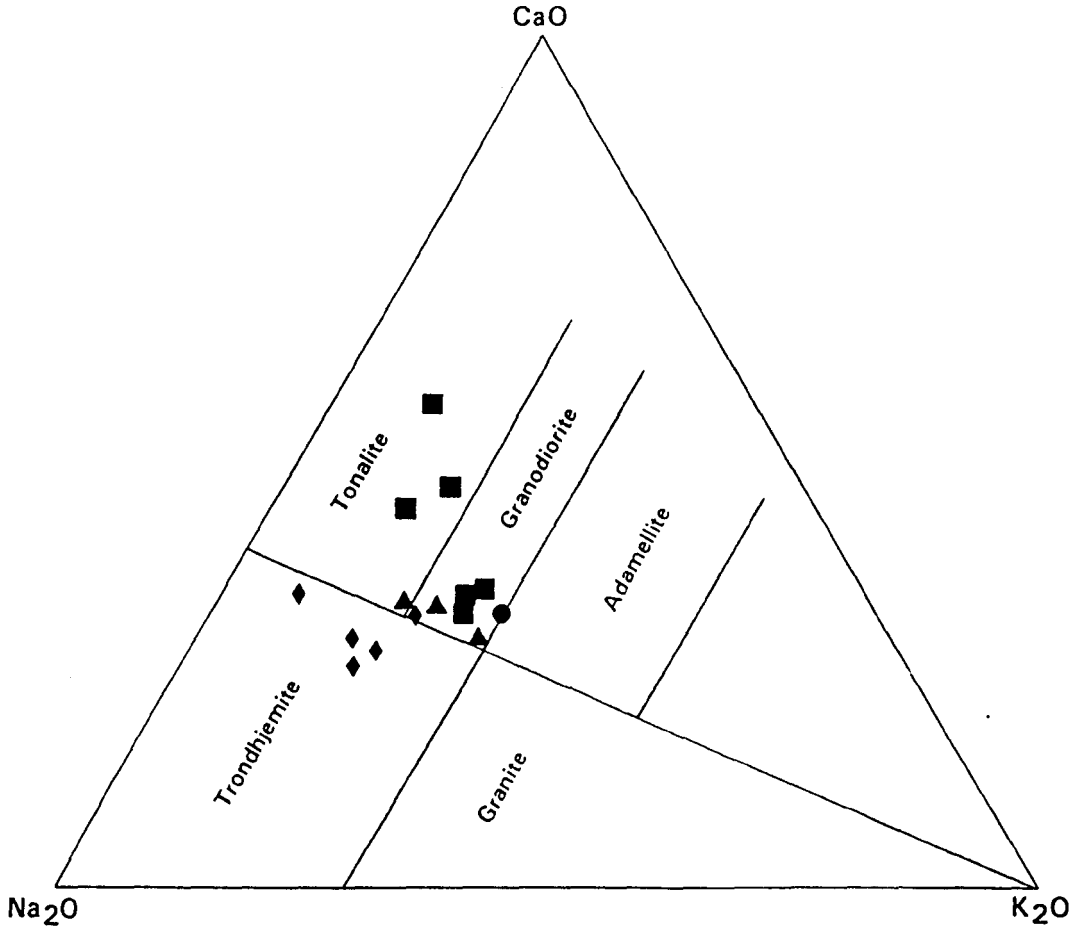

Fig. 4.8: Na_2O - CaO - K_2O ternary diagram showing a compositional classification of the Omai granitoid rocks by chemical means. Sericitisation precludes a satisfactory classification of the Omai Stock by this method, though three of the lesser altered samples (6-0626, 7-0258 and 7-1300) are shown for comparison. Field boundaries from Robb and Myer (1990). Symbols as for Fig. 4.4.

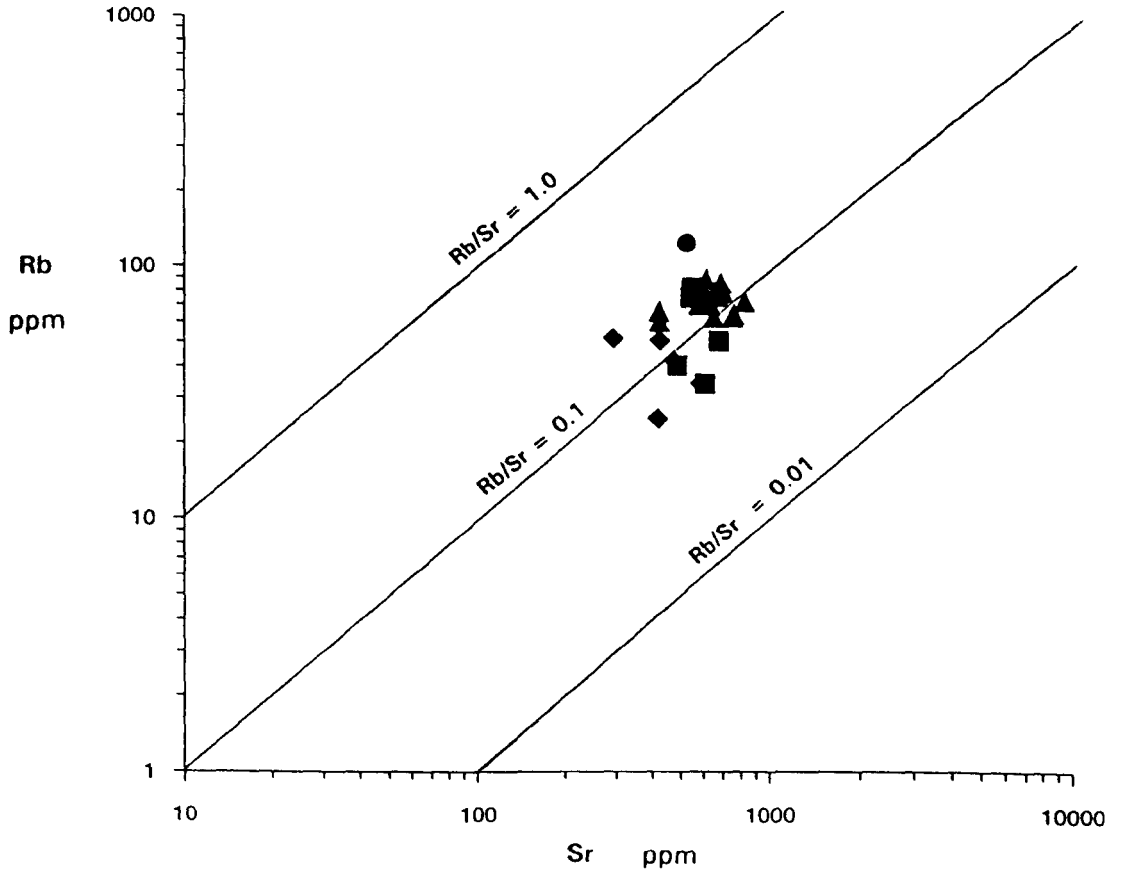

Fig. 4.9: Log Rb - Sr plot for the Omai granitoid rocks. Symbols as for Fig. 4.4, i.e. triangles - Omai Stock; squares - Tigri pluton; diamonds - Mariaba pluton; circle - Mowasi pluton.

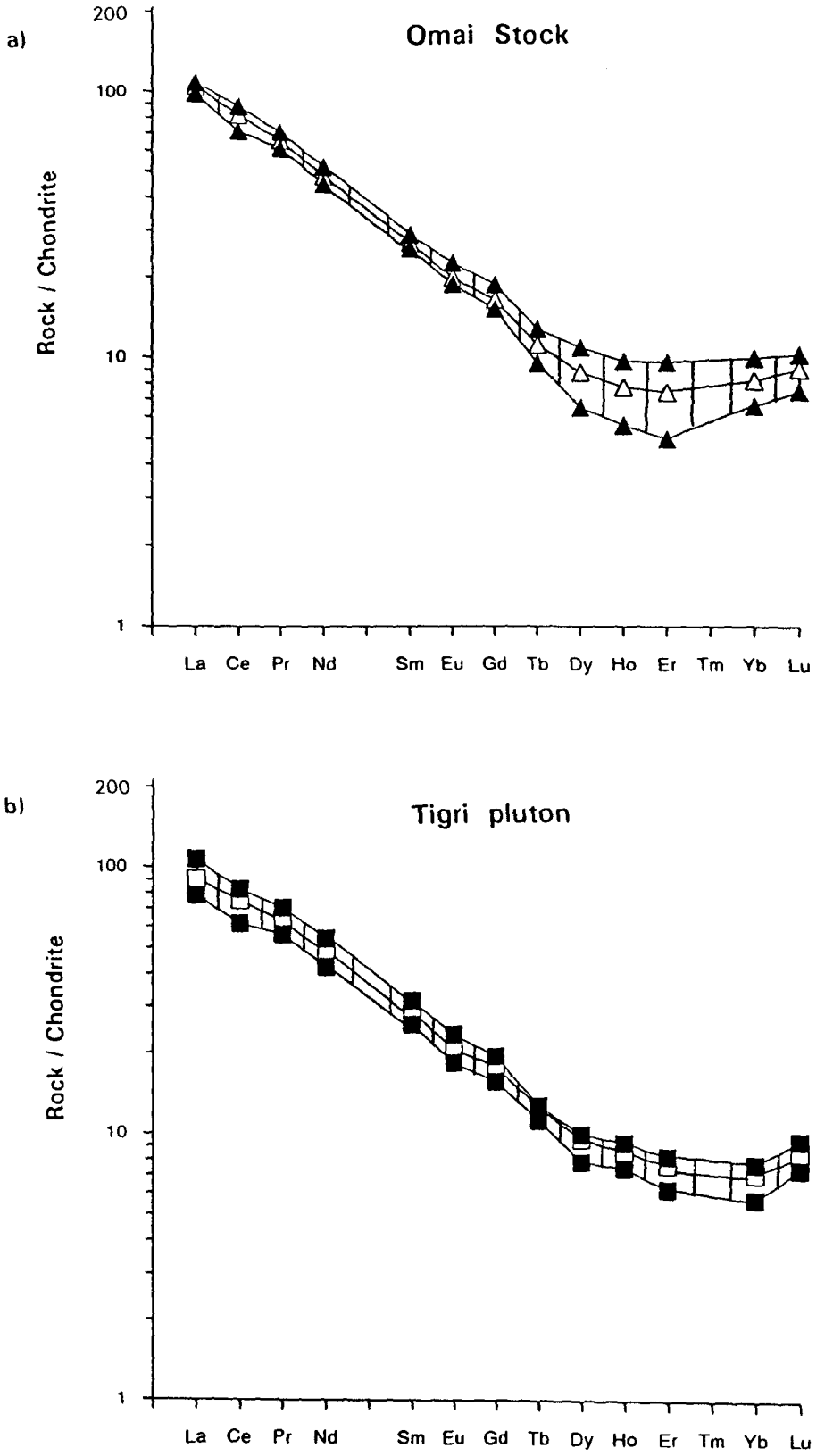

Fig. 4.10: Chondrite-normalised REE patterns for a) Omai Stock, and b) Tigri pluton. Solid symbols represent maximum and minimum values obtained; open symbols indicate average values (Omai Stock, n = 17; Tigri pluton, n = 6). Normalising values from Nakamura (1974).

Note: In the REE patterns of the Omai granitoid rocks, Tm data are not plotted. This is due to erratic values which are believed to be related to analytical uncertainties (see Table 4.2, note 5).

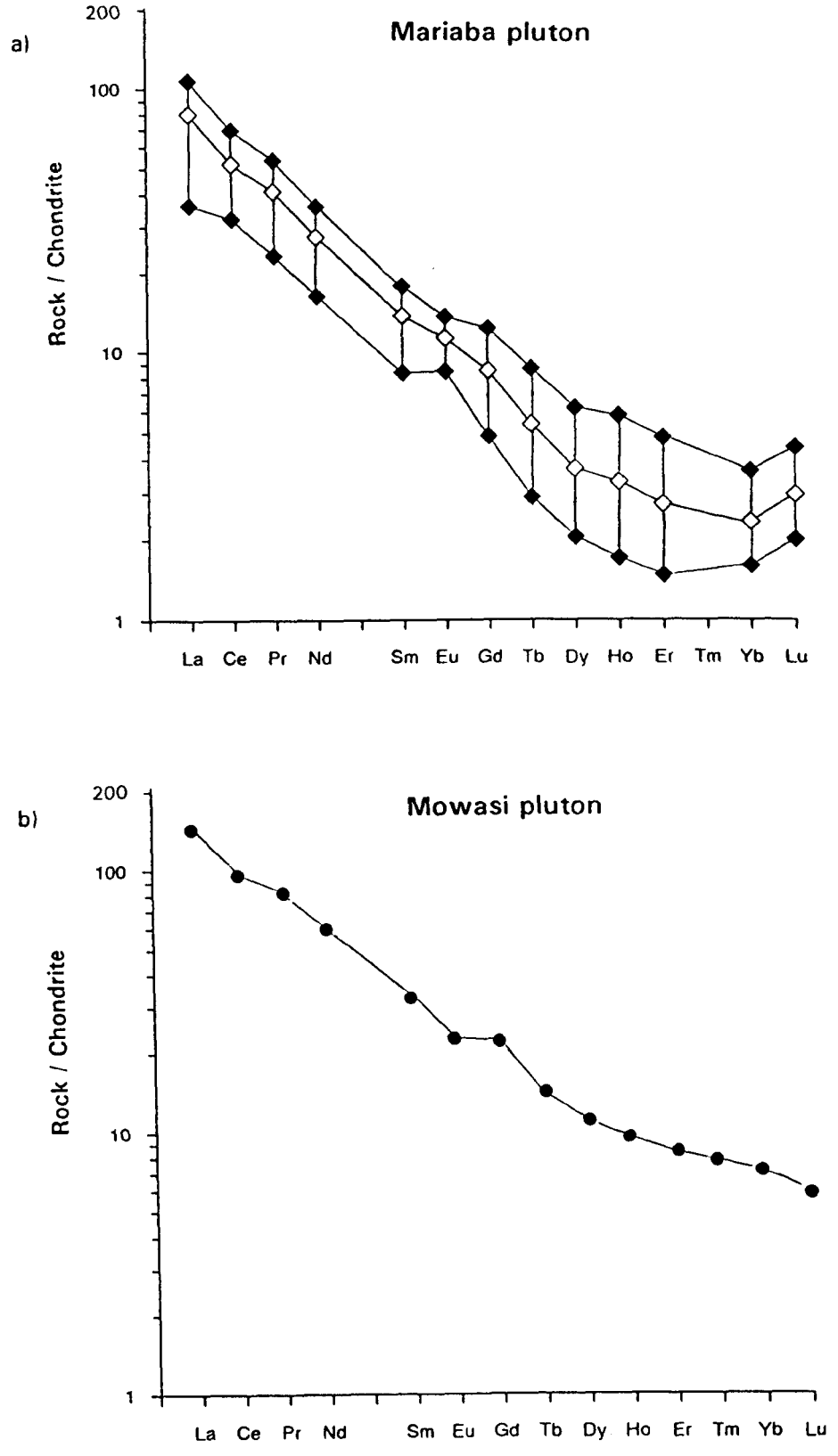

Fig. 4.11: Chondrite-normalised REE patterns for a) Mariaba pluton, and b) Mowasi pluton. In a), solid symbols represent maximum and minimum values obtained whilst open symbols indicate average values (n = 5 for Mariaba pluton). Normalising values from Nakamura (1974).

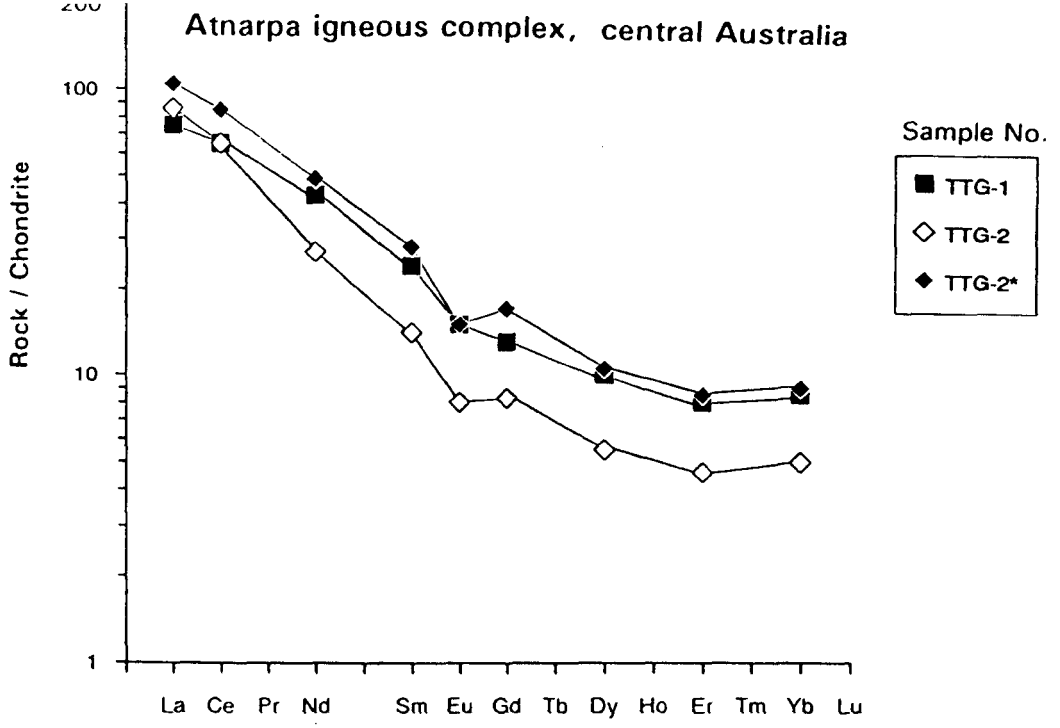

Fig. 4.12a: Chondrite-normalised REE patterns for Palaeoproterozoic granitoid rocks of the Atnarpa igneous complex, central Australia. Data from Zhao and Cooper (1992); normalising values from Nakamura (1974). Sample TTG-2 corresponds to sample 87106, sample TTG-2* to sample 88032. Note how Atnarpa REE patterns compare to those of the Omai Stock, Tigri pluton and Mowasi pluton (see Figs. 4.10a, 4.10b and 4.11b respectively).

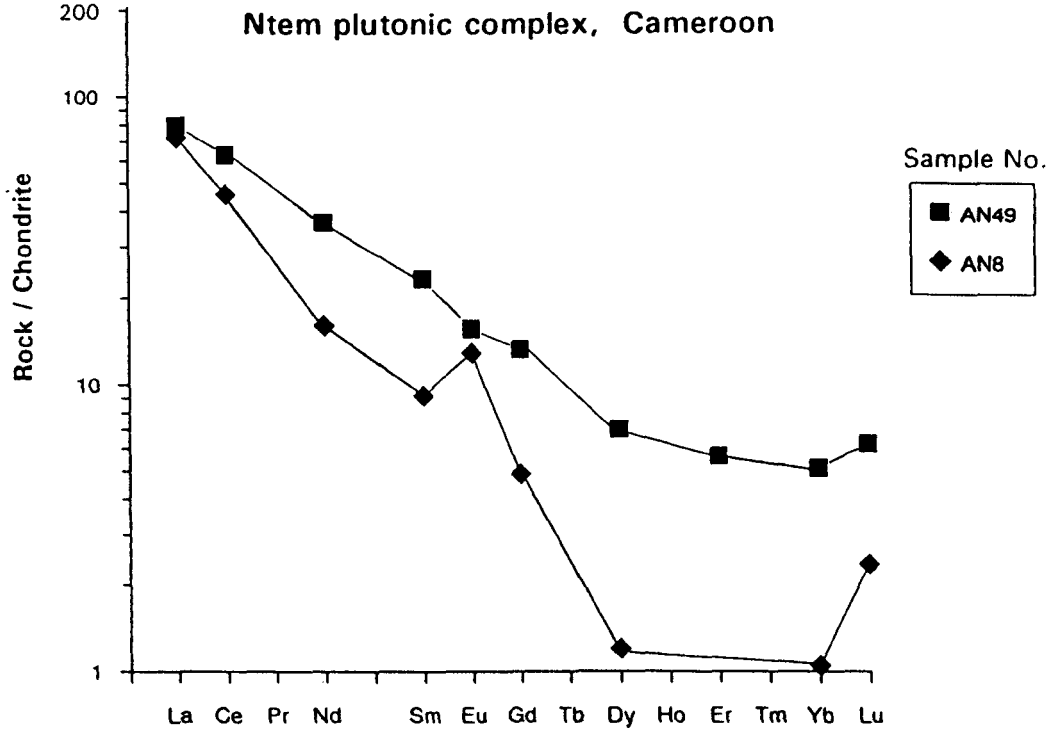

Fig. 4.12b: Chondrite-normalised REE patterns for the Soo tonalites of the (Archaean) Ntem plutonic complex, Cameroon. Data from Nedelec et al., (1990); normalising values from Nakamura (1974). Note how the REE patterns of the Ntem samples compare to those of the Mariaba pluton (Fig. 4.11a).

level. Such high compatible element abundances reflect the pluton's rich mafic assemblage of amphibole, biotite and epidote. The pluton has a distinct soda affinity with Na_2O values ranging from 3.58% to 4.32%. Na_2O/K_2O ratios vary between 1.46 and 3.25.

The chondrite-normalised REE data define a tight regular trend exemplified by fractionated LREE/HREE patterns (Fig. 4.10b) which closely correspond to those of the Omai Stock in terms of La_n/Yb_n ratios, negligible Eu anomalies and total REE and Y abundances. The close similarity in REE signatures may therefore suggest that the two granitoid bodies are genetically related.

Previous field and petrographic studies by Cannon (1963) classified the Tigri pluton as a granodiorite with an adamellite (granite) core. However, the fresh petrographic assessment presented in this thesis (see Fig. 2.4) shows that the Tigri pluton has a compositional range of quartz diorite to granodiorite with the majority of samples plotting in the tonalite field. This most recent petrographic classification is largely upheld by geochemical data which intimates that the Tigri pluton is tonalitic to granodioritic in composition (see Fig. 4.8). Moreover, on the basis of the limited field and sample data, it is tentatively proposed that the Tigri pluton is comprised of a granodioritic core mantled by a tonalitic rim.

4.8.3 The Mariaba pluton.

The Mariaba pluton, which was originally classified as a "biotite trondhjemite" according to petrographic criteria (Cannon, 1963), is chemically distinct from its granitoid neighbours and shows several major oxide similarities to the (high Al) trondhjemites defined by Barker (1979). In brief, the Mariaba pluton is characterised by its comparatively acid nature (65.63 to 70.66% SiO_2), high soda values (4.40 to 6.25% Na_2O) and low K_2O, $Fe_2O_3^T$ and MgO contents. The trondhjemitic character of the pluton is further endorsed by the data distribution on the Na_2O-CaO-K_2O ternary diagram of Fig. 4.8. The petrographic evidence clearly demonstrates that the pluton has strong tonalitic affinities (see Fig 2.4) and therefore the true composition of the Mariaba pluton is most likely tonalite-trondhjemite. The mean Rb/Sr ratio for the pluton of about 0.1 roughly corresponds with that of the Tigri pluton (see Fig. 4.9).

Relative to the Omai Stock and Tigri pluton, the Mariaba samples define a broader but regular range of chondrite-normalised REE patterns exemplified by highly fractionated La_n/Yb_n ratios of 15.6 to 66.5 (see Fig. 4.11a). The Mariaba REE signatures also differ by their severe HREE depletion and the presence of a moderately positive Eu anomaly at the lower SiO_2 levels. Total REE abundances also tend to be lower in the Mariaba pluton compared with the Omai Stock and Tigri pluton (see Fig. 4.14b).

4.8.4 The Mowasi pluton.

The sample MW-85 yields SiO_2, Na_2O and K_2O values of 65.09%, 4.13% and 3.21% respectively. The chondrite-normalised REE pattern shown in Fig. 4.11b is to some extent comparable with those shown by the Omai Stock and Tigri pluton, however, the Mowasi sample can be distinguished by its higher total REE contents (202 ppm), higher La_n/Yb_n ratio (20.1) and its straighter, steeper HREE "tail". The Rb/Sr ratio of 0.23 yielded by sample MW-85 is also relatively high compared to the other Omai granitoid rocks (see Fig. 4.9). Petrographically, the Mowasi sample plots as a tonalite (Fig. 2.4) though according to the chemical data (Fig. 4.8) the sample has a granodioritic composition.

4.9 Petrogenesis

I-type versus S-type granitoids.

A combination of chemical attributes, including calc-alkaline magmatic affinity, a meta- to weakly peraluminous nature and relatively high soda-contents, intimates that the Omai granitoids were not generated by anatexis of a sedimentary source. This hypothesis is supported by the predominance of modal hornblende and minor sphene in thin section and by the lack of such minerals as cordierite, garnet, tourmaline and primary muscovite. According to the criteria laid down by Chappell and White (1974), the Omai granitoids display typical I-type granitoid affinities as opposed to S-type ones.

Mantle source versus crustal source.

In the absence of local isotopic data, it is not possible to ascertain whether the Omai granitoids are mantle-derived or whether they are partial-melt products of older sialic crust. However, in the closely analogous Inini greenstone belt of French Guiana, Gruau et al., (1985) have recorded mantle-type intial $^{87}Sr/^{86}Sr$ ratios of 0.7019 ± 4 (2σ) in the Trans-Amazonian orthogneiss complexes of Arawa and Degrad Roche. Teixeira et al., (1989) indicate that such values are representative of the orogenic granitoid complexes which form the backbone of the Maroni-Itacaiunas mobile belt. Moreover, the fact that no record of Archaean basement has been documented in the Guiana Shield, save the fault-bounded Imataca complex of eastern Venezuela, also suggests that the regional Trans-Amazonian granitoids are not the products of reworked sialic crust.

Archaean TTG suites versus Phanerozoic I-type suites.

The Precambrian orogenic granitoid complexes which comprise substantial portions of ancient

proto-continental cores may be classified according to one of two main petrogenetic associations (see Martin, 1986; Cassidy et al., 1991). The first and most widespread of these is referred to as the so-called Archaean TTG (tonalite-trondhjemite-granodiorite) suites. Secondly, some Precambrian granitoid rocks have petrogenetic affinities akin to Phanerozoic I-type suites (also known here as Post-Archaean granitoids) of relatively recent orogenic belts. Martin (1986) maintains that Archaean TTG suites are characterised by highly fractionated La_n/Yb_n ratios ranging from 5.0 to 150 and depleted HREE and Y values with Yb_n contents in the order of 4.5 to 8.0. These trends appear to contrast with the more moderate La_n/Yb_n ratios of less than 20 which typify Post-Archaean granitoids. Yb_n values of 4.5 to 20 in the latter are relatively more enriched than those found in Archaean TTG suites (see also Table 4.1).

The La_n/Yb_n-Yb_n diagram (Fig. 4.13) demonstrates that the Mariaba pluton has clear petrogenetic affinities to Archaean TTG suites whilst the Omai Stock, Tigri pluton and the Mowasi pluton show transitional tendencies with a slight bias towards the Post-Archaean granitoid field. The rationale underpinning this diagram remains a contentious issue and merits elaboration at this juncture. Martin (1986), among others, proposes the global TTG magmas were generated as a result of the higher geothermal gradients operating in Archaean tectono-thermal settings relative to those found in post-Archaean subduction environments. Apparently, the elevated geothermal gradients of the Archaean facilitated the partial fusion of "subducted" amphibolitic/eclogitic oceanic crust, before dehydration could occur, generating large volumes of trondhjemitic liquids and an amphibole and/or garnet-rich residue. These residual amphibole/garnet phases are thought to have been the controlling factors behind the highly fractionated, HREE-depleted REE patterns which characterise Archaean TTG suites. Support for this hypothesis has been recently provided by the vapour-absent experimental work of Rapp et al., (1991). In contrast, lower geothermal gradients in post-Archaean orogenic regions gave rise to a vastly different petrogenetic regime. The relatively low geothermal gradients apparently permit the dehydration of the subducted oceanic slab before melting can begin. In turn, the dehydration process triggers off hydrous partial melting in the overlying mantle (peridotite ?) wedge, from which calc-alkaline Phanerozoic I-type granitoid magmas are produced.

The petrogenetic origin of the Omai granitoids is best considered by surveying the broader regional picture which embraces all Trans-Amazonian granitoid complexes in northern Guyana. On the whole, such regional characteristics as tonalite-dominated petrological associations, calc-alkaline magmatic affinity, prolonged plutonism and a progression from early soda-granitoids to later potassic types is more consistent with Phanerozoic (Cordilleran) I-type suites as opposed to Archaean TTG magmatism. However, one must be wary in carrying the analogy to far as comparable rocks do not necessarily imply comparable

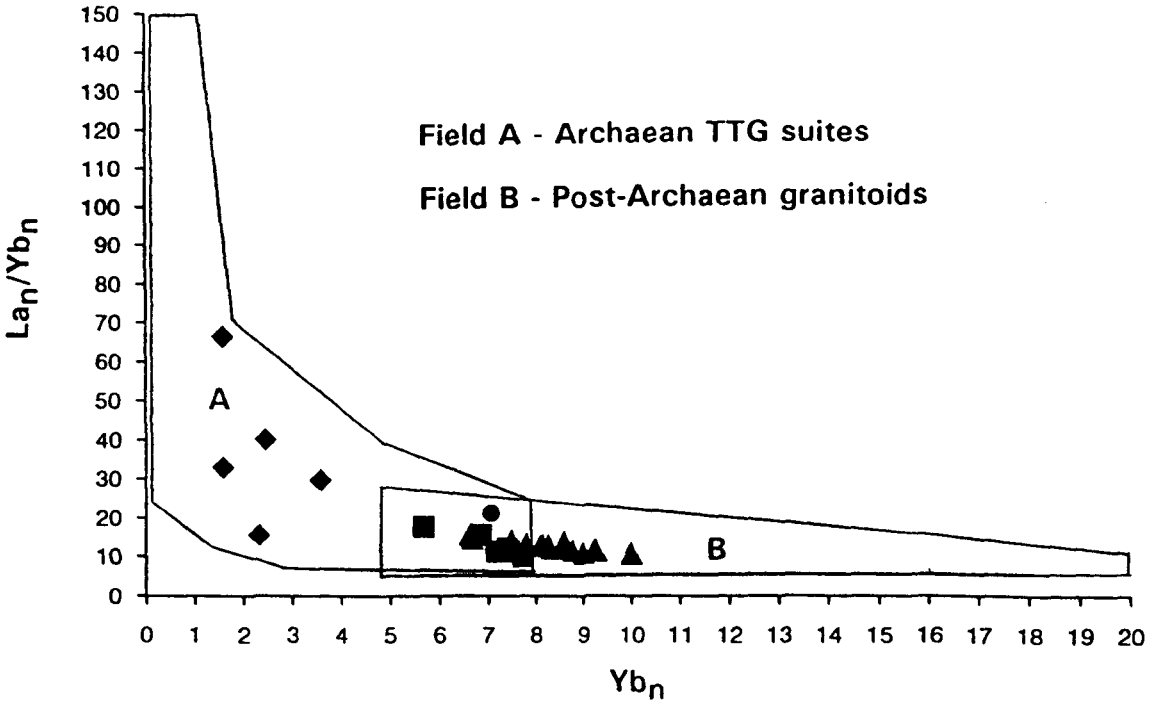

Fig. 4.13: La_n/Yb_n - Yb_n diagram showing the REE geochemistry of the Omai granitoid rocks in relation to Archaean TTG (tonalite-trondhjemite-granodiorite) suites and Post-Archaean granitoid rocks (also known here as Phanerozoic I-type suites). Field boundaries from Martin (1986). See text for discussion.

Symbols as for Fig. 4.4

Table 4.1: Comparison of the Omai granitoid rocks with Archaean TTG suites and Phanerozoic I-type suites.

Table 4.1: Comparison of Omai granitoid rocks with[1] Archaean TTG suites and Phanerozoic I-type suites.

	Archaean TTG Suites	Phanerozoic I-type Suites	Omai - Tigri Complex	Mariaba Pluton
Compositional variation	tonalite-trondhjemite-granodiorite	gabbro-diorite-granodiorite-tonalite-granite	diorite-quartz diorite-tonalite-granodiorite	tonalite-trondhjemite
Na_2O/K_2O	> 2	< 2	range: 1.46-3.25; mean: 2.37 (Tigri pluton only)	range: 2.21-7.02; mean: 2.76
REE geochemistry	highly fractionated REE patterns; depleted HREE & Y values; negligible-positive Eu anomalies La_n/Yb_n: 5 - 150 Yb_n: 0.3 - 8.5	moderatley fractionated REE patterns; moderate HREE & Y values; negligible Eu anomalies La_n/Yb_n: ≤ 20 Yb_n: 4.5 - 20	moderately fractionated REE patterns; moderate HREE & Y values; negligible Eu anomalies La_n/Yb_n: 10.1 - 17.7 Yb_n: 5.7 - 9.2 Mean Eu/Eu^* = 1.0	highly fractionated REE patterns; depleted HREE & Y values; negligibe-positive Eu anomalies La_n/Yb_n: 15.6 - 66.5 Yb_n: 1.6 - 3.6 Mean Eu/Eu^* = 1.1
Isotopic data	homogeneous and mantle-type Sr, Nd and Pb isotopic ratios	variable initial Sr, Nd and O isotope compositions, depending on crustal component in source region.	no data	no data

Definitive criteria for Archaean TTG suites and Phanerozoic I-type suites from Martin (1986) and Cassidy et al., (1991).

petrogenetic origins. The spatial and temporal intimacy between the Omai Stock and appinite intrusions is an additional feature which aligns the Omai granitoids with Phanerozoic I-type suites. This lamprophyre - felsic pluton association, which is a common attribute of the Caledonian Fold Belt (see Rock and Hunter, 1987) is generally absent from Archaean TTG terrains, though some examples have been documented in the Superior Province of Canada (see Wyman and Kerrich, 1989).

Petrogenetic trends in the Omai granitoid rocks: implications.

The closely compatible sub-horizontal trends and strongly overlapping data displayed by the Omai Stock and Tigri pluton in the Ce_n/Yb_n-SiO_2 and Total REE-SiO_2 diagrams (Figs. 4.14a and 4.14b respectively) affirm the fact that these two granitoid bodies are genetically related, though this does not necessarily imply that they were emplaced during the same pulse of magmatism. By the same token, the sharply discordant trend exhibited by the Mariaba pluton in both these diagrams implies that this body experienced a somewhat different petrogenetic history and/or source from the Omai-Tigri complex.

Fig. 4.14a clearly shows that Ce_n/Yb_n ratios in the Mariaba pluton rapidly increased during differentiation. This trend can be accounted for by the fractionation of phases such as hornblende, garnet, zircon and clinopyroxene which have high mineral/melt distribution coefficients (Kd's) for HREE relative to LREE. However, minerals such as hornblende and garnet tend to deplete the melt in total REE contents whereas Fig. 4.14b plainly demonstrates that total REE contents in the Mariaba pluton have a strong positive correlation with SiO_2. Nevertheless, the overall configuration of the REE profiles, i.e. highly fractionated, HREE-depleted patterns with minor to moderately positive Eu anomalies at the lower silica levels suggest that residual phases such as amphibole and/or garnet, as opposed to fractionating phases are the primary controls behind the Mariaba REE trends. The fractionating mineral phases have therefore only a secondary influence. The Ce-Yb mineral vector diagram (Fig. 4.15) intimates that the main fractionating phases included components from the cpx-kfsp-opx-bio-ol-plag assemblage, possibly in combination with zircon (and/or xenotime).

With respect to the Omai-Tigri complex, Figs. 4.14a and 4.14b indicate that Ce_n/Yb_n ratios and total REE contents remained fairly constant, though there might be a slight reduction in total REE contents during differentiation (Fig. 4.14b). In the Ce-Yb mineral vector diagram (Fig. 4.15), the Mariaba and the Omai-Tigri trends appear to be sub-parallel, though the data is so tightly clustered in the latter case that no definitive trends can be unequivocally discerned. However, the overall configuration of the REE patterns for the Omai-Tigri complex implies that clinopyroxene was a dominant fractionating phase. The fact that Eu anomalies in the Omai-Tigri complex are largely negligible is of further interest. Elsewhere, Hanson

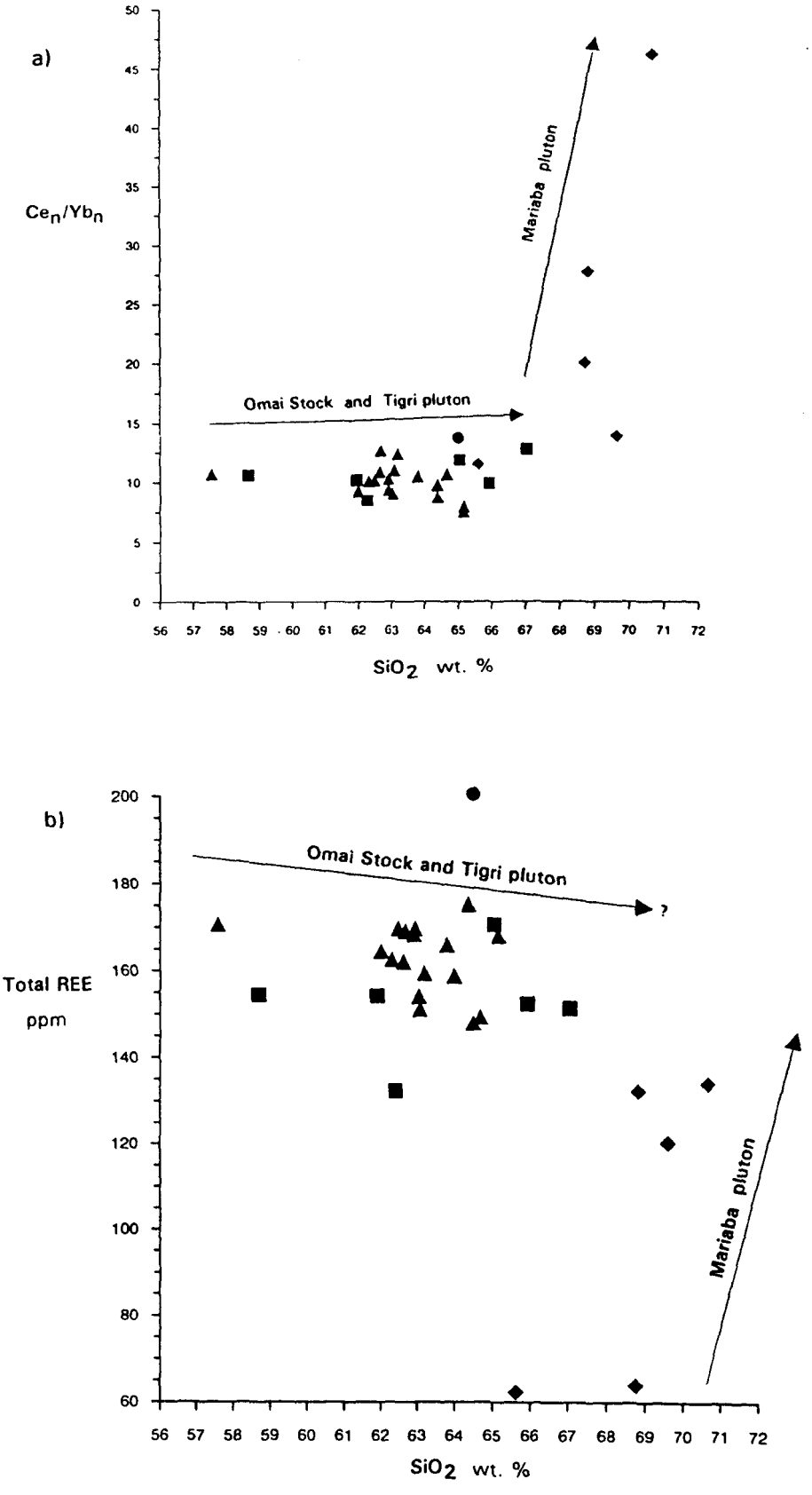

Fig. 4.14: Co-variation diagrams showing petrogenetic trends in the Omai granitoid rocks with increasing SiO_2 contents. a) Ce_n/Yb_n - SiO_2; b) Total REE - SiO_2. Symbols as for Fig. 4.4.

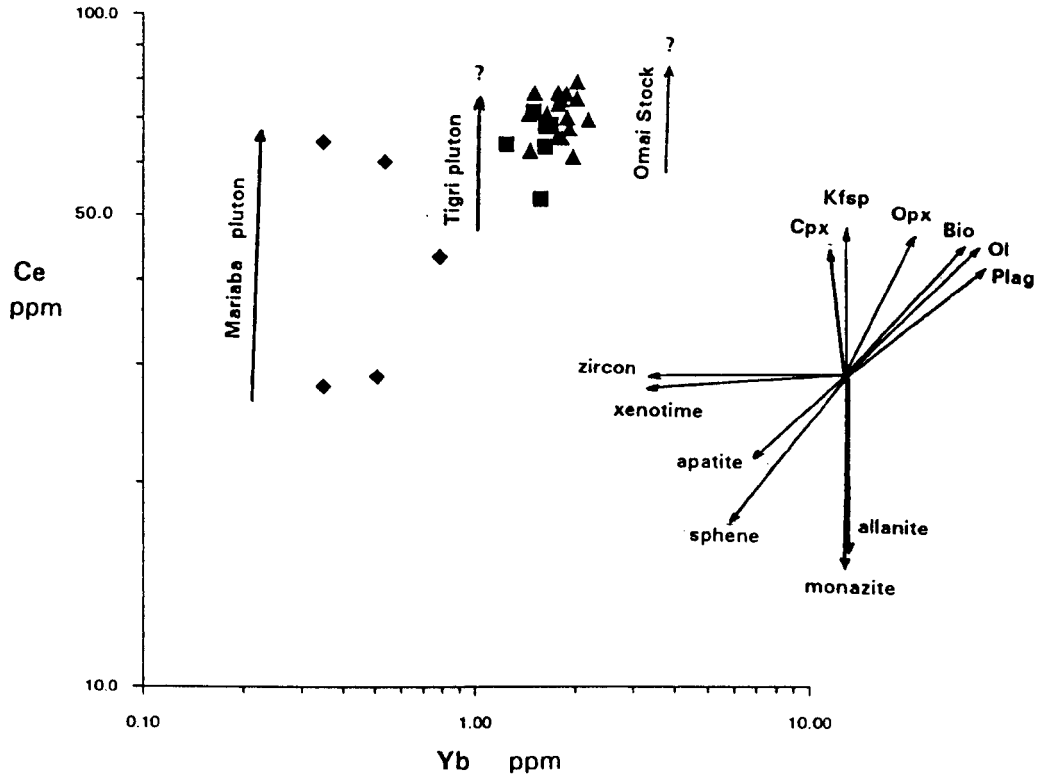

Fig. 4.15: Ce - Yb mineral vector diagram showing petrogenetic trends in the Omai granitoid rocks. Mineral vectors from Tindle and Pearce (1981) assuming Rayleigh fractionation. Symbols as for Fig.4.4.

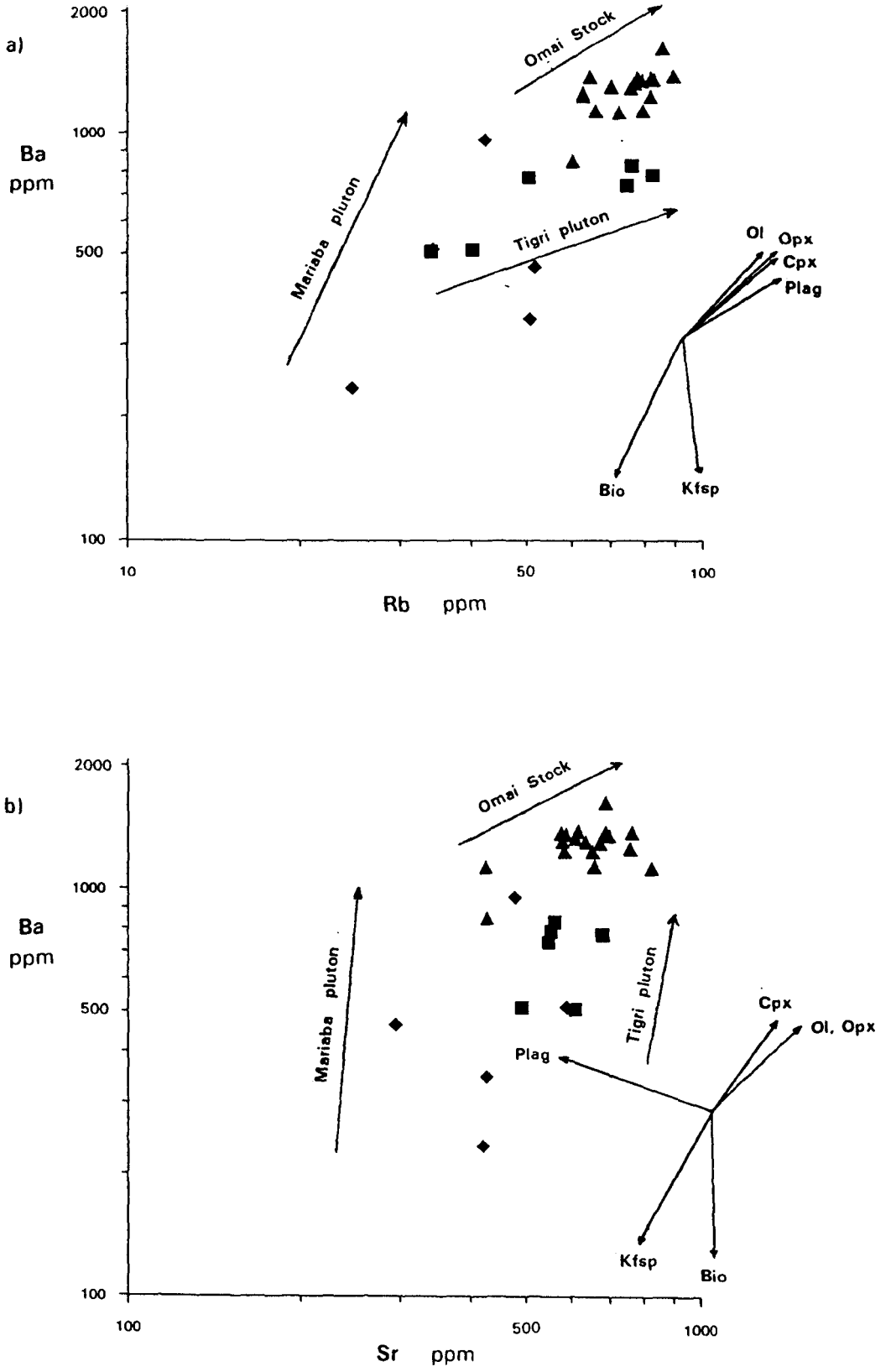

Fig. 4.16: Mineral vector diagrams showing petrogenetic trends in the Omai granitoid rocks. a) Ba - Rb; b) Ba - Sr. Mineral vectors from Tindle and Pearce (1981) assuming Rayleigh fractionation. Symbols as for Fig. 4.4.

(1978) suggests that granitic melts displaying this phenomenon are produced by equal proportions of plagioclase and clinopyroxene, or twice as much plagioclase as hornblende, remaining in the residue. On the other hand, Witt and Swager (1989) note that negligible Eu anomalies may be the result of a balancing effect brought about by amphibole and plagioclase removal from the melt.

Further insight into the magmatic evolution of the Omai granitoid rocks is given by the Ba-Rb and Ba-Sr mineral vector diagrams (Figs. 4.16a and 4.16b respectively). Both these diagrams show that LIL element distribution in the Tigri pluton and the Mariaba pluton were chiefly governed by clinopyroxene and plagioclase fractionation with a minor influence exerted by olivine-orthopyroxene removal from the melt. LIL element trends in Omai Stock have undoubtedly been modified by sericitisation, though in the Ba-Rb diagram (Fig. 4.16a) the trends exhibited by the Omai Stock and Tigri pluton are sub-parallel.

On a wider regional basis, the spatial relationship between amphibolite supracrustal rocks and Trans-Amazonian intrusions, especially those with a TTG affinity, may have a far-reaching petrogenetic significance. In the Amapa territory of northern Brazil, Joao and Marinho (1982) observed that amphibolite facies meta-volcanic rocks of the Vila Nova supracrustal suite showed evidence of partial melting in the proximity to a soda-rich TTG complex known as the Papa Vento tonalites. This complex also carries amphibolitic xenoliths which João and Marinho (1982) interpreted as precursors of the granitoid rocks. Similar relationships between tonalite-trondhjemite complexes and amphibolite supracrustal rocks have been documented in the Stonbroekoe area of Surinam (Veenstra, 1978) and in the Upper Supamo area of Venezuela (Moreno and Mendonza, 1975). Bearing these relationships in mind, it is of interest to note that large volumes of amphibolite, presumably derived from the adjacent Barama-Mazaruni Supergroup, are interspersed with the granitoid-gneisses of the Bartica Assemblage which the Mariaba pluton intrudes on its northern margin. Amphibolite-facies meta-volcanic country rocks have been mapped along the borders of the Tigri and Mariaba plutons in the Omai area (Cannon, 1963), though this feature may merely be the result of contact metamorphism with little or no petrogenetic significance. Further afield, additional supporting evidence for this amphibolite-TTG model has been recorded in the Archaean terrain of north central Newfoundland (Payne and Strong, 1979). These authors concluded from field and geochemical data that the Twillingate trondhjemite pluton was generated by the partial melting of low-K tholeiites under amphibolite facies conditions in the root zone of an island arc complex.

In summary, it is possible to say that the trace element characteristics, especially the REE data, demonstrate that the Mariaba pluton was derived from a source which differed from that of the Omai-Tigri granitoid complex. The REE trends, supported by field data from

analogous granitoid bodies in other parts of the Guiana Shield, strongly suggest that the Mariaba pluton was generated by the partial melting of an amphibole/garnet-rich mafic protolith, probably associated with the greenstone supracrustal rocks of the Barama-Mazaruni Supergroup. The petrogenetic history of the Omai-Tigri complex is less certain, but two source scenarios are tentatively proposed. These are: 1) partial hydrous melting of a mantle (peridotite ?) wedge above a subduction-type zone, and 2) partial fusion of amphibole/garnet-poor greenstones of the Barama-Mazaruni Supergroup.

4.10 Tectonic association.

As stated earlier in this thesis, Precambrian plate tectonic processes are poorly understood and ancient terrains do not necessarily have modern analogues in terms of tectonic setting. However, the calc-alkaline character of the Omai granitoids coupled with their Trans-Amazonian stratigraphic position, clearly implies that these rocks have an orogenic origin. Moreover, as summarised in Table 4.1, the Omai granitoids share several physical and chemical attributes with global Archaean and Phanerozoic orogenic granitoid suites. A point worth noting at this stage is that not all Precambrian granitoid belts are strictly orogenic in origin. For example, Kerr (1989) remarks that some alkalic-calcic components within the Proterozoic Trans-Labrador Granitoid Belt (TLGB) of eastern Canada have trace element characteristics which invite comparison with Phanerozoic A-type or within-plate granites (WPGs). In southern Guyana, south of the Takutu Break, the huge P2-type Trans-Amazonian granitoid complexes may have a similar anorogenic association.

The ORG (Ocean Ridge Granite)-normalised spidergrams* displayed by the Omai granitoids in Figs. 4.17a and 4.17b demonstrate a couple of points. Firstly, the remarkably consistent spiky profiles with fractionated LILE/HFSE ratios and characteristic Ta-Nb trough intimates that the Omai granitoids were generated in a subduction-related environment, though not necessarily in a conventional linear subduction zone as found in modern magmatic arc settings. Secondly, the extremely comparable ORG-normalised profiles shown by the Omai Stock and the Tigri pluton affirm that these two rock-types are genetically related and are probably part of the same plutonic complex.

In the Rb-Y+Nb discrimination diagram (Fig. 4.18), the Omai granitoids show unambiguous tectonic affinities with Phanerozoic volcanic arc granites (VAGs). (Three representative samples from the Omai Stock are plotted, despite mild Rb enrichment due to sericitisation. Overall, the degree of Rb enrichment is insignificant relative to the scale of the diagram). However, such diagrams have their limitations. For example, granitoid rocks plotting in the VAG field may have been generated during remobilisation of the mantle wedge in a post-

* In the Omai ORG-normalised values, Ta* is calculated as Nb/12 (see Jochum et al., 1986) and K represents K_2O.

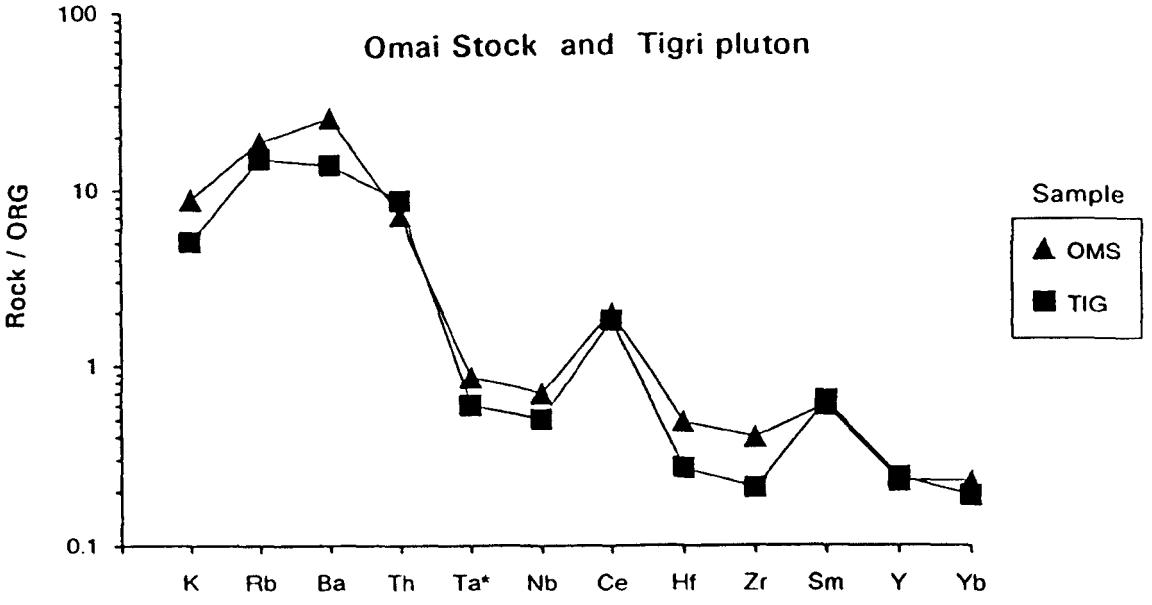

Fig. 4.17a: Average ORG-normalised spidergram profiles for the Omai Stock and Tigri pluton. Sample OMS represents the mean profile of the Omai Stock (n = 18, 17 for REE data); sample TIG represents the mean profile for the Tigri pluton (n = 6). Normalising values from Pearce et al., (1984).

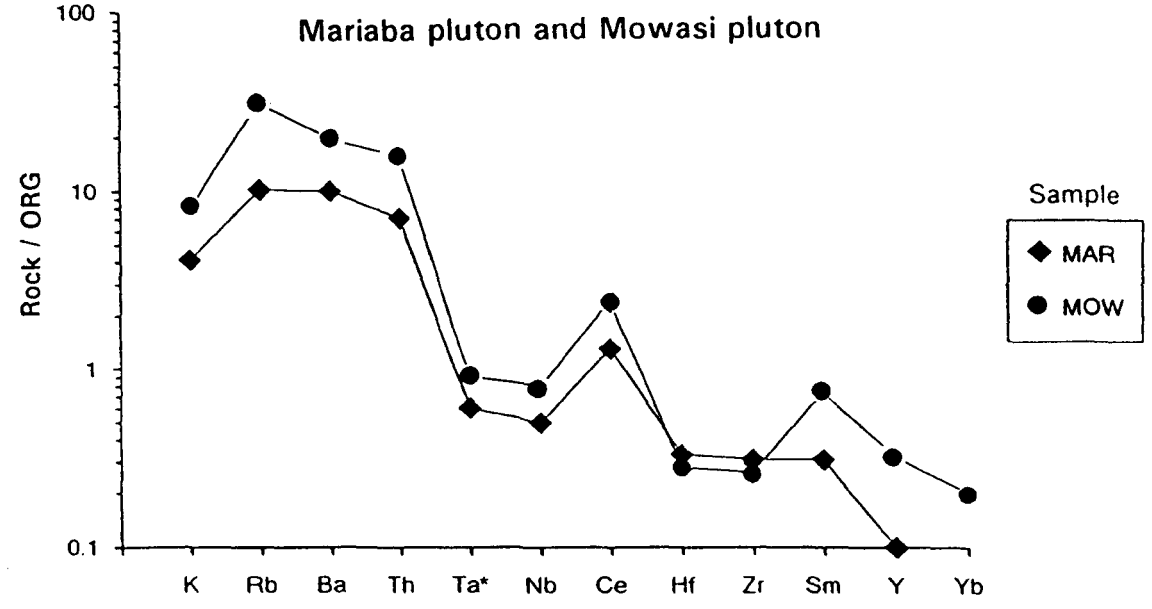

Fig. 4.17b: Average ORG-normalised spidergram profiles for the Mariaba pluton and the Mowasi pluton. Sample MAR represents the mean Mariaba profile (n = 5) whilst sample MOW represents the Mowasi sample, MW-85. Normalising values from Pearce et al., (1984).

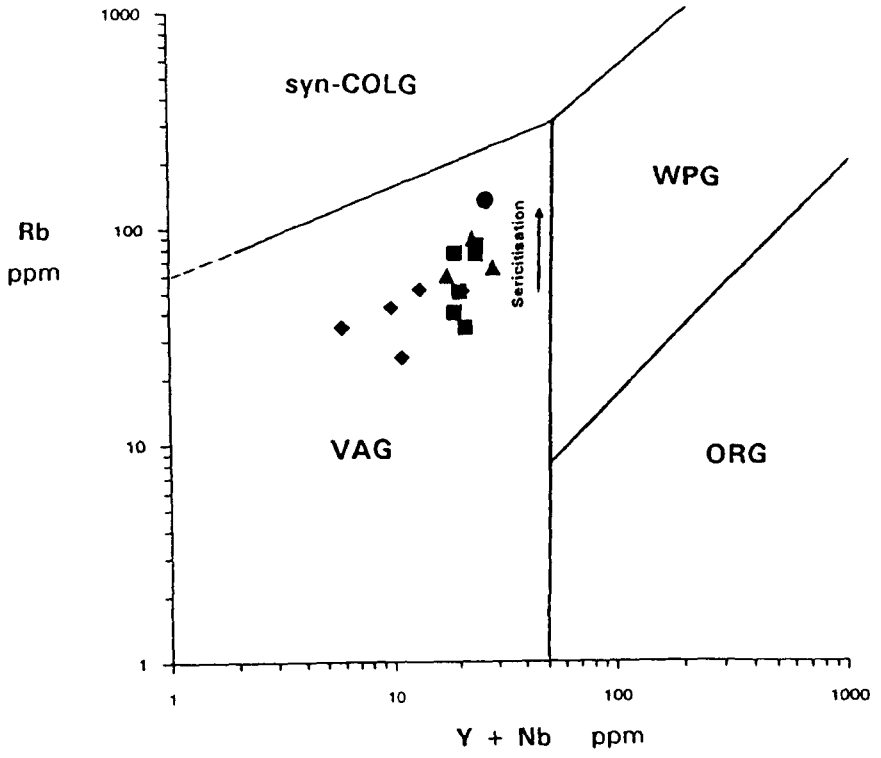

Fig. 4.18: Rb - Y + Nb discrimination diagram showing the tectonic association of the Omai granitoid rocks relative to Phanerozoic granitoid settings. The sericitisation vector for the Omai Stock is also shown. Symbols as for Fig. 4.4. Field boundaries from Pearce et al., (1984): VAG - volcanic arc granites; syn-COLG - syn-collision granites; WPG - within-plate granites; ORG - ocean ridge granites.

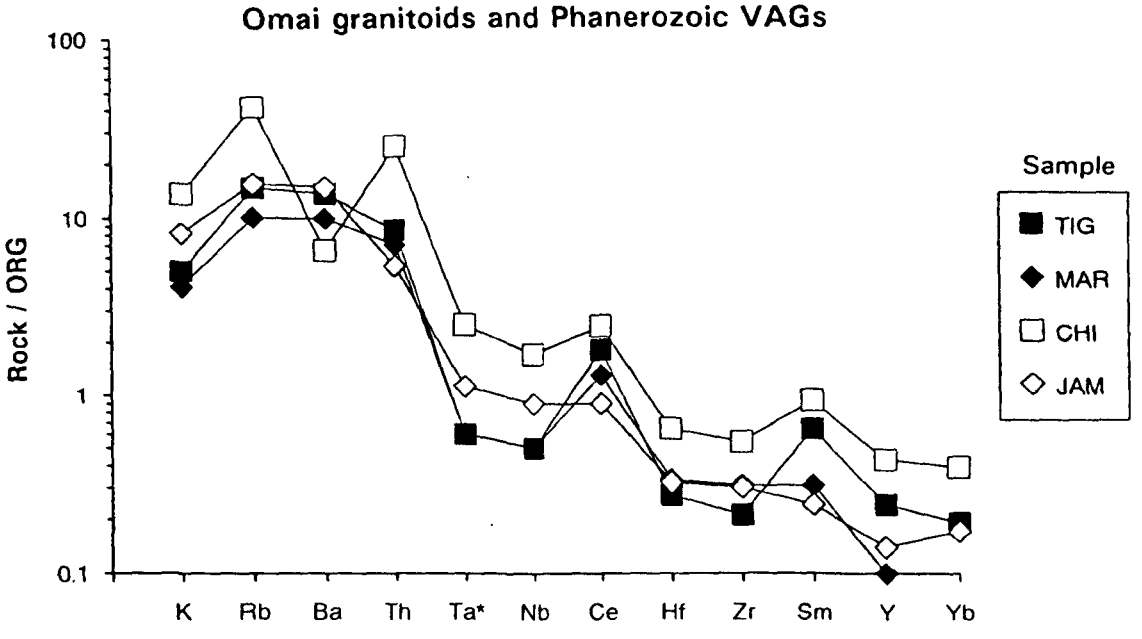

Fig. 4.19: ORG-normalised spidergram profiles comparing average Tigri (TIG) and Mariaba (MAR) profiles with representative Phanerozoic VAGs from Jamaica (JAM) and Chile (CHI). Phanerozoic data and normalising values from Pearce et al., (1984). See text for details.

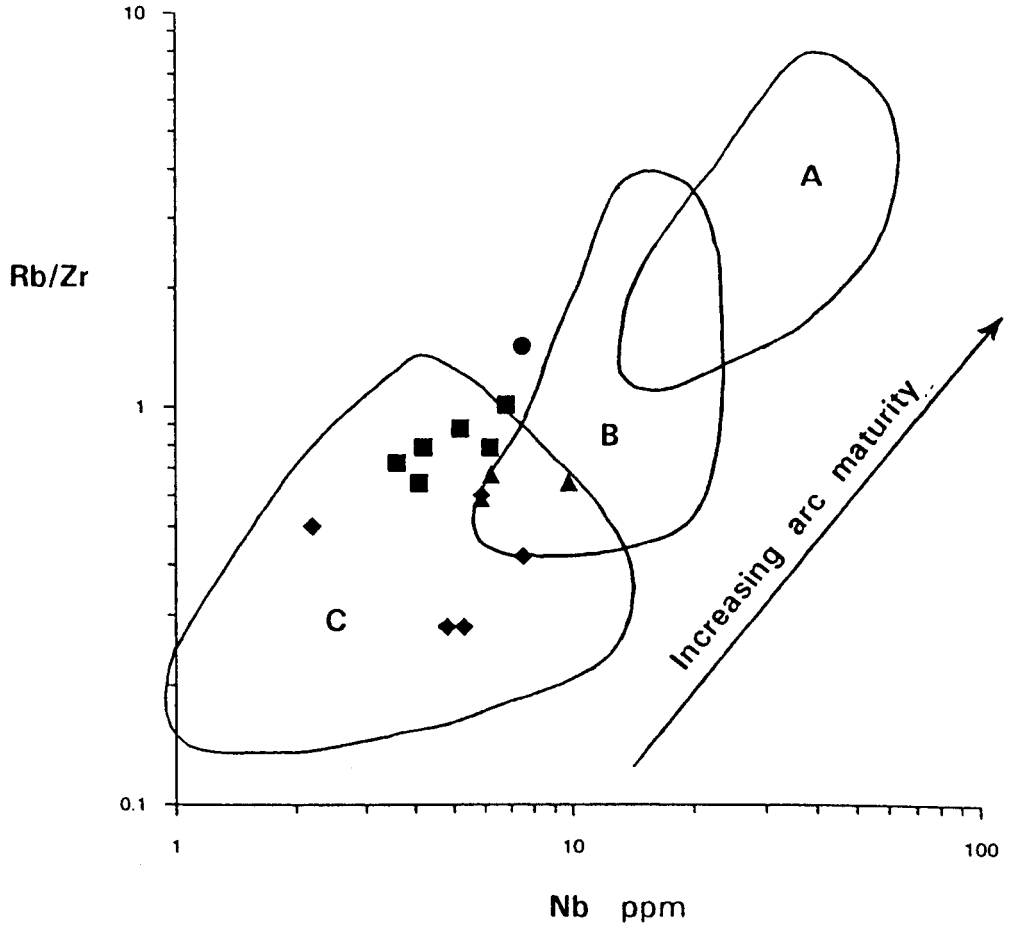

Fig. 4.20: Rb/Zr - Nb diagram showing the tectonic association of the Omai granitoid rocks with respect to Mesozoic-Cenozoic magmatic arc settings. To avoid congestion of data, only three representative samples of the Omai Stock are shown. Symbols as for Fig. 4.4. Field boundaries after Brown et al., (1984): A - mature continental arcs; B - normal continental arcs; C - primitive island arcs and continental arcs.

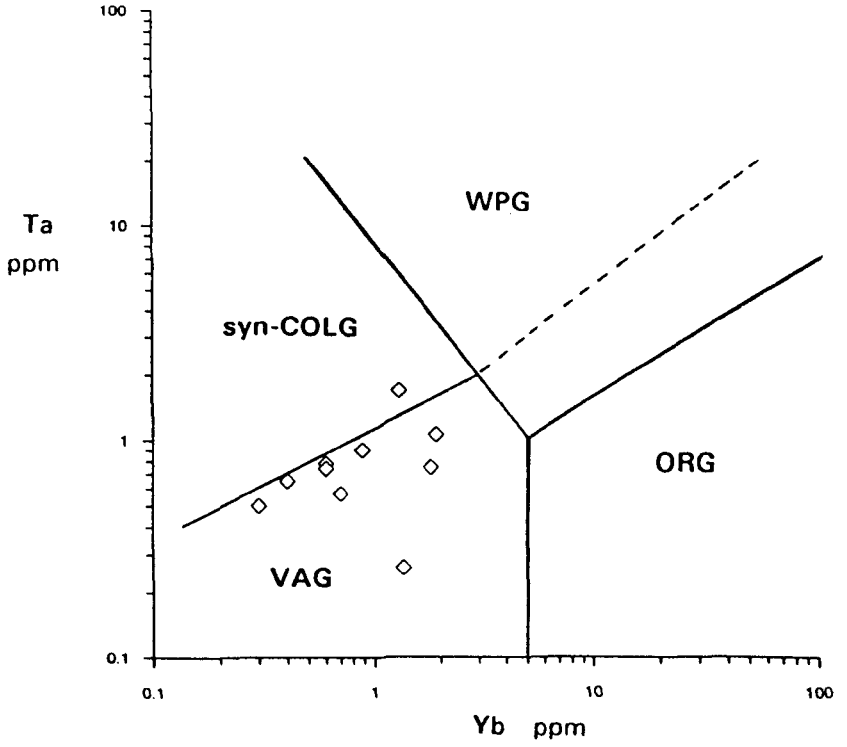

Fig. 4.21: Ta - Yb discrimination diagram showing the tectonic association of the (Palaeoproterozoic) Saramacca TTG complex, Surinam with respect to Phanerozoic granitoid settings. Saramacca data from Veenstra (1978). Field boundaries from Pearce et al., (1984). For explanation - see Fig. 4.18. The dashed line represents the upper compositional boundary for ORG from anomalous ridge segments.

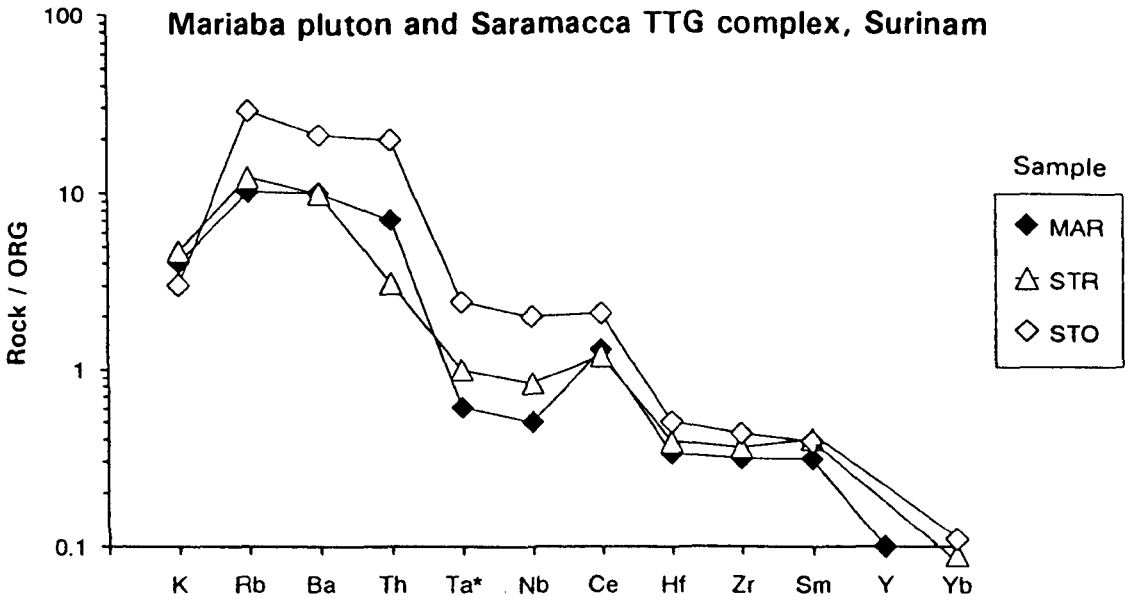

Fig. 4.22: ORG-normalised spidergram profiles comparing the average Mariaba profile (MAR) with tonalites (STO, n = 3) and trondhjemites (STR, n = 2) from the Saramacca TTG complex, Surinam. Saramacca data from De Vletter and Kroonenberg (1987), (primary Sm values interpolated from REE patterns). Normalising values from Pearce et al. (1984).

-collision environment or by partial fusion of calc-alkaline crust. Other limitations are listed in Pearce et al., (1984). Nevertheless, in Fig. 4.19, the ORG-normalised diagrams for the Tigri and Mariaba plutons correlate extremely well with representative Cenozoic volcanic arc granites from Jamaica (oceanic arc) and Chile (continental arc).

Finally, according to the Rb/Zr-Nb diagram of Fig. 4.20, the Omai granitoids show a strong tectonic affinity with Mesozoic and Cenozoic granitoids from primitive oceanic and continental arc settings. This evidence concurs with the fact that in the Trans-Amazonian orogenic cycle the Omai granitoids occur as early soda-types as opposed to late-stage potassic ones.

4.11 Regional correlation.

The paucity of critical trace element data for the Trans-Amazonian granitoid rocks of northern Guyana and beyond is regrettable as detailed chemical correlations are limited. Nevertheless, Gibbs and Barron (1992) note that the "biotite granites" of Surinam show good field and petrological associations with the Younger Granite Group of northern Guyana. The Saramacca TTG complex located in the Stonbroekoe area of northeast Surinam is one such "biotite granite" for which key trace element data are available (see Veenstra, 1978; De Vletter and Kroonenberg, 1987). These rocks, like the Omai granitoids, shown strong VAG affinities as demonstrated by the Ta-Yb diagram of Fig. 4.21. In terms of ORG-normalised signatures the Mariaba pluton and Saramacca tonalites are very closely compatible (see Fig. 4.22). In general, these profiles differ slightly from those of the Omai Stock, Tigri and Mowasi signatures in that they have noticeably lower Sm/Zr and Ce/Nb ratios and are more depleted in Y and Yb.

On a global scale, the Omai Stock and Tigri pluton have REE patterns very similar to the Palaeoproterozoic tonalite-trondhjemite-granodiorite suite of the Atnarpa Igneous Complex of central Australia (see Fig. 4.12a and Zhao and Cooper, 1992). As previously mentioned, the Mariaba pluton has REE patterns similar to those found in Archaean TTG suites. Examples of characteristic REE trends from a typical Archaean TTG suite are provided by the Soo tonalites of the Ntem plutonic complex of southern Cameroon (see Fig. 4.12b and Nedelec et al., 1990).

Table 4.2: Geochemical analyses of the Omai granitoid rocks (overleaf).

Notes:

1. Major oxide values are recalculated to 100 % anhydrous basis.
2. Major oxide values in weight percent (wt.%), trace element concentrations in ppm.
3. Total Fe analysed as $Fe_2O_3^T$.
4. LOI denotes loss-on-ignition values (wt.%).
5. Non-commercial standards used for Tm (and Lu) analyses appears to have induced erratic Tm values.

Table 4.2: Geochemical analyses of the Omai granitoid rocks.

	Omai Stock								
	6-1205	6-0786	6-1507	6-0251	6-1815	5-0811	7-1220	6-0139	7-2124
SiO2	57.57	62.01	62.31	62.48	62.64	62.68	62.90	62.94	63.05
Al2O3	20.50	19.10	18.65	18.75	18.61	19.03	18.54	18.79	18.18
$Fe_2O_3^T$	4.25	3.95	3.95	3.58	3.71	3.65	3.74	3.79	3.82
MgO	1.65	1.41	1.59	1.45	1.66	1.41	1.96	1.36	2.18
CaO	7.34	5.06	5.19	5.17	4.68	4.89	4.55	4.66	4.45
Na2O	3.54	3.81	3.88	4.06	4.48	3.66	4.38	3.96	4.06
K2O	4.42	3.93	3.71	3.83	3.53	4.01	3.23	3.78	3.58
TiO2	0.39	0.40	0.41	0.37	0.38	0.38	0.37	0.41	0.36
MnO	0.17	0.15	0.12	0.15	0.12	0.12	0.13	0.14	0.11
P2O5	0.17	0.18	0.19	0.16	0.19	0.17	0.20	0.17	0.21
Total	100.00	100.00	100.00	100.00	100.00	100.00	100.00	100.00	100.00
LOI	6.87	5.58	5.46	5.38	4.58	5.56	4.47	5.83	2.85
Rb	81.9	82.8	78.9	89.1	70.2	77.6	85.6	81.9	77.0
Sr	688	588	698	617	638	577	691	585	612
Ba	1378	1362	1353	1389	1306	1371	1631	1239	1329
Li	9.91	19.3	6.87	7.18	5.87	3.72	5.55	6.24	4.53
Y	18.0	17.9	14.5	17.3	13.7	12.2	19.1	18.0	17.1
Zr	135	138	149	132	130	131	140	130	160
Nb	7.16	8.57	7.61	6.22	6.21	6.78	7.70	6.41	7.70
Hf	5.32	5.48	4.25	3.89	4.01	3.58	3.87	4.04	3.72
Th	5.24	5.37	5.43	6.22	4.72	5.78	7.30	5.33	5.81
U	1.82	1.67	1.77	2.04	1.50	1.92	2.02	1.87	1.61
Co	19.9	21.4	20.7	19.9	20.2	20.7	20.9	20.2	20.7
Cr	80.2	81.9	128	104	98.5	51.9	107	141	153
Ni	13.7	11.9	16.9	16.5	11.9	9.9	19.2	9.2	24.2
V	63.1	58.0	58.4	63.4	63.3	58.2	65.9	59.2	61.8
Sc	3.2	2.9	3.3	3.0	3.0	2.4	4.0	2.9	3.7
Cu	32.3	33.4	46.0	35.0	35.2	35.4	54.0	51.3	39.9
Pb	15.7	12.3	13.7	13.6	13.9	11.2	18.9	14.3	10.3
Zn	72.6	73.5	56.5	69.1	50.4	53.8	74.9	63.7	59.8
As	2.5	1.0	2.5	0.5	1.5	1.0	2.1	0.5	1.9
La	35.0	34.7	34.3	35.6	35.0	35.5	35.0	35.5	33.4
Ce	76.0	69.9	68.1	75.8	70.7	76.0	74.6	74.3	65.2
Pr	8.10	8.10	8.19	8.00	7.80	8.08	8.00	8.20	7.60
Nd	30.9	31.1	31.4	30.2	29.7	30.5	29.9	30.9	28.4
Sm	5.70	5.56	5.83	5.40	5.46	5.50	5.50	5.70	5.17
Eu	1.69	1.66	1.71	1.60	1.57	1.65	1.59	1.60	1.45
Gd	5.00	4.70	4.90	4.66	4.25	4.53	4.72	4.80	4.52
Tb	0.59	0.59	0.58	0.56	0.51	0.56	0.60	0.58	0.56
Dy	3.10	3.18	2.94	3.03	2.61	2.62	3.15	3.18	2.94
Ho	0.58	0.60	0.52	0.57	0.57	0.55	0.64	0.67	0.58
Er	1.70	1.75	1.62	1.71	1.41	1.35	1.87	1.70	1.72
Tm	0.28	0.27	0.25	0.29	0.23	0.26	0.28	0.28	0.26
Yb	1.79	1.90	1.72	1.89	1.65	1.52	2.03	1.82	1.83
Lu	0.29	0.31	0.29	0.33	0.29	0.32	0.33	0.32	0.28
La_n/Yb_n	13.1	12.2	13.3	13.8	14.2	15.6	11.5	13.1	12.2
Total REE	170.7	164.3	162.4	169.6	161.8	168.9	168.2	169.6	153.9

Table 4.2 (cont'd): Geochemical analyses of the Omai granitoid rocks.

	Omai Stock								
	5-0485	7-0309	7-1808	8-0179	6-0626	7-0258	8-1596	8-2434	7-1300
SiO2	63.08	63.19	63.80	63.99	64.38	64.50	64.69	65.18	65.20
Al2O3	18.68	18.65	18.26	18.36	18.08	17.78	17.87	17.46	17.27
$Fe_2O_3^T$	3.74	3.50	3.55	3.56	3.67	3.74	3.55	3.38	3.51
MgO	1.27	1.32	1.32	1.23	1.69	1.38	1.41	1.29	1.36
CaO	4.66	4.89	4.48	4.38	3.79	3.99	4.17	4.11	3.50
Na2O	4.04	4.46	4.25	4.30	5.12	5.66	4.30	4.91	5.04
K2O	3.85	3.34	3.67	3.51	2.59	2.25	3.36	3.00	3.43
TiO2	0.39	0.39	0.37	0.40	0.37	0.40	0.39	0.36	0.38
MnO	0.12	0.09	0.11	0.11	0.12	0.12	0.11	0.12	0.12
P2O5	0.17	0.17	0.19	0.16	0.19	0.18	0.15	0.19	0.19
Total	100.00	100.00	100.00	100.00	100.00	100.00	100.00	100.00	100.00
LOI	5.28	5.28	3.88	5.32	3.40	3.42	5.00	3.18	1.62
Rb	75.9	60.2	72.4	66.1	62.9	62.8	70.2	79.5	64.6
Sr	675	428	829	426	654	761	581	659	765
Ba	1295	848	1128	1134	1236	1255	1309	1136	1377
Li	3.07	3.97	2.48	2.68	7.20	5.98	13.5	13.7	3.55
Y	15.7	12.2	16.5	12.3	19.5	21.5	13.4	19.0	21.5
Zr	130	102	160	122	137	125	124	123	137
Nb	6.90	5.87	6.09	6.89	7.52	7.50	8.29	9.80	7.70
Hf	3.60	2.86	4.63	3.83	3.84	3.70	7.50	7.91	3.70
Th	4.90	4.59	5.43	5.36	6.06	5.89	6.62	5.28	6.67
U	1.92	1.29	1.48	1.85	2.12	1.85	2.54	2.49	1.87
Co	20.4	23.7	19.5	16.2	20.5	21.0	16.4	19.7	21.0
Cr	39.1	107	138	189	134	165	61.2	76.8	62.7
Ni	11.1	12.6	13.7	25.4	17.8	20.0	12.1	14.0	11.2
V	53.8	64.0	58.2	63.0	59.0	65.2	54.0	57.6	62.0
Sc	2.4	3.0	3.0	3.0	2.8	3.4	3.9	3.1	3.3
Cu	45.2	52.7	48.0	63.9	37.0	38.3	63.7	46.4	58.9
Pb	13.2	26.2	11.2	15.6	14.7	13.0	17.6	38.6	184.0
Zn	54.2	62.0	62.9	73.1	74.7	83.6	55.6	59.8	68.8
As	0.6	1.0	1.0	1.5	1.2	3.2	1.2	2.1	2.6
La	33.7	34.2	34.8		33.9	35.1	32.3	32.6	35.4
Ce	65.4	70.7	73.3		67.3	79.0	62.3	61.1	69.4
Pr	7.70	7.90	8.00		7.80	8.17	7.41	7.45	8.44
Nd	28.4	29.2	30.0		29.3	30.6	27.9	28.1	31.7
Sm	4.40	5.27	5.43		5.30	5.85	5.16	5.19	5.84
Eu	0.60	1.48	1.57		1.54	1.61	1.45	1.50	1.74
Gd	2.81	4.18	4.61		4.63	5.18	4.18	4.35	5.28
Tb	0.60	0.50	0.56		0.58	0.67	0.53	0.58	0.66
Dy	2.81	2.21	2.98		3.26	3.54	2.86	3.21	3.72
Ho	0.60	0.48	0.56		0.66	0.70	0.43	0.63	0.74
Er	1.59	1.12	1.69		1.87	1.99	1.29	1.88	2.17
Tm	0.30	0.24	0.24		0.29	0.33	0.23	0.28	0.34
Yb	1.78	1.46	1.79		1.93	2.04	1.47	1.98	2.20
Lu	0.33	0.28	0.30		0.31	0.35	0.25	0.32	0.35
La_n/Yb_n	12.7	15.7	13.0		11.8	11.5	14.7	11.0	10.8
Total REE	151.0	159.2	165.8		158.7	175.1	147.8	149.2	168.0

Table 4.2 (cont'd): Geochemical analyses of the Omai granitoid rocks.

	Tigri pluton					
	TG-03	TG-06	TG-02	TG-07	TG-04	TG-05
SiO2	58.69	61.92	62.42	65.07	65.96	67.07
Al2O3	14.97	14.88	14.73	15.40	15.05	15.01
$Fe_2O_3^T$	7.11	6.02	5.84	4.30	4.32	3.83
MgO	7.40	5.58	5.65	4.12	3.75	3.11
CaO	6.13	5.03	4.67	3.58	3.47	3.29
Na2O	3.58	3.86	4.39	3.94	4.14	4.32
K2O	1.10	1.80	1.42	2.70	2.51	2.63
TiO2	0.66	0.58	0.58	0.51	0.48	0.45
MnO	0.13	0.12	0.10	0.10	0.09	0.07
P2O5	0.23	0.21	0.20	0.28	0.23	0.22
Total	100.00	100.00	100.00	100.00	100.00	100.00
LOI	1.79	1.18	1.90	0.89	0.93	0.83
Na_2O/K_2O	3.25	2.14	3.09	1.46	1.65	1.64
Rb	34.1	50.5	40.3	82.5	74.8	76.0
Sr	611	680	493	554	548	562
Ba	505	771	511	785	738	827
Li	19.8	16.0	12.1	27.3	25.0	20.1
Y	17.7	16.9	15.2	17.6	18.2	14.3
Zr	53.4	70.4	51.0	75.8	94.9	86.8
Nb	4.12	3.60	4.18	6.80	6.16	5.15
Hf	2.00	2.30	2.27	2.61	2.91	2.54
Th	4.23	5.49	4.28	9.05	9.95	8.53
U	0.96	1.62	0.67	3.10	3.22	2.40
Co	53.6	38.8	39.1	30.4	31.9	28.0
Cr	288	337	126	236	92.2	156
Ni	188	122	116	81.4	61.1	66.0
V	161	135	124	95.6	86.7	81.2
Sc	18.2	13.6	13.0	10.8	9.0	9.0
Cu	59.8	90.0	47.3	79.0	50.1	44.2
Pb	8.95	43.1	31.2	15.4	13.5	17.0
Zn	98.1	79.6	79.4	88.6	58.3	57.4
As	0.9	0.4	0.9	1.2	1.0	0.7
La	28.0	25.7	26.4	35.0	29.5	33.0
Ce	67.8	68.2	52.8	71.2	63.1	63.7
Pr	7.40	7.56	6.81	8.54	7.57	7.64
Nd	30.0	31.0	26.6	33.9	30.2	28.7
Sm	5.82	6.07	5.22	6.36	6.11	5.39
Eu	1.63	1.64	1.42	1.82	1.54	1.50
Gd	4.99	5.04	4.55	5.38	5.24	4.33
Tb	0.67	0.65	0.66	0.66	0.69	0.58
Dy	3.33	3.40	3.12	3.37	3.56	2.69
Ho	0.69	0.66	0.70	0.63	0.67	0.56
Er	1.81	1.81	1.73	1.66	1.85	1.40
Tm	0.29	0.27	0.32	0.25	0.27	0.23
Yb	1.64	1.70	1.58	1.51	1.63	1.25
Lu	0.29	0.29	0.32	0.25	0.25	0.25
La_n/Yb_n	11.4	10.1	11.2	15.5	12.1	17.7
Total REE	154.4	154.0	132.2	170.5	152.2	151.2

Table 4.2: (cont'd): Geochemical analyses of the Omai granitoid rocks.

	Mariaba pluton					Mowasi pluton
	MB-10	MB-12	MB-08	MB-11	MB-13	MW-85
SiO2	65.63	68.76	68.83	69.62	70.66	65.09
Al2O3	16.50	16.98	15.72	16.30	15.59	14.69
$Fe_2O_3^T$	3.62	1.98	3.08	2.85	2.64	4.40
MgO	2.70	0.92	2.38	1.45	0.85	4.15
CaO	3.76	3.22	3.00	2.58	2.55	3.48
Na2O	6.25	5.99	4.40	4.91	5.49	4.13
K2O	0.89	1.77	1.99	1.78	1.75	3.21
TiO2	0.44	0.26	0.39	0.34	0.31	0.58
MnO	0.06	0.02	0.07	0.04	0.03	0.01
P2O5	0.15	0.10	0.14	0.13	0.13	0.26
Total	100.00	100.00	100.00	100.00	100.00	100.00
LOI	1.51	0.68	3.37	1.45	1.14	1.27
Na_2O/K_2O	7.02	3.38	2.21	2.76	3.14	1.29
Rb	24.8	34.3	51.8	50.8	42.4	125.2
Sr	421	590	294	427	478	535
Ba	235	512	464	348	954	992
Li	17.1	12.5	27.1	27.2	19.6	17.5
Y	6.36	3.73	7.61	13.7	4.66	22.6
Zr	90.0	68.4	86.3	122	153	89.7
Nb	4.76	2.19	5.91	7.53	5.27	7.66
Hf	2.15	2.92	2.67	4.76	3.62	2.5
Th	2.17	5.00	5.17	4.26	4.82	12.6
U	0.96	1.23	1.33	1.18	1.15	2.73
Co	25.6	18.4	21.4	20.8	20.2	37.7
Cr	146	43.6	57.1	68.5	181	105
Ni	32.5	16.8	30.2	20.3	19.2	88.4
V	64.7	28.3	43	42.3	31.9	92.8
Sc	8.7	2.8	6.2	4.0	3.0	9.6
Cu	80.4	44.3	43.1	106	48.0	80.4
Pb	5.38	10.2	5.91	9.60	14.6	15.2
Zn	66.7	36.5	52.6	69.2	68.6	58.9
As	0.5	0.2	0.6	0.4	0.5	0.5
La	11.9	17.3	32.4	35.2	34.8	46.5
Ce	28.7	27.8	60.0	43.2	64.2	83.8
Pr	2.84	2.93	6.49	6.27	6.27	10.0
Nd	10.6	10.3	22.5	22.3	20.9	37.7
Sm	2.28	1.70	3.55	3.61	2.82	6.72
Eu	0.84	0.65	0.95	1.05	0.85	1.74
Gd	2.03	1.34	2.87	3.40	2.06	6.09
Tb	0.27	0.15	0.33	0.45	0.21	0.73
Dy	1.26	0.70	1.41	2.12	0.82	3.75
Ho	0.23	0.13	0.27	0.44	0.16	0.71
Er	0.61	0.33	0.64	1.08	0.39	1.87
Tm	0.11	0.06	0.11	0.18	0.07	0.26
Yb	0.51	0.35	0.54	0.79	0.35	1.55
Lu	0.10	0.07	0.11	0.15	0.08	0.25
La_n/Yb_n	15.6	33.1	40.2	29.8	66.5	20.1
Total REE	62.3	63.8	132.2	120.2	134.0	201.7

CHAPTER 5

GEOCHEMISTRY OF THE OMAI MAFIC DYKE SUITES

5.1 Aims of chapter.

Drill-core projections combined with field, petrographic and geochemical evidence presented in this study have led to the identification of at least four episodes of mafic dyke intrusion in the immediate Omai area. These dykes are significant in two respects. Firstly, on a local scale, they act as excellent stratigraphic markers and help to constrain the age of mineralisation. Secondly, on a regional scale, their trace element characteristics can be used to monitor the tectonic evolution of the Guiana Shield from Palaeoproterozoic to Mesozoic times.

The primary aim of this chapter is to define the main geochemical features of each episode of mafic dyke intrusion and, wherever possible, to establish each intrusive phase within the context of regional and even global tectono-magmatic events.

5.2 Description of the mafic dyke subset (22 samples).

As in the previous two chapters, the geochemical samples are largely drawn from the 1986 GSR drill-core collection. However, the appinite samples, HP-01 and HP-04, were collected from a large tailing dump near the former mine shaft at Red Hill whilst the gabbroic samples RX-21, RX-22 and MB-09 were obtained from fresh surface exposure in river sections (see Appendix I and Fig.2.3 for sample location). All the subset samples been analysed for a broad spectrum of major and trace elements with selected samples analysed for the rare earth elements (see Table 5.2). The analytical procedures outlined in Chapter 3 also apply to the mafic dyke subset. With the exception of samples HP-01 and HP-04, all geochemical samples have corresponding thin section specimens. Unless stated otherwise, all data presented in diagrams in this chapter are taken from Table 5.2.

5.3 Constraints.

Hypogene alteration, especially in regionally metamorphosed and/or hydrothermally altered samples, is reflected in some cases by excessive LOI values. The potential for element

mobility in such cases has already been discussed in detail (section 3.6) and no further comment is required at his point, except to say that by using a cautionary approach, emphasising petrogenetic trends, valuable data can still be obtained from altered samples. This statement is vindicated by the consistent petrogenetic trends presented throughout this chapter.

5.4 General overview.

The geology of the four main mafic dyke suites recorded in the immediate Omai area is summarised in Table 5.1. These suites range from the Palaeoproterozoic, greenstone-related minor basic intrusives of the Majuba Suite to the Mesozoic gabbroic dykes of the Apatoe Suite. The Jensen cation diagram (Fig. 5.1) shows that major element geochemistry can be used to roughly discriminate between each of the mafic dyke suites. However, in all cases, the respective REE patterns prove to be extremely diagnostic.

5.5 Minor basic intrusives of the Majuba Suite (3 samples, see Table 3.4).

These rocks which represent the earliest mafic dyking episode at Omai have already been discussed in detail in sections 2.5.1. and 3.7.3. Essentially, they are medium- to coarse-grained equivalents of the high-Fe tholeiitic (HFT) greenstone basalts of the Majuba Suite with which they are spatially and temporally associated. Apart from Fe-enrichment, the HFTs as a whole are characterised by low K, Zr and Ti abundances and by flat to moderately fractionated REE patterns of around 8 to 12 times chondrite (see Figs. 3.10a and 3.11a). Overall, the trace element geochemistry of the HFTs is consistent with primitive low-K tholeiitic basalts from contemporary island arc settings. On a regional scale, the minor basic intrusives of the Majuba Suite occupy a similar stratigraphic position to the meta-gabbros of the Issineru Formation as documented by Renner (1985).

5.6 Appinite pipes (Badidku Suite ?) (3 samples).

The petrography and field relations of these very distinctive lamprophyric bodies have been outlined in section 2.5.1. To recapitulate, these rocks are noted for their striking hornblende-porphyritic texture and occur as sub-vertical pipes along the margin of the Omai Stock.

5.6.1 Geochemical characteristics.

According to the chemical data for the three samples analysed, one with mild hydrothermal alteration, the appinites range in composition from ultrabasic (picro-basaltic) to basaltic with

Table 5.1: Geology of the Omai mafic dyke suites.

Description	Regional correlation	Age
Post-orogenic gabbroic dykes (POMDs)	Apatoe Suite (?)	Mesozoic (?)
Ultrabasic to intermediate sills and dykes (Gilt Creek Suite)	two-pyroxene sills at Issineru**	late Trans-Amazonian (?)
Appinite pipes	Badidku Suite or Younger Granite Group	Trans-Amazonian (i.e. 2.25 - 1.95 Ga.)
Greenstone-related minor basic intrusives (Majuba Suite)	meta-gabbros in the Issineru Formation (more widely, Barama-Mazaruni Supergroup)	Palaeoproterozoic (ca 2.25 Ga.)

** Gibbs (1987a) tentatively correlates these rocks with the Uatuma Supergroup (1.92- 1.69 Ga.)

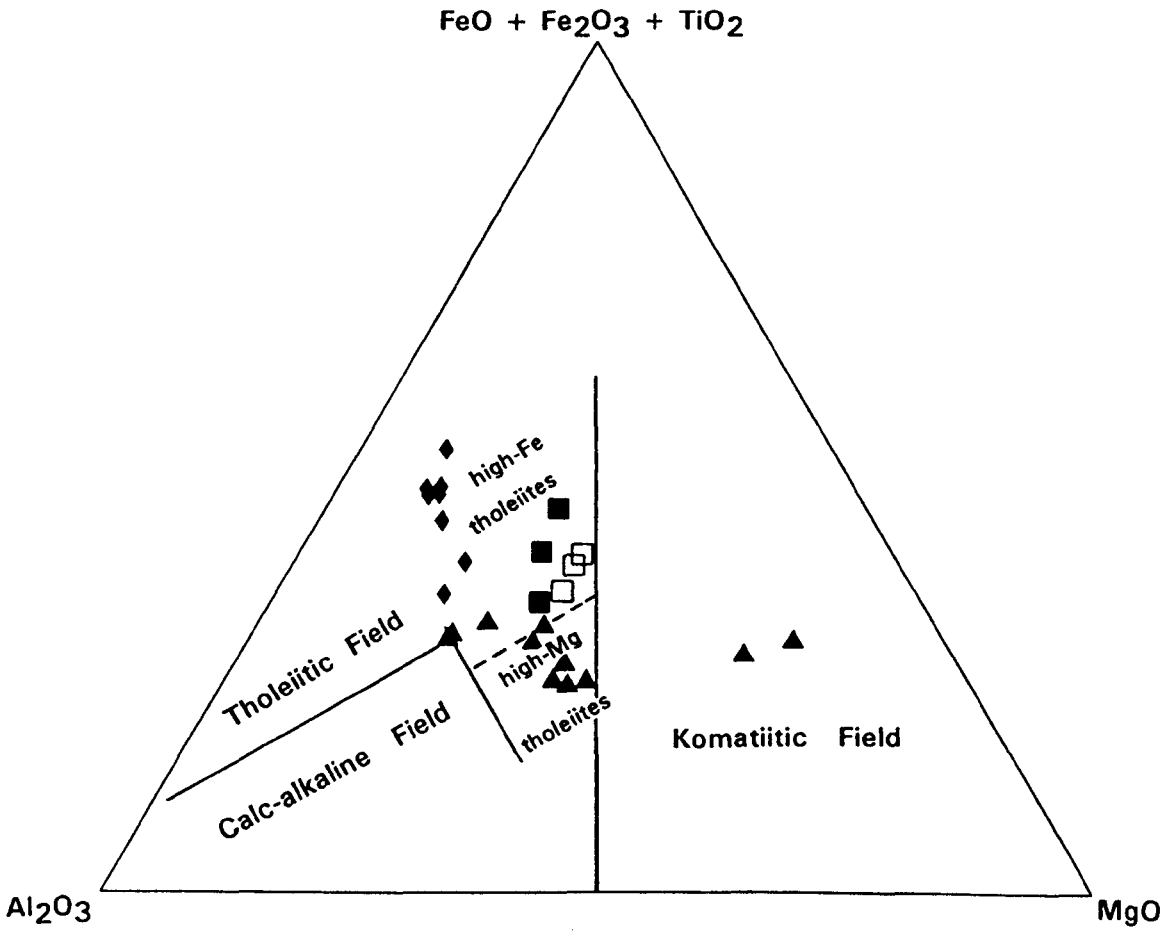

Fig. 5.1: Jensen cation diagram showing the magmatic affinity of the Omai mafic dyke suites. Field boundaries after Jensen (1976). Total Fe in the Omai rocks is represented by $Fe_2O_3^T$.

Symbols: solid squares - minor basic intrusives of the Majuba Suite; open squares - appinite pipes; solid triangles - Gilt Creek Suite; solid diamonds - post-orogenic mafic dykes (POMDs).

SiO_2 values ranging from 43.7% to 46.7%. Total alkali ($Na_2O + K_2O$) contents vary from 2.75% to 3.39% with an estimated primary Na_2O/K_2O ratio of 5.5. The magmatic affinity expressed by the appinite samples is ambiguous. For example, in terms of total alkali - SiO_2 relationships the samples show weakly alkaline tendencies though, this alkalinity is not confirmed by high Nb/Y ratios. On the Jensen Cation Plot (Fig. 5.1) the appinites clearly fall within the high-Fe tholeiite field, close to the minor basic intrusives of the Majuba Suite.

The appinite samples contain a consistent trace element geochemistry, as reflected by the regular nature of the chondrite-normalised REE profiles (see Fig. 5.2). These sub-parallel patterns are gently fractionated with an average La_n/Yb_n ratio of 4.67 and average total REE contents of 95.5 ppm. Globally, such relatively low La_n/Yb_n ratios found in lamprophyres are thought to be indicative of plagioclase-bearing types such as spessartites and camptonites (Rock, 1987; 1991). The REE patterns displayed by the Omai appinites are further characterised by a humped LREE configuration, rather similar to trends observed in some olivine-gabbro Scourie dykes from northwest Scotland (see Weaver and Tarney, 1981; 1983). This humped profile is also characteristic of the accessory mineral, sphene (see inset of Fig. 5.2) and it is possible that the relatively coarse sphene grains, observed in appinite thin section, have contributed to the overall REE patterns. The appinite REE patterns also display minor, but regular, negative Ce anomalies. The cause and significance of these negative Ce anomalies are uncertain, though, as previously mentioned, similar features have been interpreted as the effects of sea-water alteration of ocean-floor basalts (Ludden and Thompson, 1979) or due to the incorporation of subducted sediments into the petrogenetic cycle in magmatic arc settings (Hole et al., 1984).

The MORB-normalised signatures of the three Omai appinite samples are closely comparable in terms of pattern and element abundances (see Fig. 5.3a) However, from this diagram it can be computed that sample 5-1142 has sustained selective enrichment of the LIL elements K, Rb and especially Ba. For example, Rb and Ba have been enriched by the respective amounts of 12 ppm and 400 ppm. Other LIL elements such as Sr and Th are relatively unaffected. These trends can be accounted for by mild degrees of hydrothermal (sericitic) alteration observed in the corresponding thin section specimen.

5.6.2 Petrogenesis.

In view of the diverse geological association and chemical character of global lamprophyres, no single petrogenetic model can be applied across the board, though some popular models involve elements of crustal hybridisation/contamination and volatile enrichment of mantle-derived ultrabasic to basic magmas (Rock, 1991). In section 2.5.1., it has been shown that the appinites and the Omai Stock have a close spatial and temporal association. Therefore

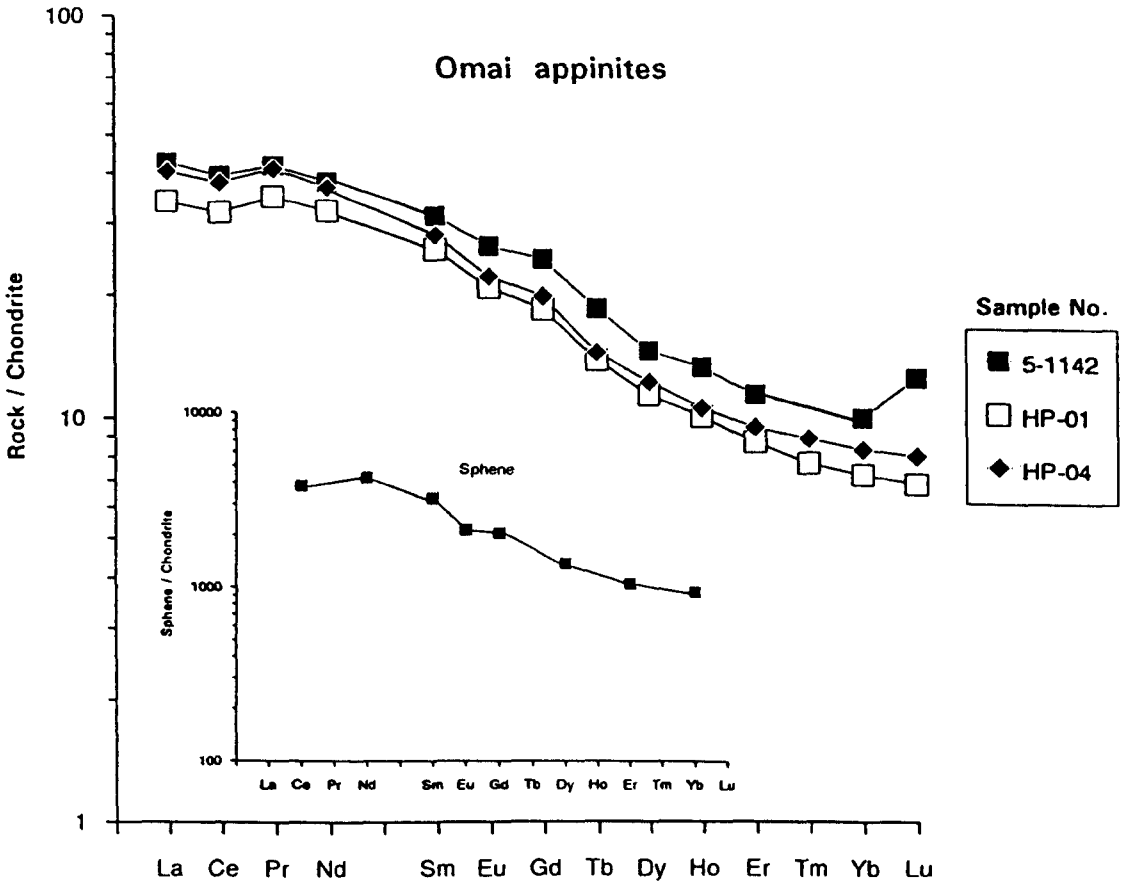

Fig.5.2: Chondrite-normalised REE patterns of the Omai appinites and sphene (inset). Sphene data from Gromet and Silver (1983). Normalising values from Nakamura (1974).

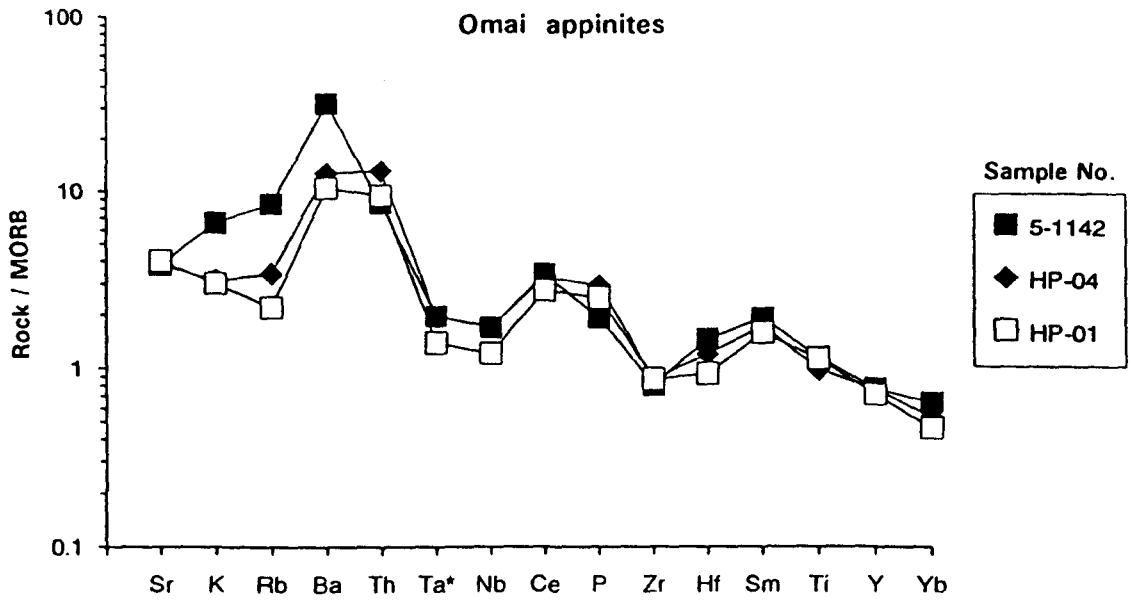

Fig. 5.3a: MORB-normalised geochemical signatures of the Omai appinites. Normalising values from Pearce (1982).

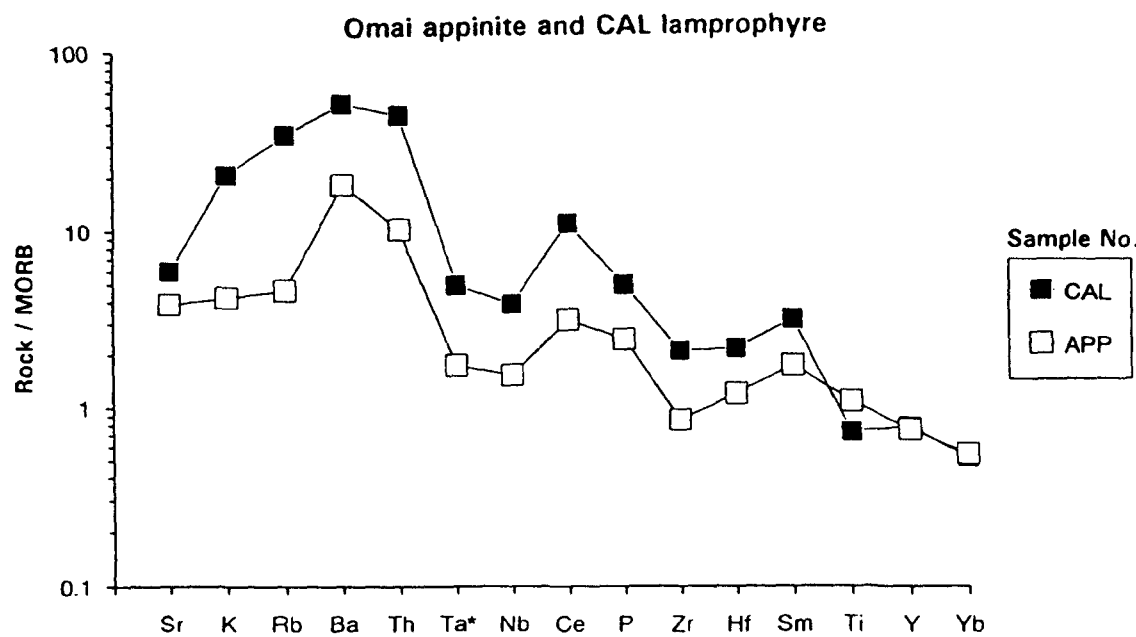

Fig. 5.3b: MORB-normalised geochemical signatures showing the similarity between the average Omai appinite (APP) and the average global calc-alkaline lamprophyre (CAL) of Rock (1991). Normalising values from Pearce (1982).

it is reasonable to assume that these two different lithologies may have evolved from the same pulse of magmatism. Unfortunately, the geochemical data does not provide any conclusive evidence to support this hypothesis. In fact, to the contrary, the sharply discordant REE patterns displayed by the appinites and the Omai Stock (see Figs 5.2 and 4.10a) imply that there is no simple genetic link between these two rock types. Therefore, for the time being, the petrogenetic origin of the Omai appinites remains undetermined.

5.6.3 Tectonic association.

The spiky MORB-normalised geochemical signatures shown in Fig. 5.3a are characterised by a marked subduction zone component (SZC) as reflected by high LILE/HFSE ratios. These trends suggest that the Omai appinites were emplaced in a magmatic arc-type setting, though again it must be emphasised that such arcs, if active in the Precambrian, were not necessarily linear subduction zones typical of modern destructive plate margins. Figure 5.3b shows that the average Omai appinite has a MORB-normalised signature comparable to the average global calc-alkaline (CAL) lamprophyre of Rock (1991). According to Rock (1991), this type of pattern, with its diagnostic coupled negative TNT (Ta-Nb-Ti) anomaly, is peculiar to the calc-alkaline (CAL) lamprophyres of orogenic belts and is not found in the other main branches of the lamprophyre clan, i.e alkaline (Al), ultramafic (UML), kimberlite (KIL) or lamproite (LL). A further point worth noting is that the Omai appinites are strongly sodic whereas 98% of CAL lamprophyres, according to Rock (1987), are potassic in nature.

5.6.4 Regional correlation.

In the context of Guyana's national geology, the exact stratigraphic position of the Omai appinites remains speculative, though their geochemistry, and to a certain extent field relations, appear to constrain them within the time frame of the Trans-Amazonian orogeny (ca 2.25-1.95 Ga.). It is possible that the appinites are the stratigraphic equivalents of the ultrabasic to gabbroic bodies of the Badidku Suite which mainly outcrop in southern Guyana. According to Gibbs and Barron (1992) the Badidku Suite intruded the Guiana Shield in the interval between the two main episodes of acid magmatism (P1 and P2) in the Trans-Amazonian orogeny. Alternatively, the appinites may be assigned to the Younger Granite Group along with the Omai Stock.

5.7 The Gilt Creek Suite (11 samples).

The petrography and field relations of these dykes are described in detail in section 2.5.1. To reiterate, these rocks occur as narrow (1m to 10m) ultramafic to intermediate sheets which intruded along sub-horizontal shear zones in the Omai Stock and adjacent country

rocks. In section 3.8, the geochemical data indicated that the Captain Mann Sill may also be classified as a member of the Gilt Creek Suite.

5.7.1 Geochemical characteristics.

Chemically, the Gilt Creek dykes vary in composition from ultrabasic (picritic) to intermediate with SiO_2 contents ranging from 41.5% to 55.8%. In terms of major elements, the Suite is typified by Mg-enrichment and low K and Ti values. The least evolved samples contain MgO values in the order of 21% to 25% with Mg-numbers of around 80. According to the Al_2O_3-FFM diagram (Fig. 5.4) the majority of samples fall within the komatiitic field, though this does not necessarily mean that this rocks are true komatiites. (For a detailed definition of komatiites (s.s.) the reader is referred to Arndt and Nisbet, 1982). With respect to trace element geochemistry, the Gilt Creek Suite is characterised by elevated Sr, Ba, Th, P, LREE, Ni and Cr abundances. The most diagnostic features are the steeply fractionated REE patterns which show a systematic increase in La_n/Yb_n ratios and total REE abundances with increasing SiO_2 contents (see Fig. 5.5). La_n/Yb_n ratios vary from 7.84 to 32.6 with maximum total REE contents of 419 ppm. These trends are normally characteristic of alkalic, shoshonitic or high-K calc-alkaline volcanic rocks from modern magmatic arc settings (see Morrison 1980).

5.7.2 Petrogenesis.

The most primitive components of the Gilt Creek Suite, i.e. samples 6-1975 and 4-1816, have several geochemical characteristics which are typical of primary mantle-derived basaltic melts. The chemical criteria for such primary mantle-melts are listed in Harnois and Mineau (1991) and include Mg-number = 70 to 83, Ni = 90 to 670 ppm, Co = 27 to 80 ppm, Sc 15 to 28 ppm and Ni (ppm) / MgO (wt.%) = 23 to 39. Theoretically, it is conceivable that the primitive nature of the Gilt Creek samples could have been induced by the accumulation of olivine and/or clinopyroxene, though the petrographic data does not support this hypothesis. Moreover, the small-scale nature of the dykes also precludes such a mechanism.

The linearity of the trends demonstrated by the three mineral vector diagrams of Figs. 5.6 a, b, and c indicates that the Gilt Creek Suite rocks are related by simple Rayleigh fractionation processes. These diagrams further imply that some combination of plagioclase, olivine, magnetite, orthopyroxene and clinopyroxene fractionation was active during petrogenesis, with pyroxene as the dominant fractionating phase(s). This latter supposition is largely supported by the behaviour of the REE. The steep, LREE-enriched profiles which systematically increase in total REE abundances with increasing SiO_2 contents is consistent with the separation of clinopyroxene from the melt. This hypothesis can be tested by using

a simple petrogenetic modelling technique involving the Rayleigh fractionation equation $C_l/C_o = F^{(D-1)}$, where C_o is the elemental concentration in the original melt, C_l is the elemental concentration in the residual melt, F is the weight fraction of the melt remaining and D (or, Kd) is the bulk distribution coefficient for the particular element. For example, by taking the REE contents of the ultrabasic sample 6-1975 as an arbitrary starting composition, the effects of REE behaviour during differentiation can then be computed by fractionating hypothetical amounts of clinopyroxene from the initial liquid.

Figure 5.7 illustrates that the modelled trends for clinopyroxene removal closely parallel the actual analysed patterns yielded by the rocks. For example, sample 8-1888 ($SiO_2 = 53.2\%$) can be generated by fractionating approximately 30% clinopyroxene from the starting liquid composition (i.e. sample 6-1975). However, as anticipated, the model breaks down for the more intermediate compositions, say above 54% SiO_2, as control of LREE partition is transferred to other mineral phases. The development of a negative Eu anomaly at about 55% SiO_2 may mark the beginning of plagioclase fractionation from the melt. The rapid increase in LREE relative to HREE at the higher silica levels almost certainly reflects the crystallisation of key LREE-rich accessory phases. The strongly positive correlations shown by the Ce-P_2O_5 and Th-P_2O_5 data (Fig. 5.8) indicate that these phases are dominated by monazite. This hypothesis is substantiated by the petrographic observations.

5.7.3 Tectonic association.

The orogenic nature of the Gilt Creek Suite is confirmed by consistently high LIL/HFS element ratios and by the shoshonitic affinity shown in the Th/Yb - Ta*/Yb discrimination diagram of Fig. 5.9. Additional evidence for a magmatic arc setting is provided by the comparable MORB-normalised patterns between the Gilt Creek dykes and modern shoshonitic volcanic rocks from both Chile (Fig. 5.10a) and Fiji (Fig. 5.10b). However, the fact that the Gilt Creek Suite is typically K-poor indicates that these rocks are not shoshonites in the strictly defined sense. Moreover, the elevated P_2O_5 values (up to 0.84%) contained in the Gilt Creek Suite strongly suggest an alkaline magmatic affinity (see Winchester and Floyd, 1976), even though Nb/Y ratios are consistently below 0.5. This hypothesis is supported by the tendency toward Mg-enrichment and by the ultrabasic to intermediate compositional range of the Gilt Creek Suite which contrasts with the predominantly intermediate nature of true shoshonites. For further information on alkaline arc magmatism the reader is referred to the suite of papers introduced by Box and Flower (1989).

5.7.4 Regional correlation.

As already demonstrated in section 3.8, the Gilt Creek Suite, is readily correlatable, in terms

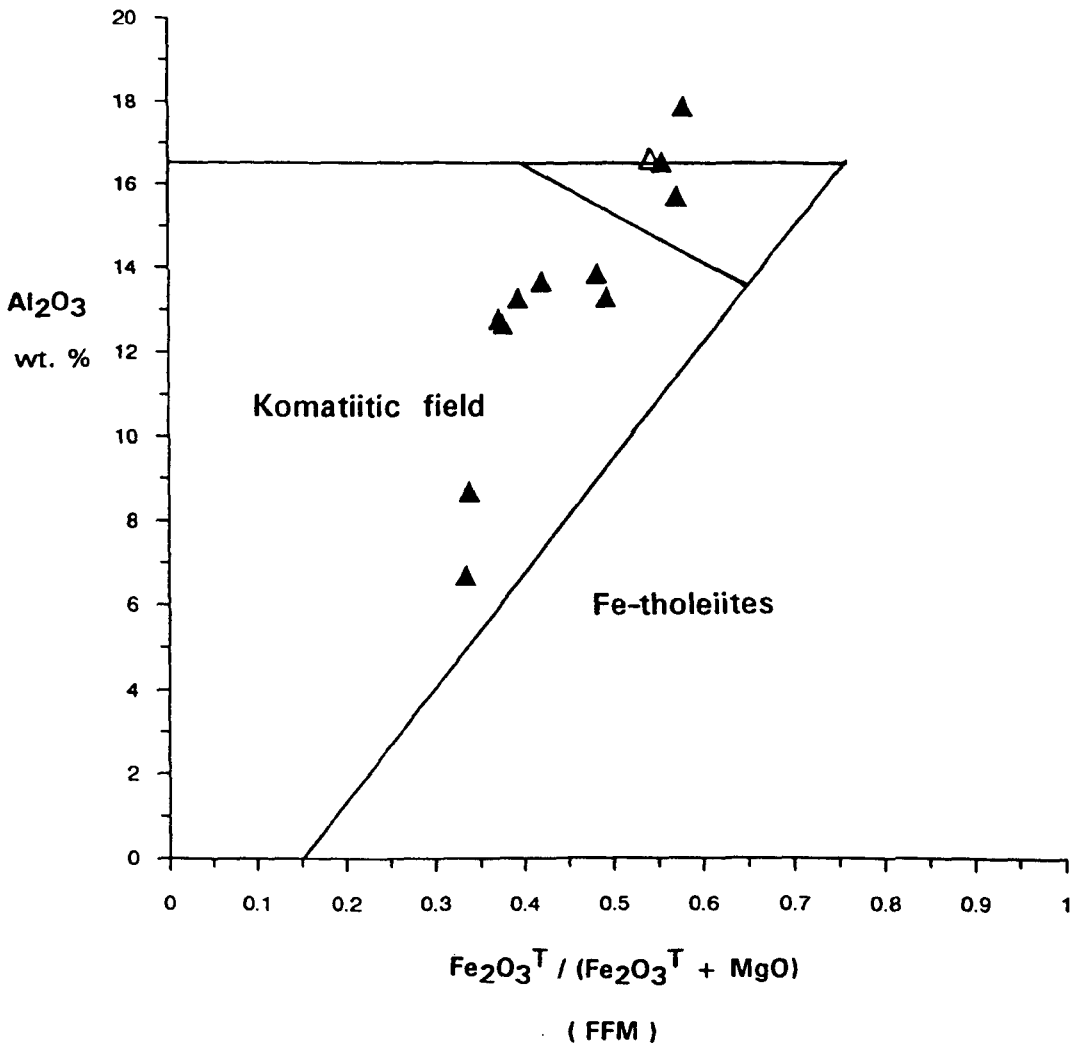

Fig. 5.4: Al_2O_3 - FFM diagram showing the largely komatiitic affinity of the Gilt Creek Suite (including the Captain Mann Sill). Field boundaries after Naldrett and Goodwin (1977).

Symbols: solid triangles - Gilt Creek Suite, Omai Stock Zone; open triangle - Captain Mann Sill (sample CM-03).

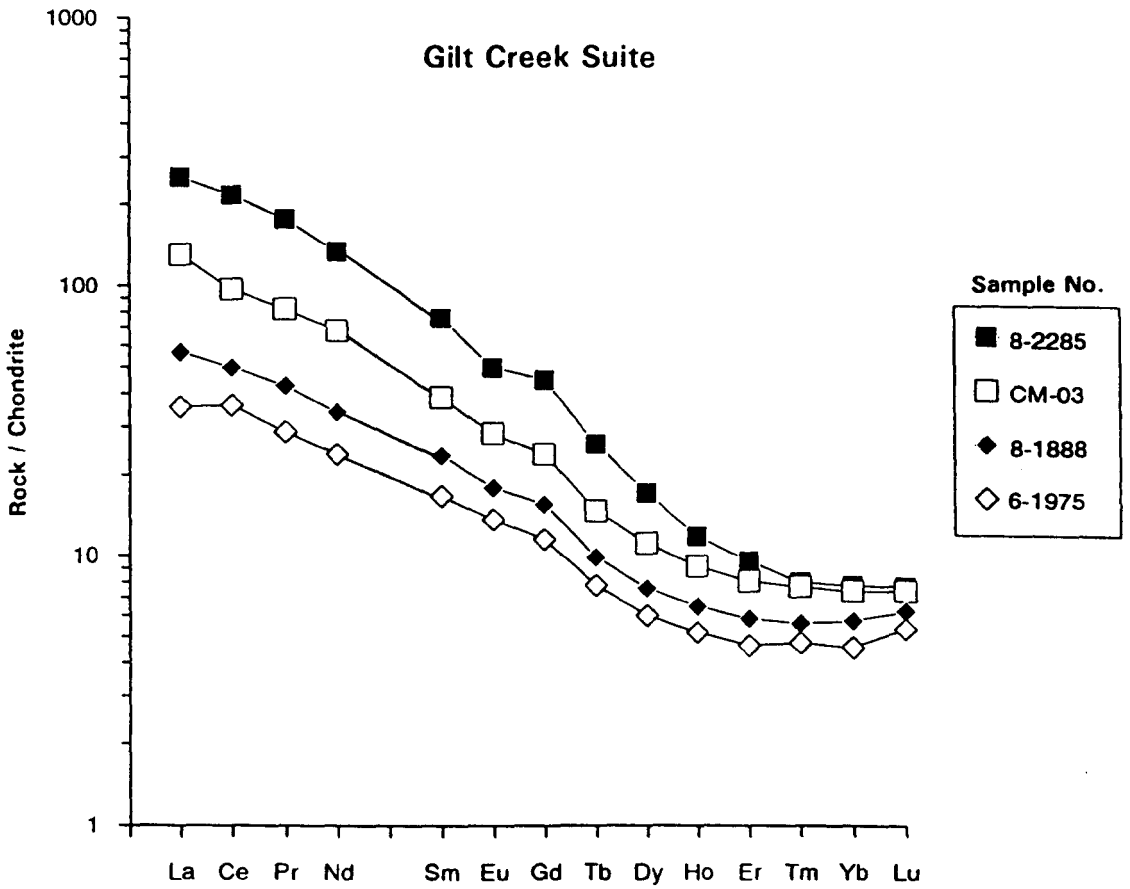

Fig. 5.5: Representative chondrite-normalised REE patterns of the Gilt Creek Suite (including sample CM-03 from the Captain Mann Sill). Normalising values from Nakamura (1974).

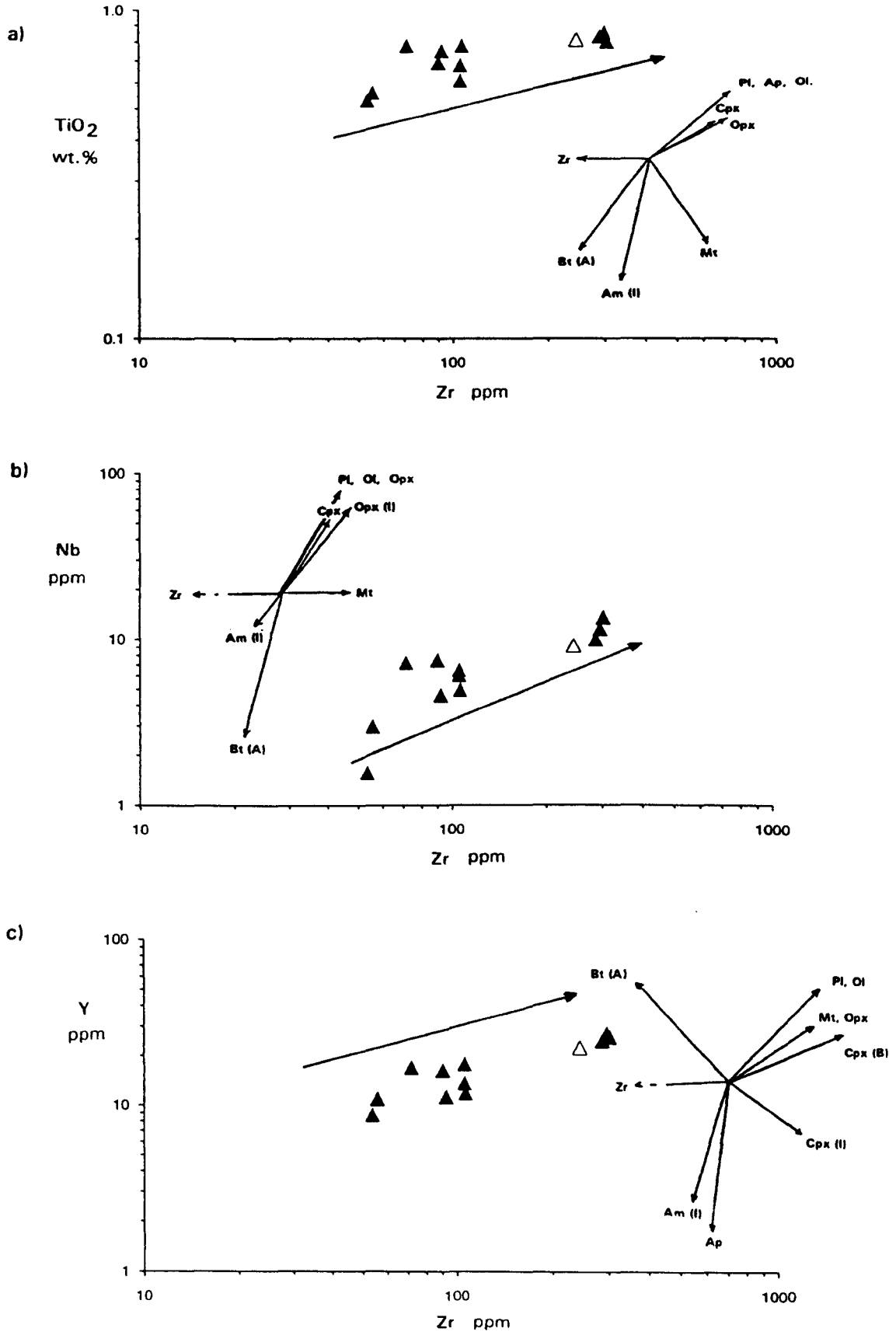

Fig. 5.6: Mineral vector diagrams showing petrogenetic trends in the Gilt Creek Suite. a) TiO_2 - Zr; b) Nb - Zr; c) Y - Zr. Mineral vectors from Pearce and Norry (1979). Gilt Creek symbols as for Fig. 5.4.

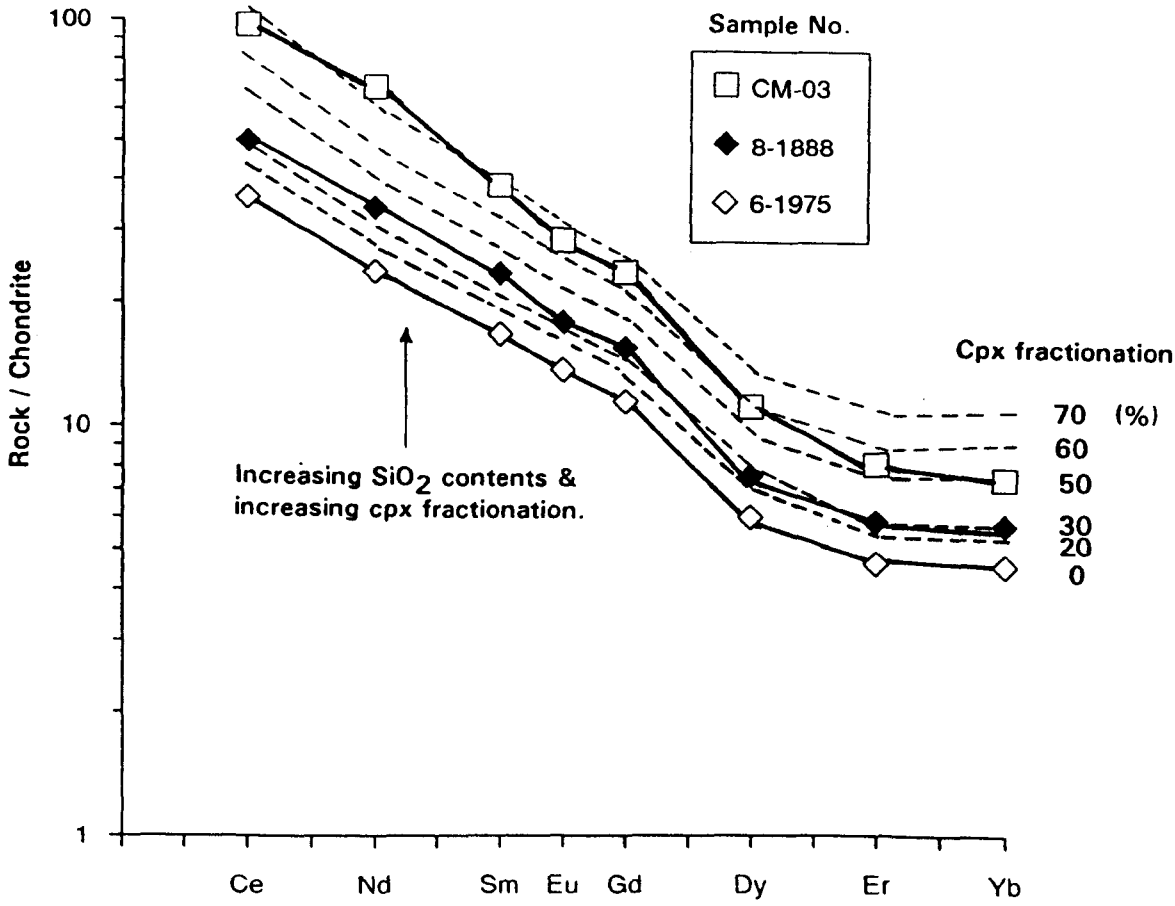

Fig. 5.7: Diagram comparing analysed chondrite-normalised REE patterns (solid lines) of the Gilt Creek Suite with modelled trends (dashed lines) involving clinopyroxene fractionation.

This modelling method is based on the Rayleigh fractionation equation $C_l/C_o = F^{(D-1)}$, where C_o is the elemental concentration in the original melt, C_l is the elemental concentration in the residual melt, F is the weight fraction of the remaining melt and D is the distribution coefficient for the particular element. Taking sample 6-1975 (SiO_2 = 41.5%) as the starting liquid composition and assuming Rayleigh fractionation processes, the behaviour of the REE (Ce, Nd, Sm, Eu, Gd, Dy, Er and Yb) can be computed by removing hypothetical amounts of clinopyroxene from the initial liquid. The distribution coefficients (D) for REE in clinopyroxene - silicate melt systems are from Grutzeck et. al., (1974). Normalising values from Nakamura (1974).

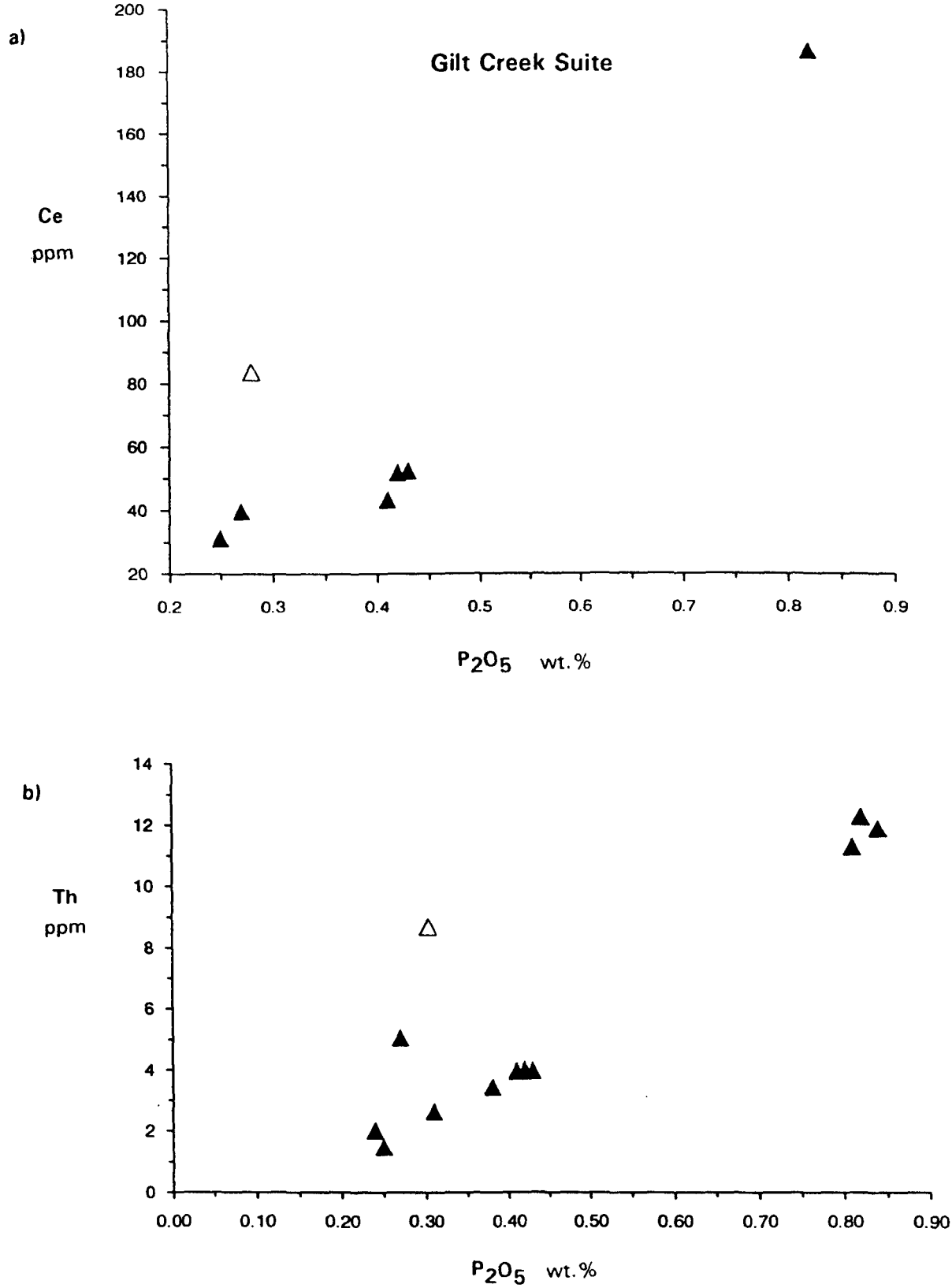

Fig. 5.8: Co-variation diagrams showing an important petrogenetic trend in the Gilt Creek Suite. The strong positive correlations shown by a) Ce - P_2O_5 and, b) Th - P_2O_5, imply that the LREE and Th were partitioning into monazite, especially at the higher silica levels. Symbols as for Fig. 5.4.

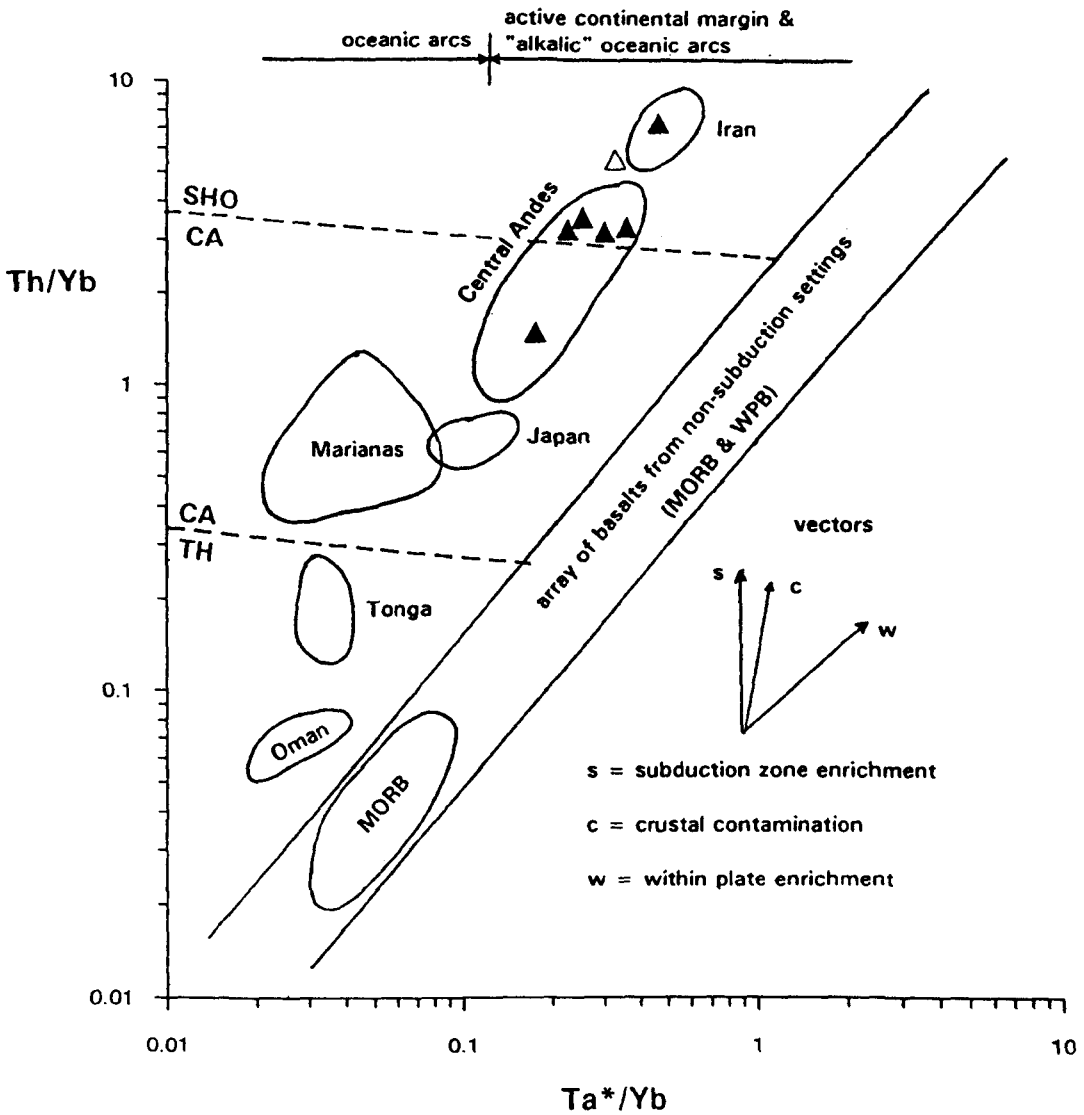

Fig.5.9: Th/Yb - Ta*/Yb discrimination diagram showing the tectono-magmatic affinities of the Gilt Creek Suite. Symbols as for Fig. 5.4. Field boundaries from Pearce (1982; 1983). SHO - shoshonitic; CA - calc-alkaline; TH - tholeiitic.

Note: Ta* indicates that Ta values for the Omai samples are calculated as a function of Nb/17 (see Jochum et al., 1986).

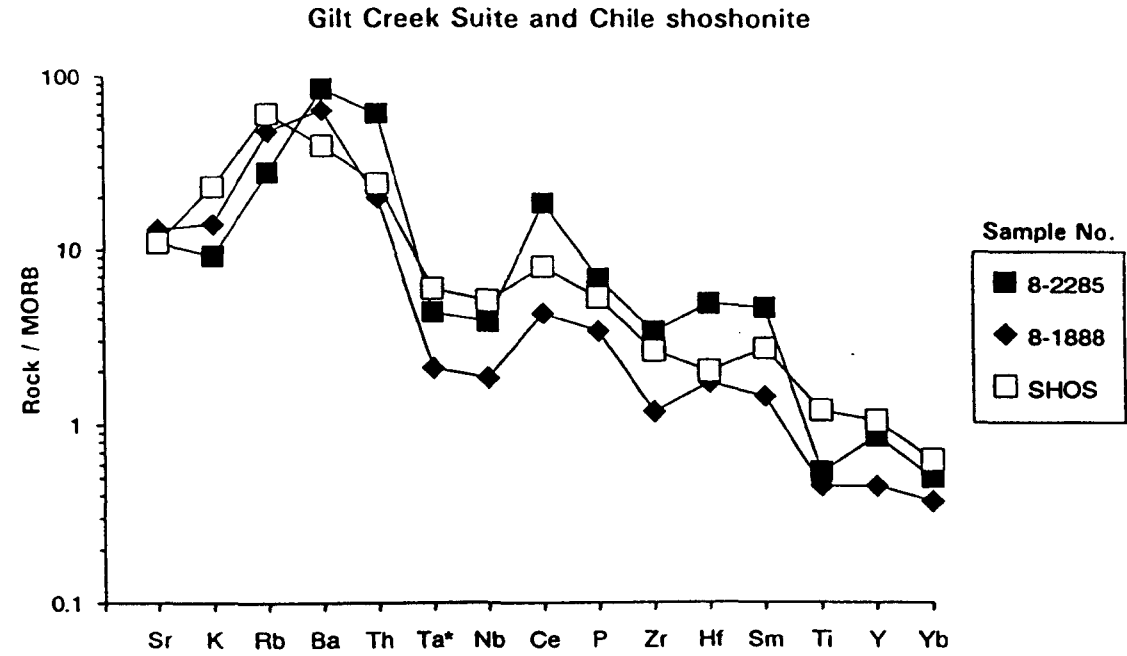

Fig. 5.10a: MORB-normalised geochemical signatures showing the similarity between the Gilt Creek Suite (8-2285 and 8-1888) and a shoshonitic basalt (SHOS) from central Chile. Chile data from Pearce (1983). Normalising values from Pearce (1982).

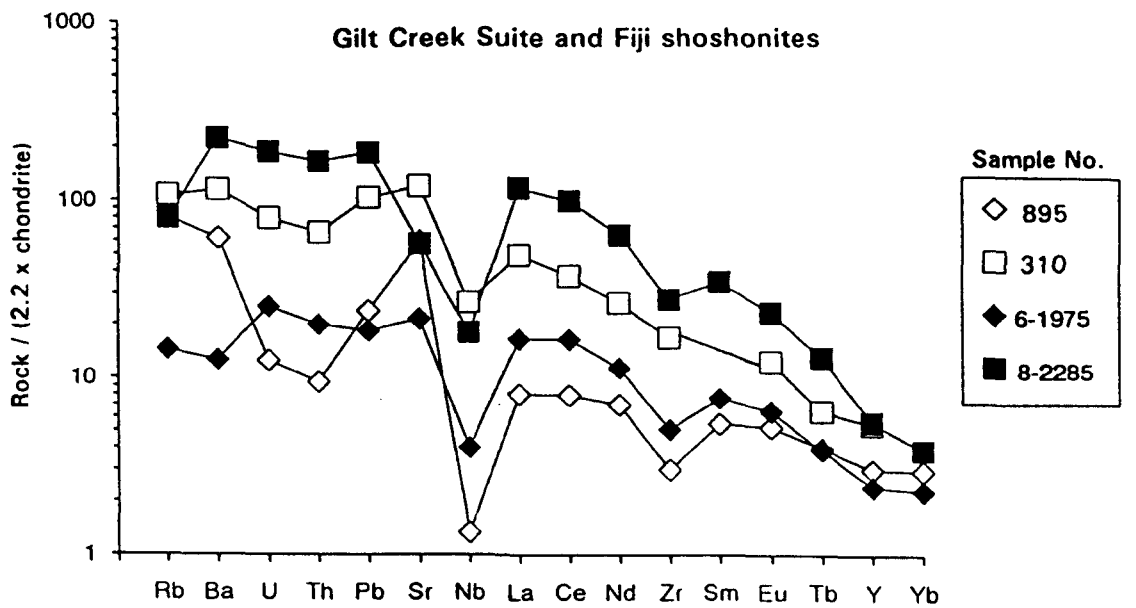

Fig. 5.10b: Chondrite-normalised geochemical signatures showing the similarity between the Gilt Creek Suite (6-1975 and 8-2285) and Miocene shoshonitic basic volcanic rocks (895 and 310) from Fiji. Fiji data from Gill and Whelan (1989). Normalising values also from Gill and Whelan (1989).

of stratigraphic and geochemical characteristics, with the two-pyroxene andesitic sills recorded at Issineru by Renner and Gibbs (1987). In turn, Gibbs (1987a) has equated the two-pyroxene sills with the high-K ("shoshonitic") continental felsic volcanic rocks of the Uatuma Supergroup (1.92 to 1.69 Ga) which have a widespread occurrence throughout the Guiana Shield. In central Guyana, these rocks and their associated intrusives are well-represented by the Iwokrama Formation which outcrop about 80 km south of Omai. However, the ultrabasic to intermediate, low-K, orogenic nature of the Gilt Creek Suite appears to contrast with the intermediate to dominantly acid, high-K, anorogenic character of the Uatuma Supergroup and any correlation between the two groups must remain tentative.

At Omai, the field relations clearly show that the Gilt Creek Suite dykes post-date the Omai Stock, whereas the orogenic geochemical signatures and mineralised nature of the dykes intimate that they were emplaced within the time frame of the Trans-Amazonian orogeny. It is conceivable, however, that the Gilt Creek dykes (and the two-pyroxene sills at Issineru) intruded the granite-greenstone basement towards the end of the Trans-Amazonian orogeny, immediately prior to the regional-scale anorogenic magmatic events which gave rise to the Uatuma Supergroup.

5.8 Post-orogenic mafic dykes (POMDs) (8 samples).

In northern Guyana, and in the Guiana Shield as a whole, three pulses of anorogenic mafic magmatism punctuate the geological record following the Trans-Amazonian orogeny. The first phase of unmetamorphosed, undeformed, non-mineralised tholeiitic intrusions is represented by the Mesoproterozoic (1.7 to 1.5 Ga) Avanavero Suite which consists of large-scale, erratic, differentiated gabbro-norite sills, dykes and inclined sheets up to 500 m thick. These bodies, which may continue laterally for hundreds of kilometres, have an estimated accumulated volume of some 30,000 km^3 (Gibbs, 1987b). Traditionally, this magmatic event has been associated with an abortive attempt at continental rifting (Choudhuri and Milner, 1971) whereas the erratic morphology of the intrusions has been interpreted to reflect emplacement into a weak, juvenile crust (Gibbs and Barron, 1983).

The PAPA (Post-Avanavero, Pre-Apoteri) dykes which intruded basement and cover throughout the Palaeozoic are smaller and less numerous than their Avanavero counterparts. In Guyana, there are only a few documented occurrences to date, mainly in the Rupununi area in the south of the country (see Berrangé, 1977). Elsewhere in the Shield, the PAPA dykes are typified by the Tiano dyke which outcrops near Boa Vista in the Roraima Territory of northern Brazil.

The third post-orogenic mafic dyking episode is largely concentrated on the Atlantic margin and is referred to as the Apatoe Suite (see Fig. 5.11). This suite is well-represented by swarms of narrow, linear, doleritic dykes which rarely exceed 50 m in width but extend in a regular north or northeast direction for several hundred kilometres. Traditionally these dykes have been associated with an extensional tectonic regime related to the opening of the Atlantic Ocean and fragmentation of Gondwanaland during the Mesozoic (May, 1971; Berrangé and Dearnley, 1975). In Guyana, the Apatoe Suite has been officially assigned a Triassic age (Walrond, 1987a), though these mafic dykes appear to have intruded from Permian to early Cretaceous times and are generally linked with the tholeiitic basalts of the Apoteri Volcanic Formation which line the floor of the Takutu graben (Berrangé and Dearnley, 1975).

At Omai, three previously unnamed and undated gabbroic POMDs are discussed in this study. The first of these is the GSR dyke (see section 2.5.1) which cuts the Omai Stock at a depth of 280m to 300m. The Point dyke and Ya-Ya dyke are more regional-scale features which intersect in an X-shaped fashion approximately 3.2 km southeast of the Omai Stock Zone (see Fig. 2.3).

5.8.1 Geochemical characteristics.

The pristine nature of the Omai POMDs, which is expressed by low LOI values ranging from 0 to 1.71%, facilitates accurate petrographic and chemical assessment. The POMDs are characterised by marked Fe-enrichment which is well-reflected by the high $Fe_2O_3^T/MgO$ ratios ranging from 1.80 to 5.16 and by a strong Fe-tholeiitic character as shown in the Jensen cation diagram of Fig. 5.1. Essentially, the POMDs are basaltic in composition and define a narrow range of SiO_2 values from 52.3 to 53.5 %. On a chemical basis, all three dykes are very similar, though the GSR dyke is slightly more Fe- and Ti-enriched than its neighbours. Petrographically, Point dyke (sample RX-22) is generally finer grained, more doleritic, that the other two dykes.

The characteristic REE patterns yielded by the Omai POMDs prove to be diagnostic of this type of mafic dyking episode (see Fig. 5.12). These sub-parallel patterns are typified by moderately fractionated La_n/Yb_n ratios ranging from 3.56 to 4.83 with HREE abundances between 12 to 18 times chondrite. Minor to moderately negative Eu anomalies (maximum $Eu/Eu^* = 0.79$) also help to characterise these profiles.

5.8.2 Petrogenesis and tectonic association.

In concurrence with the tectonic models deduced from regional field evidence (see above) the

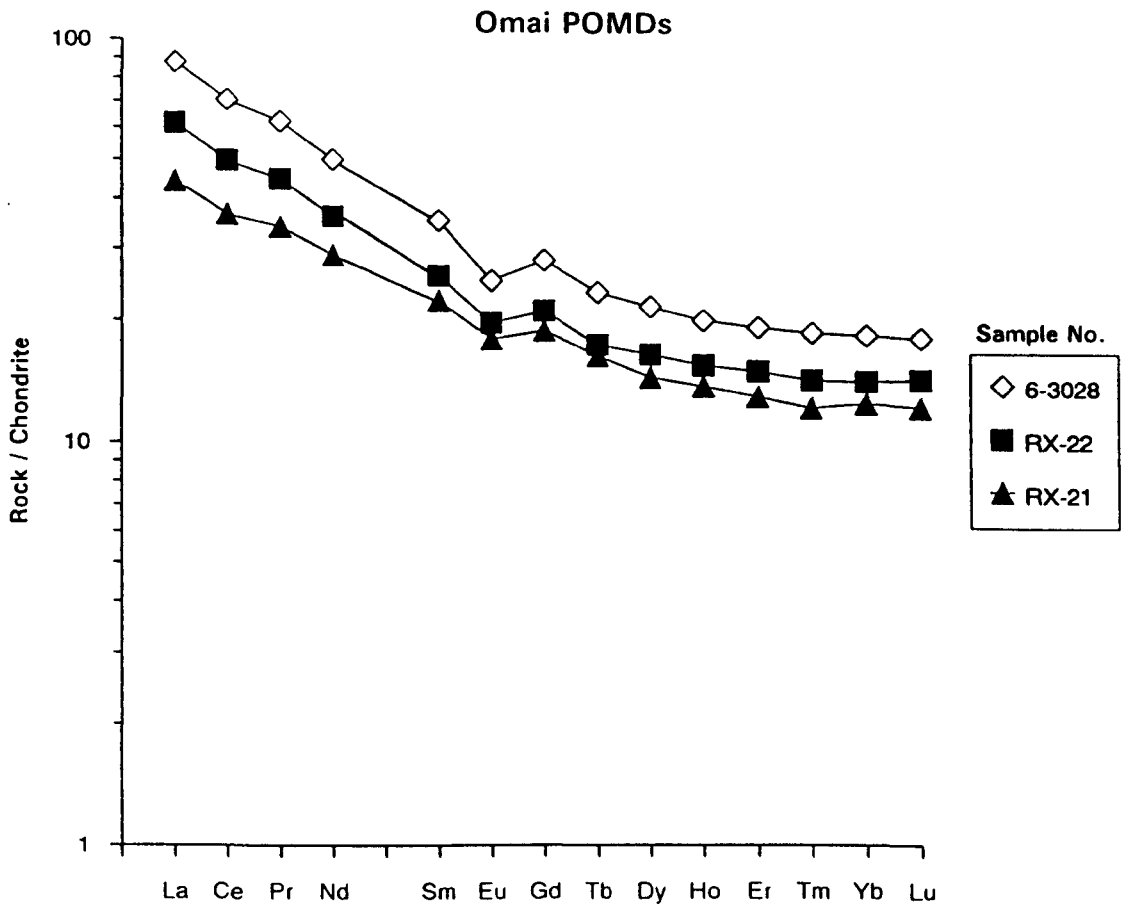

Fig. 5.12: Chondrite-normalised REE patterns of the Omai POMDs (post-orogenic mafic dykes). Sample 6-3028 - GSR dyke; RX-22 - Ya-ya dyke; RX-21 - Point dyke. Normalising values from Nakamura (1974).

major and trace element discrimination diagrams presented in Figs. 5.13 and 5.14 respectively, strongly intimate that the Omai POMDs were emplaced in a continental (within-plate), rift-related setting. Globally, such settings are centres of expansive continental flood basalt (CFB) magmatism (including major dyking episodes) associated with extensional tectonic regimes (e.g Parana province, Brazil and the Karoo province of southern Africa).

According to Thompson et al., (1983; 1984), CFB-related rocks generally yield one of two types of trace element signatures. These are: a) OIB (ocean island basalt) type, and b) the more dominant, non-OIB type (see Figs 5.15 a and b). This simple classification, however, is hotly disputed by Marsh (1987) who advocates more complex processes in CFB settings. Regardless, Fig. 5.16 clearly shows that the Omai POMDs have MORB-normalised spidergram patterns akin to the representative non-OIB type signatures which are essentially similar to the signatures of subduction-related basalts. The origin of the subduction zone component (SZC) in MORB-normalised CFB trace element patterns is another contentious issue which is outside the scope of this study. The traditional view, as championed by Thompson et al., (1983), is that non-OIB type signatures in CFB-related rocks are produced by the contamination of mantle-derived magmas by fusible crustal components. However, the universal consistency of such patterns has led Ahmad and Tarney (1991) to challenge the traditional model. These authors argue that the global uniformity of non-OIB type, CFB-related trace element patterns would be difficult to duplicate by random crustal contamination/assimilation processes, but rather, that the patterns are more likely to be a mantle-source characteristic. Ahmad and Tarney (1991) further propose that LILE-rich mineral phases such as phlogopite, which may have stabilised during the development of the sub-continental mantle lithosphere, would greatly contribute to the formation of non-OIB type, CFB signatures.

The REE data provide some further pointers into the petrogenetic history of the POMDs. Firstly, the relatively elevated HREE abundances and flattish chondrite-normalised trends rule out garnet and/or amphibole as major fractionating components or residual phases. Secondly, the minor to moderately negative Eu anomalies indicate that plagioclase was fractionating from the melt at silica levels of 52.5% upwards. The low Mg-numbers (39 to 51) and low Ni contents (67-117 ppm) suggest substantial removal of olivine from the parent melt. This latter supposition is consonant with the work of Choudhuri et al., (1984) who applied a model of continuous olivine fractionation from a rapidly rising liquid to account for the petrogenesis of the Mesozoic tholeiitic dykes from the northern Guiana Shield.

5.8.5 Regional correlation.

The narrow, relatively regular and linear morphology of the Omai POMDs suggests that these

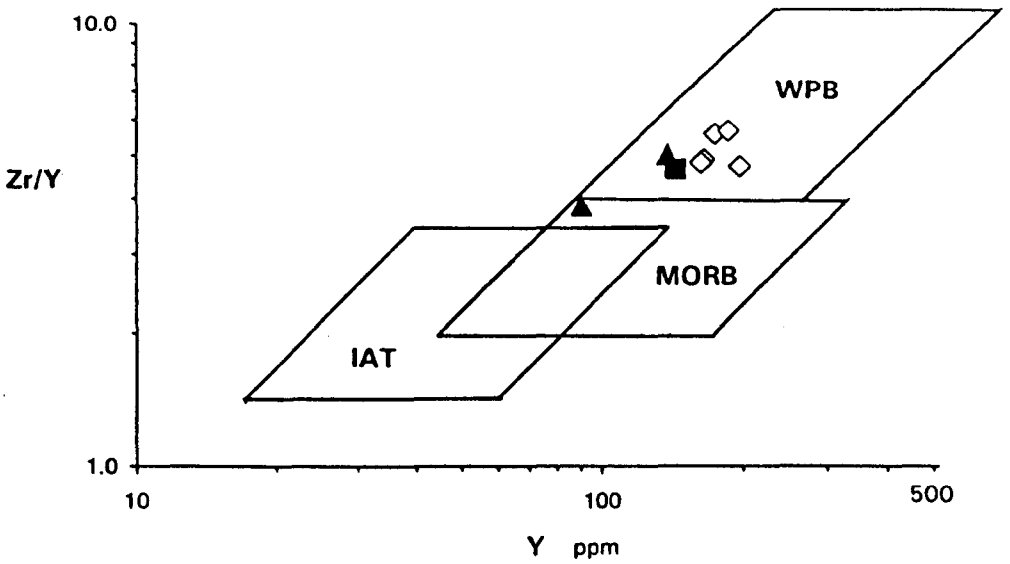

Fig. 5.13a: Zr/Y - Y discrimination diagram showing the within-plate tectonic association of the Omai POMDs. Field boundaries from Pearce and Norry (1979): WPB - within-plate basalts; MORB - mid-ocean ridge basalts; IAT - island arc tholeiitic basalts. Symbols: open diamonds -GSR dyke; solid square - Ya-ya dyke; solid triangles - Point dyke.

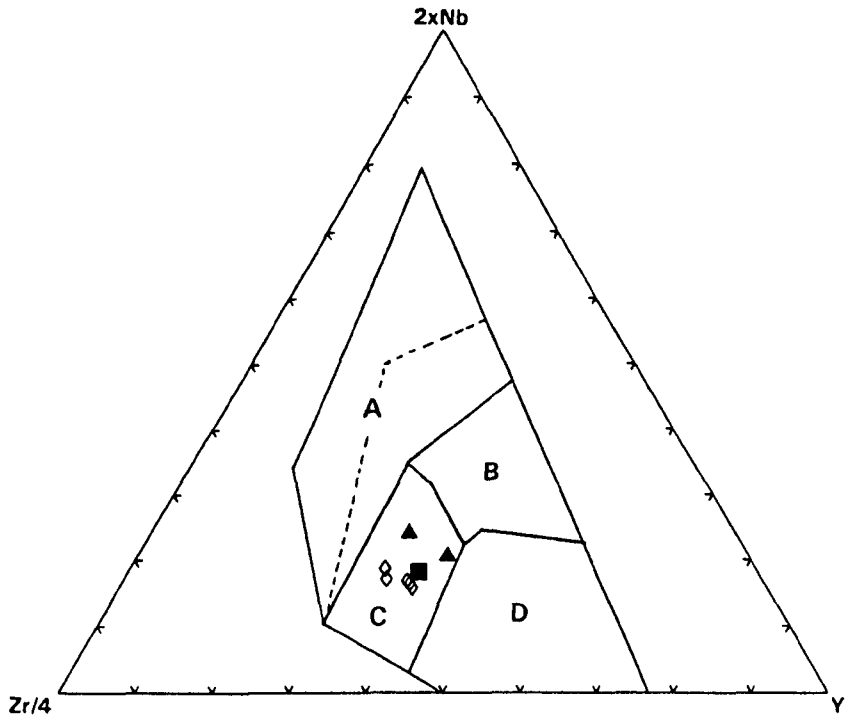

Fig. 5.13b: Zr - Nb - Y discrimination diagram showing the tectonic association of the Omai POMDs in relation to global basalt settings. Field boundaries from Meschede (1986): A - within-plate alkalic, within-plate tholeiites (below dashed line); B - plume-MORB; C - within-plate tholeiites, volcanic arc basalts; D - N-MORB, volcanic arc basalts. Symbols as for Fig. 5.13a.

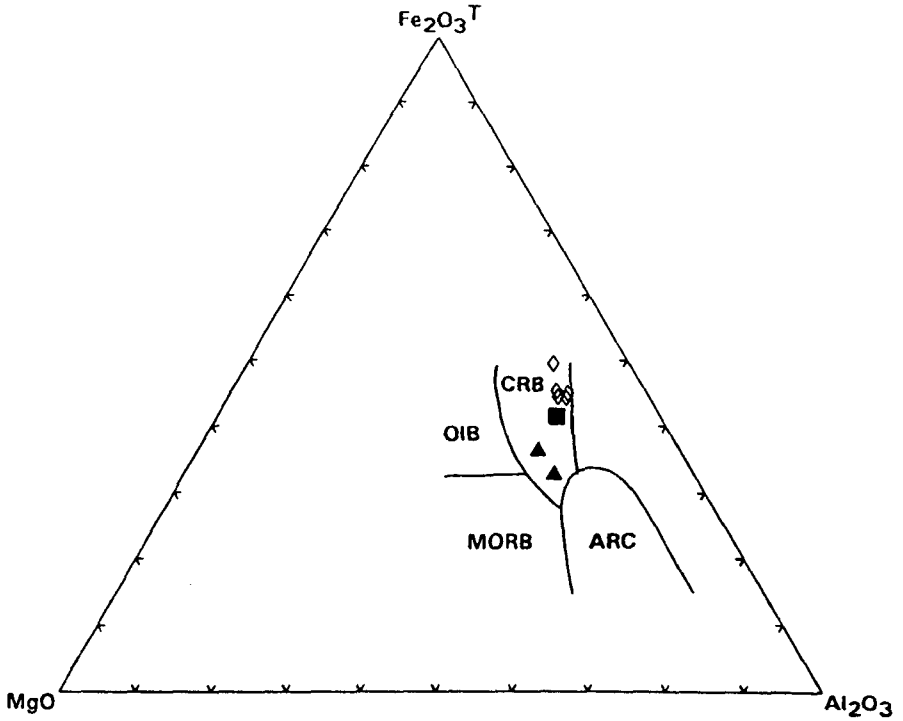

Fig. 5.14a: MgO - $Fe_2O_3^T$ - Al_2O_3 discrimination diagram showing the continental association of the Omai POMDs. Field boundaries from Pearce et al., (1977): CRB - continental rift basalts; OIB - oceanic island basalts; MORB - mid-ocean ridge basalts; ARC - island arc and continental margin basalts. Symbols as for Fig. 5.13a.

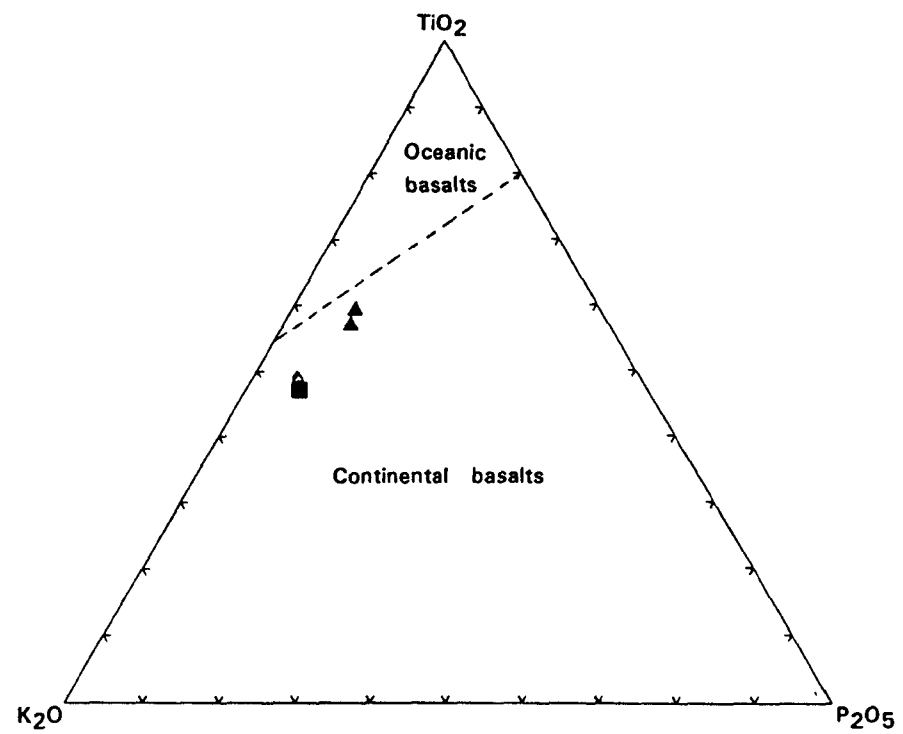

Fig. 5.14b: K_2O - TiO_2 - P_2O_5 discrimination diagram showing that the Omai POMDs have continental as opposed to oceanic affinities. Field boundaries after Pearce et al., (1975). Symbols as for Fig. 5.13a.

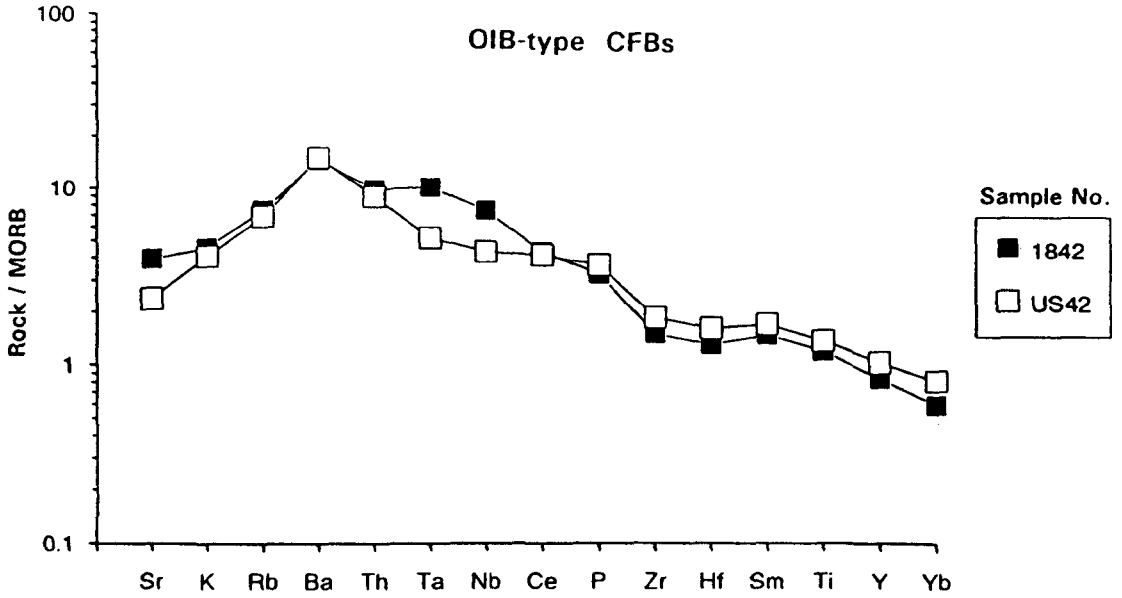

Fig. 5.15a: Representative MORB-normalised geochemical signatures of OIB (ocean island basalt) type, continental flood basalts (CFBs). Sample data from Thompson et al., (1983): 1842 - basalt, Addis Ababa, Ethiopia; US42 - basalt, Snake River Plain, USA. Normalising values from Pearce (1982).

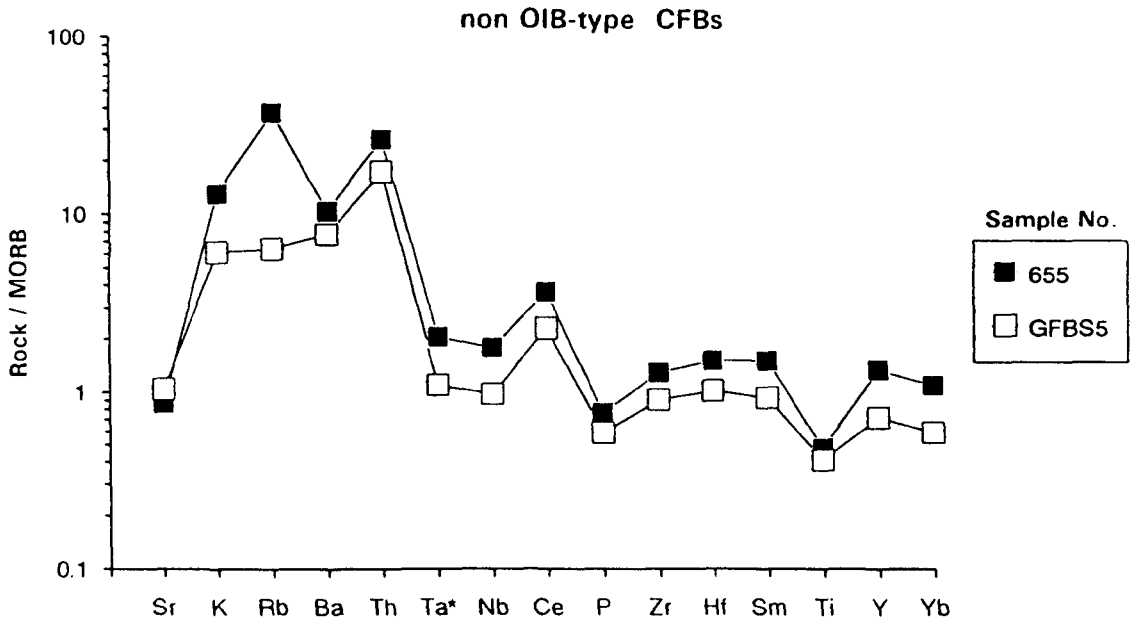

Fig. 5.15b: Representative MORB-normalised geochemical signatures of non-OIB type, continental flood basalts (CFBs). Sample data from Thompson et al., (1983): 655 - quartz dolerite, Serra di Tingua, Brazil; GFBS5 -dolerite, Wright Valley, Antarctica. Normalising values from Pearce (1982).

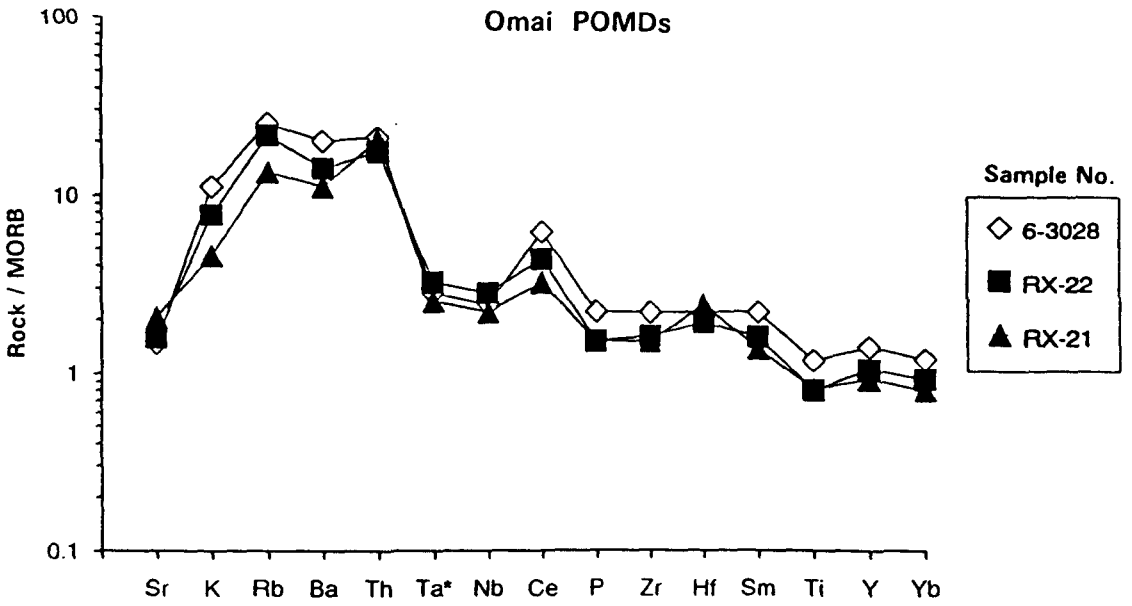

Fig. 5.16: MORB-normalised geochemical signatures of the Omai POMDs which are similar to those of the non-OIB type, CFBs as shown in Fig. 5.15b. Sample 6-3028 - GSR dyke; RX-22 - Ya-ya dyke; RX-21 - Point dyke. Normalising values from Pearce (1982).

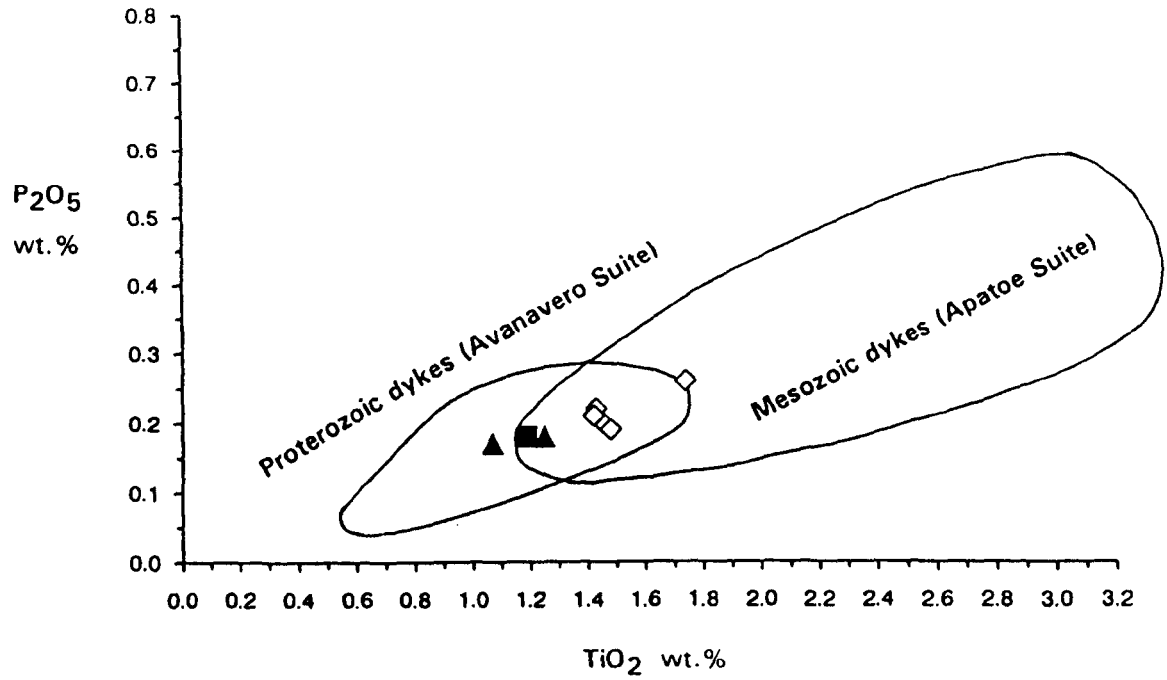

Fig. 5.17a: P_2O_6 - TiO_2 diagram showing the relation of the Omai POMDs with respect to regional Mesozoic and Proterozoic mafic dyke suites of the Guiana Shield. Symbols as for Fig. 5.13a. Field boundaries after Sial et al., (1987).

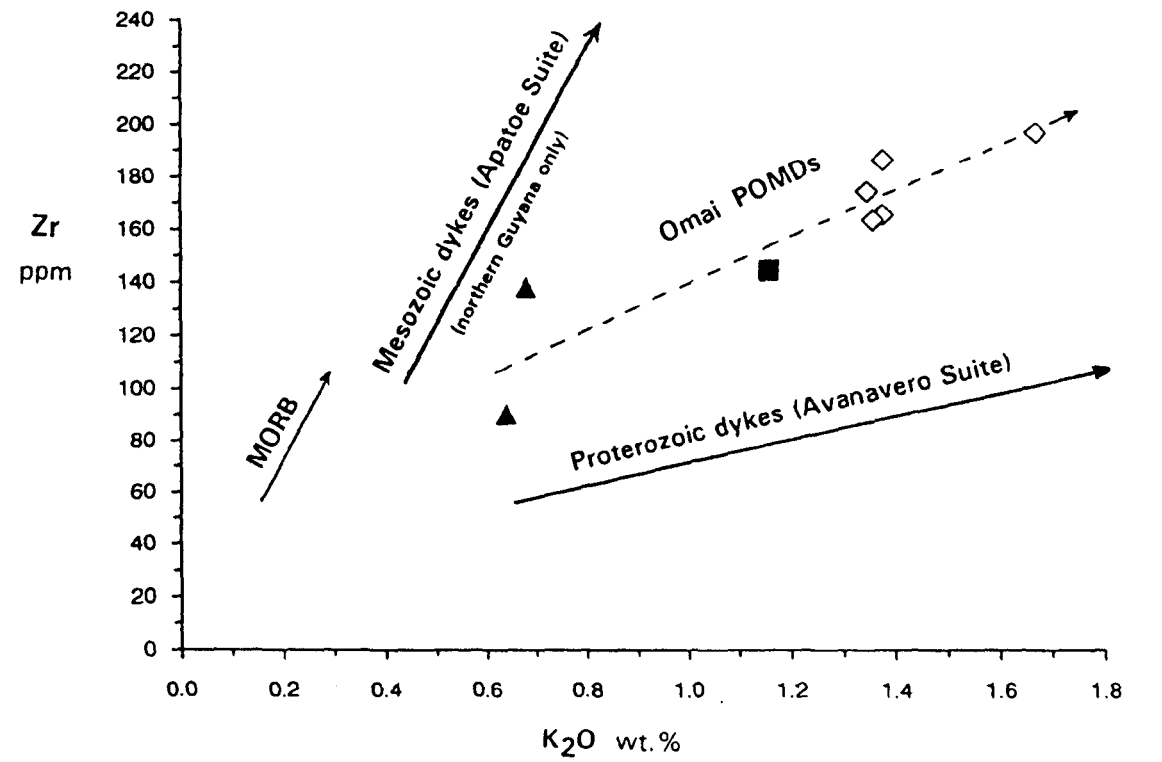

Fig. 5.17b: Zr - K_2O diagram showing the main petrogenetic trend of the Omai POMDs in relation to those of regional Mesozoic and Proterozoic mafic dyke suites in the Guiana Shield. Definitive trends for regional dyke suites and MORB are from Choudhuri et al., (1991). Symbols as for Fig. 5.13a.

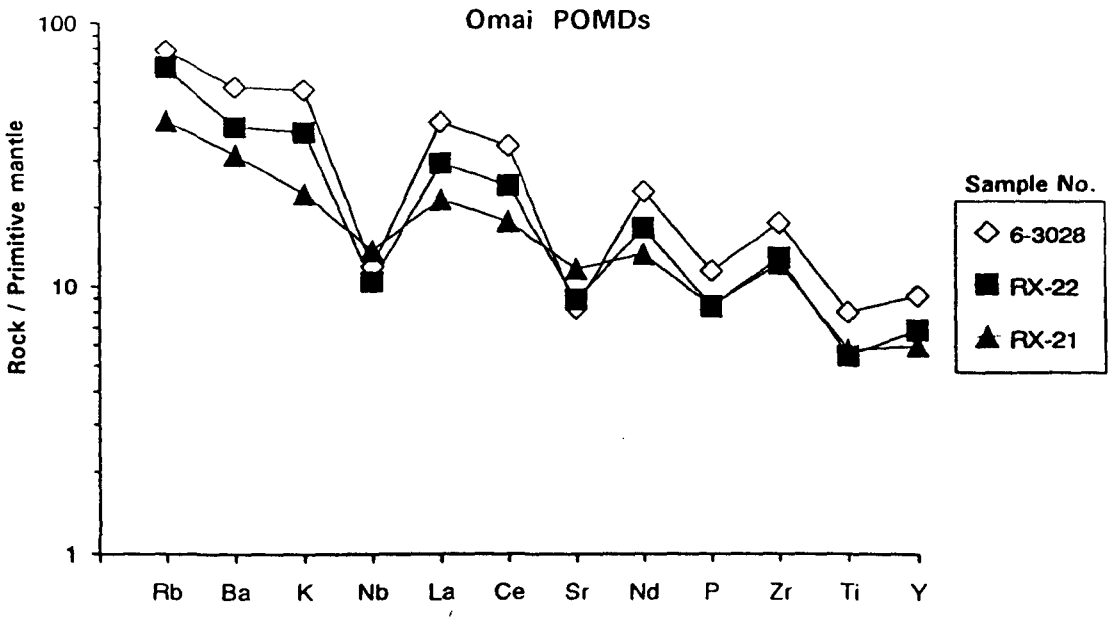

Fig. 5.18a: Mantle-normalised spidergram patterns of the Omai POMDs. Sample 6-3028 - GSR dyke; RX-22 - Ya-ya dyke; RX-21 - Point dyke. Normalising values from Sun and McDonough (1989).

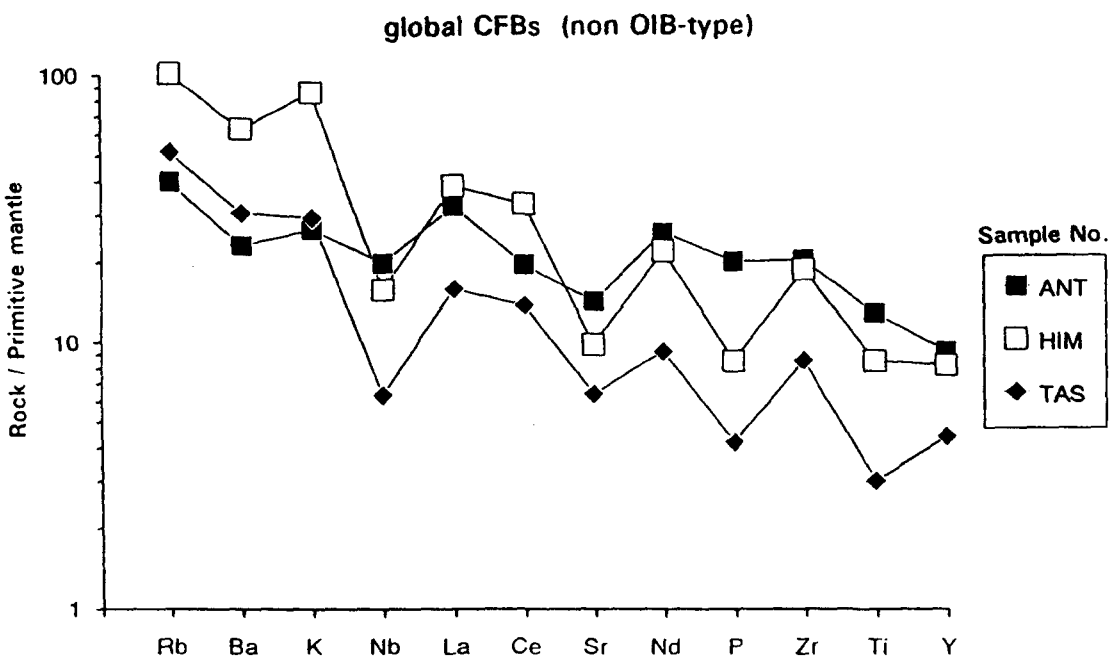

Fig. 5.18b: Mantle-normalised spidergram patterns of global CFB-related mafic dykes (non-OIB type). ANT - average of three Mesozoic dolerites from western Dronning Maud Land, Antarctica (data from Harris et al., (1991); HIM - average of ten Proterozoic mafic dykes from the Indian Himalayas (data from Ahmad and Tarney, 1991); TAS - average of twenty-one dolerites from Tasmania (data from Hergt et al., 1989). Normalising values from Sun and McDonough (1989).

dykes are members of the Mesozoic Apatoe Suite as opposed to the Avanavero Suite of the Mesoproterozoic. On the basis of geographical location, it is unlikely, but not impossible, that the Omai POMDs belong to the sub-ordinate PAPA dyke suite which chiefly occur as Palaeozoic intrusions south of the Takutu break in southern Guyana.

According to Choudhuri (pers. comm. to C.N. Barron, 1988) only minor petrological and chemical differences separate the three main dyke suites of the Guiana Shield. However, on the premise that the younger mafic dykes have relatively higher TiO_2 contents than their ancient counterparts, Sial et. al., (1987) have attempted to discriminate between Precambrian and Mesozoic dykes in the Guiana Shield by the application of a P_2O_5-TiO_2 co-variation diagrams. The ranges of TiO_2 values for the respective dyke suites are reported in Gibbs and Barron (1992) as follows: Avanavero dykes - 0.5 to 1.8% TiO_2; Apatoe dykes 1.2 to 3.6% TiO_2. It can be seen in Fig. 5.17a that the Omai POMDs generally plot within the overlap and therefore their temporal and magmatic association cannot be satisfactorily resolved using these parameters.

More recently, Choudhuri et. al., (1991) have proposed an age-related Zr-K_2O variation that distinguishes between Avanavero- and Apatoe-type magmatism (see Fig. 5.17b). According to this diagram, Apatoe dykes from northern Guyana tend to follow steep MORB-like trend whereas Avanavero dykes follow a shallow, island arc tholeiite (IAT) fractionation path. The Omai POMDs, however, appear to define a unique intermediate trend and therefore their true association cannot be resolved unambiguously by this method. However, it could be argued that the Ya-ya dyke follows the Apatoe trend, though obviously more data are required before any firm conclusions can be drawn. The picture is further complicated by the fact that Mesozoic dykes from southern Guyana lie along the Avanavero trend, which suggests that post-orogenic dykes in Guyana may contain provincial as well secular geochemical variations.

On a global scale, the Omai POMDs show a remarkable similarity in trace element geochemistry when compared to other CFB-related mafic dykes such as Mesozoic dykes from Tasmania and Antarctica and Proterozoic dykes from the Indian Himalayas (see Figs. 5.18 a and b). In all cases, the mantle-normalised spidergram patterns of these rocks are characterised by regular negative Nb-Sr-P-Ti anomalies.

Table 5.2: Geochemical analyses of the Omai mafic dyke suites (overleaf).

Notes:
1. Major oxide values are recalculated to 100% anhydrous basis.
2. Major oxide values in weight percent (wt.%), trace element concentrations in ppm.
3. Total Fe analysed as $Fe_2O_3^T$.
4. LOI denotes loss-on-ignition values (wt.%).
5. Mg-number = 100 x MgO/(MgO + FeO) atomic ratio, where FeO = $Fe_2O_3^T$/1.15.
6. * indicates semi-quantitative values by ICP-MS analysis.

Table 5.2: Geochemical analyses of the Omai mafic dyke suites.

	Appinite pipes			Gilt Creek Suite				
	5-1142	HP-01	HP-04	6-1975	4-1816	7-1594	3-1396	4-2050
SiO2	46.71	43.70	45.51	41.48	45.57	48.41	50.05	50.79
Al2O3	14.06	13.32	13.33	6.69	8.69	17.87	16.53	13.28
$Fe_2O_3^T$	12.14	15.04	14.03	12.33	10.91	10.14	10.69	9.64
MgO	11.52	12.33	11.72	24.46	21.30	7.39	8.56	9.89
CaO	10.02	10.66	10.06	13.36	11.99	9.07	8.66	11.20
Na2O	2.48	2.30	2.82	0.17	0.28	2.73	2.89	2.86
K2O	0.99	0.45	0.47	0.29	0.28	3.02	1.36	1.03
TiO2	1.72	1.70	1.47	0.56	0.53	0.69	0.78	0.75
MnO	0.13	0.20	0.24	0.41	0.21	0.25	0.17	0.18
P2O5	0.23	0.30	0.35	0.25	0.24	0.43	0.31	0.38
Total	100.00	100.00	100.00	100.00	100.00	100.00	100.00	100.00
LOI	3.32	2.97	2.65	14.42	18.33	5.30	8.00	11.60
Mg-number	66.0	62.7	63.1	80.3	80.0	59.9	62.1	67.8
$Fe_2O_3^T$/MgO	1.05	1.22	1.20	0.50	0.51	1.37	1.25	0.97
Rb	16.7	4.40*	6.80*	10.2	6.30	73.1	42.2	32.7
Sr	458	480*	458*	497	432	461	256	337
Ba	619	207*	253*	95.9	69.5	634	304	732
Li	14.8			33.8	47.7	12.7	36.2	22.5
Y	23.2	21.4	23.1	10.9	8.70	16.2	16.9	11.2
Zr	73.6	78.1*	78.4*	55.8	53.7	90.5	71.6	92.6
Nb	5.87	4.23*	6.00*	3.00	1.57	7.48	7.24	4.60
Hf	3.50	2.24*	2.89*	2.09	1.32	2.45	5.06	2.20
Th	1.75	1.87*	2.62*	1.48	2.02	3.97	2.65	3.43
U	0.59	1.43*	1.51*	0.51	0.66	1.28	1.16	0.54
Co	103	82.5	78.3	116	103	63.6	60.5	53.8
Cr	171	45.7	60.5	1688	1536	230	71.2	226
Ni	131	78.9	79.5	557	467	52.7	43.3	70.2
V	437	473	411	234	193	232	219	237
Sc	74.1	63.6	58.4	24.0	25.4	26.6	27.3	28.9
Cu	230	70.1	65.3	55.5	45.5	336	125	32.0
Pb	13.7			4.63	42.6	10.3	9.61	6.04
Zn	93.8	117	128	261	112	140	93.2	105
As	3.7			2.5	29.4	2.9	6.4	3.2
La	14.0	11.2	13.3	11.7		22.3		
Ce	34.0	27.6	32.7	31.2		52.4		
Pr	5.10	4.26	4.99	3.50		6.02		
Nd	23.9	20.2	23.2	14.9		24.8		
Sm	6.35	5.21	5.67	3.36		5.16		
Eu	2.02	1.60	1.70	1.05		1.59		
Gd	6.72	5.08	5.46	3.14		4.74		
Tb	0.96	0.72	0.75	0.40		0.55		
Dy	4.96	3.89	4.20	2.04		2.77		
Ho	1.00	0.76	0.80	0.39		0.58		
Er	2.54	1.94	2.11	1.03		1.32		
Tm	0.46	0.26	0.30	0.16		0.19		
Yb	2.17	1.57	1.81	1.00		1.21		
Lu	0.42	0.23	0.27	0.18		0.17		
La_n/Yb_n	4.32	4.76	4.91	7.84		12.32		
Total REE	104.6	84.5	97.3	74.1		123.8		

Table 5.2 (cont'd): Geochemical analyses of the Omai mafic dyke suites.

	Gilt Creek Suite (cont'd)					
	2-1546	8-1888	6-0399	7-0979	2-1534	8-2285
SiO2	52.27	53.24	53.26	53.25	54.77	55.79
Al2O3	12.77	13.67	15.71	13.84	13.26	12.66
$Fe_2O_3^T$	7.28	8.45	8.47	9.05	6.93	6.65
MgO	12.28	11.63	6.34	9.71	10.66	10.99
CaO	9.28	7.96	8.86	8.56	6.87	7.41
Na2O	3.90	1.69	3.27	2.56	4.66	3.39
K2O	0.45	2.11	2.70	1.98	1.04	1.38
TiO2	0.84	0.68	0.78	0.61	0.86	0.81
MnO	0.12	0.16	0.19	0.17	0.11	0.10
P2O5	0.81	0.41	0.42	0.27	0.84	0.82
Total	100.00	100.00	100.00	100.00	100.00	100.00
LOI	10.82	22.70	12.01	3.75	9.55	5.75
Mg-number	77.6	73.8	60.5	68.7	75.9	77.2
$Fe_2O_3^T$/MgO	0.59	0.73	1.34	0.93	0.65	0.61
Rb	17.1	95.8	75.0	49.3	40.7	56.4
Sr	765	1580	583	330	712	1311
Ba	871	1273	774	558	763	1699
Li	33.5	28.9	10.7	14.7	19.4	39.9
Y	24.5	13.6	11.8	17.7	27.0	25.8
Zr	289	106	107	106	298	304
Nb	9.96	6.48	4.94	6.07	11.50	13.50
Hf	7.53	4.13	2.63	3.01	7.91	11.70
Th	11.3	3.96	4.02	5.07	11.9	12.3
U	3.47	1.23	1.29	2.46	3.67	3.75
Co	68.6	61.5	58.3	67.6	60.5	53.6
Cr	404	204	112	250	243	460
Ni	350	78.9	27.5	141	286	293
V	143	197	166	221	153	147
Sc	18.3	26.1	22.5	29.1	15.3	16.1
Cu	87.6	46.1	43.6	56.1	76.4	124
Pb	8.50	6.36	9.29	7.23	21.2	46.5
Zn	86.9	182	144	100	95.8	104
As	3.0	1.9	2.5	4.0	3.8	3.3
La		18.6	22.3	19.6		82.9
Ce		43.2	51.8	39.7		187.0
Pr		5.20	5.50	4.80		21.5
Nd		21.4	23.0	18.9		84.0
Sm		4.75	4.70	4.10		15.3
Eu		1.37	1.38	1.13		3.80
Gd		4.25	4.30	3.98		12.3
Tb		0.51	0.48	0.54		1.34
Dy		2.58	2.32	2.99		5.83
Ho		0.49	0.42	0.58		0.89
Er		1.30	1.12	1.61		2.13
Tm		0.19	0.16	0.25		0.27
Yb		1.25	1.14	1.57		1.70
Lu		0.21	0.18	0.24		0.26
La_n/Yb_n		9.95	13.0	8.38		32.6
Total REE		105.3	118.8	100.0		419.2

Table 5.2 (cont'd): Geochemical analyses of the Omai mafic dyke suites.

Post-orogenic mafic dykes (POMDs)

	GSR dyke					Point dyke		Ya-ya dyke
	8-3046	6-2908	5-2936	6-2806	6-3028	MB-09	RX-21	RX-22
SiO2	52.57	52.66	52.95	53.00	53.12	52.23	53.52	52.48
Al2O3	14.66	14.79	15.11	15.05	13.55	16.16	14.77	15.25
$Fe_2O_3^T$	15.29	14.92	14.78	15.02	16.36	10.73	11.86	14.06
MgO	3.81	3.88	3.52	3.32	3.17	5.96	6.06	4.55
CaO	7.96	8.01	7.82	7.75	7.13	10.67	9.21	8.49
Na2O	2.54	2.54	2.64	2.66	2.60	2.21	2.30	2.47
K2O	1.35	1.38	1.38	1.36	1.67	0.64	0.68	1.16
TiO2	1.45	1.43	1.42	1.48	1.74	1.07	1.25	1.19
MnO	0.17	0.17	0.17	0.17	0.18	0.16	0.17	0.17
P2O5	0.20	0.22	0.21	0.19	0.26	0.17	0.18	0.18
Total	100.00	100.00	100.00	100.00	100.00	100.00	100.00	100.00
LOI	0.00	0.09	0.00	0.00	0.22	0.63	1.71	0.40
Mg-number	51.1	50.2	49.4	50.0	54.7	39.9	44.5	48.0
$Fe_2O_3^T$/MgO	4.01	3.85	4.20	4.52	5.16	1.80	1.96	3.09
Rb	47.3	44.5	54.5	42.9	50.3	19.0	26.8	43.0
Sr	192	187	229	182	174	186	247	188
Ba	355	362	411	366	400	243	221	281
Li	20.6	15.7	14.5	9.77	13.4	8.77	24.4	19.1
Y	31.0	33.6	32.6	33.8	41.5	23.3	27.4	30.9
Zr	174	165	186	163	197	90.3	138	144
Nb	7.70	7.55	9.10	7.34	8.47	5.93	9.78	7.41
Hf	6.11	4.85	6.11	4.88	5.30	2.69	5.68	4.62
Th	3.51	3.78	3.88	3.67	4.20	2.48	4.12	3.49
U	0.97	0.75	1.25	0.83	0.93	0.47	0.82	0.80
Co	80.6	89.4	91.6	91.4	99.4	75.8	83.4	85.8
Cr	112	106	132	143	90.0	213	116	88.0
Ni	72.7	74.0	75.3	76.7	67.0	117	106	85.9
V	337	354	362	359	391	356	331	310
Sc	34.3	36.3	38.6	37.4	38.4	37.8	34.0	33.8
Cu	225	218	226	234	253	200	192	202
Pb	26.2	8.50	10.2	8.67	8.59	4.34	15.2	8.50
Zn	152	148	151	151	160	103	115	136
As	2.0	2.1	2.5	1.9	2.0	0.4	0.9	1.5
La					28.8		14.5	20.2
Ce					60.7		31.5	42.8
Pr					7.57		4.14	5.43
Nd					31.3		18.2	22.7
Sm					7.15		4.52	5.22
Eu					1.92		1.38	1.51
Gd					7.72		5.18	5.79
Tb					1.21		0.85	0.90
Dy					7.39		4.94	5.63
Ho					1.51		1.04	1.17
Er					4.30		2.90	3.35
Tm					0.63		0.41	0.48
Yb					4.00		2.72	3.08
Lu					0.61		0.41	0.48
La_n/Yb_n					4.83		3.56	4.39
Total REE					164.8		92.7	118.7

CHAPTER 6

MINERALISATION

6.1 Aims of chapter.

The first part of this chapter is devoted to reviewing the main characteristics of primary mineralisation at Omai. Following this, preliminary attempts are made to establish the nature and origin of the hydrothermal fluid using advanced analytical techniques. These techniques include: SEM-EDS micro-analysis, fluid inclusion studies and light stable isotope analyses. The chapter is concluded with a brief review of secondary gold mineralisation in the oxidised zone.

6.2 Ore-sample subset.

Seventy-four drill-core samples, selected mainly from hydrothermal veins and adjacent wall-rocks in the Omai Stock Zone, provide the raw material for this aspect of the research. The subset includes 61 polished thin section specimens (reflected-light microscopy and SEM-EDS analysis), three polished-wafer sections (fluid inclusion studies) and 11 crushed vein samples (light stable isotope considerations). A full list of samples is presented in Appendix I.

6.3 Aspects of the primary ore zones.

As outlined in Chapter 2, the Omai goldfield consists of two primary ore zones, separated on the ground by a distance of about 800m (see Fig 2.3). These are known as the **Omai Stock Zone** and the **Wenot Lake Zone**. The Omai Stock Zone has been exploited periodically for over a century, whereas, the Wenot lake Zone was discovered relatively recently, in 1989. Sizeable amounts of saprolitic and alluvial placer deposits are associated with the primary ore zones (see Table 1.1 and section 6.6).

6.3.1 Style of Mineralisation

The style of primary mineralisation at Omai is essentially epigenetic, lode-type. In both the main ore zones, mineralisation is spatially and temporally related to a series of narrow (5mm to 50mm) shallow-dipping, laterally discontinuous, hydrothermal, quartz-carbonate veins. In

the Omai Stock Zone, these lodes are largely hosted within the granitic Omai Stock. Graphic analyses of the drill-core sections in the Omai Stock illustrate that the lodes occupy less than 1.0% volume of the ore body with local concentrations of veins occurring at, and sub-parallel to, the margins of intruding mafic dykes such as the Gilt Creek Suite. In the Wenot Lake Zone, the hydrothermal veins are hosted within narrow bands of acid volcanic rocks where they occur as anastomosing and en echelon veins and veinlets (see Bertoni et al., 1990). In this thesis, the acid volcanic rocks of the Wenot Lake Zone are known as the high-silica rhyolites of the Majuba Suite.

6.3.2 Structural controls on mineralisation.

Undoubtedly, structural controls on mineralisation are related to the relatively high competency of the acid host rocks. Field observations indicate that both the Omai Stock and the high-silica rhyolites of the Wenot Lake Zone responded to regional stresses by the brittle failure whereas the bulk of mafic greenstone country rocks accommodated external forces by ductile deformation. In the former case, enhanced open-space permeability has been generated, permitting the subsequent concentration and advection of hydrothermal fluids into the ore bodies. The overall structural picture at Omai is still poorly understood, though localised ESE-trending shear zones recorded by Guardia (1969) and Bertoni et al., (1990) in the immediate Omai area are thought to be of key structural significance (see also Chapter 7).

6.3.3 Timing of mineralisation.

Working on the hypothesis that the Omai Stock Zone and the Wenot Lake Zone were mineralised at the same time, the maximum age of the mineralisation can be constrained by the age of the youngest host rocks. Field relations clearly show that the youngest host rocks at Omai are the dykes of the Gilt Creek Suite which cut the Omai Stock. No radiometric dates are available for these dykes though, the field and geochemical evidence suggest that they were emplaced towards the end of the Trans-Amazonian orogeny, ca 1.95 Ga.(see also section 5.7.4). A minimum age of mineralisation can be estimated from the non-mineralised, post-orogenic gabbroic (GSR) dyke which also intrudes the Omai Stock. Unfortunately, this dyke is also undated, though its morphology suggests that it was emplaced along with the Apatoe Suite during the Mesozoic. The question of mineralisation timing is briefly addressed in a regional context in Chapter 7.

6.3.4 Alteration paragenesis.

Wall-rocks in Omai Stock Zone has been affected by at least six phases of episodic hypogene alteration which include: albitisation, propylitisation, silicification, sericitisation, carbonatisation and sulphidisation. These alteration phases, with the exception of the first two, are largely related to hydrothermal activity associated with the quartz-carbonate veins. In the Omai Stock, sericite-carbonate alteration is dominant. Generally, spatial and temporal overlaps between all the phases are common, making it difficult to untangle the paragenesis of alteration events. The assemblage of wall-rock alteration phases in the Wenot Lake Zone is largely comparable to that of the Omai Stock Zone, the major difference being that intensive sericitic wall-rock alteration is generally absent in the former.

6.3.5 Mineral paragenesis (Omai Stock Zone).

The hydrothermal mineral paragenesis for Omai Stock Zone was first established by Johnston (1960). A generalised version of this paragenetic sequence is presented as follows:

quartz ± carbonate ± pyrite ± scheelite ± sphalerite ± chalcopyrite ± galena ± tellurides ± gold

Minor gangue phases such as albite and tourmaline may also be added. However, in the discussion below, only the key gangue and metallic ore minerals are addressed.

Gangue minerals (quartz, carbonate).

Quartz.

Quartz is by far the most dominant gangue phase and on average accounts for approximately 75-80% of the vein-filling mode (see Plate 6.1). In general, the quartz is colourless or milky white and massive. No evidence of crustiform banding is observed, implying that the hydrothermal fluids were introduced during a single episode, rather than repeated cycles. Microscopic examination reveals that the vein-quartz consists of mosaics of anhedral grains which contain ubiquitous fluid inclusions. These inclusions tend to be aligned along micro-fractures and grain boundaries (see section 6.4.2).

Carbonate (ankerite).

According to Bertoni et al., (1990), possibly three pulses of hydrothermal carbonatisation are recorded in the Omai Stock Zone. The second of these is considered to be coeval with

Plate 6.1: Drill-core specimen 6-1465 showing a 5cm-thick quartz-carbonate vein from the Omai Stock. Note how the grey carbonate (ankerite) is confined to the vein margin.

Plate 6.2: Drill-core specimen 2-1566 showing a 1cm-thick quartz-carbonate vein in a mafic meta-volcanic rock of the Majuba Suite. In this specimen, the grey carbonate (ankerite) occupies most of the vein-filling mode.

mineralisation. Normally, carbonate minerals constitute between 10% and 15% of the vein-filling mode. In general, they are represented by a steely grey, scaly species which occurs as ribbons along the vein margins (Plate 6.1), as sprawling masses (Plate 6.2) or as regular, saw-tooth arrangements within the quartz. On the basis of optical properties, Johnston (1960) ascertained that the chief carbonate species was ankerite (Fe-carbonate). This contention is supported by the staining tests of Morton (1987). In the field, ankerite may be distinguished from common calcite by its relatively milder reaction to cold 10% HCl.

Metallic ore minerals (pyrite, scheelite, galena, tellurides and gold).

Apart from pyrite, which has a prolonged paragenetic history, metallic ore formation in the Omai Stock Zone can be conveniently classified according to early or late paragenetic episodes. The early phase of mineralisation is dominated by scheelite whereas the later phase, which provides the economic interest, consists of a galena-tellurides-gold assemblage.

Pyrite

Pyrite is by far the most abundant metallic ore mineral at Omai. Concentrations of idiomorphic cubes are commonly located in the alteration haloes of mineralised wall-rocks, adjacent to hydrothermal veins. Disseminations of pyrite are also recorded within the veins as random grains, as "float" in a carbonate matrix, or associated with other sulphides (see Plate 6.3). Minor inclusions of pyrrhotite and chalcopyrite are often observed in some of the coarser pyrite grains.

Scheelite

Scheelite can be readily detected by running an ultra violet (UV) lamp over the drill-core sections in the dark. Such simple surveys clearly demonstrate that occurrences of this mineral are spatially related to the quartz-carbonate veins within the Omai Stock. Generally, the scheelite takes the form of off-white to yellow-brown, medium-grained, sub-granular aggregates which invariably occur as ragged ribbons along the vein margins or as detached masses within the veins (see Plate 6.4). In this respect, scheelite shows a similar paragenesis to early carbonate formation. The overall distribution of scheelite is sporadic and sub-economic, though a spectacular mass, weighing some 400 g, is cited by Bracewell (1943).

Galena

Galena is common companion of visible gold in drill-core sections. This spatial association is confirmed by microscopic examination which shows galena, gold and tellurides in close

proximity, usually confined to micro-fractures and micro-cavities within vein-quartz or carbonate, near the vein margin. In the few specimens examined, it is difficult to ascertain whether galena rims gold, or whether the gold invades galena (see Plates 6.5 and 6.6). Complex textural relationships involving galena and Bi-telluride (see Plates 6.7 and 6.8) indicates that these minerals shared a similar paragenesis.

Tellurides

Apparently, telluride minerals were first recorded at Omai by E. Lungwitz, back in 1899. In an attempt to identify individual telluride phases Johnston (1960) carried out a series of microchemical tests on samples supplied by Anaconda geologist, G. C. Waterman. Although these tests proved to be inconclusive, they gave tentative indications of nagyagite, wehrlite or tetradymite, and hessite or petzite. One of the aims of this thesis is to identify individual telluride phases by SEM-EDS micro-analysis using a JEOL 840 instrument interfaced with a LINK software system. However this method is not without limitations, mainly related to the minute (10 μm) size of some telluride grains (see Appendix IV for details).

In spite of the drawbacks, micro-analyses of galena-telluride-gold mineralisation in polished section 6-2017 proved to be extremely fruitful, as five, possibly six, different telluride phases were positively identified by this method. These phases, which are listed along with their formula in Table 6.1, consist of Au-, Ag- and Bi-bearing species and include calaverite, hessite, petzite, wehrlite, tellurobismuthite and volynskite (?). These minerals can occur as discrete grains, as complex intergrowths, or as zoned crystals. An example of the latter is shown in Plate. 6.9 where the Ag-Au telluride, petzite, is rimmed by the Ag-telluride, hessite.

Gold

Native gold is the only ore mineral at Omai that is found in economic concentrations. Its primary grade has been estimated at 1.34 g/t in the Omai Stock Zone and 1.23 g/t in the Wenot Lake Zone (see Table 1.1). As already mentioned, gold has a close paragenetic association with galena and tellurides, though native gold grains may occur in isolation in micro-fractures and micro-cavities within vein-quartz (see Plate 6.10).

A series of micro-analyses carried out across a 1 mm gold grain in polished thin section, 6-2107, indicated that native gold may contain 6 to 8 wt.% silver. Under reflected-light, the purity of gold may be gauged by its colour. A hypothesis proposed here is that relatively pure gold is indicated by a deep, rich, golden yellow colour, whereas gold containing impurities, such as silver or tellurium, tends to be a paler yellow, like chalcopyrite. In polished thin section, 5-0315, microscopic inclusions of chalcopyrite and a Bi-sulphosalt (?) were identified

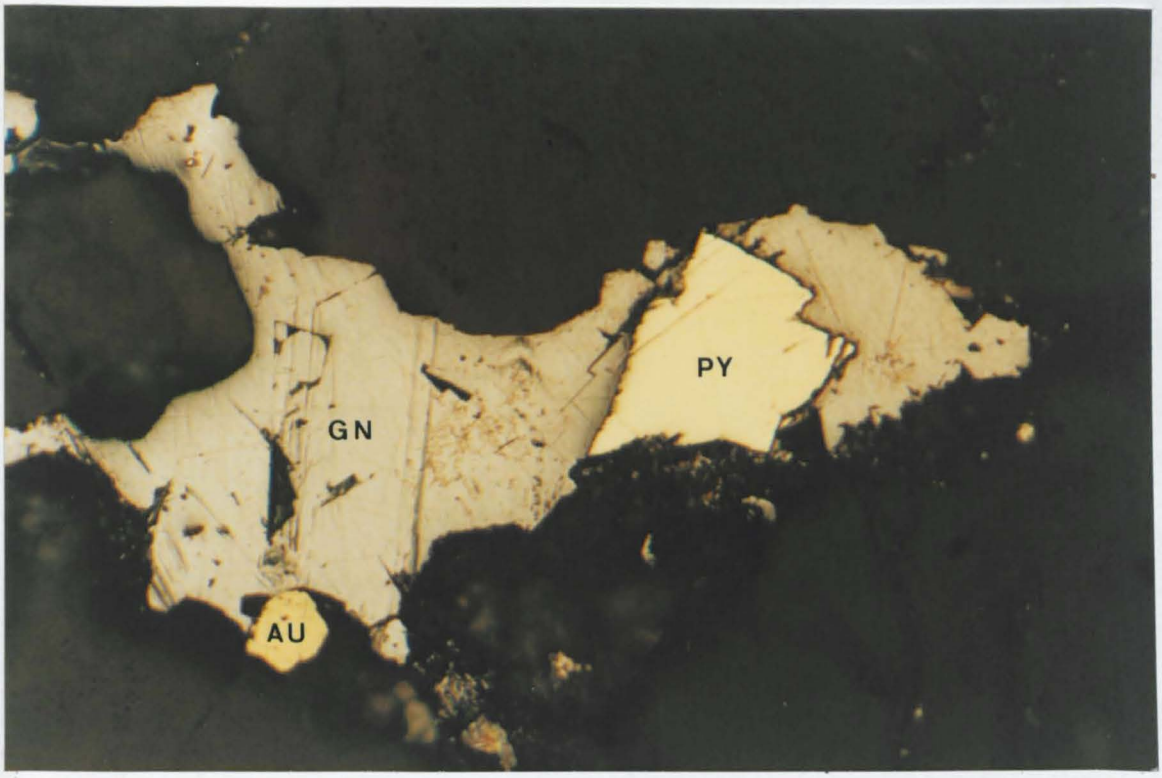

Plate 6.3: Reflected-light micrograph (oil immersion) showing pyrite (PY), galena (GN) and minor gold ? (AU) mineralisation in vein-quartz. Polished thin section, 6-2107; Mag. x 275.

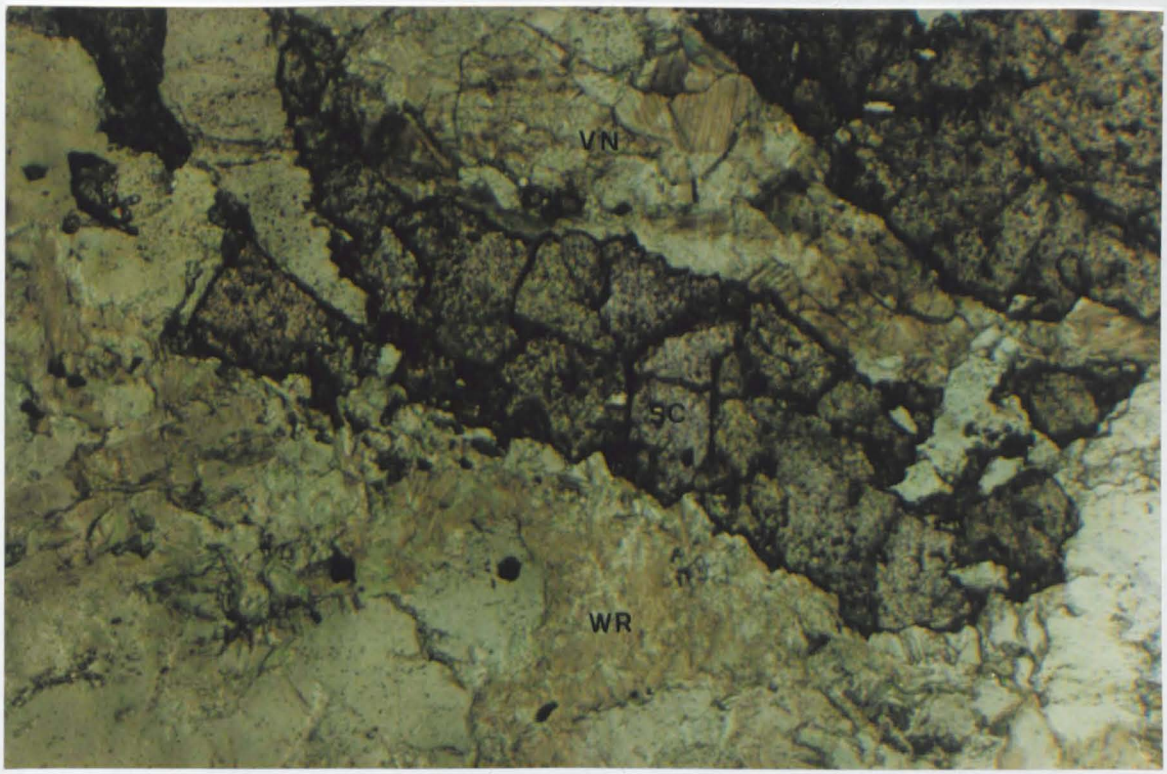

Plate 6.4: PPL micrograph showing scheelite (SC) mineralisation at the margin of a quartz-carbonate vein (VN) above granitic wall-rock (WR). Polished thin section, 5-0315; Mag. x 75.

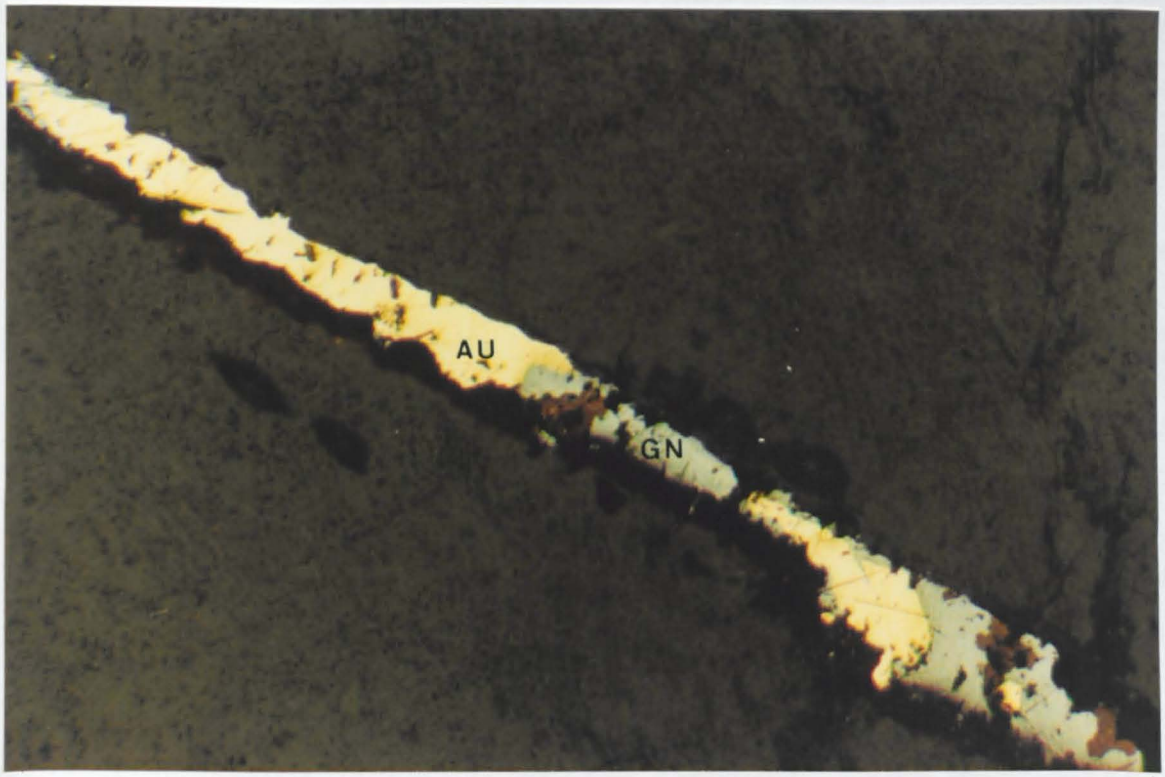

Plate 6.5: Reflected-light micrograph (oil immersion) showing gold (AU) and galena (GN) mineralisation occupying a linear micro-fracture within vein-quartz. Polished thin section, 6-2107; Mag. x 140.

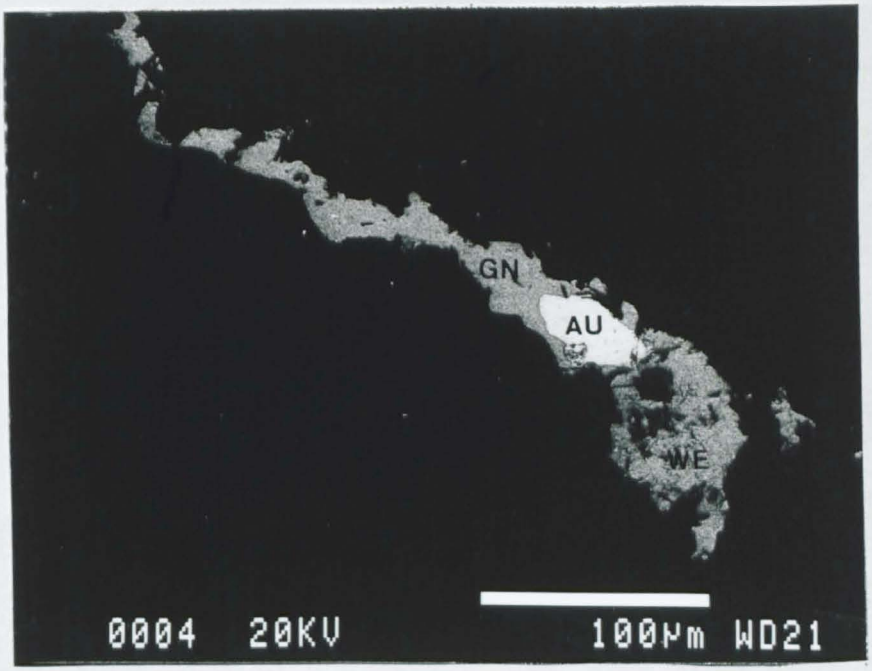

Plate 6.6: SEM-EDS backscatter image showing textural relations between galena (GN), gold (AU) and a Bi-telluride, wehrlite (WE) in vein-quartz. Polished thin section 6-2107. Note scale bar is 100 μm.

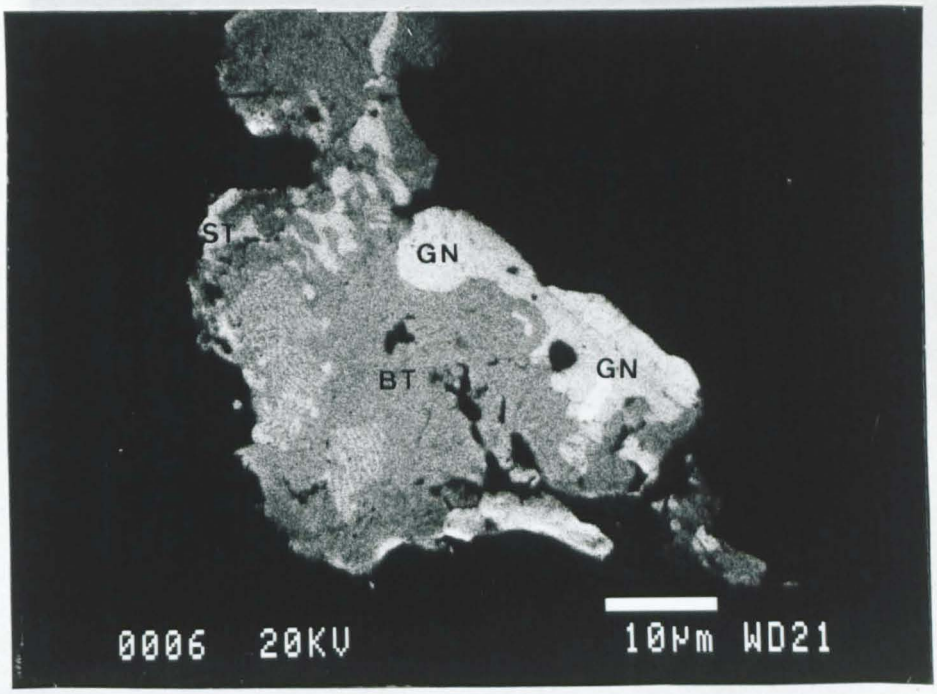

Plate 6.7: SEM-EDS backscatter image showing complex textural relations between galena (GN), a Bi-telluride (BT) and a Ag-telluride (ST) in vein-quartz. Polished thin section, 6-2107. Note scale bar is 10 μm.

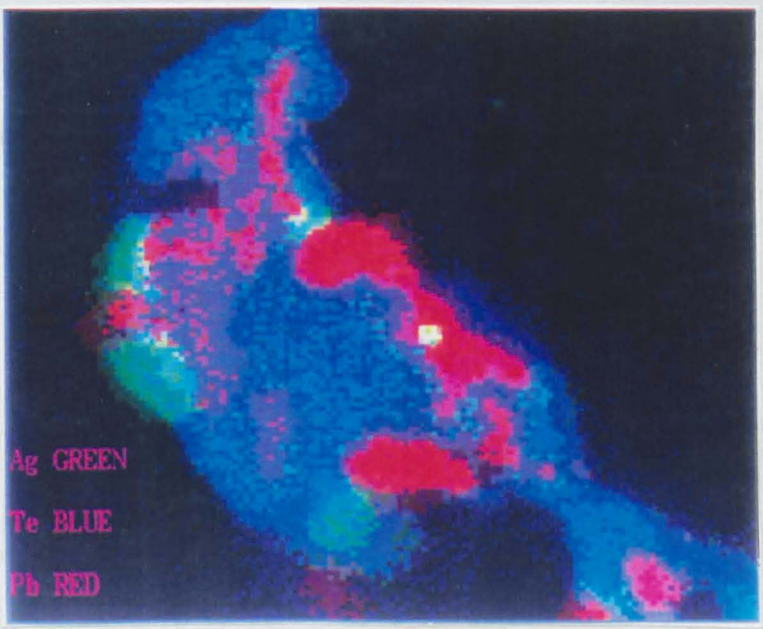

Plate 6.8: Digital X-ray emission (DRXM) map high-lighting the complex textural relations of the mineral grain shown in Plate 6.7. Red areas (Pb) in the DRXM image correspond to galena (GN), blue areas (Te) to a Bi-telluride and green areas (Ag) to a Ag-telluride. Areas of mixed colour indicate intergrowths between the three main phases. Scale approximates that of Plate 6.7.

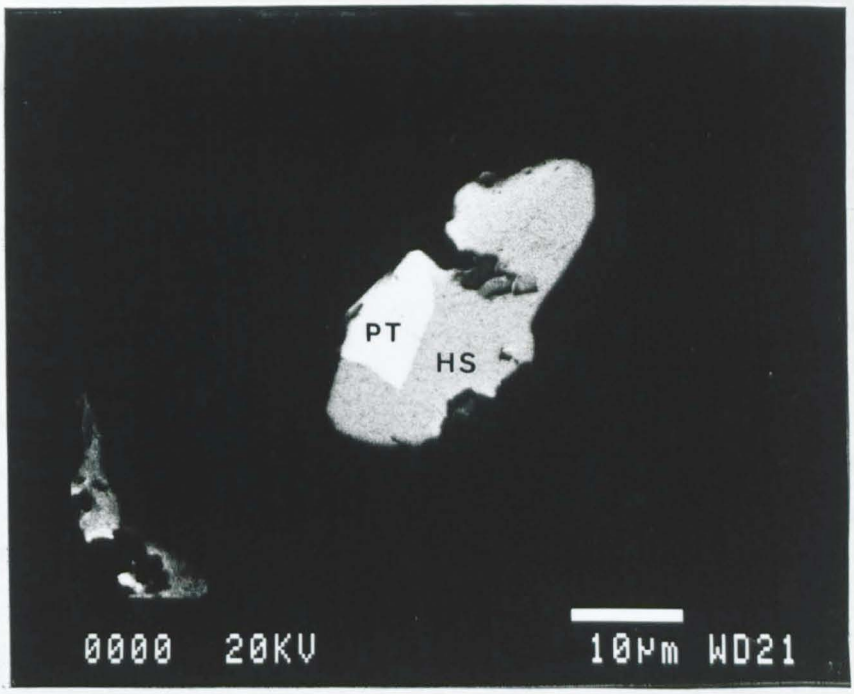

Plate 6.9: SEM-EDS backscatter image showing overgrowth/zoning texture between the telluride phases petzite (PT) and hessite (HS). The host material is vein-quartz. Polished thin section, 6-2107. Note the scale bar is 10 μm.

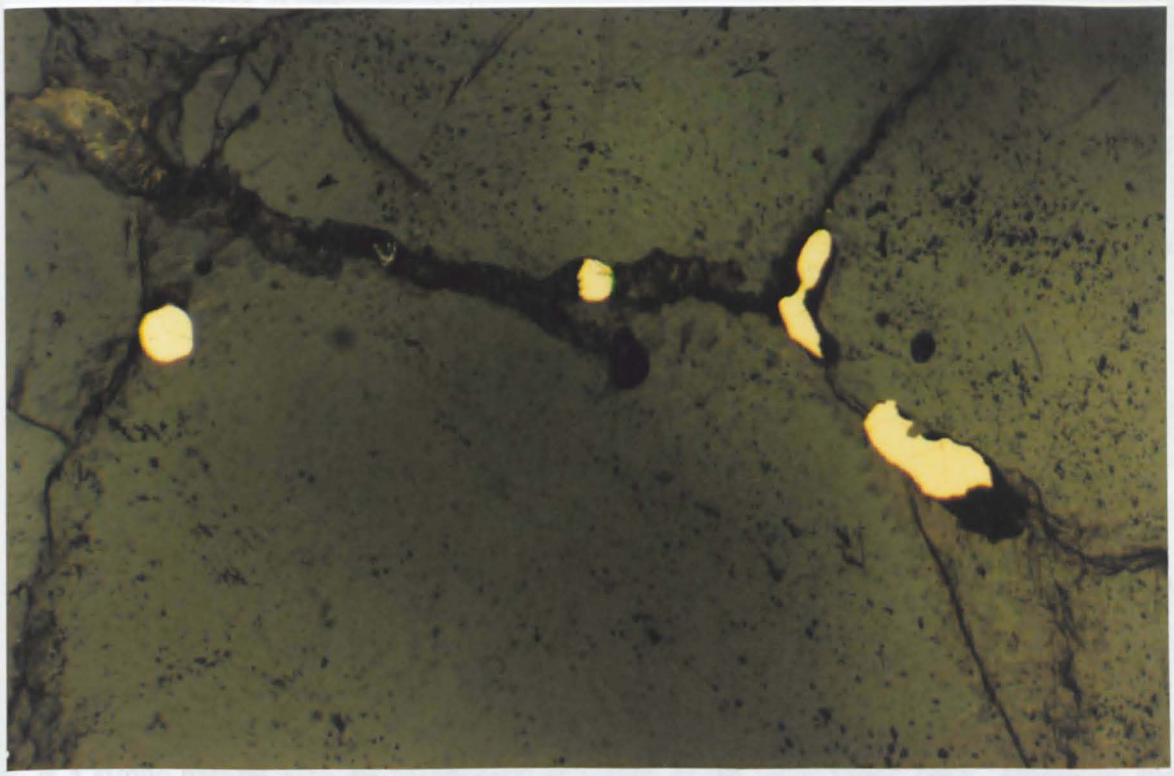

Plate. 6.10: Reflected-light (oil immersion) micrograph showing native gold grains aligned along micro-fractures in vein-quartz. Polished thin section, 7-1284; Mag. x 140.

at the margin of a native gold grain, in close proximity to galena.

Table 6.1: Telluride minerals identified in the Omai Stock Zone by SEM-EDS micro-analysis (sample 6-2107).

Telluride	Formula
Calaverite	$AuTe_2$
Petzite	Ag_3AuTe_2
Hessite	Ag_2Te
Wehrlite	BiTe
Tellurobismuthite	Bi_2Te_3
Volynskite (?)	$AgBi_{1.6}Te_2$

Notes:

1. Stoichiometric behaviour of elements is assumed when calculating formulae. (see Utytenbogaardt and Burke (1971) and Afifi et al. (1988a, 1988b) for further details on telluride minerals).

2. Representative micro-analyses of the above tellurides, along with X-ray spectra, are presented in Appendix IV.

3. Telluride minerals may provide a rough indication of the depositional temperature of the mineralising fluid. For example, Afifi et al. (1988a, 1988b) suggest that the presence of Au-Ag telluride phases (sylvanite and krennerite) in greenstone terrains reflects a maximum depositional and subsequent metamorphism temperature and of 400°C at 2 kbars.

4. The list of tellurides recorded at Omai is by no means exhaustive, as only one polished thin section was examined in detail by SEM-EDS microscopy.

6.3.6 Mineral paragenesis (Wenot Lake Zone).

On the basis of limited sample data, Bertoni et al., (1990) list the main gangue constituents of the hydrothermal veins of the Wenot Lake Zone as quartz and ankerite. Accessory albite, epidote and tourmaline are also noted. The metallic ore minerals are documented as pyrite, scheelite, chalcopyrite, galena and gold. With the exception of the telluride minerals, there is a strong parallel with the paragenetic sequence of the Omai Stock Zone. Moreover, the likelihood is, that in due course, tellurides will be discovered in the Wenot Lake Zone.

6.4 Fluid inclusion studies.

The objective of this preliminary investigation is to constrain provisional P-T-X (pressure-temperature-composition) characteristics of the hydrothermal fluid at Omai so that comparisons can be made with global gold-related deposits.

6.4.1 Analytical technique.

Three unmounted, doubly-polished, 200 μm thick wafers of hydrothermal vein-quartz were analysed using a LINKHAM THM 600 heating-freezing stage. Following the operational procedure outlined by Shepherd (1981), the stage was attached to a Leitz petrological microscope which was fitted with a times 30 LWD (long working distance) objective. Accuracy is estimated at $\pm$ 0.1°C in the temperature range -50°C to 0°C, $\pm$ 4°C between 0°C and 200°C, and $\pm$ 6°C above 200°C.

6.4.2 Sample description.

All three wafer samples were prepared from narrow (< 5cm) hydrothermal veins contained in drill-core samples from the Omai Stock. Samples 5-0550 and 6-0305 consist of non-mineralised quartz whereas sample 5-0315 is composed of quartz-carbonate gangue, containing visible scheelite, galena and gold. All wafer samples are replete with planar trails of minute (<10 μm) secondary fluid inclusions aligned along micro-fractures and grain boundaries. Each sample also hosts relatively good quality primary inclusions which lend themselves to microthermometric analysis. In contrast to the secondary ones, primary fluid inclusions are relatively large (10-40 μm), isolated and randomly distributed.

Following the classification scheme of Nash (1976), four types of primary fluid inclusions are recognised at room temperature in the wafer samples. Type I is represented by water-rich monophase and two phase inclusions, type II by vapour-rich monophase and two-phase inclusions (see Plate 6.11), type III by multi-phase inclusions incorporating daughter minerals, possibly micas and type IV by three-phase, H_2O liquid + CO_2 liquid + CO_2 vapour. The majority of the microthermometric data was obtained from the type IV class which comprise approximately 40% of total primary inclusions. Fluid inclusions in the type IV class are also known as "bubble within bubble" inclusions (see Plate: 6.12). Primary inclusions which showed evidence of leakage or necking were not considered.

6.4.3 Results and interpretation of data.

In ideal situations, five temperature-related microthermometric measurements can be

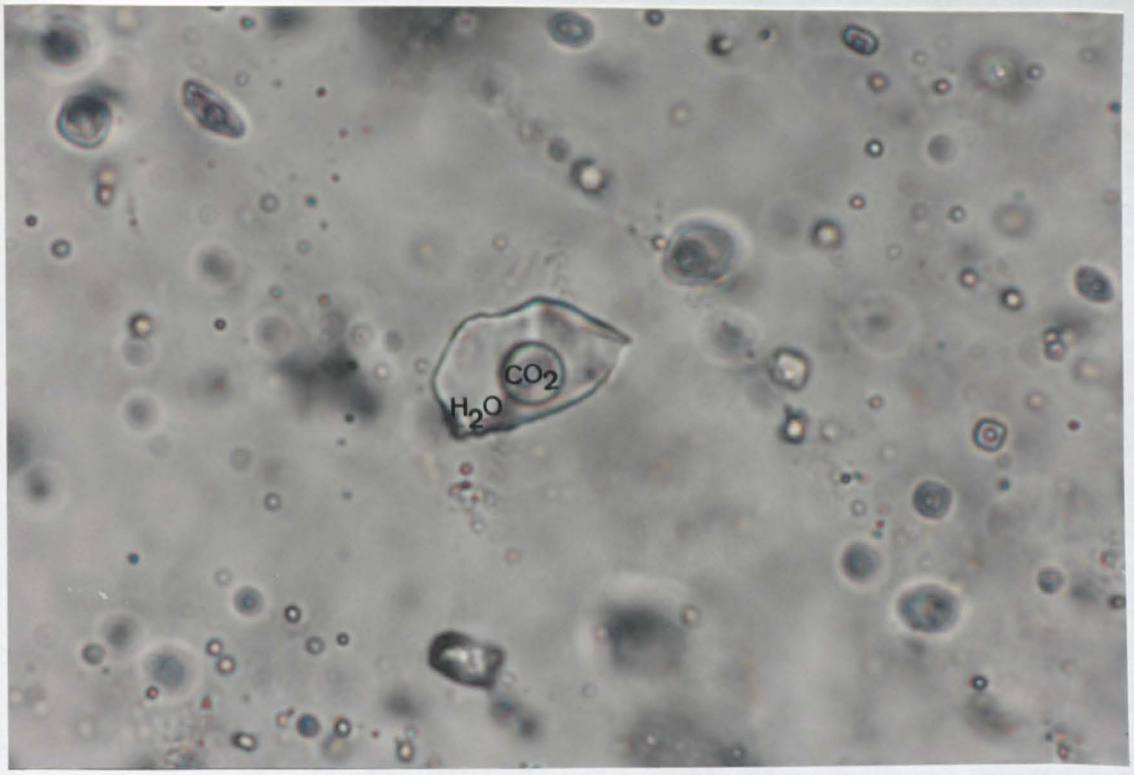

Plate 6.11: PPL micrograph showing primary fluid inclusions in vein-quartz from the Omai Stock. The relatively large (40 μm) inclusion in the centre of the field of view is a type II, two-phase inclusion consisting of H_2O liquid and CO_2 liquid. Polished wafer specimen, 5-0550.

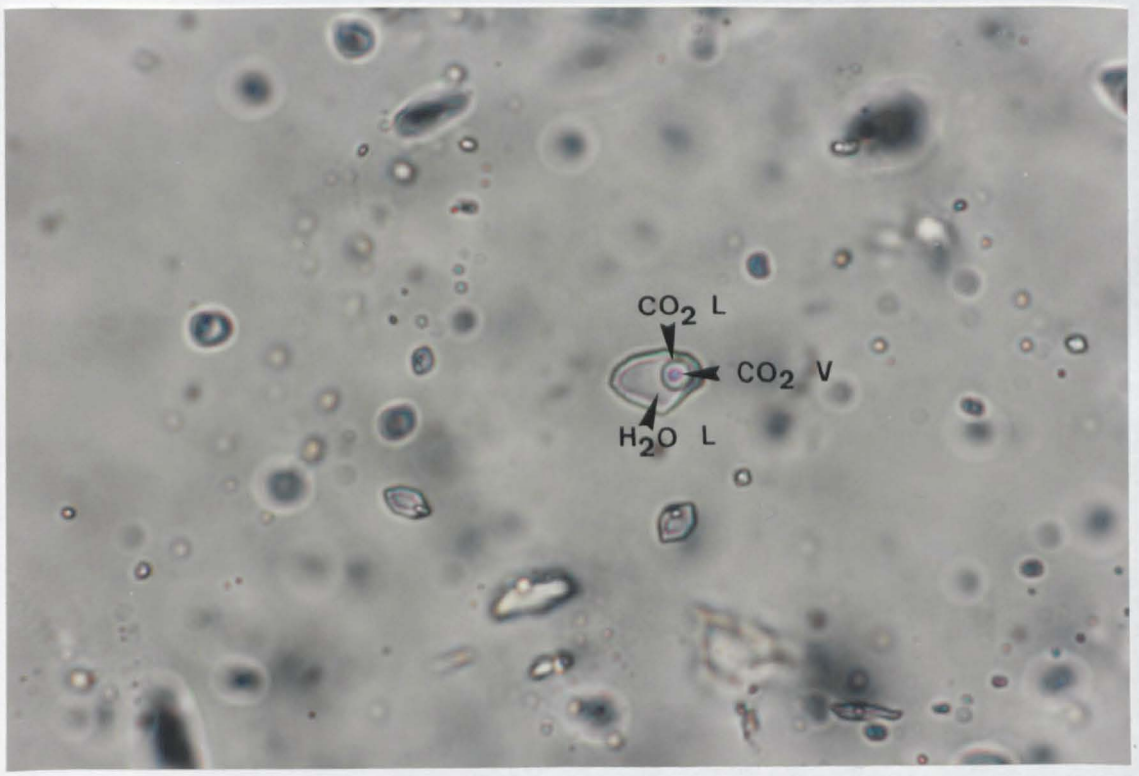

Plate 6.12: PPL micrograph showing primary three-phase fluid inclusions (type IV) in vein-quartz from the Omai Stock. The annotated inclusion, which has a diameter of about 20 μm, illustrates that these "bubble within bubble" inclusions consist of H_2O liquid (L), CO_2 liquid (L) and CO_2 vapour (V). Polished wafer specimen, 5-0550.

determined from any one three-phase fluid inclusion. These determinations, which include solid CO_2 melting (TM_{CO2}), ice melting (TM_{ice}), ice-clathrate melting (TM_{clath}), partial homogenisation (TH_{CO2}) and bulk homogenisation (TH_{tot}), can then be used to assess the P-T-X characteristics of the parent hydrothermal fluid. However, owing to the extremely small size and poor clarity of the inclusions in the Omai wafer samples, no single three-phase inclusion yielded a full compliment of measurements. Therefore, the summary of microthermometric data presented in Table 6.2 is essentially a hybrid compilation derived from a range of two- and three-phase fluid inclusions. Nevertheless, these data proved adequate for a provisional assessment of the following parameters of the fluid: volume fraction of H_2O and CO_2 phases; density of the CO_2 phase; methane content of the CO_2 phase; salinity of the fluid; bulk density of the fluid; mole % of CO_2 in the fluid and the bulk homogenisation temperature (minimum trapping temperature) of the fluid.

Table 6.2: **Summary of microthermometric measurements of fluid inclusions (Omai Stock Zone).**

Parameter	Temp. range (°C)	Mean temp.(°C)	Readings
TH_{tot}	+171 to +307	+207	23
TH_{CO2}	+15.3 to +30.4	+25.8	20
TM_{clath}	+8.4 to +10.9	+9.9	10
TM_{ice}	- not determined -		
TM_{CO2}	-59.0 to -56.4	-57.6	03

Note: The above parameters were established from measurements made on three polished wafer samples (5-0315, 5-0550 and 6-0305).

Volume fraction of CO_2 and H_2O phases.

By their very nature, "bubble-within bubble", three-phase inclusions are CO_2-bearing and H_2O-rich (see Plate. 6.12) The volume fraction of CO_2 (V_{CO2}) in any one inclusion is estimated visually and is essentially the combined volume fraction of the CO_2 liquid and vapour phases. The volume fraction of the surrounding H_2O (V_{H2O}) is calculated by subtracting V_{CO2} from 1. In the Omai samples, V_{CO2} generally ranges from 0.05 to 0.3 (two-phase inclusions included) with a rough average value of 0.15. The average V_{H2O} value is therefore taken as 0.85. The volumetric proportions between phases in fluid inclusions is also referred to as "degree of fill".

Density of the CO_2 phase.

The temperature at which the CO_2 liquid and vapour phases homogenise in three-phase inclusions is known as the partial homogenisation temperature, TH_{CO2}. This temperature is density-dependent, and therefore once it is known, the overall density of CO_2 in the fluid (d_{CO2}) can be calculated (see Fig. 6.17 of Shepherd et al., 1985). However, the manner in which the CO_2 phases homogenise also needs to be considered when estimating the density. (Note: the CO_2 will homogenise into either the liquid or vapour state.) In the Omai samples, TH_{CO2} values for twenty readings ranged from 15.3°C to 30.8°C (see Fig. 6.1), with homogenisation consistently occurring into the liquid state. The mean TH_{CO2} value of 25.8°C corresponds to a d_{CO2} value of 0.71 g/cm^3, according to the temperature-density diagram of Shepherd et al., (1985). However, a bias in the data towards the higher TH_{CO2} values may have been induced by relatively high ambient temperatures. For example, on cooling the stage a few degrees below room temperature (21 °C), several two-phase inclusions were seen to develop a third phase. Therefore, many of these three-phase inclusions, which partially homogenised below room temperature, may have gone undetected. Correction of this bias would give rise to a lower mean $TH_{(CO2)}$ value, which, in turn would translate into a higher mean value of d_{CO2}, though it is unlikely that the true mean d_{CO2} value is higher than 0.75 g/cm^3.

Methane (CH_4) content of the CO_2 phase.

Often, CO_2-bearing phases contain variable amounts of methane (CH_4) and to a lesser extent nitrogen (N_2). At room temperature, CO_2- and CO_2-CH_4-(N_2) fluid inclusions are visually similar and can only be distinguished by their contrasting behaviour at sub-zero temperatures. The presence of CH_4 and N_2 have a tendency to depress the melting point of solid CO_2 in much the same way as NaCl lowers the melting point of ice. Therefore, by freezing fluid inclusions containing CO_2-CH_4-(N_2) mixtures and recording the final melting temperature (TM_{CO2}) upon reheating, the mole CO_2:CH_4 ratios can be estimated.

In the Omai samples, three values of TM_{CO2} were obtained. These are -56.4°C, -57.5°C and -59.5°C. Bearing in mind that TM_{CO2} for pure CO_2 is -56.6°C, one can provisionally conclude that CO_2 phase of the fluid contained high proportions of CO_2 relative to CH_4. A numerical value for mole % CH_4 can be obtained graphically from the intersection of the appropriate curves in Fig. 6.19a of Shepherd et al., (1985). By applying a mean TM_{CO2} value of -57.6°C and a mean TH_{CO2} value of 25.8°C, the mean CH_4 composition of the CO_2 phase is interpolated at 5 or 6 mole %.

Salinity of the fluid.

It is generally known that the H_2O phase of hydrothermal fluids generally contain variable amounts of NaCl with lesser amounts of other salts such as KCl and $CaCl_2$. The salinity of a particular fluid, usually expressed in weight % NaCl equivalent, can be estimated by the following method. First of all, suitable fluid inclusions are froze until the H_2O-rich phase of the inclusion turns to ice. The temperature at which the last of the ice melts upon reheating (TM_{ice}) is recorded and then used to gauge the salinity of the fluid (see Fig. 4.10 of Shepherd et al., 1985). However, the final melting temperature of ice is often obscured by the formation of low-temperature gas hydrates, or "clathrates", which decompose in the temperature range -6°C to +12°C. Fortunately, the final melting temperature of clathrates (Tm_{clath}) can be used to estimate the salinity of a fluid in much the same way as TM_{ice} data (see Collins, 1979). In the Omai samples, ten values of TM_{clath} were obtained, ranging from +8.4°C to +10.9°C. These values, when projected unto the clathrate-melting curve (CDC) in Fig. 6.22 of Shepherd et al., (1985), indicate that the Omai hydrothermal fluids were weakly saline with an estimated salinity of 0 to 1.8 wt.% NaCl equivalent.

Bulk density (B_d) of the fluid.

Shepherd et al., (1985) show that the overall bulk density (B_d) of a fluid can be calculated from the following formula:

$$B_d = (V_{CO2} \times d_{CO2}) + (V_{H2O} \times d_{H2O})$$

where V_{CO2} is the volume fraction of CO_2 in the fluid, d_{CO2} is the density of CO_2 in the fluid and d_{H2O} is the density of the H_2O phase of the fluid. For the Omai fluid, V_{CO2} is taken as 0.15, and d_{CO2} as 0.71 g/cm^3 (see above). As the Omai fluid has been shown to be very weakly saline, i.e. less than 1.8 wt.% NaCl equiv., the d_{H2O} value for pure water is used, i.e. 1.0 g/cm^3. Therefore, the bulk density (B_d) of the hydrothermal fluid at Omai is estimated as follows:

$$B_d = (0.15 \times 0.71) + (0.85 \times 1.0)$$

$$B_d = 0.96 \text{ g/cm}^3$$

Mole % of CO_2 in the fluid.

Having established the bulk density of the fluid, the weight % of CO_2 in the fluid can be

calculated as:

$$\text{wt.\% } CO_2 = 100 \times (V_{CO2} \times d_{CO2}) / B_d$$
$$= 100 \times (0.15 \times 0.71) / 0.96$$
$$= 11.1$$

The weight % of H_2O in the fluid is therefore 100 - 11.1 = 88.9. Now that the respective weights % of CO_2 and H_2O are known, the overall mole % of CO_2 in the fluid can be calculated from the following formula:

$$\text{Mole \% } CO_2 = \frac{100 \times (\text{wt.\% } CO_2 / \text{mol. wt. } CO_2)}{(\text{wt.\% } CO_2 / \text{mol. wt. } CO_2) + (\text{wt.\% } H_2O / \text{mol. wt. } H_2O)}$$

When the appropriate values are applied to this formula, the mole % CO_2 of the Omai fluid is estimated at 4.9.

Bulk homogenisation temperature (TH_{tot}) of the fluid inclusions.

The temperature at which two- or three phase fluid inclusions totally homogenise upon heating is referred to as the final or bulk homogenisation temperature, denoted as TH_{tot}. In effect, TH_{tot} is indicative of the minimum formational or trapping temperature of the fluid inclusions, which in turn, constrains a minimum temperature for the parent hydrothermal fluid. However, the true trapping temperature (T_T) of the fluids is notably higher than TH_{tot}. The differential between these two temperatures is known as the "pressure correction" which is a function of the pressure and density of the parent fluid. (For methods of estimating pressure correction see pp 155-160 of Shepherd et al., 1985).

In the Omai samples, a total of twenty-three values of TH_{tot} were recorded. These values indicate that the bulk homogenisation or minimum trapping temperature for the Omai hydrothermal fluids was between 171°C to 307°C with a mean TH_{tot} value of 207°C (see Fig 6.2). Therefore, it is reasonable to assume that the true trapping temperature (T_T) of the Omai fluid was in excess of 200°C. The maximum depositional of temperature of the fluid is tentatively estimated from the presence of telluride minerals at 400°C (see Table 6.1, note 3.).

Summary of fluid characteristics.

According to the preliminary investigations outlined above, the Omai hydrothermal fluid was

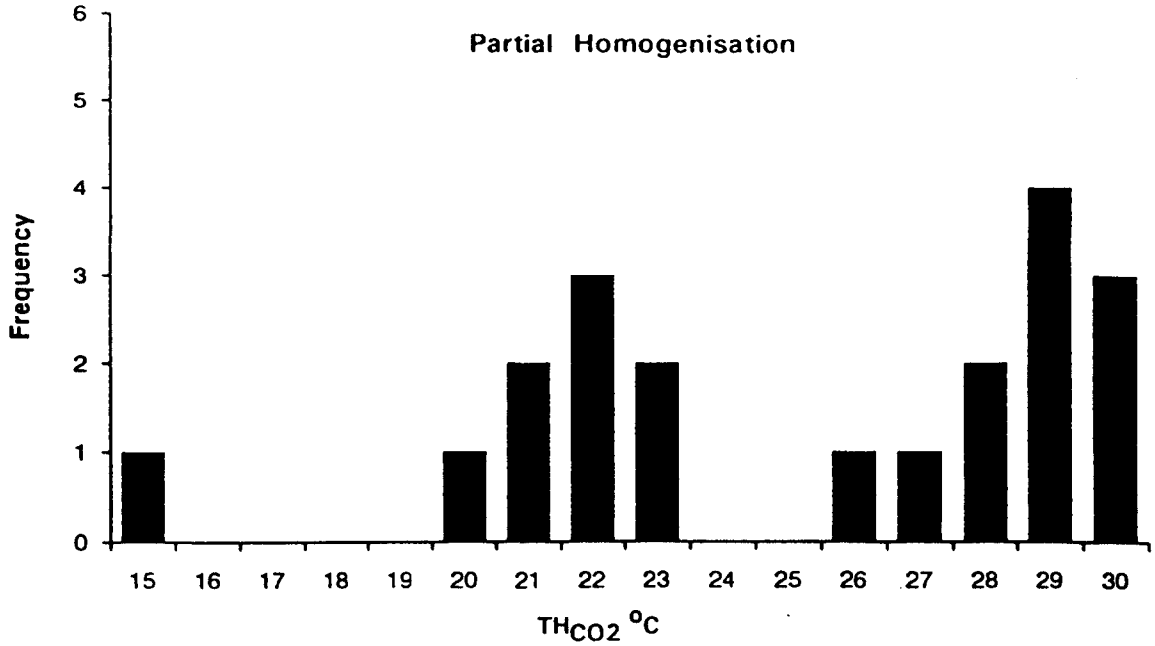

Fig. 6.1: Histogram showing the frequency and range of partial homogenisation temperatures (TH_{CO2}) recorded in veins from the Omai Stock (see text for details).

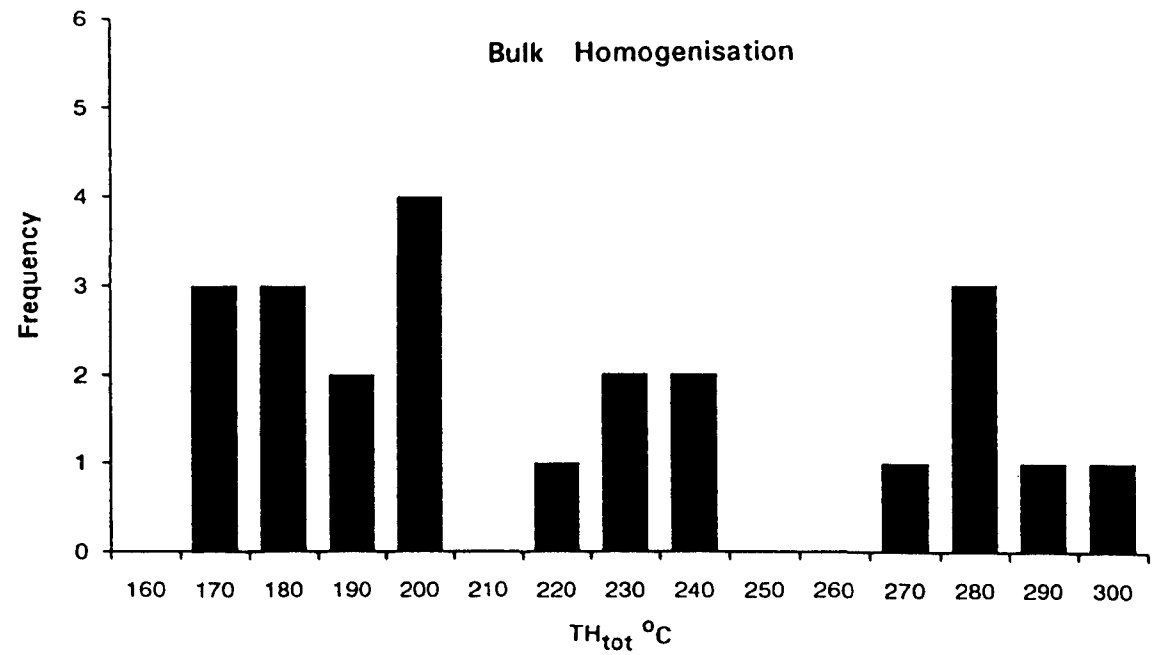

Fig. 6.2: Histogram showing the frequency and range of bulk homogenisation temperatures (TH_{tot}) recorded in veins from the Omai Stock (see text for details). Note three decrepitation temperatures (245, 260 and 307 °C) are also included in these results.

CO_2-bearing (4.9 mole % CO_2) and weakly saline (0 to 1.8 wt. % NaCl equiv.) with a moderate bulk density (B_d) of 0.96 g/cm^3. The fluid was deposited at a minimum (bulk homogenisation) temperature somewhere in the range of 171°C to 307°C with a true trapping temperature (T_T) probably in excess of 200°C. The maximum depositional temperature is estimated from the presence of Au-Ag tellurides at around 400°C.

6.4.4 Comparison with global gold deposits.

At Omai, the geological setting, style of mineralisation, ore association and the dominant sericite-carbonate alteration readily invite comparison with the mesothermal lode gold deposits which characterise the mineralised terrains of global Precambrian shields. This analogy is strengthened by the fact that the Omai fluid properties are similar to those of Archaean-style lode gold deposits (see Table 6.3). Like Omai, the Archaean fluids are also relatively CO_2-rich and weakly saline which contrast with the CO_2-poor and variably saline hydrothermal fluids of epithermal and porphyry-hosted gold deposits of the Mesozoic and Tertiary (see Barley et al., 1989). However, the preliminary nature of the Omai fluid inclusion data again needs to be emphasised and a more comprehensive study is required before detailed comparisons can be made.

Table 6.3: Comparison between the hydrothermal fluid characteristics of Omai and Archaean lode gold deposits.

Parameter	Omai	Archaean
T, °C	200 - 400 ? (171 - 307*)	200 - 450 (generally 250 - 350)
Mole % CO_2	4.9	3 - 25 (generally 10 - 15)
Salinity, wt.% NaCl equiv.	0 - 1.8	< 6 (generally, < 2)
B_d, g/cm^3	0.96	0.8 - 1.0

Notes: Archaean data from Groves and Foster (1991); * indicates range of minimum trapping (bulk homogenisation) temperatures.

6.5 Light stable isotope characteristics (O and C).

In contrast to radiogenic isotopes, in which isotopic variations are the result of the radioactive decay of elements, stable isotope (O, H, C and S) characteristics are based on mass fractionation effects in chemical reactions. In view of the vastly different isotopic signatures between crustal and mantle reservoirs, stable isotopes are widely used in ore deposit studies to "trace" the origin of hydrothermal fluids. In the following preliminary study, light stable isotopic (O and C) considerations are used to provide further insight into the nature and origin of the hydrothermal fluid at Omai.

6.5.1 $\delta^{13}C$ and $\delta^{18}O$ systematics of hydrothermal carbonate.

Table 6.3, has shown that the Omai hydrothermal fluid has P-T-X characteristics similar to mesothermal lode gold deposits of the Archaean. According to Kerrich (1987), the ubiquitous presence of hydrothermal carbonate minerals (dolomite, ankerite, siderite, magnesite and calcite) in these Precambrian deposits, more or less confirms that the parent fluid reservoir, or reservoirs, contained oxidised carbon compounds. Therefore, by measuring the stable isotopic ($\delta^{13}C$, $\delta^{18}O$) compositions of ankerite, the dominant hydrothermal carbonate at Omai, comparisons can be made with similar deposits in other shield areas. Moreover, some provisional conclusions, concerning the ultimate source of the Omai fluid, may also be drawn.

Analytical technique

Approximately two to three grammes of ankerite were extracted from each of five quartz-carbonate veins contained in drill-core specimens collected from the Omai Stock Zone. Three samples (6-0568, 7-1261 and 8-2297) were collected from the heart of the Stock whilst the two remaining samples (2-1565 and 3-1496) were taken from basic meta-volcanic rocks of the Majuba Suite. Following the traditional procedure, first proposed by McCrea (1950), roughly 200 mg of each sample were dissolved in 105% phosphoric acid at a temperature of 90°C over a eight minute period . The $\delta^{13}C$ and $\delta^{18}O$ values for the liberated CO_2 gas were then measured using a VG "prism" mass spectrometer. These values correspond directly to the $\delta^{13}C$ and $\delta^{18}O$ contents of ankerite in each sample, hereafter referred to as $\delta^{13}C_{carb}$ and $\delta^{18}O_{carb}$. Carbon isotopic measurements are calculated with reference to a Pee Dee Belemnite (PDB) standard whilst oxygen isotopic values are calculated relative to Standard Mean Ocean Water (SMOW). Minor adjustments were made to the measured $\delta^{18}O_{carb}$ values to compensate for the specific mass fractionation effects generated by ankerite (see Rosenbaum and Sheppard 1986).

The results obtained from the above experiments are summarised as follows: $\delta^{13}C_{carb}$ range: +1.34 to +3.82‰; $\delta^{18}O_{carb}$ range: +12.22 to +14.48‰. Table 6.4 shows that the Omai $\delta^{18}O_{carb}$ values correlate well with mesothermal lode gold deposits of the Canadian and Australian shields. However, the $\delta^{13}C_{carb}$ data are anomalously positive with respect to global trends. In fact, positive, enriched $\delta^{13}C_{carb}$ values for hydrothermal carbonate are extremely rare in mesothermal lode gold deposits of Precambrian age. However, Wood et al., (1986) propose that $\delta^{13}C_{carb}$ values of up to +7.0‰ could be generated through decarbonation of sea-floor carbonate in greenstone sequences. Elsewhere, Ohmoto and Rye (1979) show that strongly enriched $\delta^{13}C_{carb}$ values of up to +10.0‰ occur late in the paragenetic sequence of Phanerozoic Pb-Zn deposits of the Mississippi Valley type (MVT). At Omai, the most likely explanation for the elevated $\delta^{13}C_{carb}$ values is that the hydrothermal fluid reacted with oxidised carbon-rich country rocks, such as limestone, during its ascent through the crust.

6.5.2 $\delta^{13}C$ and $\delta^{18}O$ systematics of the hydrothermal fluid.

The $\delta^{13}C$ contents of the parent hydrothermal fluid can be determined by analysing the CO_2 phase of fluid inclusions contained in vein-quartz. The $\delta^{18}O$ contents of the fluid, on the other hand, cannot be analysed directly owing to its reaction with quartz, though estimates of this parameter can be made mathematically using the calcite-water fractionation equation.

$\delta^{13}C$ systematics of fluid inclusions ($\delta^{13}C_{fluid}$).

Analytical technique.

Six samples of vein-quartz, five from the Omai Stock Zone and one from the Wenot Lake Zone, were crushed and cleaned with 10% HCl. One-millimetre diameter grains of pure quartz were hand-picked to make up six corresponding sub-samples of a few grammes each. After the method outlined by Mattey et al. (1989), approximately 100 mg of quartz grains from each sample were, in turn, step-heated over a period of six hours to a decrepitation temperature of 1000°C. For each sample, the $\delta^{13}C_{fluid}$ contents of the liberated CO_2 gas was then measured after purification, using a VG "prism" mass spectrometer. In passing, it is of interest to note that the corresponding polished thin section of one sample (5-0315) contains visible scheelite, gold and galena.

Results and interpretation.

The $\delta^{13}C_{fluid}$ results as presented in Table 6.4 reflect a wide spread of values, i.e from -13.24

to +0.56‰. This large variation is most unusual for contemporaneous samples from such a limited geographical area. For example, the range of average $\delta^{13}C_{fluid}$ values for global Archaean lode gold deposits varies from -7.0 to +1.0‰ , though individual mining camps usually cluster in the range -4.0 to -2.0‰ (see Table 6.4 and Groves and Foster, 1991). At Omai, the depleted $\delta^{13}C_{fluid}$ values of around -13.0‰ suggest that a portion of the fluid may have interacted with a reduced carbon source such as graphite. Analytical error in the Omai samples is not suspected as blanks, duplicates and precision checks gave good results (see Appendix III).

Reconciliation of $\delta^{13}C_{carb}$ and $\delta^{13}C_{fluid}$ data.

According to Ohmoto and Rye (1979), the $\delta^{13}C$ values of hydrothermal fluids in the temperature range 200-500°C, under oxidising conditions, neutral pH and in the absence of graphite, should closely approximate the $\delta^{13}C$ value of ferroan dolomite in equilibrium with the fluid. In other words, if these conditions hold at Omai, then the $\delta^{13}C_{carb}$ and $\delta^{13}C_{fluid}$ data should be correlatable, or at least overlapping. However, at Omai, a huge disparity exists between these two parameters (see Table 6.4). The most likely explanation for this disparity is that the fluid (quartz) and the carbonate (ankerite) were not coeval - a hypothesis largely endorsed by the textural evidence, where, on the whole, carbonate deposition post-dates quartz. However, the picture may be further complicated by possible contamination of the fluid by a reduced secondary carbon source, such as graphite (see above).

Table 6.4: Comparison between the O and C isotopic characteristics of Omai and Archaean lode gold deposits.

Parameter	Omai	Archaean
$\delta^{13}C_{carb}$, ‰	+1.34 to +3.82	-10.0 to +2.2 (generally -8.5 to -2.5)
$\delta^{18}O_{carb}$, ‰	+12.22 to +14.48	+9.1 to +15.4*
$\delta^{13}C_{fluid}$, ‰	-13.24 to +0.56	-7.0 to +1.0 (generally -4.0 to -2.0)
$\delta^{18}O_{fluid}$, ‰	+4.95 to +7.01	+2.5 to +10.0 (generally +5.0 to +8.0)

Note: All Archaean data from Groves and Foster (1991), except *, from Kerrich (1989a).

$\delta^{18}O$ contents of the fluid ($\delta^{18}O_{fluid}$) - estimates from the calcite-water system.

As mentioned above, the $\delta^{18}O$ contents of a fluid cannot be analysed owing to interaction with quartz. However, this parameter can be estimated mathematically using the calcite-water fractionation equation of Faure (1986) which reads:

$$\delta^{18}O_{calcite} - \delta^{18}O_{water} = 2.78 \times 10^6 \ T^{-2} - 2.89 \ldots\ldots\ldots\ldots (1)$$

In relation to the Omai situation, this equation may be rewritten as:

$$\delta^{18}O_{carb} - \delta^{18}O_{fluid} = 2.78 \times 10^6 \ T^{-2} - 2.89 \ldots\ldots\ldots\ldots\ldots (2)$$

The above equations are based on the premise that the difference between the $\delta^{18}O$ content a mineral (carbonate) and water (fluid) in equilibrium is fixed, and is related to the equilibrium temperature T (°K) and the mass fractionation factor of the mineral. In the above examples, the mass fractionation factor is -2.89 (calcite), where 2.78×10^6 is a constant.

In order to calculate the $\delta^{18}O$ content of the hydrothermal fluid at Omai, two basic assumptions are necessary. These are:

1. The mass fractionation factor of ankerite, which is unknown, closely approximates the mass fractionation factor of calcite, i.e. -2.89.

2. The equilibrium temperature (T) of the fluid is taken as 250°C (523°K). This value is to a large extent arbitrary, based on the fact that the fluid inclusion data tentatively established a minimum temperature range of 170°C to 300°C , with a mean minimum temperature of 207°C.

In order to constrain a maximum $\delta^{18}O$ content of the fluid, the maximum $\delta^{18}O_{carb}$ is selected from Table 6.4. This value of 14.48‰ corresponds to $\delta^{18}O_{carb}$ in equation 2 above. Leading on from equation 2, the maximum $\delta^{18}O$ content of the Omai fluid, which corresponds to $\delta^{18}O_{fluid}$ in equation 2 is expressed as follows:

$$\delta^{18}O_{fluid} = \delta^{18}O_{carb} + 2.89 - 2.78 \times 10^6 / T^2$$

$$= 14.28 + 2.89 - 2.78 \times 10^6 / 523^2$$

$$= 7.01‰$$

Likewise, the minimum value of $\delta^{18}O_{fluid}$ can be calculated by inserting the minimum $\delta^{18}O_{carb}$ value of 12.22‰ into the above equation. The minimum $\delta^{18}O_{fluid}$ value works out at 4.95‰. To summarise, the $\delta^{18}O_{fluid}$ content of the hydrothermal fluid at Omai is estimated at 4.95 - 7.01‰. This range of values correlates well with global Archaean-style mesothermal deposits (see Table 6.4).

6.5.3 Origin of the Omai hydrothermal fluid.

As already intimated, light stable isotope data may be used to constrain the origin of hydrothermal fluids. However, no general consensus of opinion has been reached regarding the origin of the auriferous mesothermal fluids which characterise the Archaean. Colvine et al., (1988) equate the average $\delta^{13}C_{carb}$ value of -4.0‰ for such fluids with a juvenile mantle CO_2 reservoir ($\delta^{13}C$ = -6 ± 2‰) whilst Burrows et al., (1986) infer that $\delta^{13}C_{carb}$ values close to -3.0‰ reflect a magmatic source. Kerrich (1987, 1989a, 1989b) demonstrates that average $\delta^{13}C_{carb}$ values for Archaean lode gold deposits generally fall outside the range of both mantle and magmatic carbon reservoirs and suggests that the mesothermal fluids were generated by greenschist/amphibolite metamorphic processes. At Omai, the wide spread of $\delta^{13}C$ data precludes any satisfactory assessment regarding the origin of the fluid.

$\delta^{18}O_{fluid}$ values are also often used to discriminate between magmatic and metamorphic fluids. According to Taylor (1979), magmatic fluids have $\delta^{18}O_{fluid}$ values within the tight range of +5.0 to +10.0‰. In contrast, metamorphic fluids define a broad spectrum of $\delta^{18}O_{fluid}$ values ranging from +5.0 to +25.0‰. In the case of Omai, Table 6.4 shows that the $\delta^{18}O_{fluid}$ values range from +4.95 to +7.01‰. These values straddle the overlap between the magmatic and metamorphic fluids and therefore they do not provide a clear-cut indicator regarding the ultimate source of the Omai fluid.

6.5.4 Summary of O and C isotope characteristics.

In terms of oxygen isotopic values ($\delta^{18}O_{carb}$ and $\delta^{18}O_{fluid}$), the Omai hydrothermal fluid shows good compatibility with global Archaean-style mesothermal lode-gold deposits (see Table 6.4). Carbon isotope data ($\delta^{13}C_{carb}$ and $\delta^{13}C_{fluid}$), on the other hand, are less conclusive. The large disparity between $\delta^{13}C_{carb}$ and $\delta^{13}C_{fluid}$ data implies that the respective quartz and carbonate phases of the Omai hydrothermal fluid were not coeval. This hypothesis is supported by the textural evidence. However, the picture may be further complicated by possible contamination from a reduced secondary carbon source such as graphite which may account for depleted $\delta^{13}C_{fluid}$ values of around -13.0‰. $\delta^{18}O_{fluid}$ values of +4.75 to +7.01‰, are consistent with a magmatic or metamorphic origin for the Omai hydrothermal fluid. A more comprehensive study is required to confirm the above trends.

6.6 Gold in the oxidised zone (see also section 2.5.3).

Over the last decade or so, especially in the Australian Shield, much attention has been paid to secondary gold deposits contained in the deeply weathered laterite profiles overlying primary ore bodies (see Webster and Mann, 1984; Wilson, 1984 and Monti, 1987). The majority of these laterite-gold deposits tend to be small though at Boddington, in the Yilgarn Block, over 45 million tonnes of laterite reserves contain an average of 1.8 g/t Au (Butt, 1988). At Omai, the combined laterite (saprolite) and alluvial deposits comprise a sizeable fraction (18%) of the total geological reserves (see Table 1.1). Moreover, these "soft-rock" deposits are economically significant in that they can be mined quickly and cheaply, providing essential up-front capital for the mining operation.

Careful correlation of pit-logs and assay results from the Omai Stock Zone indicate that the colluvial horizon of the laterite profile is relatively enriched in gold. The dominant concentration mechanisms cannot be pin-pointed, but by analogy with other deposits, mechanical transportation and gravity settling are likely to be the main contributing factors. Lower down the laterite profile, high gold values tend to be spatially related to relict quartz-carbonate veins. However, the bulk of laterite-gold at Omai is contained in the Wenot Lake Zone where Bertoni et al., (1991) have identified a 30m-thick, enriched seam spanning the duricrust and mottled zone in the laterite profile. Gold mineralisation in this body is not strictly associated with relict quartz veining and appears to be the product of supergene enrichment.

At Omai, there is also some biogeochemical evidence indicating chemical solution and re-deposition of gold in the surficial environment. For example, Lungwitz (1908) demonstrated that wood ash from Iron Mary and Baromalli trees assayed at 3.0 g/t Au and 300 ppb Au respectively (cited in Inasi and Gibbs, 1982). More recently, just across the Amazon basin, in the Carajas region of the northern Brazilian Shield, Andrade et al., (1991) recorded levels of 65-400 ppb Au in vegetation growing on the Bahia Cu-Au deposit. These findings suggest that vegetation may serve as a useful sample medium for gold exploration in tropically weathered terrains.

CHAPTER 7

ASPECTS OF REGIONAL MINERALISATION

7.1 Aims of chapter.

The main aim of this chapter is to examine the geological and structural setting of the Omai goldfield in the context of regional mineralisation in northern Guyana and also with respect to lode gold deposits in other Precambrian shields. Some recommendations are made that may assist in the planning of future regional gold exploration programmes in northern Guyana.

7.2 Geological and structural characteristics of the Guyana gold deposits.

The majority of gold occurrences in Guyana show a compelling spatial correlation with the Palaeoproterozoic granite-greenstone terrain of the northern geological province (see Fig 7.1). According to Barnard (1990), approximately 84 tonnes of gold have been won from this terrain in the period 1885-1990. In most cases, the source of the gold can be traced, via eluvial and alluvial placer deposits to primary quartz lodes hosted in the fractured contact zones between granitoid batholiths and greenstone country rocks (Macdonald, 1968; Barron, 1970). However, the three largest of Guyana's historic gold mines (Omai, Aurora and Peters' Mine) are hosted within small, altered, granitic stocks. In west-central Guyana, significant amounts of gold (and diamonds) have been shed from the Mesoproterozoic continental sediments of the Roraima Group into the adjacent drainage systems, though its very possible this gold too was originally contained in the granite-greenstone basement. In southern Guyana, gold deposits are minor and sporadic, though this part of the country is relatively remote and unexplored. Here, the most significant gold deposit is the Marudi Mountain camp, which is apparently analogous with BIF-type (banded ironstone formation) deposits.

In northern Guyana, localised shearing, competent host rocks and to a lesser extent carbonatisation, appear to be the common denominators of the lode gold deposits. Shearing is normally evidenced by closely spaced arrays of quartz veins and/or a mappable sheared fabric in the host rocks. On a regional scale, Gibbs (1980) has recorded the predominance of major sub-parallel shear zones which trend intermittently in a southeast direction. The most significant of these is the Makapa-Kuribrong shear zone, first described by Barron (1969).

Fig. 7.1: (cont'd) Key to the main granite-greenstone hosted lode gold deposits in Guyana.

1. Tassawini*
2. Five Star
3. Aurora
4. Akaiwong
5. Aremu
6. Groete Creek (sedex Au-Cu)
7. Peters' Mine
8. Tamakay
9. Tikwah
10. Issano**
11. Honey Camp
12. Kaburi
13. Omai* (including Quartz Hill)
14. Winters' Mine (Appaparu)
15. Pott Falls
16. Mahdia-Eagle Mountain (also includes the proto-Mahdia fossil placer deposit**)
17. Marudi Mountain (BIF-greenstone association ?)

Notes:

a) Most of the above deposits have been worked in the past. * denotes historic mines that are soon to go into commercial production, e.g. Omai; ** indicates deposits where gold is presently being mined on a relatively large scale.

b) The majority of primary gold deposits have spatially associated eluvial (laterite-saprolite) and alluvial placer deposits.

c) The Takutu break is a Mesozoic graben structure and is not associated in any way with gold mineralisation. However, diamond drilling operations have intersected pockets of crude oil in fractured basalts on the floor of the graben.

This structure can be traced for over 200 km, cutting both the Cuyuni and Mazaruni greenstone belts. Gibbs (1980) suggests that such structures may reflect lithological competency contrasts along regional fold axes in the Barama-Mazaruni Supergroup, though he makes no definite connection with the distribution of gold camps.

According to Walrond (1985), the overall distribution is of gold occurrences in northern Guyana is controlled by structural breaks. This hypothesis appears to hold for the Mazaruni greenstone belt where a cluster of gold camps appear to lie along a well-defined, bifurcating, linear southeast trend (see Fig. 7.2). The major part of this trend is broadly co-incident with the Makapa-Kuribrong shear zone mentioned above, and neatly incorporates the Tamakay, Tikwah, Mahdia-Eagle Mountain, Konawaruk and Pott Falls gold camps. It is here proposed that an ESE-trending arm of the main shear zone also exists, sweeping through the Issano, Honey Camp, Kaburi, Quartz Hill, Omai and Winters' Mine (Appaparu) goldfields (see Fig. 7.2). However, in addition to the localised ESE-trending shear zones documented at Omai, and at nearby Quartz Hill, more firm field evidence is required to confirm the existence of such a shear zone (hereafter known as the Issano-Appaparu shear zone). The way that gold camps in the greater Omai area show a distinct ESE alignment was first recognised by Bracewell (1943).

Elsewhere in the Guiana Shield, the fragments of evidence available to date also suggest that auriferous lode deposits are spatially related to regional-scale linear structures. For example, in neighbouring Surinam, Brinck (1955) perceived that gold deposits could be divided into two linear zones - an E-W trending belt running northwest of Lake van Blommenstein and a second belt running from the lake in a southeasterly direction. In French Guiana, relatively recent investigations by Lassere et al., (1988) have shown that gold camps are clearly cospatial with ESE-trending sub-parallel linear belts (shear zones ?) which can be traced along strike for over 100 km, extending across the border into Surinam. On a greater regional scale, Ledru and Milesi (1991) note that gold-bearing shear zones in French Guiana have a geological and metallogenetic association with similar features in the Palaeoproterozoic terrain of Ghana, west Africa. In the northern Brazilian Shield, Oliveira and Leonardos (1990) report the occurrence of auriferous deposits along the length of the E-W to ENE-trending Diadema shear belt which cuts across the granite-greenstone basement. In the Tapajos region, 500 km to the west, extensive gold deposits aligned along a regional-scale lineament are currently being investigated (X. João, pers. comm, 1992).

In summary, on the basis of limited field evidence and the alignment of numerous gold camps, it is proposed that the Omai goldfield lies along a ESE-trending regional lineament, here known as the Issano-Appaparu shear zone. This structure is a subsidiary arm of the main Makapa-Kuribrong shear zone. In the Guiana Shield at large, preliminary observations

indicate that regional gold mineralisation is also related to major EW to SE-trending structures, though more data are required to verify this hypothesis.

7.3 The Omai goldfield and Archaean-style lode gold deposits.

In terms of regional geological setting, structural control, ore association, wall-rock alteration and physicochemistry of hydrothermal fluid, the Omai goldfield is readily comparable to the Archaean mesothermal lode gold deposits which dominate the Canadian and Australian shields, among others (see Groves and Foster, 1991 for a review of this type of gold deposit). This statement may also ring true for all the Palaeoproterozoic lode gold deposits in the Guiana Shield.

One of the key characteristics of Archaean lode gold deposits is a consistent spatial relationship with steeply-dipping, crustal-scale shear zones, or breaks, of brittle to ductile deformation (see Eisenlohr et al., 1989). In addition to permitting the diapiric emplacement of alkaline to trondhjemitic magmas - the eventual hosts of mineralisation, these shear zones also act as conduits for the advection of auriferous, CO_2-rich fluid from deep sources (Colvine et al., 1988). The possibility, that primary lode gold deposits in northern Guyana and beyond are related to major shear zones has yet to be fully explored, though the local and regional field evidence presented in section 7.2 above gives good indications that such a relationship exists.

At this juncture, it must be noted that mesothermal lode gold deposits are not entirely restricted to the Archaean (or Proterozoic), but also occur in Phanerozoic terrains, albeit on a much more diminished degree. These Phanerozoic mesothermal deposits are commonly located in tectonically active continental margins such as the North American Cordillera (see Nesbitt, 1991 for a review). In the Guiana Shield at large, the lode gold deposits are, without exception, hosted in Palaeoproterozoic granite-greenstone rocks. Moreover, it is widely accepted that regional mineralisation is a late by-product of the Trans-Amazonian orogeny which consolidated the Guiana Shield between 2.25 and 1.95 Ga. This hypothesis is in accord with the model invoked by Colvine et al., (1988) who propose that gold metallogeny in the Superior Province of Canada was generated during cratonisation. However, unlike the Canadian Shield, significant volcanogenic massive sulphide (VMS) deposits have yet to be discovered in the Guiana Shield.

7.3.1 Possible genetic models.

No consensus of opinion has so far been reached regarding the formation of Archaean-style lode gold deposits and consequently at least four genetic models are in vogue. These are

briefly reviewed below and include, magmatic, metamorphic, mantle degassing-granulitisation and lamprophyric models.

1. **Magmatic model** (e.g. Burrows et al., 1986), - auriferous hydrothermal fluids have a magmatic origin and are derived from granitoid or porphyry intrusions with which they are spatially associated.

2. **Metamorphic model** (e.g. Groves et al, 1987) - metamorphic fluids circulating at depth extract gold from the overlying greenstone sequences. Effective focusing of these fluid ensures that the concentrations of precipitated gold are greatly enriched.

3. **Mantle degassing-granulitisation model** (e.g. Colvine et al., 1988) - mantle-derived Au-CO_2-LILE-rich fluids in association with granulitisation of the lower crust during cratonisation are the fundamental components of the ore-forming process.

4. **Lamprophyric model** (e.g. Rock and Groves, 1988) - a cross between magmatic and metamorphic models in which lamprophyric magmas act as transporting agents for the gold from mantle sources. These magmas then undergo extensive crustal interactions, generating felsic magmas or releasing their gold into metamorphic-hydrothermal systems.

The Omai goldfield contains elements of all four of the above models and therefore no unambiguous statement can be made regarding the genetic origin of the gold. For example, $\delta^{18}O_{fluid}$ values at Omai are consistent with both magmatic and metamorphic fluids. Regional gold mineralisation in the Guiana Shield has been correlated with cratonisation processes during the Trans-Amazonian orogeny (mantle degassing-granulitisation model ?). Finally,the cospatial relationship between gold and felsic and lamprophryic intrusions at Omai is, in part, consistent with the lamprophyric model of Rock and Groves (1988).

7.4 Suggestions for future regional exploration in Guyana.

Over the last decade or so, much emphasis has been placed on the location and development of known historic gold workings, and as a result, conventional geological mapping programmes have received little attention. This is understandable, given Guyana's economic problems coupled with the fact the that dense tropical rainforest which blankets the mineralised terrain does not permit easy or economic mobility on the ground. However, a comprehensive geological data base is fundamental to any mineral exploration programme, and sooner or later, detailed geological surveys will need to be resumed. On the bright side, most of the country has been mapped on a scale of 1:200,000 and excellent geological and mineral maps have been compiled by Walrond (1987a, 1987b respectively) at a scale of 1:1

million.

It is apparent from the discussion in sections 7.2 and 7.3 above that the lode gold deposits of northern Guyana, at least in the Mazaruni greenstone belt, tend to lie along regional scale-shear zones or lineaments in much the same way as the Archaean lode gold deposits do in the more celebrated Precambrian shields. It is therefore proposed that more emphasis be placed on identifying and defining such structures in Guyana and the Guiana Shield at large. This may be achieved by a fresh analysis of the aeromagnetic data available and by detailed geological mapping on the ground. The spatial relationship between gold and minor felsic and/or lamprophyric intrusions which is well-documented in analogous terrains (see Cherry, 1983; Perring, 1988) provides another pointer for future exploration. Certainly, known granitoid-lamprophyre complexes, such as the one exposed at Temple Bar Falls on the Konawaruk River, warrant further investigation.

A simple and rapid field method for identifying potential auriferous quartz lodes using a fluid-inclusion crushing-stage has been developed by Diamond and Marshall (1990). The underpinning principle of this technique is based on the fact that fluid inclusions in mesothermal gold-quartz deposits are relatively CO_2-rich. When the compressed CO_2 gas within the fluid inclusion is liberated by crushing the quartz under a mineral oil, such as glycerine, vapour bubbles are can be readily observed in the oil under low-power magnification, as they expand against atmospheric pressure. This technique could be adopted as a useful exploration tool in northern Guyana.

CHAPTER 8

SUMMARY AND CONCLUSIONS

8.1 Introduction.

The Omai goldfield is essentially a mesothermal lode gold deposit, with associated saprolite and alluvial deposits, hosted within the Palaeoproterozoic granite-greenstone terrain of northern Guyana. Total mining reserves are estimated at 44.8 million tonnes, grading at 1.43 g/t Au (Mining Magazine, Sept., 1991). The goldfield is located in dense tropical rainforest close to the west bank of the mighty Essequibo River at the eastern extremity of the Mazaruni greenstone belt, some 230 km south-southwest of Georgetown.

8.2 Regional mineralisaton.

The alignment of gold camps in the Mazaruni belt, combined with local structural evidence, suggests that regional mineralisation is spatially related to an ESE-trending lineament, here known as the Issano-Appaparu shear zone. This structure stems from the Makapa-Kuribrong shear zone which runs for some 200 km in a southeasterly directly, along the length of the Mazaruni belt (see Fig. 7.2).

8.3 Primary mineralisation in the Omai goldfield.

Primary lode gold mineralisation at Omai is concentrated in two discrete ore zones, separated on the ground by a distance of 800 m. These are the Omai Stock Zone and the Wenot Lake Zone. The bulk of mineralisation is centred on the Omai Stock Zone, especially in the Omai Stock - a small, altered granitoid boss where wall-rock alteration is dominated by a sericite-carbonate-(pyrite) assemblage. The primary ore package, which consists of Au-W-Te-S mineralisation, is contained in a series of narrow (5-50mm) quartz-carbonate (ankerite) veins. Visible gold is commonly associated with galena and microscopic tellurides. Scheelite occurs in sub-economic, sporadic concentrations. SEM-EDS micro-analyses have positively identified at least five, possibly six, telluride minerals. These are: calaverite, petzite, hessite, wehrlite, tellurobismuthite and volynskite (?). Provisional fluid inclusion studies have indicated that the parent hydrothermal fluid was H_2O-CO_2 -bearing ($\approx$5.0 mol % CO_2), weakly saline (0 to 1.8 wt.% NaCl equiv.) with a moderate bulk density of 0.96 g/cm^3. The depositional temperature

of the fluid was probably in the region of 200-400°C. These values readily correspond to those of Archaean mesothermal lode gold deposits which are prevalent in the Canadian and Australian shields. Preliminary oxygen and carbon isotope analyses also demonstrate that the Omai fluid is conformable to Archaean lode gold deposits. $\delta^{18}O_{fluid}$ values of +4.95 to +7.01‰ obtained for the Omai fluid are consistent with a magmatic and/or metamorphic source. Primary mineralisation in the Wenot Lake Zone has yet to be fully investigated, though a provisional examination by Bertoni et al. (1990) reveals that both the mineral and alteration paragenesis compare favourably with the Omai Stock Zone.

The structural permeability of the primary ore bodies (Wenot Lake Zone included) is attributed to the highly competent nature acid host rocks which responded to regional stresses by brittle failure, thus opening up depositional sites for the focusing and advection of the hydrothermal fluids. No precise or absolute age is available for the mineralisation, though it is widely accepted that regional gold mineralisation in the Guiana Shield was introduced during the Trans-Amazonian orogeny (ca 2.25-1.95 Ga).

8.4 The geology and geochemistry of the Omai Stock Zone.

As already mentioned, the Omai Stock is the main mineralised component in the Omai Stock Zone. However, the adjacent greenstone country rocks of the Majuba Suite and some minor igneous intrusions in and around the Stock are also partially mineralised.

The combined effects of albitisation (Na-autometasomatism), propylitisation (regional metamorphism) and intensive sericitisation-carbonatisation (hydrothermal alteration) have obscured the primary mineral and chemical components of the Omai Stock. Nevertheless, systematic petrographic analysis of 17 representative thin sections by the point-counting method shows that the Stock is fairly homogenous in composition, with the majority of samples forming a tight cluster of data straddling the quartz diorite and tonalite fields on a standard QAP plot. This homogeneity is also reflected by the chemical data.

The Omai Stock, plus the regional Tigri, Mariaba and Mowasi plutons, are collectively known as the Omai granitoids. These rocks have a chemistry which is largely characteristic of the metaluminous to weakly peraluminous, I-type, calc-alkaline, volcanic arc granitoid rocks of Phanerozoic orogenic belts. The Omai granitoids are broadly coeval and form part of the extensive P1-type Trans-Amazonian granitoid complexes of northern Guyana and beyond. The REE geochemistry of the Omai Stock and the Tigri pluton are strongly comparable, intimating that both bodies are genetically related and probably form part of the same granitoid complex. The Mariaba pluton, on the other hand, is distinguished by its steeply fractionated, HREE-depleted REE patterns (La_n/Yb_n = 15.6 to 66.5) which also characterise

granitoid rocks from Archaean TTG (tonalite-trondhjemite-granodiorite) terrains. Such trends in the Mariaba pluton are interpreted to reflect partial melting from an amphibole- and/or garnet-rich protolith.

The Majuba Suite, which shows excellent lithogical and chemical similarities to the type greenstone locality of the Barama-Mazaruni Supergroup at Issineru, is dominated by primitive, low-K, high-Fe tholeiitic basalts and minor basic intrusives (HFTs). These rocks are characterised by flat to slightly fractionated REE patterns of about 10 times chondrite. A sub-ordinate calc-alkaline series (CAS), mostly of andesitic composition, is interbedded with the HFTs within the volcanic pile. The CAS andesites are characterised by moderately inclined REE profiles with La_n/Yb_n ratios in the order of 4.6 to 6.5. Sharply positive Ce anomalies were obtained from both HFT and CAS rocks. This phenomenon is thought to reflect the mobility of LREE under hydrous conditions during regional metamorphism, though analytical uncertainty may also be a contributing factor. In terms of trace element geochemistry, the Majuba Suite rocks correlate well with volcanic rocks from contemporary island arc settings.

Several petrographically distinctive lamprophyric (appinite) pipes are located around the periphery of the Omai Stock. The stratigraphic relationship between the appinites and the Omai Stock is uncertain, though it is assumed that they are roughly coeval. The appinites have a distinct trace element chemical signature epitomised by moderately fractionated REE patterns with a diagnostic humped LREE profile. This trend suggests that the REE were extracted from the melt by the crystallisation of sphene. Although the appinites are only weakly mineralised, they may have some significance regarding the genetic origin of the gold (see Rock and Groves, 1988; Wyman and Kerrich, 1988). Moreover, the fact that the gold-lamprophyre-felsic intrusion association is well-documented in analogous Precambrian terrains should provide an impetus for future exploration programmes in northern Guyana.

Towards the end of the Trans-Amazonian orogeny, a series of ultrabasic to intermediate, arc-related alkaline dykes intruded the Omai Stock and adjacent greenstone rocks along shallow-dipping, subhorizontal fracture or shear zones. The ESE- to SE-trending Captain Mann Sill, which is exposed about 1 km north of the main ore zone, is also included in this suite of rocks. On a regional-scale the Gilt Creek Suite is stratigraphically and chemically comparable to the two-pyroxene andesites recorded at Issineru. In the Omai Stock Zone, many of the Gilt Creek dykes have suffered severe hydrothermal alteration, though they are only weakly mineralised, notably at the margins. Chemically, the Gilt Creek dykes are typified by Mg-enrichment, low K and Ti values and elevated Sr, Ba, Th, P, LREE, Ni and Cr abundances. The least evolved samples, with MgO values of 21 to 25 wt% and Mg-numbers of around 80, may represent primary mantle melts. The dykes are further characterised by steeply

fractionated REE patterns which systematically increase in total REE abundances with increasing SiO_2 contents. La_n/Yb_n ratios vary from 7.84 to 32.6 with maximum total REE contents of 419 ppm. Mineral vector diagrams and REE modelling clearly demonstrate that clinopyroxene was the primary controlling phase behind the magmatic evolution of the Suite.

A gently-dipping, unmetamorphosed, non-mineralised gabbroic sheet, known as the GSR dyke, cuts the Omai Stock Zone at a depth of around 300 m. This dyke has a marked Fe-tholeiitic character and in terms of petrography and chemical composition correlates well with the two regional gabbroic dykes (Point dyke and Ya-ya dyke) which intersect in an X-shaped fashion 3.2 km to the southeast. The gabbroic dykes in the Omai area clearly post-date the Trans-Amazonian orogeny and are therefore known as post-orogenic mafic dykes (POMDs). The regular, linear morphology of the Omai POMDs imply that they are members of the regional-scale Apatoe Suite which consists of swarms of Mesozoic basic dykes. These dyke swarms are related to an extensional tectonic regime associated with the opening of the Atlantic Ocean. This hypothesis is supported by the geochemical characteristics of the Omai POMDs. For example, several tectonic discrimination diagrams indicate that the POMDs were emplaced in a continental rift-related setting. Moreover, mantle-normalised spidergrams show that the POMDs have strongly comparable geochemical signatures to global mafic dykes from known continental flood basalt (CFB) tectonic settings.

8.5 The geology and geochemistry of the Wenot Lake Zone.

The Wenot Lake Zone is essentially bimodal and consists of a narrow (200m) tract of mafic meta-volcanic rocks, intercalated with thin bands of felsic meta-volcanic rocks, here known as high-silica rhyolites (HSRs). The field evidence to the north indicates that the Wenot Lake volcanic rocks are contiguous with the Majuba Suite greenstones of the Omai Stock Zone. However, at its southern margin, the Wenot Lake Zone rocks show sheared contacts with a sub-parallel belt of phyllitic tuffs. Mineralisation is contained in narrow quartz-carbonate veins and veinlets which are almost exclusively hosted by the HSRs. As their name implies, the HSRs are characterised by elevated (>75%) SiO_2 contents. The rocks are also enriched in Na_2O, Nb, Zr, Hf and REE. At the other extreme, MgO, TiO_2, CaO, K_2O and P_2O_6 occur in trace amounts along with anomalously low concentrations of Rb, Sr, and Ba. The HSRs are further characterised by wing-shaped REE patterns with deep negative Eu anomalies. The petrogenesis of the HSRs is unclear. One theory is that they were generated by partial fusion and magma mixing brought about by the ponding of mafic magma at the base of the lower crust.

8.6 The oxidised zone.

At Omai, both the primary ore zones are overlain by a deeply weathered mantle of saprolitic material which attains a maximum thickness of 50 m. This oxidised zone, which includes minor alluvial placer deposits, is a unique, self-contained gold depositional environment.

8.7 Recommendations for further research.

It is clear from the above discussions that the geology and geochemistry of the host rocks to mineralisation at Omai have been fairly well constrained. However, some more analyses of the HSR rocks of the Wenot Lake Zone are required as only two samples were analysed. The mafic meta-volcanic rocks of the Wenot Lake Zone have yet to be examined though it is reasoned that they are petrologically and chemically similar to the Majuba Suite greenstones of the Omai Stock Zone.

Preliminary SEM-EDS micro-analyses, fluid inclusion studies and light stable isotope analyses have paved the way for a comprehensive investigation of primary mineralisation. Such a study may strive to attain a better understanding of the metallic ore paragenesis and the physicochemical properties of the hydrothermal fluid. Transport mechanisms of gold in the hydrothermal fluid have yet to be established. Also, much scope remains for a comparative study of mineralisation in the Omai Stock Zone and the Wenot Lake Zone.

The advent of mining operations in 1993 may preclude any further research into the nature and distribution of gold in the oxidised zone. However, the wealth of drill-core data available could be used to constrain the structural architecture of the primary ore bodies. Finally, there is much need for detailed geological mapping programmes so that the local and regional structural controls of mineralisation can be better understood.

BIBLIOGRAPHY

AFIFI, A.M., KELLY, W.C. & ESSENE, E.J., 1988a. Phase relations among tellurides sulphides and oxides: Part I: Thermochemical data and calculated equilibria. Econ. Geol., 83: 377-384.

AFIFI, A.M., KELLY, W.C. & ESSENE, E.J., 1988b. Phase relations among tellurides, sulphides and oxides: Part II: Application to telluride-bearing ore deposits. Econ. Geol., 83: 385-404.

AHMAD, T. & TARNEY, J., 1991. Geochemistry and petrogenesis of Garwhal volcanics: implications for evolution of north Indian lithosphere. Precambrian Res., 50: 69-88.

ALLEN P.M., 1963. A preliminary report on the classification of the Younger Granite Group of British Guiana and a description of some of the complexes. Geol. Surv. Br. Guiana, Report PMB 3/63.

AMBROSI, J.P. & NAHON D., 1986. Petrological and geochemical differentiation of lateritic iron crust profiles. Chem. Geol., 57: 371-393.

ANDRADE, W.O., MACKESKY, M.L., & ROSE, A.W., 1991. Gold distribution and mobility in the surficial environment, Carajas region, Brazil. J. Geochem. Explor., 40: 95-114.

ARNDT, N.T. & NISBET, E.G., 1982. What is a komatiite ? In: ARNDT, N.T. & NISBET, E.G., (eds.), Komatiites. George Allen & Unwin, London, pp 19-27.

ASLIN, G.E.M., 1976. The determination of arsenic and antimony in geological materials by flameless atomic absorption spectrometry. J. Geochem. Explor., 6: 321-330.

BAILEY, J.G., 1981. Chemical criteria for a refined tectonic discrimination of andesites. Chem. Geol., 32: 139-154.

BARKER, F., 1979. Trondhjemite: definition, environment and hypotheses of origin. In: BARKER, F. (ed.), Trondhjemites, dacites and related rocks. Elsevier, pp 1-12.

BARLEY, M.E., EISENLOHR, B.E., GROVES, D.I., PERRING, C.S. & VEARNCOMBE, J.R., 1989. Late convergent margin tectonics and gold mineralization: A new look at the Norseman-Wiluna Belt, Western Australia. Geology, 17: 826-829.

BARNARD, F., 1990. Gold in Proterozoic greenstones, Guyana, South America. Presented at GOLD '90 session, SME, Salt Lake City, USA, February, 1990.

BARNARD, F., 1991. Guyana: Mining evaluation profile (10/91). Available from the author at 1835 Alkire St., Golden, Colorado, 80401, USA, 3 pp.

BARRON, C.N., 1969. Notes on the stratigraphy of Guyana. Proc. 7th Geol. Conf., Paramaribo, Surinam, 1966. Rec. Geol. Surv. Guyana, 6: 1-28.

BARRON, C.N., 1970. A further guide to mineral exploration in Guyana (supplement to Bulletin 38). In: Proc. 8th Guiana. Geol. Conf., Georgetown, Guyana, 1969, Paper XVII.

BARRON, C. N., 1986. The 1986 Geological Map of Guyana (text only). Unpub. report, CNB: 6/86, G.G.M.C., Georgetown, Guyana, 7 pp.

BERRANGÉ, J.P., 1977. The geology of southern Guyana, South America. Institute of Geological Sciences, London, Overseas Division Memoir 4: 112 pp and map.

BERRANGÉ, J.P. & DEARNLEY, R., 1975. The Apoteri volcanic formation - tholeiitic flows in the north savannas graben of Guyana and Brazil. Geol. Rundsch., 64: 883-889.

BERTONI, C.H., SHAW, R.P., SINGH, R., BELZILE, E., MINAMOTO, J., RICHARDS, J.M. and NORGAN, R., 1990. Report on the geology and gold mineralisation of the Omai Property, Guyana. Internal report, Golden Star Resources Ltd - Cambior Inc, 66 pp.

BERTONI, C.H., SHAW, R.P., SINGH, R., MINAMOTO, J. & RICHARDS, J.M., 1991. Geology and gold mineralization of the Omai property, Guyana. In: LADEIRA, E.A., (ed.), Brazil Gold '91, Balkema, Rotterdam, pp 767-771.

BLACK. R., 1980. Precambrian of West Africa. Episodes, 4: 3-8.

BOX, S.E. & FLOWER, M.F.J., 1989. Introduction to special section on alkaline arc magmatism. J. Geophys. Res., 94: 4467-4468.

BRACEWELL, S., 1943. Report on an occurrence of scheelite at Omai Mine, British Guiana. Unpub. report, Geol. Surv. of British Guiana, 9 pp.

BREWER, T.S. & ATKIN B.P., 1989. Element mobilities produced by low-grade metamorphic events. A case study from the Proterozoic supracrustals of southern Norway. Precambrian Res., 45: 143-158.

BRINCK, T.W., 1955. Gold deposits in Suriname. Ph.D. thesis (in Dutch with English summary), Liedse Geol. Meded. 21; 246 pp.

BROWN, G.C., THORPE, R.S. & WEBB, P.C., 1984. The geochemical characteristics of granitoids in contrasting arcs and comments on magma sources. J. Geol. Soc. London, 141: 413-426.

BURROWS, D.R., WOOD, P.C., SPOONER, E.T.C., 1986. Carbon isotope evidence for a magmatic origin for Archean gold-quartz vein deposits. Nature, 321: 851-854.

BUTT, C.R.M., 1988. Genesis of lateritic and supergene gold deposits in the Yilgarn Block, Western Australia. In: Proc. of Gold '88 Symposium, Melbourne, pp. 359-364.

BUTT, C.R.M. & ZEEGERS, H., 1989. Classification of geochemical exploration models for tropically weathered terrains. J. Geochem. Explor., 32: 65-74.

B.V.S.P. (BASALTIC VOLCANISM STUDY PROJECT), 1981. Basaltic Volcanism on Terrestrial Planets. Pergammon Press, New York, 1286 pp.

CAEN-VACHETTE, M., 1988. Le craton ouest-africain et le bouclier guyanais: un seul craton au Proterozoic inferieur. J. African Earth Sci., 7, (2): 479-488.

CANNON, R.T., 1963. A preliminary report on the geology of the area between Akenna Falls and Waraputa Falls, Essequibo River. Unpub. report RTC 1/63, Geol. Surv. of British Guiana, 15 pp.

CASSIDY, K.F., BARLEY, M.E., GROVES. D.I., PERRING, C.S. & HALLBERG, J.A., 1991. An overview of the nature, distribution and inferred tectonic setting of granitoids in the late-Archaean Norseman-Wiluna Belt. Precambrian Res., 51: 51-83.

CHAPPELL, B.W. & WHITE, A.J.R., 1974. Two contrasting granite types. Pacific Geology, 8: 172-174.

CHERRY, M.E., 1983. Association of gold and felsic intrusions - examples from the Abitibi

belt. In Colvine, A.C., (ed)., The Geology of Gold in Ontario. Ontario Geological Survey, Miscellaneous Paper 110, pp 48-55.

CHOUDHURI, A., IYER, S.S. & VASCONCELLOS, M.B.A., 1984. U, Th and rare earth elements in tholeiite dykes from the northern Guiana Shield. Anais II Symposium Amazonico, Manaus, Brazil, pp. 171-177.

CHOUDHURI, A. & MILNER, M.W., 1971. Basic magmatism in Guiana and continental drift. Nature Phys. Sci., 232: 154-155.

CHOUDHURI, A., OLIVEIRA, E.P. & SIAL, A.N., 1991. Mesozoic dyke swarms in northern Guiana and northern Brazil and the Cape Verde Fernando de Noronha plume vortices: a synthesis. In: TEIXEIRA, W., ERNESTO, M. & OLIVEIRA, E.P., International Symposium on Mafic Dykes: Extended Abstracts, Sao Paulo, Brazil, pp 17-22.

CLAOUE-LONG, J.C., KING, R.W. & KERRICH, R., 1990. Archaean hydrothermal zircon in the Abitibi greenstone belt: constraints on the timing of gold mineralisation. Earth Planet. Sci. Lett., 98: 109-128.

COLLEY, H. & WALSH, J.N., 1987. Genesis of Fe-Mn deposits of southwest Viti Levu, Fiji. Trans. Instn. Min. Metall. (Sect B: Appl. ear. sci.), 96: B201-212.

COLLINGS, S.P., 1969. The geology and geochemistry of the Omai Mine area, Omai SW, Guyana. Unpub. MSc thesis, Colorado School of Mines, Golden, Colorado, USA, 224 pp.

COLLINS, P.L.F., 1979. Gas hydrates in CO_2-bearing fluid inclusions and the use of freezing data for estimation of salinity. Econ. Geol., 74: 1435-1444.

COLVINE, A.C., FYON, J.A., HEATHER, K.B., MARMONT, S., SMITH, P.M. & TROOP, D.G., 1988. Archean lode gold deposits in Ontario. Ontario Geol. Surv. Misc. Paper 139, 136 pp.

CONDIE, K.C., 1989. Geochemical changes in basalts and andesites across the Archean-Proterozoic boundary: Identification and significance. In: GORBATSCHEV, R., (ed.), Proterozoic Geochemistry. Lithos, 13: 1-18.

COREY M.C. & CHATTERJEE A.K., 1990. Characteristics of REE and other trace elements in response to successive and superimposed metasomatism within a portion of the South Mountain Batholith, Nova Scotia, Canada. Chem. Geol., 85: 265-285.

DAVY, R. & EL-ANSARY, M., 1986. Geochemical patterns in the laterite profile at the Boddington gold deposit, Western Australia. J. Geochem. Explor., 26: 119-144.

DESPRAIRIES, A. & BONNOT-COURTOIS, C., 1980. Relation entre la composition des smectites d'alteration sous-marine et leur cortege de terres rares. Earth Planet. Sci. Lett., 48: 124-130.

DE VLETTER, D.R. & KROONENBERG, S.B., 1987. The granitoid-volcanic complex of Suriname. Extended abstract for the the final meeting of IGCP project 204, The Precambrian evolution of the Amazon region, Carajas, Brazil, pp 55-65.

DIAMOND, L.W. & MARSHALL, D.D, 1990. Evaluation of the fluid-inclusion crushing-stage as an aid in exploration for mesothermal gold-quartz deposits. J. Geochem. Explor., 38: 285-297.

ELLIOTT, R.G., 1985. Preliminary report on the Mowasi River cassiterite and gold expedition.

Unpub. rep., G.G.M.C., Georgetown, Guyana. 11 pp.

FAURE, G., 1986. Principles of isotope geology (2nd ed.), Wiley, New York.

EISENLOHR, B.N., GROVES, D. & PARTINGTON, G.A., 1989. Crustal-scale shear zones and their significance to Archaean gold minerlisation in Western Australia. Mineral. Deposita, 24: 1-8.

FLOYD, P.A., KELLING, G., GOKCEN, S.L. & GOKCEN, N., 1991. Geochemistry and tectonic environment of basaltic rocks from the Misis ophiolite melange, south Turkey. Chem. Geol., 89: 263-280.

FLOYD, P.A. & WINCHESTER, J.A., 1978. Identification and discrimination of altered and metamorphosed volcanic rocks using immobile elements. Chem. Geol. 21: 291-306.

GAUDETTE, H.E. & OLSZEWSKI Jr., W.J., 1985. Geochronology of the basement rocks, Amazonas Territory, Venezuela and the tectonic evolution of the western Guiana Shield. Geol. en Mijnbouw, 64: 131-143.

GIBBS, A.K., 1980. Geology of the Barama-Mazaruni Supergroup of Guyana. Unpub. PhD thesis, Harvard University, Mass., USA, 374 pp.

GIBBS, A.K., 1987a. Proterozoic volcanic rocks of the northern Guiana Shield, South America. In: PHARAOH, T.C., BECKINSALE, R.D. & RICKARD, D., (eds.), Geochemistry and Mineralization of Proterozoic Volcanic Suites, Geological Society Special Publication No. 33, pp 275-288, (Blackwell Scientific Publications).

GIBBS, A.K., 1987b. Contrasting style of continental mafic intrusions in the Guiana Shield. In: HALLS, H.C. & FAHRIG, W.F., (eds.), Mafic Dyke Swarms, Geological Association of Canada Special Paper 34, pp 457-465.

GIBBS, A.K. & BARRON, C.N., 1983. The Guiana Shield reviewed. Episodes, 2: 7-13.

GIBBS, A. K. & BARRON, C.N., 1992. The geology of the Guiana Shield. Oxford University Press, New York, 304 pp.

GIBBS, A.K. & OLSZEWSKI, Jr., W.J., 1982. Zircon U-Pb ages of Guyana greenstone-gneiss terrain. Precambrian Res., 17: 199-214.

GIBSON, C., 1987. Surface geology of the Omai gold deposit, Guyana. Unpub. internal report, Placer Dome., 15 pp.

GILL, J. & WHELAN, P., 1989. Early rifting of an ocean island arc (Fiji) produced shoshonitic to tholeiitic basalts. J. Geophys. Res., 94 (B4): 4561-4578.

GOVINDARAJU, K., 1989. 1989 compilation of the working values and sample descriptions for 272 geostandards. Geostandards Newsletter: 13, Special issue, pp 1-113.

GRAHAM, C.M., 1976. Petrochemistry and tectonic significance of Dalradian metabasaltic rocks of the S.W. Scottish Highlands. J. Geol. Soc. London, 132: 61-84.

GROMET, L.P. & SILVER, L.T., 1983. Rare earth element distributions among minerals in a granodiorite and their petrogenetic implications. Geochim. Cosmochim. Acta, 47: 925-939.

GROVES, D.I. & FOSTER, R.P., 1991. Archaean lode gold deposits. In: FOSTER, R.P., (ed.), Gold Metallogeny and Exploration, Blackie, pp 63-103.

GROVES, D.I., PHILLIPS, N., HO, S.E., HOUSTON, S.M. & STANDING, C.A., 1987. Craton-scale distribution of Archean greenstone gold deposits: predictive capacity of the metamorphic model. Econ. Geol., 82: 2045-2058.

GRUAU, G., MARTIN, H., LEVEQUE, B. & CAPDEVILA, R., 1985. Rb-Sr and Sm-Nd geochronology of the Lower Proterozoic granite-greenstone terrrains in French Guiana, South America. Precambrian Res., 30: 63-80.

GRUTZECK, M., KRIDELBAUGH, S & WEILL, D., 1974. The distribution of Sr and REE between diopside and silicate liquid. Geophys. Res. Lett., 1: 273-275.

GUARDIA, F.J.L., 1969. The Omai Mine area: report on the geological and geochemical surveys, Sept. - Dec., 1967. Unpub. report, Geol Surv. Guyana, 50 pp.

HANSON, G.N., 1978. The application of trace elements to the petrogenesis of igneous rocks of granitic composition. Earth Planet. Sci. Lett., 38: 26-43.

HARRIS, C., WATTERS, B.W. & GROENEWALD, P.B., 1991. Geochemistry of Mesozoic regional basic dykes of western Dronning Maud Land, Antarctica. Contrib. Mineral. Petrol., 107: 100-111.

HARRISON, Sir J.B., 1908. The geology of the goldfields of British Guiana. Dulau & Co., London, 320 pp.

HART, S.R., ERLANK, A.T. & KABLE, E.J.B., 1974. Sea floor basalt alteration: some chemical and Sr isotopic effects. Contrib. Mineral. Petrol., 44: 219-230.

HELLMAN, P.L., SMITH, R.E. & HENDERSON, P., 1979. The mobility of rare earth elements: evidence and implications from selected terrains affected by burial metamorphism. Contrib. Mineral. Petrol., 71: 23-44.

HERGT, J.M., CHAPPELL, B.W., McCULLOCH, M.T., McDOUGALL, I. & CHIVAS, A.R., 1989. Geochemical and isotopic constraints on the origin of the Jurassic dolerites of Tasmania. J. Petrol., 30: 841-883.

HILDRETH, W., 1981. Gradients in silicic magma chambers: Implications for lithospheric magmatism. J. Geophys. Res., 86: 10153-10192.

HOLE, M.J., SAUNDERS, A.D., MARRINER, G.F. & TARNEY, J., 1984. Subduction of pelagic sediments: implications for the origin of Ce-anomalous basalts from the Mariana Islands. J. Geol. Soc. London, 141: 453-472.

HUMPHRIS, S.E. & THOMPSON, G., 1978. Trace element mobility during hydrothermal alteration of oceanic basalts. Geochim. Cosmochim. Acta, 42: 127-136.

HYNES, A., 1980. Carbonatization and mobility of Ti, Y, and Zr in Ascot Formation metabasalts, S.E. Quebec. Contrib. Mineral. Petrol., 75: 79-87.

IGE, O.A. & ASUBIOJO, O.I., 1991. Trace element geochemistry and petrogenesis of some meta-ultramafites in Apomu and Ife-Ilesa areas of southwestern Nigeria. Chem. Geol., 91: 19-32.

INASI, J.C. & GIBBS, A.K., 1982. Baromalli heartwood sampling in Guyana. In: LAMING, D.J.C. & GIBBS, A.K., (eds.), Hidden wealth: mineral exploration techniques in tropical forest areas. AGID Report No.7, pp 89-94.

IRVINE, T.N. & BARAGAR, W.R.A., 1971. A guide to the chemical classification of the common volcanic rocks. Can. J. Earth. Sci., 8: 523-548.

JAKES, P. & WHITE, A.J.R., 1972. Major and trace element abundances in volcanic rocks of orogenic areas. Geol. Soc. Am. Bull., 83: 29-40.

JARVIS, K.E., 1988. Inductively coupled plasma mass spectrometry: a new technique for the rapid or ultra-trace level determination of rare-earth elements in geological materials. Chem. Geol., 68: 31-39.

JEMIELITA, R.A., DAVIS, D.W. & KROGH, T.E., 1990. U-Pb chronological constraints on the origin of Archean Superior Province lode gold deposits. Mineral Deposits Study Group (MDSG) Annual Conference, Trinity College, Dublin, Dec., 1990.

JENNER, G.A., LONGERICH, H.P., JACKSON, S.E. & FRYER, B.J., 1990. ICP-MS - A powerful tool for high-precision trace element analysis in Earth sciences: Evidence from the analysis of selected U.S.G.S. reference samples. Chem. Geol., 83: 133-148.

JENSEN, L.S., 1976. A new cation plot for classifying subalkalic volcanic rocks. Miscellaneous Paper, 66, Ontario Division of Mines, 22 pp.

JOÃO, X. da S. & MARINHO, P.A., 1982. Granitoides sodicos da regiao centro leste do Territorio Federal do Amapa. Anais do simposio de Geologia da Amazonia, Belem, May, 1992. Sociedade Brasileira de Geologia - Nucleo Norte, Vol. 2, pp 162-183.

JOCHUM, K.P., SEUFERT, H.M., SPETTEL, B. & PALME, H., 1986. The solar system abundances of Nb, Ta and Y and their relative abundances of refractory lithophile elements in differentiated planetary bodies. Geochim. Cosmochim. Acta, 50: 1173-1183.

JOHNSTON, R., 1960. The geology of the Omai gold mine, British Guiana. Colonial Development and Welfare Scheme No. d. 1744, University of St. Andrews, Scotland, 126 pp.

KERR, A., 1989. Geochemistry of the Trans-Labrador Granitoid Belt, Canada. A quantitative comparative study of a Proterozoic batholith and possible Phanerozoic counterparts. Precambrian Res., 45: 1-17.

KERRICH, R., 1987. The stable isotope geochemistry of Au-Ag vein deposits in metamorphic rocks: Mineralogical Association of Canada Short Course Handbook 13, pp 287-336.

KERRICH, R., 1989a. Geochemical evidence on the source of fluids and solutes for shear zone hosted mesothermal gold deposits. In BURSNALL, J.T., (ed.), Mineralisation and shear zones: Mineralogical Association of Canada Short Course 6, pp 129-198.

KERRICH, R., 1989b. Archean gold: Relation to granulite formation or felsic intrusions ? Geology, 17: 1011-1015.

LASSERRE, J.L., LEDRU, P. & MILESI, J.P., 1988. Les gites d'or de Guyane dans leur environnement geologique et structural (Geological and structural setting of gold occurrences in French Guiana). Principaux Resultats Scientifiques et Techniques du BRGM, RS 2474, pp 157-158.

LE BAS, M.J. & STRECKEISEN, A.L., 1991. The IUGS systematics of igneous rocks. J. Geol. Soc. London, 148: 825-833.

LEDRU, P. & MILESI, J.P, 1991. The metallogenetic relationship between gold-bearing shear zones and conglomerates in the lower Proterozoic of Ghana and French Guiana. In: LADEIRA, E.A., (ed.), Brazil Gold '91, Balkema, Rotterdam, p 709

LESHER, C.M., GOODWIN, A.M., CAMPBELL, I.H. & GORTON, M.P., 1986. Trace-element geochemistry of ore associated and barren felsic meta-volcanic rocks in the Superior Province, Canada. Can. J. Earth Sci., 23: 222-237.

LEUBE, A., HIRDES, W., MAUER, R. & KESSE, G.O., 1990. The Early Proterozoic Birimian Supergroup of Ghana and some aspects of its associated gold mineralization. Precambrian Res., 46: 139-165.

LONGERICH, H.P., JENNER, G.A., FRYER, B.J. & JACKSON, S.E., 1990. Inductively coupled plasma - mass spectrometric analysis of geological samples: A critical evaluation based on case studies. Chem. Geol., 83: 105-118.

LUDDEN, J.N. & THOMPSON, G., 1979. An evaluation of the behaviour of the rare earth elements during the weathering of sea-floor basalt. Earth Planet. Sci. Lett., 43: 85-92.

LUNGWITZ, E.E., 1899. Uber die regionalen veranderungen der Goldlager-Stratten. Unpub. PhD thesis, Univ. of Rostock, Leipzig.

LUNGWITZ, E.E., 1908. Gold placers in British Guiana. Geol. Surv. Br. Guiana, File GL14a.

MACDONALD, J.R., 1968. A guide to mineral exploration in Guyana. Geol. Surv. Guyana, Bulletin 38, 91 pp.

MARSH, J.S., 1987. Basalt geochemistry and tectonic discrimination within continental flood provinces. In: WEAVER, S.D. & JOHNSON, R.W., (eds.), Tectonic Controls on Magma Chemistry. J. Volcanol. Geotherm. Res., 32: 35-49.

MARTIN, H., 1986. Effect of steeper Archean geothermal gradient on geochemistry of subduction zone magmas. Geology, 14: 753-756.

MATHEIS, G., 1988. Proterozoic metallogenetic belts across the Central Atlantic. J. African Earth Sci., 7, (2): 516.

MATTEY, D.P., EXLEY, R.A. & PILLINGER, C.T., 1989. Isotopic composition of CO_2 and dissolved carbon species in basalt glass. Geochim. Cosmochim. Acta, 53: 2377-2386.

MAY, P.R., 1971. Pattern of Triassic-Jurassic diabase dykes around the north Atlantic in the context of predrift position of the continents. Bull. Geol. Soc. Am., 82: 1285-1292.

McCONNELL, R.B., 1958. Provisional stratigraphic table for British Guiana. Ann. Report 1957, Geol. Surv. Br. Guiana, Appx. I, pp 33-53.

McCONNELL, R.B., 1969. Fundamental fault zones in the Guiana and West African Shields in relation to presumed axes of Atlantic spreading. Bull. Geol. Soc. Am., 80: 1775-1782.

McCREA, J.M., 1950. On the isotopic chemistry of carbonates and a paleotemperature scale. J. Chem. Phys., 18: 849-857.

MESCHEDE, M., 1986. A method of discriminating between different types of mid-ocean ridge basalts and continental tholeiites with the Nb-Zr-Y diagram. Chem. Geol., 56: 207-218.

MIDDLEMOST, E.A.K., 1975. The basalt clan. Earth-Sci. Rev., 11: 337-364.

MINING MAGAZINE, 1991. 1993 start-up for Omai, Guyana gold project ? Panorama, Sept., 1991, p 18.

MIYASHIRO, A., 1974. Volcanic rock series in island arcs and active continental margins. Am. J. Sci., 274: 321-355.

MONTI, R., 1987. The Boddington lateritic gold deposit, Western Australia: a product of supergene enrichment processes. In HO, S.E. & GROVES, D.I., (eds.), Recent Advances in Understanding Precambrian Gold Deposits. Geol. Dept. & Univ. Extension, Univ. West. Australia, Pub. 11, pp 355-368.

MORENO, L.A. & MENDOZA, V., 1975. Petroquimica de metabasitas de alto supamo sureste de la Guayana Venezolana. In Anais 10 th Conf. Geol. Interguianas, Belem, Brazil, 1975, Min. Minas Energia, D.N.P.M, pp 389-413.

MORRISON, G.W., 1980. Characteristics and tectonic setting of the shoshonite rock association. Lithos, 13: 97-108.

MORTON, R.D., 1987. Petrography and mineralogy of selected litholgies from DDH #86-8, Omai gold property, Guyana. Unpub. research report for Golden Star Resources Ltd., 13 pp.

MORTON, R.D., 1990. Preliminary petrographic and petrological observations on the host rocks of the Omai gold deposits, Guyana: A guide to exploration models and potentials. Unpub. research report, University of Alberta, Canada, 11 pp.

NAKAMURA, N., 1974. Determination of REE, Ba, Fe, Mg, Na and K in carbonaceous chondrites. Geochim. Cosmochim. Acta, 38: 757-775.

NALDRETT, A.J. & GOODWIN, A.M, 1977. Volcanic rocks of the Blake River Group, Abitibi Greenstone Belt, Ontario, and their sulphur content. Can. J. Earth Sci., 14: 539-550.

NASH, J. T., 1976. Fluid inclusion petrology - data from porphyry copper deposits and applications to exploration. U.S.G.S. Prof. Paper 907-D.

NEDELEC, A., NSFIFA, E.N. & MARTIN, H., 1990. Major and trace element geochemistry of the Archaean Ntem plutonic complex (south Cameroon): petrogenesis and crustal evolution. Precambrian Res., 47: 35-50.

NESBITT, B.E., 1991. Phanerozoic gold deposits in tectonically active continental margins. In: FOSTER, R.P., (ed.), Gold Metallogeny and Exploration, Blackie, pp 104-132.

O'DAY, P.A., 1984. Sedimentary rocks of the Barama-Mazaruni Supergroup, northern Guyana: sedimentology, petrography and geochemistry. Unpub. MSc thesis, Cornell University, Ithaca, New York, 154 pp.

OHMOTO, H. & RYE, R.O., 1979. Isotopes of sulfur and carbon. In: BARNES, H.L., (ed.), Geochemistry of Hydrothermal Ore Deposits, (2nd ed.), Wiley, pp 509-567.

OLIVEIRA, C.G. & LEONARDOS, O.H., 1990. Gold mineralization in the Diadema shear belt, northern Brazil. Econ. Geol., 85: 1034-1043.

PAYNE, J.G. (Vancouver Petrographics Ltd.), 1989a. Unpub. consultant's petrographic/mineralogical report (No. 7946) on selected drill-core samples from the Omai gold deposit, Guyana - for Placer Dome Inc., 17 pp.

PAYNE, J.G. (Vancouver Petrographics Ltd.), 1989b. Unpub. consultant's petrographic/mineralogical report (No. 8067) on selected drill-core samples from the

Omai gold deposit, Guyana - for Placer Dome Inc., 3 pp.

PAYNE, J.G. & STRONG, D.F., 1979. Origin of the Twillingate trondhjemite, north-central Newfoundland: partial melting in the roots of an island arc. In: BARKER, F., (ed.), Trondhjemites, dacites and related rocks. Elsevier, pp 489-516.

PEARCE, J.A., 1982. Trace element characteristics of lavas from destructive plate boundaries. In: THORPE, R. S., (ed.), Orogenic Andesites, John Wiley & Sons pp. 525-548.

PEARCE, J.A., 1983. Role of the sub-continental lithosphere in magma genesis at active continental margins. In: HAWKESWORTH, C.J. & NORRY, M.J. (eds.), Continental Basalts and Mantle Xenoliths, Shiva Publications, pp. 230-249.

PEARCE, J.A. & CANN, J.R., 1973. Tectonic setting of volcanic rocks determined using trace element analyses. Earth Planet Sci. Letters, 19: 290-300.

PEARCE, J.A., HARRIS, N.B.W. & TINDLE, A.G., 1984. Trace element discrimination diagram diagrams for the tectonic interpretation of granitic rocks. J. Petrol., 25: 956-983.

PEARCE, J.A. & NORRY, M.J., 1979. Petrogenetic implications of Ti, Zr, Y and Nb variations in volcanic rocks. Contrib. Mineral. Petrol., 69: 33-47.

PEARCE, T.H., GORMAN, B.E. & BIRKETT, T.C., 1975. The TiO_2-K_2O-P_2O_5 diagram: a method of discriminating between oceanic and non-oceanic basalts. Earth Planet. Sci. Lett., 24: 419-426.

PEARCE, T.H., GORMAN, B.E. & BIRKETT, T.C., 1977. The relationship between major element chemistry and the tectonic environment of basic and intermediate volcanic rocks. Earth Planet. Sci. Lett., 36: 121-132.

PECK, D.C. & SMITH T. E., 1989. The geology an geochemistry of an Early Proterozoic volcanic-arc association at Cartwright Lake: Lynn Lake greenstone belt, northwestern Manitoba. Can. J. Earth Sci., 26: 716-736.

PERRING, C.S., 1988. Petrogenesis of the lamprophyre - "porphyry" suite from Kambalda, Western Australia. In HO, S.E. & GROVES, D.I., (eds.), Advances in Understanding Precambrian Gold Deposits, Vol II. Geol. Dept. & Univ. Extension, Univ. West. Australia, Pub. 12, pp 277-294.

PHARAOH, T.C. & PEARCE, J.A., 1984. Geochemical evidence for the geotectonic setting of Early Proterozoic metavolcanic sequences in Lapland. Precambrian Res., 25: 283-308.

RAPP, R.P., WATSON, B.E. & MILLER, C.F., 1991. Partial melting of amphibolite/eclogite and the origin of Archean trondhjemites and tonalites. Precambrian Res., 51: 1-25.

RENNER, R., 1985. The geology and geochemistry of the Issineru Formation, northern Guyana. Unpub. MSc thesis, Cornell University, New York, 252 pp.

RENNER, R. & GIBBS, A.K., 1987. Geochemistry and petrology of the metavolcanic rocks of the early Proterozoic greenstone belt, northern Guyana. In: PHARAOH, T.C, BECKINSALE, R.D. & RICKARD, D., (eds.), Geochemistry and Mineralization of Proterozoic Volcanic Suites, Geological Society Special Publication No. 33, pp. 289-309. (Blackwell Scientific Publications.)

ROBB, L.J. & MYER, F.M., 1990. The nature of the Witwatersrand hinterland: conjectures

on the source area problem. Econ. Geol., 85: 511-536.

ROBERTS, R.G., 1987. Archean lode gold deposits. In: ROBERTS, R.G. & SHEENAN, P.A. (eds.), Ore Deposit Models, Geoscience Canada, Reprint Series 3, pp 1-19.

ROCK, N.M.S., 1987. The nature and origin of lamprophyres: an overview. In: FITTON, J.G. & UPTON, B.J.G., (eds.), Alkaline Igneous Rocks, Geological Society Special Publication, No. 30, pp. 191-226.

ROCK, N.M.S., 1991. Lamprophyres. Blackie & Son Ltd., Glasgow, 285 pp.

ROCK, N.M.S. and GROVES, D.I., 1988. Can lamprophyres resolve the genetic controversy over mesothermal gold deposits ? Geology, 16: 538-541.

ROCK, N.M.S & HUNTER, R.H., 1987. Late Caledonian dyke-swarms of northern Britain: spatial and temporal intimacy between lamprophyric and granitic magmas around the Ross of Mull pluton, Inner Hebrides. Geol. Rundsch., 76: 805-827.

ROSENBAUM, J. & SHEPPARD, S.M.F., 1986. An isotopic study of siderites, dolomites and ankerites at high temperatures. Geochim. Cosmochim. Acta, 50: 1147-1150.

SAUNDERS, A.D. & TARNEY, J., 1979. The geochemistry of basalts from a back-arc spreading centre in the East Scotia Sea. Geochim. Cosmochim. Acta, 43: 555-572.

SAUNDERS, A.D. & TARNEY, J., 1985. Geochemical characteristics of basaltic volcanism within back arc basins. In: KOKELAAR, B.P. & HOWELLS, B.P., (eds.), Marginal Basin Geology: volcanic and associated sedimentary and tectonic processes in modern and ancient marginal basins. Geological Society London Special Publication No. 16, pp. 59-76.

SCHELLMAN, W., 1989. Composition and origin of lateritic ore at Tagaung Taung, Burma. Mineral. Deposita, 24: 161-168.

SCHOCK, H.H., 1979. Distribution of rare-earth elements and other trace elements in magnetites. Chem. Geol. 26: 119-133.

SHAW, R.P., 1986. The nature of gold in residual laterite soils from the Omai Mine area, Guyana, South America. Unpub. undergraduate thesis, University of Alberta, Canada, 52 pp.

SHEPHERD, T.J., 1981. Temperature-programmable heating-freezing stage for microthermometric analysis of fluid inclusions. Econ Geol., 76: 1244-1247.

SHEPHERD, T.J, RANKIN, A.H. & ALDERTON, D.H.M., 1985. A practical guide to fluid inclusion studies. Blackie, 239 pp.

SHERVAIS, J.W., 1982. Ti-V plots and the petrogenesis of modern ophiolitic lavas. Earth Planet. Sci. Lett., 59: 101-118.

SIAL, A.N., OLIVEIRA, E.P. & CHOUDHURI, A., 1987. Mafic dyke swarms of Brazil. In: HALLS, H.C. & FARIG, W.F., Mafic Dyke Swarms. Geological Association of Canada Special Paper 34, pp. 467-481.

SISSON, T.W., 1991. Pyroxene-high silica rhyolite trace element partition coefficients measured by ion microprobe. Geochim. Cosmochim. Acta, 55: 1575-1585.

S.N.C. INC., 1985. An interim geological report on the Omai deposit, Guyana. Unpub. consultants' report, for Golden Star Resources Ltd.

S.N.C. INC., 1986. Feasibilty of the weathered zone. Unpub. consultants' report on the Omai Project, Golden Star Resources Ltd., 97 pp.

SNELLING, N.J., & McCONNELL, R.B., 1966. The geochronology of Guyana. Geol. Surv. Guyana Records 6: Paper IX, 23 pp. Revised version in Geol. en Mijn., 48: 201-213.

STRECKEISEN, A., 1976. To each plutonic rock its proper name. Earth Sci. Rev., 12, 1-33.

STILLMAN, C.J. & WILLIAMS, C.T., 1979. Geochemistry and tectonic setting of some Ordovician volcanic rocks in east and southeast Ireland. Earth Planet. Sci. Lett., 41: 288-310.

SUN, S.-s. & McDONOUGH, W.F., 1989. Chemical and isotopic systematics of oceanic basalts: implications for mantle composition and processes. In: SAUNDERS, A.D. & NORRY, M.J. (eds.), Magmatism in the ocean basins, Geological Society Special Publication No 42, pp 313-345.

TEIXEIRA, W., TASSINARI, C.C.G., CORDANI, U.G. and KAWASHITA K., 1989. A review of the geochronology of the Amazon Craton: tectonic implications. Precambrian Res., 42: 213-217.

TAYLOR, Jr., H.P., 1979. Oxygen and hydrogen isotope relationships in hydrothermal mineral deposits. In: BARNES, H.L., (ed.), Geochemistry of Hydrothermal Ore Deposits, (2nd ed.), Wiley, pp 236-277.

THOMPSON, R.N., MORRISON, M.A., DICKIN, A.P. & HENDRY, G.L., 1983. Continental flood basalts.... arachnids rule O.K. ? In: HAWKESWORTH, C.J. & NORRY, M.J. (eds.), Continental Basalts and Mantle Xenoliths. Shiva Publications, pp 158-185.

THOMPSON, R.N., MORRISON, M.A., HENDRY, G.L. & PARRY, S.J., 1984. An assessment of the relative roles of crust and mantle in magma genesis: an elemental approach. Phil. Trans. R. Soc. Lond. A 310, 549-590.

THURSTON. P.C. & FRYER, B.J., 1983. The geochemistry of repetitive cyclical volcanism from basalt through rhyolite in the Uchi-Confederation greenstone belt, Canada. Contrib. Mineral. Petrol., 83: 204-226.

TINDLE, A.G. & PEARCE, J.A., 1981. Petrogenetic modelling of situ fractional crystallization in the zoned Loch Doon pluton, Scotland. Contrib. Mineral. Petrol., 78: 196-207.

TLIG, S. & STEINBERG, M., 1982. Distribution of rare-earth elements (REE) in size fractions of recent sediments of the Indian Ocean. Chem. Geol., 37: 317-333.

TOPP, S.E., SALBU, B., ROALDSET, E & JORGENSEN, P., 1985. Vertical distribution of trace elements in laterite soil (Suriname). Chem. Geol. 47: 159-174.

UYTENBOGAARDT, W. & BURKE, E.A.J., 1971. Tables for microscopic identification of ore minerals (2nd revised ed.), Elsevier, 430 pp.

VEENSTRA, E., 1978. Petrology and geochemistry of Sheet Stonbroekoe, Sheet 30, Academisch Proefschrift, Univeristat Amsterdam, 161 pp. Also published as Contibutions to the Geology of Suriname, 7, 1983, 134 pp.

WALROND, G.W., 1985. A metallogenetic scheme for the Guiana Shield. In: MUNOZ, M., (ed.), Memoria, I Symposium Amazonico: Ministerio de Energia y Minas (Caracas), pp 609-624.

WALROND, G.W., 1987a. Geological map of Guyana. Scale 1:1 million. G.G.M.C.,

Georgetown, Guyana.

WALROND, G.W., 1987b. Mineral exploration map of Guyana. Scale 1:1 million. G.G.M.C., Georgetown, Guyana.

WEAVER, B.L. & TARNEY, J., 1981. The Scourie dyke suite: petrogenesis and geochemical nature of the sub-continental mantle. Contrib. Mineral. Petrol., 78: 175-188.

WEAVER, B.L. & TARNEY, J., 1983. The geochemistry of the sub-continental mantle: inferences from Archaean and Proterozoic dykes and continental flood basalts. In: HAWKESWORTH, C.J. & NORRY, M.J., (eds.), Continental Basalts and Mantle Xenoliths. Shiva Publications, pp 209-229.

WEBSTER, J.G. & MANN, A.W., 1984. The influence of climate, geomorphology and primary geology on the supergene migration of gold and silver. J. Geochem. Explor., 22: 21-42.

WHITFORD, D.J., McPHERSON, W.P.A. & WALLACE, D.B., 1989. Geochemistry of the host rocks of the volcanogenic massive sulphide deposit at Que River, Tasmania. Econ. Geol., 84: 1-21.

WILSON, A.F., 1984. Origin of quartz-free gold nuggets and supergene gold found in laterites and soils- a review and some new observations. Aus. J. Earth Sci., 31: 303-316.

WILSON, M., 1989. Igneous Petrogenesis. Unwin Hynman, London, 466 pp.

WINCHESTER, J.A. & FLOYD, P.A., 1976. Geochemical magma type discrimination: application to altered and metamorphosed basic igneous rocks. Earth Planet. Sci. Lett., 28: 459-469.

WINCHESTER, J.A. & FLOYD, P.A., 1977. Geochemical discrimination of different magma series and differentiation products using immobile elements. Chem. Geol., 20: 325-343.

WITT, W.K.& SWAGER, C.P., 1989. Structural setting and geochemistry of Archaean I-type granites in the Bardoc-Coolgardie area of the Norseman-Wiluna Belt, Western Australia. Precambrian Res., 44: 323-351.

WOOD, D.A., 1980. The application of a Hf-Ta diagram to the problems of tectonomamatic classification and to establishing the nature of crustal contamination of basaltic lavas of the British Tertiary Volcanic Province. Earth Planet. Sci. Lett., 50: 11-30.

WOOD, D.A., JORON, J. & TREUIL, M., 1979. A re-appraisal of the use of trace elements to classify and discriminate between magma series erupted in different tectonic settings. Earth Planet. Sci. Lett., 45: 326-335.

WOOD, P.C., BURROWS, D.R., THOMAS, A.V. & SPOONER, E.T.C., 1986. The Hollinger-McIntyre Au-quartz vein system, Timmin, Ontario, Canada: geologic characteristics, fluid properties and light stable isotope geochemisrty. In: Macdonald, A.J. (ed.), Proc. of Gold '86, an international symposium on the geology of gold, Toronto, Konsult International Inc., pp 56-80.

WYMAN, D.A. & KERRICH, R., 1988. Lamprophyres a source of gold (?). Nature 332: 209-210.

WYMAN, D.A. & KERRICH, R., 1989. Archean lamprophyres of the Superior Province, Canada: distribution, petrology and geochemical characteristics. J. Geophys. Res.,

94: 4667-4696.

ZHAO, J-X. & COOPER, J.A., 1992. The Atnarpa Igneous Complex, southeast Arunta Inlier, central Australia: implications for subduction at an Early-Mid Proterozoic continental margin. Precambrian Res., 56: 227-253.

APPENDICES

Appendix I: Sample Data Base

The vast majority of samples in the data base are taken from drill-core specimens and are labelled according to the drill-hole number and depth at which the specimen was taken. For example, thin section 1-0401 indicates that this particular sample was taken from drill-hole (GSR 86):1 at a depth of 40.1 m. Abbreviations used in this appendix are as follows:

CMS - Captain Mann Sill; **GCS** - Gilt Creek Suite; **MJ** - Majuba Suite; **OMS** - Omai Stock; **OMZ** - Omai Stock Zone; **WLZ** - Wenot lake Zone.

Thin section and geochemical samples (all from drill-core specimens).

* indicates that the thin section specimen has a corresponding geochemical sample.

1-0401*	basalt, MJ, OMZ.
1-0523	sub-ophitic to ophitic-textured minor basic intrusive, MJ, OMZ.
1-0579	silty-ashy intermediate tuff, MJ, OMZ.
1-0987	quartz vein with minor carbonate, in MJ, OMZ.
1-1555*	porphyritic hornblende andesite, MJ, OMZ.
1-1657*	"tapioca"-textured basaltic andesite, MJ, OMZ.
1-1712	dioritic dyke-rock, GCS, OMZ.
2-1110	sub-ophitic to ophitic-textured minor basic intrusive, MJ, OMZ.
2-1534*	dioritic dyke-rock, GCS, OMZ.
2-1546*	dioritic dyke-rock, GCS, OMZ.
2-1598*	sub-ophitic to ophitic-textured minor basic intrusive, MJ, OMZ.
2-2360*	andesite, MJ, OMZ.
3-0366	slightly weathered lamprophyre (appinite), OMZ.
3-0739*	micro-porphyritic basalt with quartz-carbonate-sericite veining, MJ, OMZ.
3-0905*	sub-ophitic basalt, MJ, OMZ.
3-1019	sheared dioritic dyke-rock cut by quartz-carbonate vein, GCS (?), OMZ.
3-1372	porphyritic "caviar" andesite, MJ, OMZ.
3-1396*	chill facies dioritic dyke-rock, GCS, OMZ.
3-1365*	sheared dioritic dyke-rock, GCS, OMZ. (geochem. analyses not listed)
3-1681*	sub-ophitic basalt, MJ, OMZ
3-1849*	sub-ophitic to ophitic basalt or minor basic intrusive, MJ, OMZ.
3-2240	dioritic dyke-rock, GCS (?), OMZ.

4-0120	mafic tuff with micro-porphyritic tecture, MJ, OMZ.
4-0145*	mafic tuff with micro-porphyritic (?) texture, MJ, OMZ.
4-0294*	sub-ophitic basalt, MJ, OMZ.
4-0578	andesitic tuff, MJ, OMZ.
4-0657	andesitic tuff, MJ, OMZ.
4-0701	extremely altered mafic volcanic rock, MJ, OMZ.
4-0775*	banded mafic tuff, MJ, OMZ.
4-1050*	strongly banded mafic tuff, MJ, OMZ
4-1272*	sub-ophitic to ophitic textured basalt, MJ, OMZ.
4-1618	sheared dioritic dyke-rock, GCS, OMZ.
4-1650	sub-ophitic to ophitic-textured minor basic intrusive, MJ, OMZ.
4-1816*	dioritic dyke-rock, GCS, OMZ.
4-2022*	porphyritic-amygdaloidal basalt, MJ, OMZ.
4-2055	dioritic dyke-rock, GCS, OMZ.
4-2409*	sub-ophitic to ophitic textured basalt or minor basic intrusive, MJ, OMZ.
5-0110	quartz diorite - tonalite, OMS.
5-0318	quartz diorite - tonalite, OMS.
5-0485*	quartz diorite, OMS.
5-0811*	tonalite, OMS.
5-0937	strongly altered contact rock - OMS/lamprophyre ?
5-1055	lamprophyre (appinite) in contact with OMS.
5-1142*	lamprophyre (appinite), OMZ.
5-1515*	"tapioca"-textured basalt, MJ, OMZ.
5-1629	dioritic dyke-rock (relatively fresh), OMZ.
5-1750*	sub-ophitic to ophitic-textured basalt with pumpellyite (?), MJ, OMZ.
5-2023	severely altered altered mafic volcanic rock with pyrite, MJ, OMZ.
5-2308	veined and strongly altered mafic volcanic rock, MJ, OMZ.
5-2492*	andesitic volcanic rock, MJ, OMZ.
5-2496	minor basic intrusive (relatively fresh), MJ, OMZ.
5-2936*	gabbro, GSR dyke, OMZ.
6-0139*	tonalite, OMS.
6-0251*	tonalite, OMS.
6-0399*	chilled dioritic dyke-rock, GCS, OMZ.
6-0626*	tonalite, OMS.
6-0786*	tonalite, OMS.
6-0841	quartz diorite - tonalite, OMS.

6-1205*	diorite, OMS.
6-1507*	quartz-diorite, OMS.
6-1745	chilled dioritic dyke-rock, GCS, OMZ.
6-1765	dioritic dyke-rock, GCS, OMZ.
6-1815*	quartz diorite, OMS.
6-1975*	sheared ultramafic dyke-rock, GCS, OMZ.
6-2119	quartz diorite - tonalite, OMS.
6-2176	chilled dioritic-dyke rock, GCS, OMZ.
6-2356	strongly altered mafic volcanic rock or chilled dioritic dyke-rock, OMZ.
6-2687	thermally (?) altered mafic volcanic rock, MJ, OMZ.
6-2802*	gabbro, GSR dyke, OMZ.
6-2908*	uralitised gabbro, GSR dyke, OMZ.
6-3028*	uralitised gabbro, GSR dyke, OMZ.
7-0135	quartz-diorite - tonalite, OMS.
7-0278	quartz vein in quartz diorite - tonalite, OMS.
7-0309*	quartz diorite - tonalite, OMS.
7-0363	quartz diorite - tonalite, OMS.
7-0364	chilled dioritic dyke-rock of GCS in contact with OMS.
7-0588	quartz diorite - tonalite, OMS.
7-0709	quartz diorite - tonalite, OMS.
7-0819	propylitised porphyritic dioritic dyke-rock, GCS, OMZ.
7-0979*	propylitised porphyritic dioritic dyke-rock, GCS, OMZ.
7-1162	quartz diorite - tonalite, OMS.
7-1220*	quartz diorite, OMS.
7-1258	quartz diorite - tonalite, OMS.
7-1300	granodiorite, OMS.
7-1312	chilled dioritic dyke-rock of GCS in contact with OMS.
7-1460	quartz diorite - tonalite, OMS.
7-1594*	dioritic dyke-rock, GCS, OMZ.
7-1808*	tonalite, OMS.
7-1956	ultramafic to dioritic dyke-rock, GCS, OMZ.
7-2059	quartz diorite - tonalite, OMS.
7-2124*	quartz diorite, OMS.
7-2464	quartz vein in OMS wall-rock (2 slides).
7-2563	thermally (?) mafic volcanic rock or chilled dioritic dyke rock, OMZ.
7-2734	uralitised gabbro, GSR dyke, OMZ.
7-3021	uralitised gabbro, GSR dyke, OMZ.

8-0179*	tonalite, OMS.
8-0393	quartz diorite - tonalite, OMS.
8-0713	quartz diorite - tonalite, OMS.
8-1389	diorite - quartz diorite, OMS.
8-1596*	tonalite, OMS.
8-1735	quartz diorite - tonalite, OMS.
8-1888*	dioritic dyke-rock, GCS, OMZ.
8-1948	dioritic dyke-rock, GCS, OMZ.
8-2009	dioritic dyke-rock, GCS, OMZ.
8-2285*	dioritic dyke-rock, GCS, OMZ.
8-2434*	tonalite, OMS.
8-2611	quartz diorite, OMS.
8-2723	chilled dioritic dyke-rock, GCS, OMZ (2 slides).
8-2792	quartz diorite - tonalite, OMS.
8-3046*	uralitised gabbro, GSR dyke, OMZ.
11-0722	greenish sericite tuff, southwest of OMZ.
11-0723	greenish sericite tuff, southwest of OMZ.
11-0756	dark grey sericite tuff, southwest of OMZ.
15-0565	quartz diorite - tonalite, OMS.
15-0566	quartz diorite - tonalite, OMS.
58-1143	lamprophyre (appinite), OMZ.
67-0716*	spherulitic acid volcanic rock (high-silica rhyolite), MJ, WLZ.
67-1474*	acid volcanic rock (high silica rhyolite), MJ, WLZ.

<u>Regional thin section and geochemical samples</u> (all from hand specimens).

* indicates that the thin section specimen has a corresponding geochemical sample.

RX-20	micro-gabbro, Point dyke, Omai landing, Essequibo River.
RX-21*	micro-gabbro, Point dyke, Omai landing, Essequibo River (see Fig. 2.3).
RX-22*	gabbro, Ya-ya dyke, near Omai Falls, Omai River (see Fig 2.3).
RX-23	gabbro, Ya-ya dyke, near Omai Falls, Omai River.
RX-89	lamprophyre (appinite), from a tailing dump, OMZ.

CM-02* porphyritic basalt, MJ, Captain Mann Creek (see Fig. 2.3).
CM-03* andesitic sill-rock, CMS, Captain Mann Creek (see Fig. 2.3).
CM-04* andesitic sill-rock, CMS, Captain Mann Creek (see Fig. 2.3).

GL-01 micro-porphyritic basalt, MJ, upper Gilt Creek.

TG-01 amphibolite, Essequibo River (5°24'28" N; 58°47'42" W).
TG-02* tonalite, Tigri pluton, Essequibo River (5°24'04" N; 58°48'45" W).
TG-03* quartz diorite, Tigri pluton, Essequibo River (5°23'38" N; 58°49'03" W).
TG-04* tonalite-granodiorite, Tigri pluton, Essequibo River (5°24'21" N; 58°49'32" W).
TG-05* granodiorite, Tigri pluton, Essequibo River (5°24'26" N; 58°49'52" W).
TG-06* tonalite, Tigri pluton, Essequibo River (5°24'35" N; 58°50'18" W).
TG-07* tonalite, Tigri pluton, Essequibo River (5°24'50" N; 58°48'34" W).

MB-08* tonalite-granodiorite, Mariaba pluton, Essequibo River (5°29'11" N; 58°38'47" W).
MB-09* gabbro, Ya-ya dyke, Essequibo River (5°29'28" N; 58°38'37" W).
MB-10* tonalite, Mariaba pluton, Essequibo River (5°31'0" N; 58°37'47" W).
MB-11* tonalite, Mariaba pluton, Essequibo River (5°31'10" N; 58°37'32" W).
MB-12* tonalite-granodiorite, Mariaba pluton, Essequibo River (5°30'37" N; 58°37'32" W).
MB-13* tonalite, Mariaba pluton, Essequibo River (5°30'07" N; 58°37'58" W).

MW-85* tonalite, Mowasi pluton, Mowasi River (approx. 5°30'16" N; 58°59'55" W).

Polished thin sections (all from drill-core specimens except RK-02 and RK-03)

1-1520 quartz vein in MJ, OMZ.

2-0555 quartz vein in sub-ophitic basalt, MJ, OMZ.
2-1565 quartz-carbonate vein in MJ, OMZ.

3-0461 mafic volcanic wall-rock with disseminated pyrite cubes, MJ, OMZ.
3-0535 quartz-carbonate vein in pyritised mafic volcanic wall-rock, MJ, OMZ.
3-0714 quartz-carbonate vein from dioritic dyke-rock, OMZ.
3-1496 quartz-carbonate vein containing pyrite, pyrrhotite and chalcopyrite, MJ, OMZ.

4-0302	pyritised mafic volcanic wall-rock cut by quartz veinlet with minor chalcopyrite, MJ, OMZ.
4-0526	mafic volcanic wall-rock sandwiched between two quartz-carbonate veins; abundant pyrite, MJ, OMZ.
4-1118	mafic volcanic wall-rock cut by quartz veinlets, MJ, OMZ. (Assay: 10 g/t Au).
4-1119	mafic volcanic wall-rock cut by quartz veinlets, MJ, OMZ. (Assay: 10 g/t Au).
4-1438	quartz-carbonate vein with coarse disseminated pyrite, MJ, OMZ.
5-0213	carbonate "vein" in quartz vein, OMS. (Assay: 6.0 g/t Au).
5-0214	quartz veinlet cutting OMS wall-rock. (Assay: 6.0 g/t Au).
5-0319	quartz vein in OMS wall-rock containing scheelite, gold, galena and a Bi-sulphosalt (2 slides).
5-0550	quartz vein from OMS containing abundant fluid inclusions. (Assay: 8.0 g/t Au).
5-0618	quartz vein from OMS ("frosty" slide).
5-0936	contact rock between OMS and appinite ? containing magnetite, pyrite, pyrrhotite and chalcopyrite.
5-1629	dioritic dyke wall-rock, OMZ.
5-1836	quartz vein in MJ near granitic dyklet, OMZ.
5-2051	quartz vein in dioritic dyke wall-rock, OMZ. (Assay: 10.4 g/t Au).
5-2415	quartz veinlet in pyritised mafic volcanic wall-rock, MJ, OMZ. (Assay: 6.7 g/t Au).
5-2713	quartz vein in mafic volcanic wall-rock with carbonate ribbon along vein margin, MJ, OMZ. Good caries textures in pyritised wall-rock.
6-0138	quartz vein in OMS containing abundant fluid inclusions.
6-0305	quartz vein in OMS containing abundant fluid inclusions.
6-0420	quartz vein cutting OMS wall-rock. (Assay: 8.1 g/t Au).
6-0568	quartz-carbonate vein cutting OMS wall-rock. (Assay: 10.3 g/t Au).
6-1097	quartz-carbonate vein cutting OMS wall-rock (frosty slide).
6-2107	quartz-carbonate vein in OMS wall-rock containing visible gold, galena and tellurides (2 slides).
6-2658	quartz vein in OMS wall-rock. Pyrrhotite and chalcopyrite in wall-rock.
7-0589	quartz vein in OMS, with pyrite.
7-0843	quartz-carbonate vein in dioritic dyke wall-rock, OMZ.
7-0844	quartz-carbonate vein in dioritic dyke wall-rock, OMZ.
7-1284	quartz vein in OMS containing visible gold. (Assay: 5.2 g/t Au).

7-1261	quartz-carbonate vein in OMS. (Assay value 5.2 g/t Au).
7-1471	quartz vein cutting OMS wall-rock.
7-1702	quartz-carbonate vein cutting OMS wall-rock.
7-1899	quartz-carbonate vein cutting OMS wall-rock ("frosty" slide).
7-1923	quartz vein, OMS.
7-1989	quartz vein cutting OMS wall-rock.
7-2274	"tapioca"-textured quartz-carbonate vein, OMS.
7-2464	quartz-carbonate vein cutting OMS wall-rock.
8-0256	quartz vein in OMS containing abundant fluid inclusions.
8-0452	quartz-carbonate vein cutting OMS wall-rock.
8-0594	quartz-carbonate vein in OMS containing scheelite. (Assay: 8.4 g/t Au).
8-0619	pyrite-rich quartz vein in OMS wall-rock.
8-2055	quartz-carbonate veins cutting OMS wall-rock.
8-2134	quartz-carbonate vein cutting OMS wall-rock.
8-2198	OMS wall-rock.
8-2297	quartz-carbonate vein cutting OMS wall-rock.
8-2968	quartz veinlet cutting heavily pyritised OMS wall-rock.
8-2969	quartz veinlet cutting pyritised OMS wall-rock; also with sphalerite.
67-1413	quartz vein cutting high-silica rhyolite wall-rock, WLZ.
67-1440	quartz vein cutting high-silica rhyolite wall-rock, WLZ.
67-1472	quartz vein cutting high-silica rhyloite wall-rock, WLZ.
RK-02	lamprophyre (appinite) from a tailing dump, OMZ - contains chalcopyrite and skeletal opaques (leucoxene).
RK-03	lamprophyre (appinite) from a tailing dump, OMZ - contains disseminated chalcopyrite.

Polished wafers (fluid inclusion studies)

5-0319	quartz-carbonate vein from OMS (contains scheelite, gold, galena and Bi-sulphosalt.
5-0550	quartz vein from OMS.
6-0305	quartz vein from OMS.

Crushed vein-carbonate samples (stable isotope studies)

2-1565	quartz-carbonate vein from MJ, OMZ.
3-1496	quartz-carbonate vein from MJ, OMZ.
6-0568	quartz-carbonate vein from OMS.
7-1261	quartz-carbonate vein from OMS.
8-2297	quartz-carbonate vein from OMS.

Crushed vein-quartz samples (stable isotope studies)

2-0550	quartz vein from MJ, OMZ.
5-0315	quartz vein from OMS.
5-0550	quartz vein from OMS.
6-0305	quartz vein from OMS.
7-1284	quartz vein containing visible gold, OMS.
67-1442	quartz vein from high-silica rhyolite, WLZ.

Appendix II: Petrographic data of the Omai granitoid rocks (point-counting method).

Tigri pluton

Sample No.	Q	A	P	%	Points
TG-03	18.8	0.4	80.8		1531
TG-06	23.3	3.8	72.9		1335
TG-02	24.0	0.5	75.5		1381
TG-07	32.4	2.9	64.7		1528
TG-04	31.8	6.4	61.8		1435
TG-05	29.6	14.7	55.7		1365

Mariaba pluton

Sample No.	Q	A	P	Points
MB-10	25.8	0.1	74.1	1282
MB-12	24.9	8.0	67.1	1448
MB-08	36.4	5.9	57.7	1363
MB-11	30.5	0.0	69.5	1452
MB-13	32.2	0.2	67.6	1373

Mowasi pluton

Sample No.	Q	A	P	Points
MW-85	28.9	5.0	66.1	1534

Omai Stock

Sample No.	Q	A	P	Points
6-1205	3.7	0.5	95.5	1451
6-0786	21.0	0.5	78.5	1550
6-1507	17.2	0.2	82.6	1552
6-0251	22.5	0.3	77.2	1464
6-1815	16.5	0.8	82.7	1541
5-0811	20.3	0.1	79.6	1549
7-1220	18.4	2.7	78.9	1511
6-0139	21.4	0.3	78.3	1458
7-2124	18.1	0.7	81.2	1447
5-0485	18.3	0.7	81.0	1548
7-0309	17.9	0.0	82.0	1370
7-1808	21.9	0.1	80.0	1547
8-0179	23.4	0.1	76.5	1450
6-0626	23.8	0.0	76.2	1544
8-1596	21.3	0.3	78.4	1478
8-2434	22.6	0.7	76.7	1517
7-1300	22.1	26.5	51.5	1457

Appendix III: Geochemical methods

General sample preparation

Drill-core or hand specimen samples, weighing 300 to 500 grammes, were trimmed on site using a Norton Clipper 3HP diamond saw to remove any signs of excessive weathering along the edges. The samples were then passed through a Lesson 1/4 inch jaw crusher before being fed into a Mine and Smelter 1/8 inch cone crusher. The crushed samples were then placed in a Siebtik tungsten-carbide tema and pulverised for two minutes. The pulp samples were then sieved to minus 80 mesh (minus 180 microns) and 100 gramme split samples were removed for analysis.

XRF analysis - Major elements

Major element analyses were carried out on rock powder pellets at the University of Durham. Rock powders were pressed into 35mm-diameter pellets and gelled with twelve drops of Mowiol under seven tonnes of pressure.

XRF - Analytical uncertainties

Table A demonstrates that a reasonable degree of accuracy was obtained during check analyses, though MgO values at low concentrations tend to be conspicuously variable with respect to the standard analysis. On the other hand, high levels of instrumental precision were attained with % RSD (Relative Standard Deviation) values generally within the range of 0.06 to 1.8 (see Table B).

ICP-MS - Trace elements

Selective trace element analyses, using a VG Elemental Plasmaquad, were carried out on sample solutions at the University College of Wales, Aberystwyth. Elements analysed by this method included Rb, Sr, Ba, Li, Zr, Nb, Hf, Th, U, Pb, REE and Y. As already mentioned in the main text, Ta was also analysed but enriched and erratic values pointed to contamination, possibily from build-ups on the sampling cone of the Plasmaquad.

By way of sample preparation, approximately 0.5 grammes of each rock powder sample were dissolved using a hot acid (HF-$HClO_4$) attack in PTFE beakers. The final sample solutions were made up to 100 ml with an acid concentration of 10% (volume/volume) HNO_3. For

analysis the sample solutions were further diluted. Two ml. of sample solution were mixed with 0.05 ml of 10 μg/ml indium (In) solution which is used as the internal standard. The final volume was then made up to 5 ml with 18 Mohm (milli-Q) water, giving an In concentration 100 ng/ml. The concentrations of the elements analysed were comfortably within the limits of detection (LOD) as listed by Jarvis (1988). For further details regarding the ICP-MS analytical method the reader is referred to Jenner et al., (1990) and Longerich et al., (1990).

ICP-MS - Analyticial uncertainties

By using REE data, Table C demonstrates that fairly high levels of accuracy and precision were achieved by the ICP-MS instrumentation at Aberystwyth. However, it must be noted that these check analyses were not run concurrently with the Omai samples. Nevertheless, it significant that in the basaltic international standard sample, BHVO-1, Ce has a very poor accuracy of +41.8 % (difference). This trend may account for the sharply positive Ce anomalies recorded in some of the basaltic rocks of the Majuba Suite at Omai and further checks are necessary. For the majority of REE, instrumental precision appears to be good with % RSD values generally less than 2.6 (see Table D). However, Ce, Tm, Lu and especially Y, yield less than satisfactory levels of precision.

ICP-MS - Quantitative versus semi- quantitative analysis

Four of the Omai samples (67-0716, 67-1460, HP-01 and HP-04) were analysed on a semi-quantitative basis, also known as the single standard calibration method, for a selected number of elements including Rb, Sr, Ba, Zr, Nb, Hf, Th, and U. The manufactures of the VG Plasmaquad suggest that the accuracy of this method is usually better than 30% (difference) and may be as low as 10% (difference). Instrumental precision is estimated at around 5.0% RSD. The accuracy claims were tested by comparing fully quantitative ICP-MS data against semi-quantitative ICP-MS data for two other Omai samples. From Table E, it can be seen that the semi-quantitative analyses of Rb, Sr, Ba, Zr, Nb and Hf attain maximum accuracy levels ranging from 0.33 to 29.2 % (difference). However, elements such as Th and U, with extremely low concentrations, gave rise to poor accuracy (75-140 % diff.) relative to the fully quantitative data.

ICP analysis - Trace elements

At Oxford Brookes University, sample solutions were analysed by the ICP method for Co, Cr, Ni, V, Sc, Y, Cu and Zn. By way of sample preparation, rock powders were dissolved by the same hot acid attack method as outlined for the ICP-MS technique. However, in the ICP analyses, sample solutions were aspirated directly into the instrument without further dilution.

Table F shows that a good degree of instrumental precision was attained for the ICP method. Percentage RSD values for the majority of elements fall within the acceptable range of 1 to 5. However, Ni and Y show less satisfactory precision with respective % RSD values of 8.9 and 11.5. Table G demonstrates that the LODs for the all the elements, except V, analysed by ICP. For the Omai samples, the concentrations of these elements nearly always exceed the LODs. Only in the highly felsic samples (e.g. 67-0716 and 67-1470) do the analysed values of certain elements (Co, Cr and Sc) fall beneath the LODs.

AAS - MHS-20 hydride generator system

This analytical method was used at Oxford Brookes University to determine the concentrations of As, a hydride forming element, in the Omai samples. Sample solutions were prepared by cold Aqua Regia digestion of 0.5 grammes of rock powder samples. The underpinning principle of this analytical method is that the hydride-forming element e.g As (or Sb, Bi, Hg) is leached from the sample solution via hydride formation with sodium borohydride as the reductant. The hydride is then passed to a heated quartz cell were atomic absorption measurement is made. According to Aslin (1976), the LOD for As, based on a 500 μg weight, is 0.16 μg/g. Precision is subject to the skill of the operator. For further details on this method the reader is referred to Aslin (1976).

Stable isotope analyses

Regarding the $\delta^{13}C$ analyses of CO_2 vapour within fluid inclusions contained in quartz veins, excellent levels of instrumental precision were attained by the VG "prism" mass spectrometer at Royal Holloway. For example, for the analyses of six samples, precision levels of 0.007 to 0.015 (Standard Deviation, SD) were achieved.

Table A: XRF - Accuracy assessment

	CRPG standard - basalt			USGS standard - basalt		
	BR (Std.)	BR (Dur.)	% Diff.	W-2 (Std.)	W-2 (Dur.)	% Diff.
SiO2 wt%	38.20	38.33	0.34	52.44	52.55	0.15
Al2O3	10.20	10.89	6.76	15.35	15.37	0.13
Fe2O3T	12.88	12.59	2.25	10.74	15.37	0.65
MgO	13.28	13.19	0.68	6.37	5.91	7.22
CaO	13.80	13.71	0.65	10.87	10.72	1.38
Na2O	3.05	3.23	5.90	2.14	2.22	3.74
K2O	1.40	1.28	8.57	0.63	0.65	3.17
TiO2	2.60	2.58	0.77	1.06	1.03	2.83
MnO	0.20	0.19	5.00	0.16	0.16	0.00
P2O5	1.04	1.02	1.92	0.13	0.17	30.80
LOI	3.29	3.00	9.67	0.15	0.60	300.00

	USGS standard - granodiorite			USGS standard - granite		
	GSP-1 (Std.)	GSP-1 (Dur.)	% Diff.	G-1 (Std.)	G-1 (Dur.)	% Diff.
SiO2 wt%	67.15	66.86	0.43	72.44	72.35	0.12
Al2O3	15.10	14.88	1.46	14.22	13.93	2.04
Fe2O3T	4.29	4.51	5.13	1.94	1.87	3.61
MgO	0.96	1.16	20.80	0.36	0.19	47.20
CaO	2.07	2.22	7.25	1.37	1.50	9.49
Na2O	2.80	2.68	4.29	3.33	3.29	1.20
K2O	5.51	5.95	7.99	5.50	6.06	10.18
TiO2	0.65	0.77	18.50	0.27	0.28	3.70
MnO	0.04	0.04	5.00	0.30	0.23	23.30
P2O5	0.28	0.31	10.70	0.08	0.11	37.50
LOI	0.59	0.64	8.47	0.36	0.41	13.89

Note: Std. - international geostandard analysis from Govindaraju (1989).
Dur. international geostandard analysis by XRF at the University of Durham.

Table B: XRF - Precision assessment

	Quartz diorite - Omai Stock					
	5-0485A	5-0485B	5-0485C	Mean	SD	% RSD
SiO2 wt%	59.76	59.84	59.79	59.8	0.033	0.06
Al2O3	17.69	17.69	17.60	17.66	0.042	0.02
Fe2O3T	3.54	3.48	3.55	3.52	0.031	0.88
MgO	1.21	1.20	1.25	1.22	0.022	1.80
CaO	4.41	4.41	4.44	4.42	0.014	0.32
Na2O	3.82	3.81	3.79	3.81	0.012	0.32
K2O	3.64	3.63	3.66	3.64	0.012	0.33
TiO2	0.37	0.38	0.38	0.38	0.005	1.32
MnO	0.12	0.12	0.12	0.12	0.000	0.00
P2O5	0.16	0.17	0.15	0.16	0.008	5.00
(LOI)	5.28	5.28	5.28			

Note: SD - Standard Deviation; % RSD - % Relative Standard Deviation.

Table C: ICP-MS - Accuracy assessment

		USGS - basalt			USGS - andesite		
		BHVO-1 (Std.)	BHVO-1 (Aber.)	% Diff.	AGV-1 (Std.)	AGV-1 (Aber.)	% Diff
La	ppm in rock	15.80	16.66	5.44	38.00	37.83	0.45
Ce		39.00	55.30	41.80	67.00	67.44	0.66
Pr		5.70	5.29	7.19	7.60	8.18	7.63
Nd		25.20	24.36	3.33	33.00	29.87	9.48
Sm		6.20	6.09	1.77	5.90	5.40	8.47
Eu		2.06	2.00	2.91	1.64	1.73	5.49
Gd		6.40	6.45	0.78	5.00	5.11	2.20
Tb		0.96	0.91	5.20	0.70	0.64	8.57
Dy		5.20	5.00	3.84	3.60	3.20	11.10
Ho		0.99	0.89	10.10	0.67	0.61	8.96
Er		2.40	2.34	2.50	1.70	1.59	6.47
Tm		0.33	0.30	9.09	0.34	0.25	26.50
Yb		2.02	1.86	7.92	1.72	1.51	12.20
Lu		0.29	0.23	20.70	0.27	0.24	11.10

		USGS - quartz latite			USGS - granite		
		QLO-1 (Std.)	QLO-1 (Aber.)	% Diff.	G-2 (Std.)	G-2 (Aber.)	% Diff.
La	ppm in rock	27.00	26.48	1.93	89.00	85.17	4.30
Ce		54.60	51.23	6.17	160.00	152.90	4.44
Pr		6.00	5.90	1.67	18.00	15.30	15.00
Nd		26.00	22.26	14.40	55.00	48.55	11.72
Sm		4.88	4.78	2.05	7.20	6.56	9.72
Eu		1.43	1.54	7.69	1.40	1.50	7.14
Gd		4.70	4.69	0.21	4.30	5.11	18.80
Tb		0.71	0.64	9.86	0.48	0.48	0.00
Dy		3.80	3.57	6.05	2.40	2.12	11.70
Ho		0.86	0.74	14.00	0.40	0.33	17.50
Er		2.30	2.15	6.52	0.92	0.82	10.90
Tm		0.37	0.33	10.80	0.18	0.12	33.30
Yb		2.32	2.05	11.60	0.80	0.55	31.20
Lu		0.37	0.35	5.40	0.11	0.09	18.20

Note: Std. - international geostandard analysis from Govindaraju (1989).
Aber. - international geostandard analysis by ICP-MS at Aberystwyth.

Table D: ICP-MS - Precision assessment

		DRF-1 (1)	DRF-1 (2)	DRF-1 (3)	Mean	SD	% RSD
La	ppm in rock	10.57	10.61	10.49	10.59	0.02	0.19
Ce		20.36	23.9	20.38	21.55	1.66	7.72
Pr		3.04	2.96	2.94	2.98	0.04	1.34
Nd		12.62	12.81	13.29	12.9	0.28	2.17
Sm		3.04	3.23	3.17	3.15	0.08	2.54
Eu		0.94	0.9	0.95	0.93	0.02	2.15
Gd		3.18	3.23	3.45	3.29	0.12	3.65
Tb		0.56	0.48	0.5	0.51	0.03	1.53
Dy		2.84	2.76	2.92	2.84	0.07	2.46
Ho		0.62	0.61	0.61	0.61	0.005	0.82
Er		1.64	1.73	1.73	1.7	0.04	2.35
Tm		0.3	0.26	0.26	0.27	0.02	7.4
Yb		1.55	1.59	1.61	1.58	0.02	1.27
Lu		0.3	0.24	0.28	0.27	0.03	9.23
Y		12.25	15.74	8.72	12.24	2.87	23.4

Note: DRF -1 is an in-house reference rock (Diorite Rhobell Fawr) at University College of Wales, Aberystwyth.

Table E: ICP-MS - Quantitative versus semi-quantitative analysis

		4-0294 - basalt, Majuba Suite			7-1594 - diorite, Gilt Creek Suite		
		Quant.	Semi-qnt	% Diff	Quant	Semi-qnt	% Diff.
Rb	ppm in rock	9.7	9.43	2.78	73.1	83.1	13.7
Sr		242	228	5.79	461	497	7.81
Ba		243	343	41	634	773	21.9
Zr		26	18.4	29.2	90.5	90.2	0.33
Nb		2.96	2.24	24.2	7.48	10.4	39
Hf		0.64	0.63	1.56	2.45	2.82	15.1
Th		0.64	1.12	75	3.97	4.5	13.4
U		0.08	0.19	138	1.28	1.99	55.5

Note: Quant - fully quantitative analysis; Semi-qnt - semi-quantitative analysis.

Table F: ICP - Precision assessment

Sample 1-1555D - andesite, Majuba Suite.

Element (ppm in rock)	n	Mean	SD	% RSD
Cu	7	77.15	1.34	1.74
Zn	7	92.15	1.62	1.76
Co	7	49.57	2.34	4.72
Cr	7	163.1	2.33	1.43
Ni	7	63.14	5.62	8.90

Sample 5-0485 - quartz diorite, Omai Stock

Element (ppm in rock)	n	Mean	SD	% RSD
Y	7	16.57	1.91	11.50
V	7	58.90	3.09	5.20

Sample 3-1635D - dioritic dyke-rock, Gilt Creek Suite

Element (ppm in rock)	n	Mean	SD	% RSD
Sc	8	26.9	1.21	1.29

Table G: ICP - Limits of detection (LOD)

Element	W'length	LOD* (ppm in rock)
Co	228.616	2.5
Cr	267.716	3.0
Ni	231.604	4.0
Sc	361.384	1.0
Y	371.030	2.0
Cu	324.754	2.0
Zn	213.856	1.0

*Note: LOD indicates limits of detection in ppm in the rock. This value is calculated from the concentration of the element in solution times the sample volume (100 ml) divided by the sample weight (0.5 grammes).

Appendix IV: SEM-EDS micro-analysis

Instrumentation: JEOL 840 interfaced with a LINK software system.

Specifications: Working distance (WD) - 39mm; Accelerating voltage - 40 KV; Probe current - 1 nano-amp.

Analytical uncertainties

1. The standards used to calibrate the instrument may not be sufficiently similar to the unknown elements for the ZAF correction to function properly.

2. Fluctuations in the beam current tend to generate (element %) analytical totals of less than, or greater than, 100 %.

3. The minute grain size (10 μm) of some minerals, especially the tellurides, poses some problems. For example, at an accelerating voltage of 40 KV, the beam interaction volume is more or less comparable to the diameter of the grain being analysed. This will result in wall-rock (vein) elements such as Si and Ca being incorporated in the micro-analysis. This phenomenon will ultimately give rise to analytical totals of less than 100 %.

4. Backscatter images demonstrate that even the smallest of grains contain complex zoning and intergrowths on a sub-micron scale. These intergrowths are substantially smaller than the beam interaction volume and will generate hybrid micro-analyses.

5. Elements such as Te may not have a simple integer stoichiometry which would hinder the calculation of mineral formulae.

6. A "bug" in the software system has ensured the normalised atomic % values do not add up to 100% and therefore these values have been re-normalised manually. This is not a serious problem as it is the ratios of atomic % values between the elements which determines the stoichiometry of the mineral being analysed (see representative micro-analyses of telluride minerals overleaf).

The accuracy of the SEM-EDS micro-analytical method cannot be assessed satisfactorily due to the lack of comparable standards. However, an estimate of the instrumental precision was made by taking 30 consecutive micro-analyses of a single point on a native gold grain,

Representative SEM-EDS micro-analyses of telluride minerals at Omai.

Spectrum R53 : Calaverite : $AuTe_2$

All elmts analysed

ELMT	ZAF	%ELMT	+-	Error	ATOM.%	ATOM.% NORM.
MoK :10	1.037	< .660	+-	.330		
AgK :10	1.117	1.951	+-	.963	2.115	2.16
SbK :10	1.024	<6.697	+-	3.349		
TeK :10	.996	53.054	+-	6.171	48.620	49.55
W L :10	.897	< .300	+-	.150		
AuL :10	.933	43.213	+-	.351	25.654	26.14
PbL :11	1.001	< .423	+-	.211		
BiL :10	.940	3.339	+-	.232	1.868	1.90
S K :11	.561	<1.697	+-	.848		
AlK :11	.604	< .236	+-	.118		
SiK :11	1.257	4.431	+-	.200	18.444	18.79
TiK :11	.618	.246	+-	.062	.600	0.61
MgK :11	.615	< .298	+-	.149		
CaK :11	.760	.286	+-	.118	.833	0.85
MnK :11	.823	< .074	+-	.037		
FeK :11	.854	< .080	+-	.040		
TOTAL		106.519				100.00

Spectrum R52 : Petzite : Ag_3AuTe_2

All elmts analysed

ELMT	ZAF	%ELMT	+-	Error	ATOM.%	ATOM.% NORM.
MoK :10	1.092	< .640	+-	.320		
AgK :10	1.069	38.771	+-	1.566	43.663	44.94
SbK :10	.986	<6.098	+-	3.049		
TeK :10	.960	31.525	+-	5.643	30.013	30.89
W L :10	.878	< .280	+-	.140		
AuL :10	.914	25.329	+-	.293	15.622	16.08
PbL :11	.980	< .382	+-	.191		
BiL :10	.921	< .365	+-	.183		
S K :11	.667	<1.621	+-	.811		
AlK :11	.587	< .217	+-	.108		
SiK :11	1.233	1.457	+-	.168	6.301	6.49
TiK :11	.574	.181	+-	.057	.458	0.47
MgK :11	.592	< .282	+-	.141		
CaK :11	.656	.363	+-	.112	1.100	1.13
MnK :11	.805	< .072	+-	.036		
FeK :11	.834	< .077	+-	.039		
TOTAL		97.625				100.00

Spectrum R12 : Hessite : Ag_2Te

All elmts analysed

ELMT	ZAF	%ELMT	+-	Error	ATOM.%	ATOM.% NORM.
MoK :10	1.189	< .640	+-	.320		
AgK :10	1.053	56.127	+-	1.796	59.059	62.15
SbK :10	.952	<5.847	+-	2.924		
TeK :10	.925	33.386	+-	5.902	29.698	31.25
W L :10	.854	< .258	+-	.129		
AuL :10	.889	.445	+-	.172	.256	0.27
PbL :11	.955	< .373	+-	.187		
BiL :10	.897	< .353	+-	.177		
S K :11	.896	<1.388	+-	.694		
AlK :11	.530	< .216	+-	.108		
SiK :11	1.134	1.318	+-	.164	5.325	5.60
TiK :11	.554	.200	+-	.061	.473	0.50
MgK :11	.525	< .287	+-	.143		
CaK :11	.663	< .166	+-	.083		
MnK :11	.771	< .073	+-	.036		
FeK :11	.798	.107	+-	.048	.218	0.23
TOTAL		91.582				100.00

Spectrum R44 : Wehrlite : BiTe

All elmts analysed

ELMT	ZAF	%ELMT	+-	Error	ATOM.%	ATOM.% NORM.
MoK :10	1.046	.652	+-	.314	.982	1.04
AgK :10	1.119	<2.051	+-	1.026		
SbK :10	1.058	<6.570	+-	3.285		
TeK :10	1.031	39.940	+-	5.919	45.206	48.09
W L :10	.944	< .272	+-	.136		
AuL :10	.948	< .332	+-	.166		
PbL :11	1.020	< .548	+-	.274		
BiL :10	.960	61.509	+-	.445	42.509	45.23
S K :11	.959	<2.217	+-	1.108		
AlK :11	.599	.347	+-	.173	1.860	1.98
SiK :11	1.239	.594	+-	.151	3.052	3.25
TiK :11	.592	< .065	+-	.032		
MgK :11	.615	< .282	+-	.141		
CaK :11	.714	< .133	+-	.067		
MnK :11	.825	< .073	+-	.036		
FeK :11	.858	.148	+-	.046	.383	0.41
TOTAL		103.191				100.00

Spectrum R02 : Tellurobismuthite : Bi_2Te_3

All elmts analysed

ELMT	ZAF	%ELMT	+-	Error	ATOM.%	ATOM.% NORM.
MoK :10	1.044	< .687	+-	.344		
AgK :10	1.122	<2.140	+-	1.070		
SbK :10	1.049	<7.082	+-	3.541		
TeK :10	1.022	44.833	+-	6.357	50.512	54.04
W L :10	.931	< .275	+-	.138		
AuL :10	.941	< .342	+-	.171		
PbL :11	1.012	< .548	+-	.274		
BiL :10	.952	52.008	+-	.436	35.777	38.27
S K :11	.944	<1.965	+-	.982		
AlK :11	.582	< .198	+-	.099		
SiK :11	1.211	.615	+-	.145	3.145	3.36
TiK :11	.595	.154	+-	.059	.463	0.50
MgK :11	.593	< .269	+-	.134		
CaK :11	.746	.999	+-	.109	3.582	3.83
MnK :11	.814	< .073	+-	.036		
FeK :11	.847	< .079	+-	.039		
TOTAL		98.608				100.00

Spectrum R16 : Volynskite: $AgBi_{1.6}Te_2$

All elmts analysed

ELMT	ZAF	%ELMT	+-	Error	ATOM.%	ATOM.% NORM.
MoK :10	1.030	< .668	+-	.334		
AgK :10	1.067	16.974	+-	1.324	16.091	16.73
SbK :10	.984	<6.701	+-	3.351		
TeK :10	.957	39.691	+-	6.418	31.807	33.08
W L :10	.890	< .271	+-	.135		
AuL :10	.905	< .325	+-	.163		
PbL :11	.972	.672	+-	.260	.332	0.35
BiL :10	.913	35.650	+-	.387	17.444	18.15
S K :11	.865	<2.022	+-	1.011		
AlK :11	.569	.478	+-	.213	1.811	1.88
SiK :11	1.190	7.709	+-	.214	28.063	29.19
TiK :11	.575	.191	+-	.062	.408	0.42
MgK :11	.572	< .306	+-	.153		
CaK :11	.707	< .166	+-	.083		
MnK :11	.792	< .075	+-	.037		
FeK :11	.821	.103	+-	.049	.188	0.20
TOTAL		101.467				100.00

containing 6-8 wt.% silver, in sample 6-2017. In each case the weight (element) % of gold and silver were recorded. Bearing in mind that each analysis slightly modifies the sample area, the levels of precision achieved were of a relatively high degree. The results are summarised below as follows:

	Number of analyses (n)	Mean (wt.%)	SD	% RSD
Au	30	93.09	0.61	0.66
Ag	30	6.51	0.59	9.06

Note: SD - Standard deviation; % RSD - % Relative standard deviation.

X-ray spectra

Representative X-ray spectra of the main ore-forming minerals (gold, galena, scheelite and tellurides) are displayed on the following three pages.

Representative X-ray spectra of the main ore minerals at Omai.

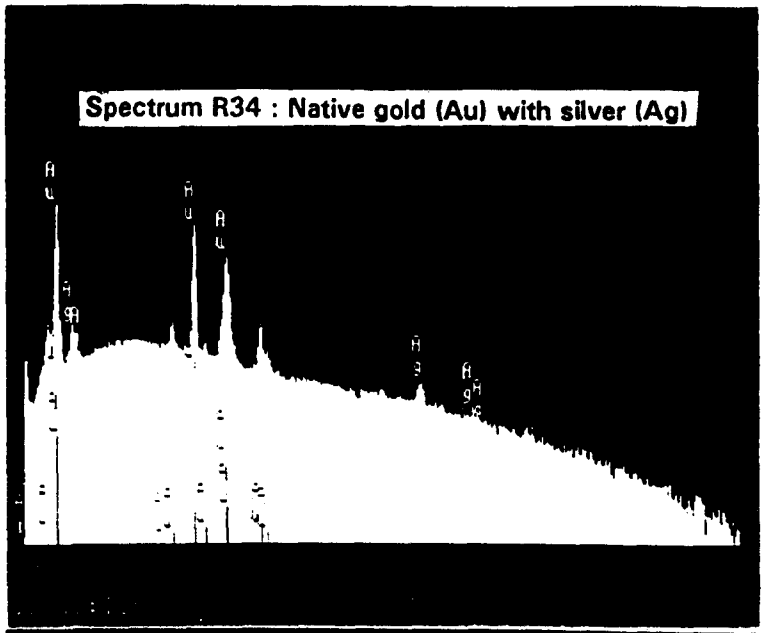

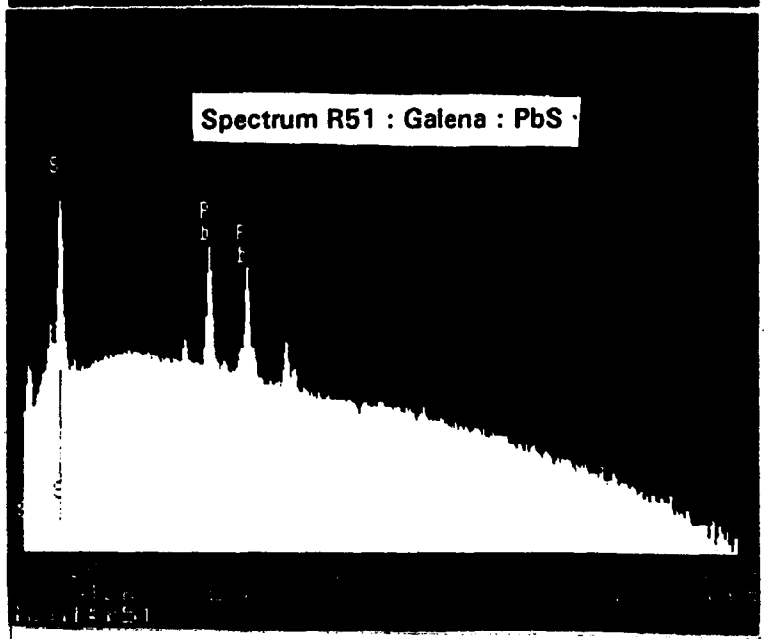

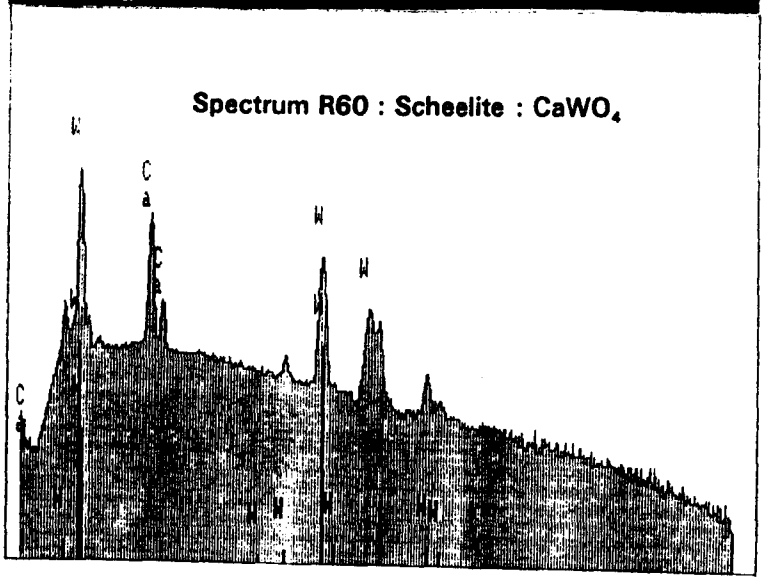

Representative X-ray spectra of the main ore minerals at Omai (cont'd).

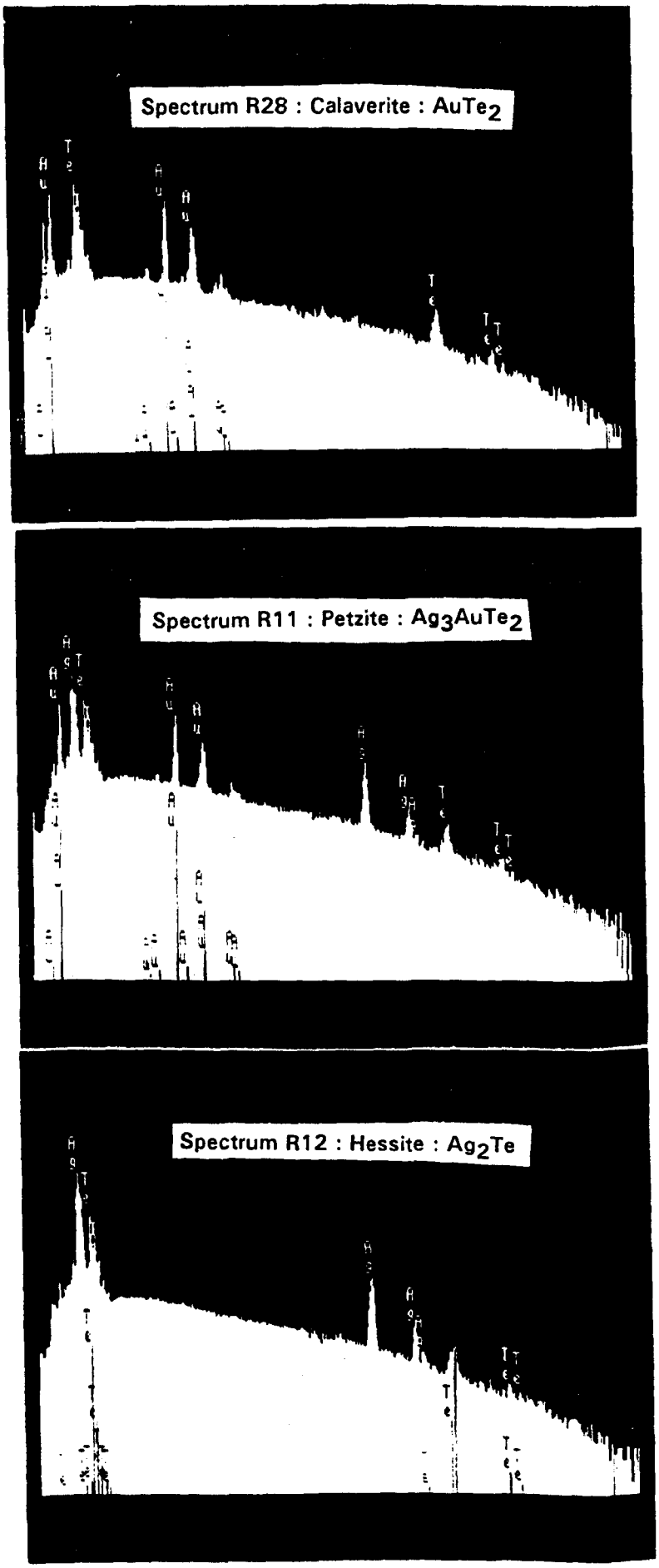

Representative X-ray spectra of the main ore minerals at Omai (cont'd).

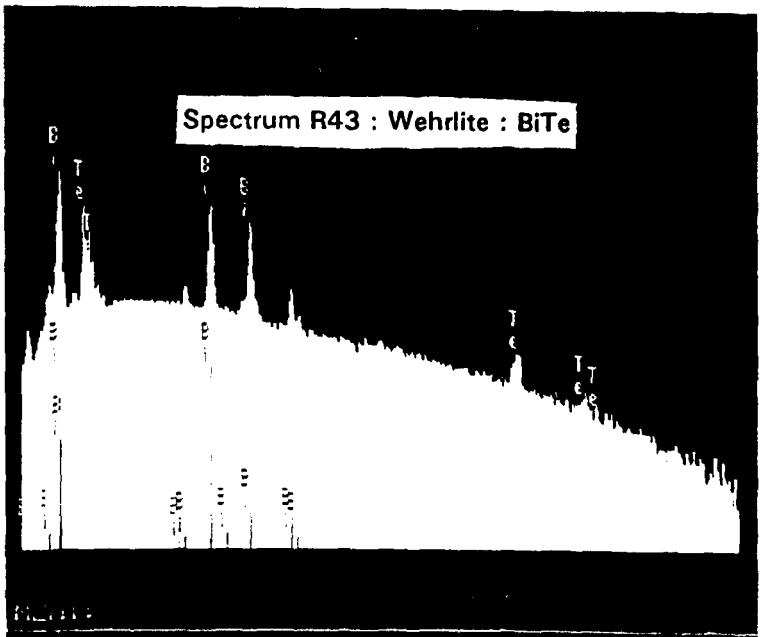

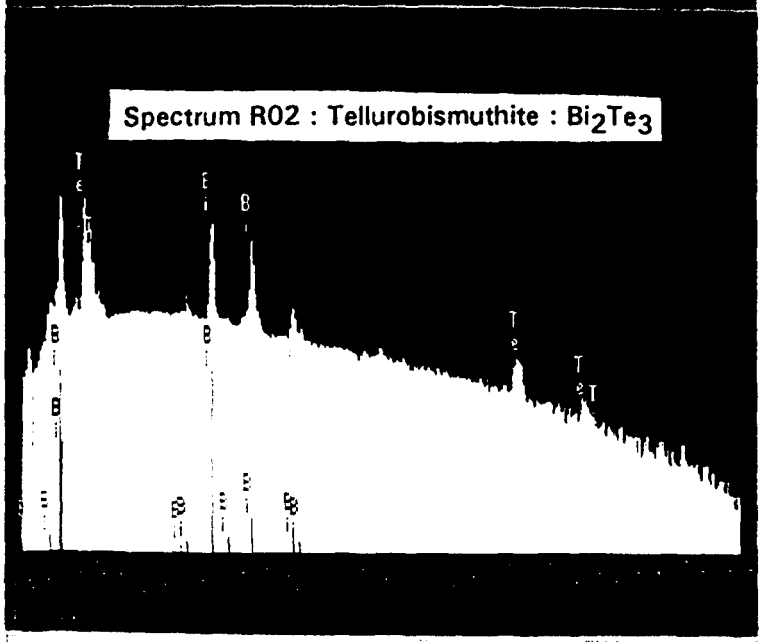

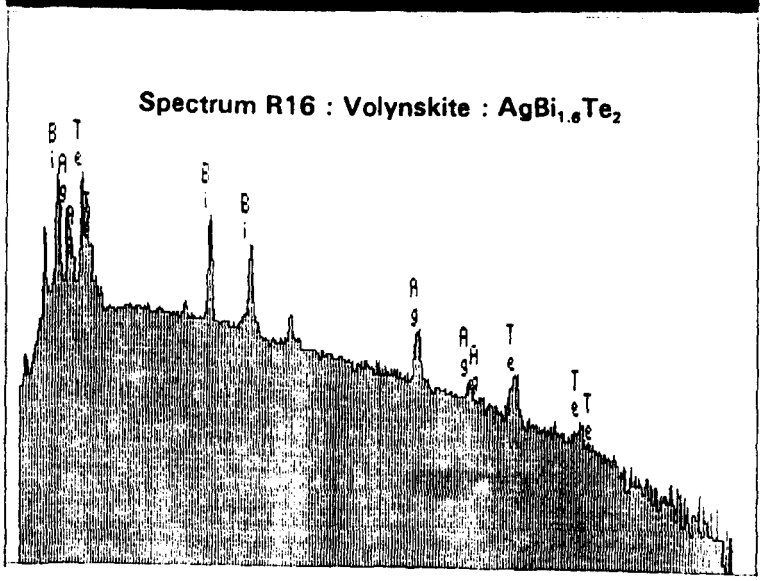

Fig. 2.3

GEOLOGICAL MAP OF THE OMAI AREA

Modified after Guardia (1969)